

ULTRASONIC STUDIES IN SIMPLE  
LIQUIDS AND BINARY MIXTURES

by

AKL MOHAMMED AWWAD

A thesis submitted to the Department of Pure and Applied  
Chemistry, University of Strathclyde, in accordance with  
the requirements for the Degree of DOCTOR OF PHILOSOPHY.

May 1983.

TO MY CHILDREN  
HYTHAM AND RANA  
AND MY WIFE, AMAL

## CONTENTS

## CONTENTS

	<u>Page</u>
Acknowledgements	vi
Summary	vii
 <u>CHAPTER 1 INTRODUCTION</u>	
1.1 General Introduction	1
1.2 Hydrocarbons	1
1.3 Alcohols	9
1.4 Morpholine Derivatives	12
 <u>CHAPTER 2 MOLECULAR ACOUSTICS AND THERMODYNAMIC FUNCTIONS</u>	
2.1 Introduction to Acoustics	14
2.2 Sound Propagation and Absorption in Liquids	16
(i) Shear viscosity contribution	
(ii) Volume viscosity contribution	
(iii) Thermal conduction contribution	
2.3 Ultrasonic Relaxation	19
2.4 Evaluation of Energy Parameters	23
(i) Kinetic	
(ii) Thermodynamic	
2.5 Thermodynamic Functions of Binary Mixtures	30
(i) Introduction	
(ii) Ideal mixture	
(iii) Molar mixing functions	
(iv) Excess functions	
 <u>CHAPTER 3 EXPERIMENTAL</u>	
3.1 Generation and Detection of Ultrasonic Waves	35
3.2 General Review of Experimental Techniques	38

	<u>Page</u>
3.3 Techniques of Specific Relevance to This Study	38
3.4 Swept Frequency Acoustic Resonator	40
(i) Principle of technique	
(ii) Experimental system	
(iii) Experimental procedure	
(iv) Analysis of data	
(v) Accuracy	
3.5 Conventional Pulse Equipment (15-72 MHz)	50
(i) Principle of technique	
(ii) Experimental system	
(iii) Experimental procedure	
(iv) Analysis of data	
(v) Accuracy	
3.6 Ultra-High Frequency Pulse Technique (100-1000 MHz)	57
(i) Principle of technique	
(ii) Experimental system	
(iii) Experimental procedure	
(iv) Analysis of data	
(v) Accuracy	
3.7 $^{13}\text{C}$ nmr Spectra	
3.8 Density Measurements	
3.9 Viscosity Measurements	
<u>CHAPTER 4</u> <u>ULTRASONIC STUDIES OF ROTATIONAL ISOMERISM IN VARIOUS METHYLPENTANES</u>	
4.1 Introduction	68
4.2 Materials	70

	<u>Page</u>	
4.3	Results	70
	(i) Viscosities	
	(ii) Densities	
	(iii) Isoentropic (adiabatic) compressibilities	
	(iv) Ultrasonic relaxation	
	(v) Theoretical prediction of rotational energy parameters	
4.4	Discussion	93
4.5	Conclusions	104
<u>CHAPTER 5 ULTRASONIC STUDIES OF ROTATIONAL ISOMERISM IN VARIOUS METHYLPENTANES</u>		
5.1	Introduction	105
5.2	Materials	106
5.3	Results	106
	(i) Viscosities and densities	
	(ii) Isoentropic (adiabatic) compressibilities	
	(iii) Ultrasonic relaxation	
	(iv) Theoretical prediction of rotational energy parameters	
5.4	Discussion	120
5.5	Conclusion	132
<u>CHAPTER 6 ULTRASONIC STUDIES OF MIXTURES OF n-HEXADECANE WITH DIMETHYLPENTANES</u>		
6.1	Introduction	133
6.2	Materials	136
6.3	Theory	138
6.4	Results	140
6.5	Discussion	151

	<u>Page</u>
6.6 Conclusion	159
<u>CHAPTER 7</u> <u>ISOENTROPIC (ADIABATIC) COMPRESSIBILITY</u> <u>OF HYDROCARBONS AND THEIR MIXTURES</u>	
7.1 Introduction	160
7.2 Materials	162
7.3 Results	162
(i) Sound velocity and density data	
(ii) Isoentropic compressibility data	
7.4 Discussion	182
(i) Pure liquids	
(ii) Binary mixtures	
7.5 Conclusions	202
<u>CHAPTER 8</u> <u>ULTRASONIC INVESTIGATION OF MIXTURES</u> <u>OF ISOMERIC OCTANOLS WITH n-OCTANE</u>	
8.1 Introduction	204
8.2 Materials	205
8.3 Results	205
(i) Excess volume data	
(ii) Acoustic velocity and isoentropic compressibility	
(iii) Ultrasonic attenuation and viscosity measurements	
8.4 Discussion	219
(i) Volume of mixing	
(ii) Acoustic velocity and isoentropic compressibilities	
(iii) Viscothermal acoustic attenuation coefficient	
8.5 Conclusions	227

	<u>Page</u>
<u>CHAPTER 9</u> <u>ULTRASONIC STUDIES OF N-FORMYL-</u> <u>MORPHOLINE-WATER MIXTURES</u>	
9.1    Introduction	228
9.2    Materials	229
9.3    Results	230
(i)    Volume of mixing data	
(ii)    Viscosity data	
(iii)    Sound velocity data	
(iv)    Isoentropic compressibility and excess isoentropic compressibility data	
(v) <sup>13</sup> C nmr spectra of N-formylmorpholine	
(vi)    Ultrasonic attenuation data	
9.4    Discussion	252
A.    Conformational dynamics of N-formylmorpholine	
B.    Conformational dynamics of N-formylmorpholine in the presence of water	
C.    Structure of N-formylmorpholine- water mixtures	
(i)    Excess volumes and compress- ibilities of mixing	
(ii)    Viscosities	
(iii)    Ultrasonic absorption	
9.5    Conclusions	256

## ACKNOWLEDGEMENTS

I wish to express my deep and sincere gratitude to Professor A.M. North and Dr R.A. Pethrick for their constant encouragement, supervision and invaluable assistance throughout the whole research period. I am equally indebted to my sponsor, The Petroleum Research Institute of Iraq for providing me with an opportunity to conduct my research work in this Department.

The high frequency ultrasonic equipment and facilities kindly made available by Professor J. Lamb of the Department of Electronic and Electrical Engineering, University of Glasgow are gratefully acknowledged. The technical assistance offered by Mr T. Wright and R. Turnbull is similarly recognised.

The efficient and accurate typing by Mrs A. White is also fully appreciated.

Finally, I must take this opportunity to express my deep appreciation to staff, technical staff, fellow post-graduates and postdoctorates for their assistance throughout the whole period of this research.

*AKL AWWAD*

## SUMMARY

## SUMMARY

This thesis is concerned with the study of four topics.

These are:-

1. Rotational Isomerism in Methylpentanes and Methylhexanes

The rotational isomerism in methylpentanes and methylhexanes has been studied using the ultrasonic relaxation technique. The observed conformational energetics obtained are compared with those predicted on the basis of non-bonded van der Waals' interaction between neighbouring groups. In general, the values of the activation and energy difference obtained from experiment are in good agreement with those obtained from the theory.

The adiabatic compressibilities and other ultrasonic parameters indicate that the propagation of sound in these liquids is controlled by the nature of the molecular structure and the effects of the basic shapes of the molecules on the intermolecular interactions.

2. Mixtures of Dimethylpentanes in n-Hexadecane

Studies of the physical and acoustic properties of binary mixtures of dimethylpentanes and n-hexadecane at 298.15K indicate a concentration dependent phenomenon. The observed acoustic attenuation is associated with a rotational isomeric process and a clustering of the molecules in the mixture.

3. Mixtures of Isomeric Octanols in n-Octane

Studies of the binary mixtures of isomeric octanols with n-octane indicate that the observed volume, adiabatic

and acoustic excesses are a consequence of competing effects of the alkane chain taking up the 'free' volume in the system and the disturbance of the distribution between cyclic, linear structures and monomer forms in the mixtures.

#### 4. N-Formylmorpholine-Water Mixtures

The acoustic,  $^{13}\text{C}$  nmr spectra and physical properties of N-formylmorpholine and its aqueous solutions indicate that N-formylmorpholine is more planar than its N-alkyl analogues and this planarity is increased by the presence of traces of water. This explains the increased efficiency in the extraction of aromatics from petroleum feedstocks.

CHAPTER 1

INTRODUCTION

## CHAPTER 1

### INTRODUCTION

#### 1.1 General Introduction

Recent developments in theoretical studies of simple liquids<sup>1-6</sup> and liquid mixtures<sup>7-10</sup> have established the relationship between the time averaged dynamic behaviour of a molecular system and its equilibrium thermodynamic properties. Studies of the time dependent behaviour of simple liquids and liquid mixtures using relaxation techniques have been performed for many years<sup>11-15</sup>. The correlation of dynamic and thermodynamic measurements has not been considered adequately, although such inter-dependence has often been inferred.

The following sections outline briefly topics that are relevant to the study of the thermodynamic and dynamic behaviour in the context of the subject to be discussed later in this thesis.

#### 1.2 Hydrocarbons

A knowledge of the physical and chemical properties of hydrocarbons and their mixtures is important both academically and industrially. Many industrial processes use both hydrocarbons and their mixtures and a knowledge of this subject area is critical to the efficient utilization and refining of crude oil. Proper development and economic design of appropriate equipment for these processes is only possible if the chemical and physical properties of the substances to be processed are known.

For this reason, the properties of hydrocarbons and their mixtures have been the subject of an international data collection exercise. Furthermore, many attempts have been made to correlate these data using semiempirical or theoretical approaches. Recently, computer-stimulated calculations<sup>16-18</sup> and neutron-scattering experiments<sup>19</sup> have given insight into the relations between molecular structure and macroscopic behaviour. Considerable progress has also been made in the development of statistical theories over recent years<sup>20,21</sup>. The calculation of physical properties using a complete, statistical theory is still not yet possible for 'complicated' molecules such as long-chain hydrocarbons, because of the range of different conformations which can occur and the effects of these various structures on the intermolecular interactions.

The most successful theories describing the thermodynamic properties of mixtures of chain-like molecules or, more generally, of molecules differing significantly in shape and size was first developed by Prigogine et al<sup>22</sup>, and later improved by Flory et al<sup>23-25</sup>. This theory has been presented in a general form by Patterson et al<sup>26</sup>. It is commonly called the Prigogine-Flory theory and its essential physical principles will be briefly discussed in the following section.

The macroscopic volume of a liquid is envisaged to be divided up into single cells, each occupied by a single molecule. The theory is based upon the concept that the

structure of a liquid is closely related to that of a solid. For chain-like molecules - linear or branched - each segment of a chain occupies a unit cell.

The calculation of thermodynamic properties usually starts from the free energy,  $F$ , of the pure component or the mixture. For that purpose the following assumptions are made:-

1. Each segment of the molecule has a hard-core volume of  $v^*$ . The hard cores of the segments of different molecules,  $i$  and  $j$ , interact with one another with an attractive potential,  $\eta_{ij}/v$ , which only extends to the next nearest neighbours of a particular segment;  $v$  is the volume of the liquid and the constant of proportionality,  $\eta_{ij}$ , characterizes the interaction between  $i$  and  $j$ . In a binary mixture, there are three types of such interactions, between segments of molecules of the same kind,  $\eta_{11}$ ,  $\eta_{22}$ , and of different kinds,  $\eta_{12}$ .
2. The segments of the chain molecules are randomly distributed within the cells. It therefore follows that the probability of 1-1 contacts with an interaction parameter  $\eta_{11}$  or of 2-2 contact with an interaction parameter  $\eta_{22}$  is proportional to the probability of finding two segments of type 1 or 2 neighbouring each other. These probabilities are proportional to  $\phi_1^2$  or  $\phi_2^2$  which are the squares of the probabilities  $\phi_1$  or  $\phi_2$  of finding a segment of type 1 or 2 in a particular cell. The values of  $\phi_1$  and  $\phi_2$  are identical with the segment fractions for

the two types of molecules present in the mixture.

$$\phi_1 = \frac{x_1 r_1 v^*}{x_1 r_1 v^* + x_2 r_2 v^*} = 1 - \phi_2 \quad 1.1$$

where  $x_i$  is the mole fraction and  $r_i$  is the number of segments of a molecule of type  $i$  present. Hence  $r_i v^*$  is the hard-core volume of one molecule,  $i$ , which is expressed as:

$$V_i^* = r_i v^* \quad 1.2$$

3. The third assumption concerns the flexibility of the segments within their cells. A single molecule consisting of one segment only ( $r_i=1$ ) has three degrees of translational freedom to move around within its cell. The volume available for unrestrained motion - free volume,  $v_f$ , is given by constant  $(v^{1/3} - v^{*1/3})^3$ . Since the diameter of a segment is proportional to  $v^{*1/3}$ , the distance between the centres of two neighbouring segments is proportional to  $v^{1/3}$ , and hence the third power of the difference in the volume is proportional to  $v_f$ . A chain segment does not have three degrees of freedom, as it is chemically bonded to neighbouring segments, and thence is constrained in its motion to within its unit cell. This effect is accounted for by  $v_f$

$$v_f = \text{constant} (v^{1/3} - v^{*1/3})^3 c \quad 1.3$$

where  $c < 1$ . The smaller the value of  $c$ , the more rigid is the chain. The general expression for the free energy  $F_M$  of a mixture of chain molecules is given by:

$$F_M = - (A_{11}\eta_{11} + A_{22}\eta_{22} + A_{12}\eta_{12})/v_M +$$

$$T[3kN\bar{r}\bar{c}\ln(v_M^{2/3} - v^{*1/3}) + k \ln W_M] +$$

$$\text{constant} \quad 1.4$$

In the first term,  $A_{ij}$  signifies that number of contacts between segments of type  $i$  and  $j$  in the mixture. Multiplication of these values by  $\eta_{ij}$  and division of the whole term by  $v_M$ , the molar volume of the mixture, yields the internal energy,  $U_M$ , of the mixture. The contribution enclosed between square brackets is the entropy  $S_M$  of the mixture, corresponding to  $F_M = U_M - TS_M$ .  $S_M$  contains the free volume,  $v_{fM}$ , of the mixture. The parameter,  $W_M$ , designates the number of distinguishable distributions of chain molecules within all cells and  $\bar{r}$  and  $\bar{c}$  respectively are the average values of the number of segments per molecule in the mixture, and of the flexibility parameter,  $c$ , of the mixture.  $A_{ij}$ ,  $W_M$ ,  $\bar{r}$  and  $\bar{c}$  depend on the mole fraction  $x_i$  or the segment fraction  $\phi_i$  of the mixture. In order to calculate the volume,  $v_M$ , of the mixture, the relation  $\partial F/\partial V = P$  is applied to equation 1.4 yielding the thermal equation of state which can then be used to calculate  $v_M$  at a given pressure and temperature.

For  $x_1 = 1$  or  $x_1 = 0$ , the free energy,  $F$ , of the pure components is obtained from equation 1.4 and the following expressions have been adequately derived elsewhere<sup>24</sup>.

$$\Delta F_M = \Delta U_M - T\Delta S_M \quad 1.5$$

$$\Delta U_M = (V_1^* x_1 + V_2^* x_2) [(\bar{v}_1^{-1} - v_M^{-1}) \phi_1 P_1^* + (\bar{v}_2^{-1} - \bar{v}_M^{-1}) \phi_2 P_2^* + \phi_1 \phi_2 \left( \frac{s_2/s_1}{\phi_1 + s_2/s_1 \phi_2} \right) \frac{\chi_{12}}{\bar{v}_M}] \quad 1.6$$

$$\Delta S_M = -k [N_1 \ln \phi_1 + N_2 \ln \phi_2] - 3 \sum_{i=1}^2 \frac{N_i V_i^*}{T_i^*} \ln \left( \frac{\bar{v}_i^{-1/3} - 1}{\bar{v}_M^{-1/3} - 1} \right) \quad 1.7$$

$$\Delta V_M = (V_1^* x_1 + V_2^* x_2) (\bar{v}_M - \phi_1 \bar{v}_1 - \phi_2 \bar{v}_2) \quad 1.8$$

$$\Delta H_M = \Delta U_M - P \Delta V_M \quad 1.9$$

$$\Delta G_M = \Delta H_M - T \Delta S_M \quad 1.10$$

The abbreviation  $\bar{v}_i = v_i/V_i^*$  has been used in equations 1.6 to 1.10. The parameter  $P_i$  has the dimensions of pressure and is proportional to  $\eta_{ii}$ ; the quantities  $T_i^*$  have the dimensions of temperature and are defined as:

$$T_i^* = P_i^* v_i^* / k c_i \quad 1.11$$

Another important definition is that of  $\chi_{12}$ :

$$\chi_{12} = \frac{s_i}{2v_i^*} (\eta_{11} + \eta_{22} - 2\eta_{12}) \quad 1.12$$

The parameters,  $s_i$ , are given as the ratio surface/volume of the hard cores which are a measure of the compactness of a molecule.

Without discussing the derivation of the above equation, the following general statements can be made:

i) The energy of mixing  $\Delta U_M$ , given by equation 1.6, is the sum of two contributions. The first term, the

interaction-energy term with  $\chi_{12}$  contains the pair-interaction parameter,  $\eta$ , of the mixture multiplied by  $\phi_1\phi_2$ . This term causes  $\Delta U_M$  to have the typical, parabolic composition dependence which is in fact observed experimentally. The second term is the equation of state term accounting for the difference of the free volumes of the pure components and the mixture. The second contribution usually is small compared to the first and takes into account the changes of volume upon mixing and the corresponding effects of  $\Delta U_M$ .

ii) The entropy of mixing also contains several contributions. The first term with  $\ln\phi_i$  is the combinatorial entropy, which takes into account the number of distinguishable distributions of all molecules of the mixture within all cells, reduced by the corresponding number for the pure components. This combinatorial entropy was first derived by Flory<sup>27</sup> and later by Huggins<sup>28</sup>. The second contribution to  $\Delta S_M$  is the equation of state term which contains the logarithmic difference of the free volumes of the mixture and the pure components, and is usually small compared to the combinatorial contribution.

iii) The enthalpy of mixing  $\Delta H_M$  differs from  $\Delta U_M$  only by the additional term  $P\Delta V_M$  which is negligible at ambient pressures, but plays a major role at high pressures.

For practical application of these theoretical expressions to the mixing properties, it is important that all parameters of the pure components,  $V_i^*$ ,  $c_i$ ,  $v_i$ ,  $s_i$  and  $p_i^*$  be obtained by fitting the theoretical thermal equation

of state to experimental data of the pure components. The thermal expansion coefficient and compressibility are suitable for such a fitting procedure. Hence, the theoretical expressions for the mixing properties are defined for any particular mixture;  $\chi_{12}$  is the only adjustable parameter. This is one of the reasons for the success of the Flory theory, using only one adjustable parameter,  $\chi_{12}$ , a good representation of the mixing properties for a wide range of mixtures of chain molecules and polymer solutions has been obtained. Binary mixtures of long-chain n-alkanes with globular molecules such as 2,2-dimethylbutane or branched isomeric nonanes have been studied extensively<sup>29-31</sup> to test the Prigogine-Flory theory.

The thermodynamic properties of binary mixtures of hydrocarbons are extensively studied. These studies include the excess volumes<sup>32,33</sup>, excess enthalpy of mixing<sup>34</sup>, excess free energy of mixing<sup>30</sup>, excess chemical potential<sup>35,36</sup> and the phenomenon of lower critical miscibility<sup>37</sup>.

The ultrasonic relaxation studies of pure hydrocarbons and their binary mixtures are very limited. Early ultrasonic relaxation studies of the lower members of the alkane series at frequencies around 5 MHz failed to indicate any relaxation behaviour<sup>38</sup>. Later low temperature measurements exhibit relaxation behaviour showing that in normal alkanes processes associated with spatial rearrangements of the backbone can be observed<sup>39</sup>.

Analysis of the acoustic data as a single relaxation process was carried out and the process ascribed to the motion of single units of the alkane backbone. Studies of the analogous branched-chain molecules<sup>40,41</sup> indicate the presence of rotational isomers in these systems. A more recent study of n-alkanes, octane to tetradecane<sup>42</sup> over the frequency range 15-270 MHz and a temperature range of ambient to their melting points, has considerably clarified the description of the relaxation behaviour in the normal hydrocarbons.

In this thesis some aspects of thermodynamic and dynamic behaviour of branched-chain hydrocarbons, namely methylpentanes, methylhexanes and binary mixtures of dimethylpentanes with n-hexadecane will be reported.

### 1.3 Alcohols

Aliphatic alcohols in their pure state exist in a variety of cyclic and linear associated forms<sup>43</sup>, the precise detail of the distribution between possible structures being a function of the stereochemistry of the alkane chain. Chemical structure has two effects:- first it can sterically inhibit the formation of hydrogen bonds between pairs or groups of molecules and, secondly, it can influence the internal rotation of the chain to which the hydroxyl group is attached.

Pure alcohols have been studied extensively by ultrasonic relaxation<sup>44-48</sup>, dielectric relaxation<sup>49-51</sup>, <sup>1</sup>H and <sup>13</sup>C nmr relaxation<sup>52-54</sup> and infra-red<sup>55</sup>. The aim of these measurements is usually twofold: firstly to

determine the nature of the hydrogen bonding structure and secondly, to quantify the dynamic changes which occur.

Aqueous solutions of alcohols exhibit abnormalities in their properties such as viscosity-composition maxima and have been studied extensively using thermodynamic measurements, i.r. and Raman spectroscopic and ultrasonic relaxation studies<sup>56-62</sup>. Recently,<sup>61</sup> ultrasonic relaxation studies have shown that the ultrasonic absorption-composition maxima depends strongly on the structure of the alcohol. The composition at which the absorption exhibits a maximum is called the PSAC (Peak Sound Absorption Composition). Andreae et al<sup>62</sup> have compiled a list of PSAC values for a number of binary mixtures. In general, it is observed that the behaviour of an aqueous mixture is very different from that observed when the same cosolvent is mixed with other polar compounds. However, not all binary aqueous mixtures show an intense absorption maximum. It appears that only those with a high degree of hydrophilic character show this behaviour.

The above acoustic observations in aqueous solutions of alcohols have been discussed in the following way:

i) Solute molecules can lead to an enhancement of the water structure with the effect that it resembles the structure observed at lower temperatures. This type of model explains the observations that the partial molar volume decreases with increase in solute concentration. The alcohol molecule therefore appears to be accommodated in voids in the lattice.

ii) Enhancement of water structure around a hydrophobic solute contributes a negative contribution to the entropy of the solution and thus a positive contribution to the free energy. In real solutions, this unfavourable entropy change can be minimised if the hydrophilic parts of different molecules come together and so minimise their contact with water.

Aqueous solutions of alcohols have been studied systematically over many years with the aim of obtaining information on solute-solvent and solute-solute interactions through thermodynamic properties<sup>56</sup>. These interactions are particularly interesting in view of the high degree of structure in aqueous solutions, both in the solvent itself and in the aggregates that can exist as a result of the structure of water. The thermodynamic excess functions of alcohol mixtures<sup>63-66</sup> and alcohol + n-alkane mixtures<sup>67-69</sup> are extensively studied.

Recently Emery et al<sup>45,46</sup> studied the relaxation behaviour of isomeric octanols. The observed dispersion in less hindered octanols is attributed to hydrogen bond exchange processes associated with structural relaxation of the liquid. In the highly hindered octanols, an additional contribution is associated with internal rotational relaxation processes.

One part of this thesis is concerned with studies of binary mixtures of isomeric octanols with n-octane. These systems have been studied extensively by Emery et al<sup>45,46</sup>.

#### 1.4 Morpholine Derivatives

In recent years, the petroleum industry has given much attention to morpholine derivatives<sup>70,71</sup> such as N-hydroxyethylmorpholine, N-dimethylmorpholine, N-formylmorpholine, N-acetylmorpholine and N-phenylmorpholine. This interest has resulted from their high selectivity and solvent power for low molecular monocyclic aromatic hydrocarbons (C<sub>6</sub>-C<sub>9</sub>).

Among these derivatives, N-formylmorpholine<sup>71</sup> is of particular interest in view of its suitability as an extractive agent in the recovery of aromatics by distillation. Moreover, it is chemically and thermally stable and non-corrosive.

N-formylmorpholine, while possessing good selectivity, also offers sufficient solvency for non-aromatics. The solubility of non-aromatics is reduced by adding 2-5 per cent by weight of water<sup>71</sup>. This small amount of water is sufficient to bring about an optimum efficiency in the N-formylmorpholine process for liquid-liquid extraction. The maintenance of the proper water volume is important; too much water would reduce the solubility of the aromatics, too little would reduce selectivity. As the individual process stages require different qualities, a change in the amount of water added permits the solvent to adapt to different requirements.

The selectivity of an extractive agent is defined as the following:

$$S = \gamma_i / \gamma_j \quad 1.12$$

where  $\gamma$  is the activity coefficient,  $i$  refers to an aromatic compound and  $j$  refers to a paraffinic compound. The selectivity and solvent power of N-formylmorpholine have been studied extensively<sup>71,73,74</sup>. However, the thermodynamic and ultrasonic properties of N-formylmorpholine and its aqueous solutions have not as yet been reported.

In this thesis, N-formylmorpholine and its aqueous solutions are reported. The aim of this study is to understand the dynamic behaviour of N-formylmorpholine and its aqueous solutions and to gain information about its efficiency in recovery of aromatic hydrocarbons from petroleum products.

## CHAPTER 2

### MOLECULAR ACOUSTICS AND THERMODYNAMIC FUNCTIONS

CHAPTER 2  
MOLECULAR ACOUSTICS AND THERMODYNAMIC  
FUNCTIONS

2.1 Introduction to Acoustics

Experimentally, sound waves can be produced in the frequency range of a few cycles to over 1.0 GHz. The acoustic spectrum can be divided into four ranges<sup>75</sup>: the infra-audible ( $10^{-2}$  to 10 Hz), the audible (10 Hz to 14 KHz), the ultrasonic (14 KHz to 800 MHz) and the hypersonic ( $\geq 10^9$  Hz).

Sound waves are propagated in a liquid as longitudinal waves. A longitudinal wave may be considered as being the superposition of a pure compressional and a pure shear wave<sup>76</sup>. This is illustrated in Figure 2.1. A compressional wave may be considered as creating an alternating periodic pressure variation which results in a given volume being successively compressed and decompressed. Since the period of pressure fluctuation is short compared with the time required for thermal equilibration with the surroundings, the process is essentially adiabatic<sup>77</sup> and can be therefore visualised correctly as a sinusoidal temperature wave. However, the adiabatic approximation fails at very high frequencies (above  $10^9$  Hz) because the mean free path becomes comparable with the wavelength of the sound wave, so that enough energy can be exchanged by direct transfer of molecular momentum (heat conduction) to simulate isothermal propagation<sup>77</sup>. Equilibria

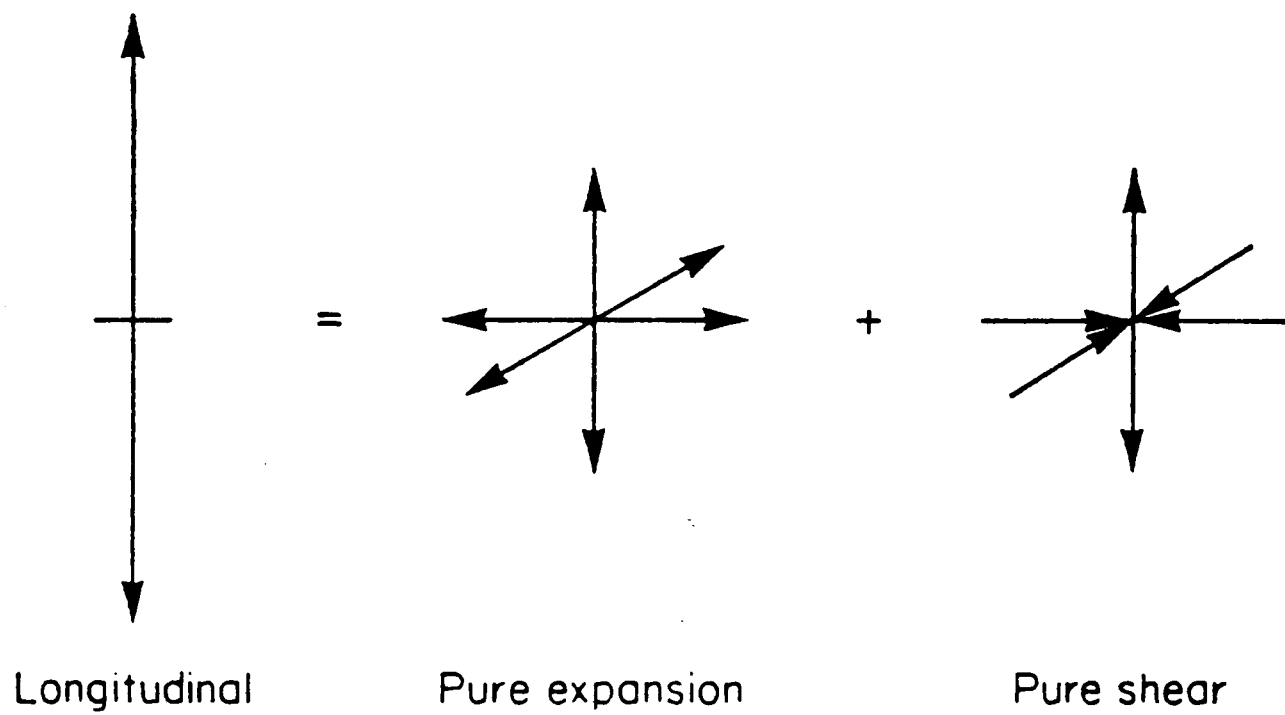


Figure 2.1. A longitudinal wave resolved into pure compression and pure shear.

sensitive to temperature or pressure variation can therefore be studied using longitudinal waves.

When a medium is subjected to shear perturbation the medium does not experience a volume or temperature change. The medium responds to the shear wave perturbation by viscous flow in the case of a liquid.

## 2.2 Sound Propagation and Absorption in Liquids

In the studies of molecular acoustics, plane waves of low amplitude are generally used. In an isotropic homogeneous medium, the pressure amplitude,  $P$ , of a one-dimensional sound wave travelling in the positive  $x$ -direction, is given by<sup>78</sup>

$$P = P_0 \exp(-\alpha x) \exp[i\omega (t - \frac{x}{c})] \quad 2.1$$

where  $P_0$  is the pressure amplitude at  $x = 0$  and time  $t = 0$ ,  $\alpha$  is the absorption coefficient related to the attenuation of the sound wave,  $c$  is the phase velocity and  $\omega = 2\pi f$  where  $f$  is the frequency of the sound wave. In equation 2.1 the quantity  $P_0 \exp(-\alpha x)$  represents the amplitude of the sound wave at a distance  $x$  from the source. The real part of equation 2.1 can be seen to be analogous to the Beer-Lambert Law governing light absorption. The imaginary part of equation 2.1 represents the particle velocity or density variation.

The total absorption coefficient,  $\alpha$ , is made up of three main components as expressed in equation 2.2

$$\alpha_t = \alpha_s + \alpha_v + \alpha_{th} \quad 2.2$$

where

$\alpha_s$  = the attenuation contribution arising from shear viscosity,  $\eta_s$

$\alpha_v$  = the attenuation contribution arising from volume viscosity,  $\eta_v$

$\alpha_{th}$  = the attenuation contribution arising from thermal conductivity,  $Q$ .

These contributions are assumed to be additive and can be discussed separately.

(i)  $\alpha_s$  - shear viscosity contribution

Calculation of the shear viscosity contribution to the total absorption attenuation,  $\alpha$ , based on the Stokes-Navier equation and its use in the description of ultrasonic propagation has been reviewed by Herzfeld and Litovitz<sup>76</sup>. The contribution arising from shear viscosity is:-

$$\alpha_s = \frac{2\pi^2}{\rho c^3} \cdot \frac{4}{3} \eta_s f^2 \quad 2.3$$

where  $\rho$  and  $c$  are the density and sound velocity of the liquid respectively.

(ii)  $\alpha_v$  - volume viscosity contribution

Truesdell<sup>79</sup> has shown that the concept of 'volume' viscosity can be accommodated within hydrodynamic theory and leads to an expression for the absorption coefficient of the sound wave of the form:

$$\alpha_v = \left( \frac{2\pi^2}{\rho c^3} \right) \eta_v f^2 \quad 2.4$$

(iii)  $\alpha_{th}$  - thermal conduction contribution

The thermal conduction contribution due to thermal conduction,  $Q$ , and the relationship obtained by Kirchoff<sup>80</sup> is:-

$$\alpha_{th} = \left(\frac{2\pi^2}{\rho C^3}\right) \left\{ \left(\frac{\gamma-1}{C_p}\right) Q f^2 \right\} \quad 2.5$$

where  $\gamma$  is the ratio  $C_p/C_v$ ,  $C_p$  is the specific heat per unit mass at constant pressure and  $C_v$  the specific heat per unit mass at constant volume.

It is normal to term the combined effects of viscosity and thermal conductivity as the 'classical' absorption. The classical absorption can thus be given in the form:

$$\left(\frac{\alpha}{f^2}\right)_{\text{classical}} = \left(\frac{2\pi^2}{\rho C^3}\right) \left\{ \underbrace{\left(\eta_v + \frac{4}{3} \eta_s\right)}_{\text{viscous}} + \underbrace{\frac{(\gamma-1)Q}{C_p}}_{\text{thermal}} \right\} \quad 2.6$$

The classical absorption is important in the analysis of results from measurements of acoustic absorption. For a given liquid at a stated pressure and temperature it is a constant value and usually is denoted by B.

The difference between the measured absorption coefficient  $\left(\frac{\alpha}{f^2}\right)$  and the classical absorption coefficient represents all absorptions in excess of that due to the additive effects of shear viscosity, volume viscosity and thermal conductivity and is usually referred to as the 'excess' absorption:

$$\left(\frac{\alpha}{f^2}\right)_{\text{exc.}} = \left(\frac{\alpha}{f^2}\right)_{\text{obs.}} - \left(\frac{\alpha}{f^2}\right)_{\text{class.}} \quad 2.7$$

### 2.3 Ultrasonic Relaxation

In order to explain the principles involved in ultrasonic relaxation, Litovitz<sup>81</sup> has described the energy content of a liquid in terms of the energy boxes shown diagrammatically in Figure 2.2. In brief, the total energy content of the liquid is the sum of many components, including translational, rotational, and vibrational components and the less familiar contributions from the existence of conformational and structural equilibria.

When a sound wave is passed through a liquid, the periodic compression and decompression accompanying the propagation of the pressure wave will produce a corresponding alternation in the temperature and hence energy content of the translational box. Since the energies of all the boxes are coupled, an increase in the translational energy content will lead to energy being transferred to all other modes until a new equilibrium is reached<sup>82</sup>.

The behaviour of the acoustic parameter during a single relaxation process is shown in Figure 2.3. At any given temperature the absorption coefficient ( $\alpha/f^2$ ) will decrease with increasing frequency,  $f$ , in accordance<sup>76,83</sup> with equation 2.8 and the derivation of this equation has been described adequately elsewhere<sup>76-78</sup>.

$$\left(\frac{\alpha}{f^2}\right) = \frac{A}{1 + (f/f_c)^2} + B \quad 2.8$$

where  $A$  is a relaxation parameter,  $f_c$  is the relaxation frequency ( $1/2\pi\tau$ ) and  $B$  represents contributions to ( $\alpha/f^2$ )

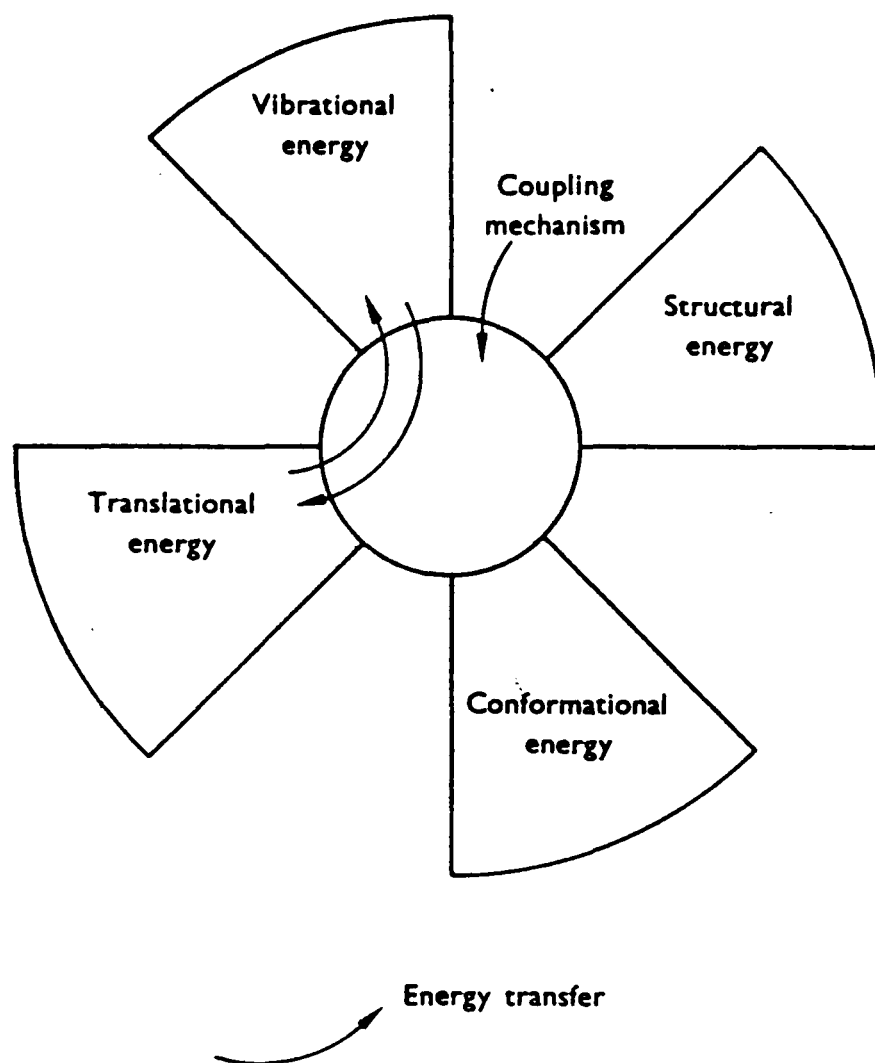


Figure 2.2. Simplified diagram of the energy box.

which are not related to the relaxation (equation 2.6). These contributions are shear viscosity and any excess absorption due to a relaxation process with a relaxation frequency much higher than  $f_c$ . The loss per cycle or absorption per unit wavelength,  $\mu$ , relating to the relaxation is

$$\mu = \alpha' \lambda \quad 2.9$$

where  $\alpha'$  is the excess absorption for the relaxation process. Thus

$$\begin{aligned} \mu &= (\alpha - Bf^2)\lambda \\ &= \frac{Acf}{1 + (f/f_c)^2} \end{aligned} \quad 2.10$$

where  $f = f_c$  ( $\omega\tau=1$ ),  $\mu$  reaches a maximum value  $\mu_{\max}$  given by equation 2.11.

$$\mu_{\max} = \frac{1}{2} Acf_c \quad 2.11$$

The dispersion in the sound velocity,  $c$ , is given by the expression:

$$c^2 - c_o^2 = \left( \frac{2\mu_{\max}}{\pi} \right) c_o c_\infty \frac{(\omega\tau)^2}{1+(\omega\tau)^2}$$

where the subscripts  $o$  and  $\infty$  refer to the sound velocity at low and high frequencies. Typical variation of the acoustic parameters for a single relaxation process can be seen in Figure 2.3.

Provided that the relaxation can be described by a single relaxation time, then only two parameters,  $\mu_{\max}$  and  $f_c$  (or  $\tau$ ), are involved in a complete specification of the behaviour within the region of relaxation. The

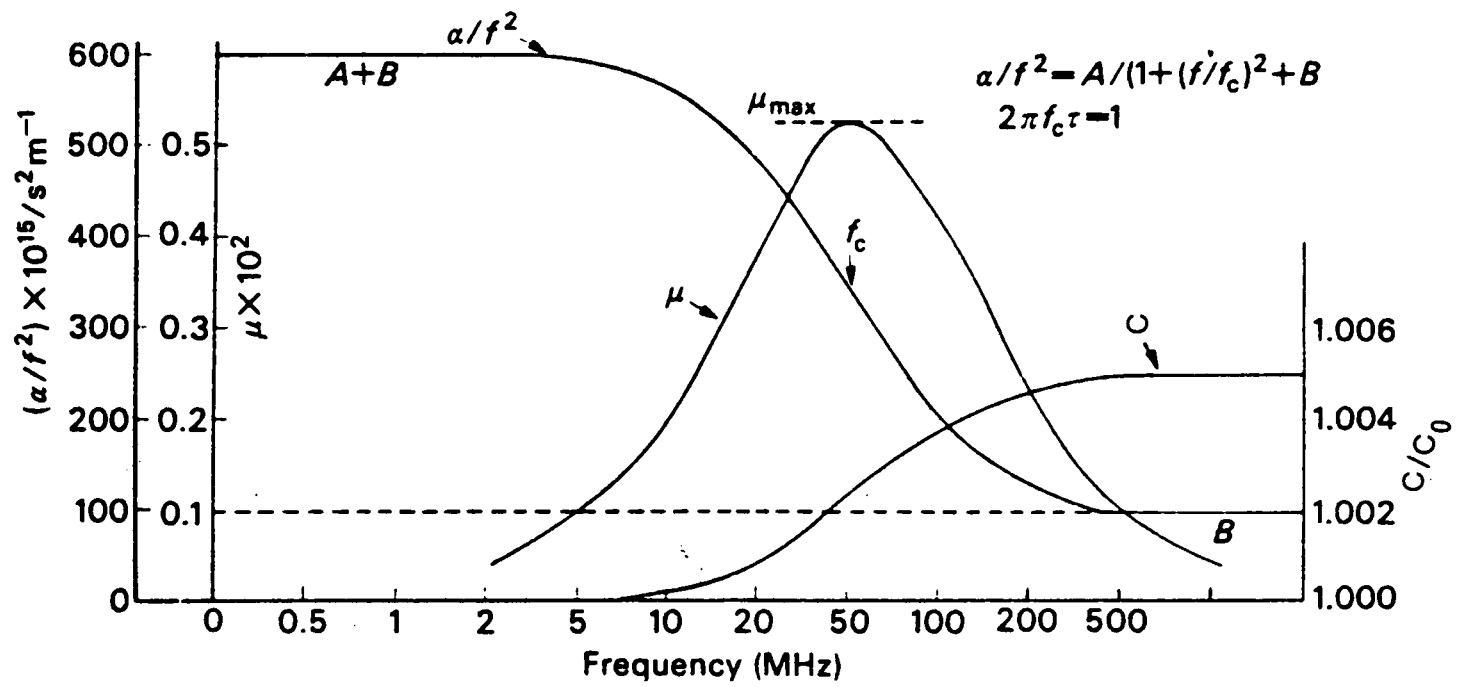


Figure 2.3. Variation of typical ultrasonic parameters with frequency for a single-relaxation process.

objective of ultrasonic experiments is to be able to derive these two parameters from experimental results so that further analysis can be carried out. Moreover, it is desired to determine the dependence of  $\mu_{\max}$  and  $f_c$  on temperature and pressure in order to make possible a complete interpretation of the relaxation process. There is a fundamental difference in principle between these two parameters;  $\mu_{\max}$  is given in terms of thermodynamic quantities while  $f_c$  is determined by kinetic considerations.

#### 2.4 Evaluation of Energy Parameters

A unimolecular equilibrium of the type  $A \xrightleftharpoons[k_{21}]{k_{12}} B$  can be represented by the Gibbs free energy diagram of Figure 2.4. The various kinetic and thermodynamic parameters of the system can be determined through ultrasonic studies and the method of evaluation is outlined below.

##### (i) Kinetic

The derivation of the kinetic parameters are based on three important assumptions:-

- (a) A unimolecular reaction is considered.
- (b) All reactions take place in an ideal solution.
- (c) The backward rate is faster than that of the forward reaction.

The relaxation frequency,  $f_c$  of the first-order reaction is given by:

$$f_c = \frac{1}{2\pi} \tau = (k_{12} + k_{21})/2\pi \quad 2.13$$

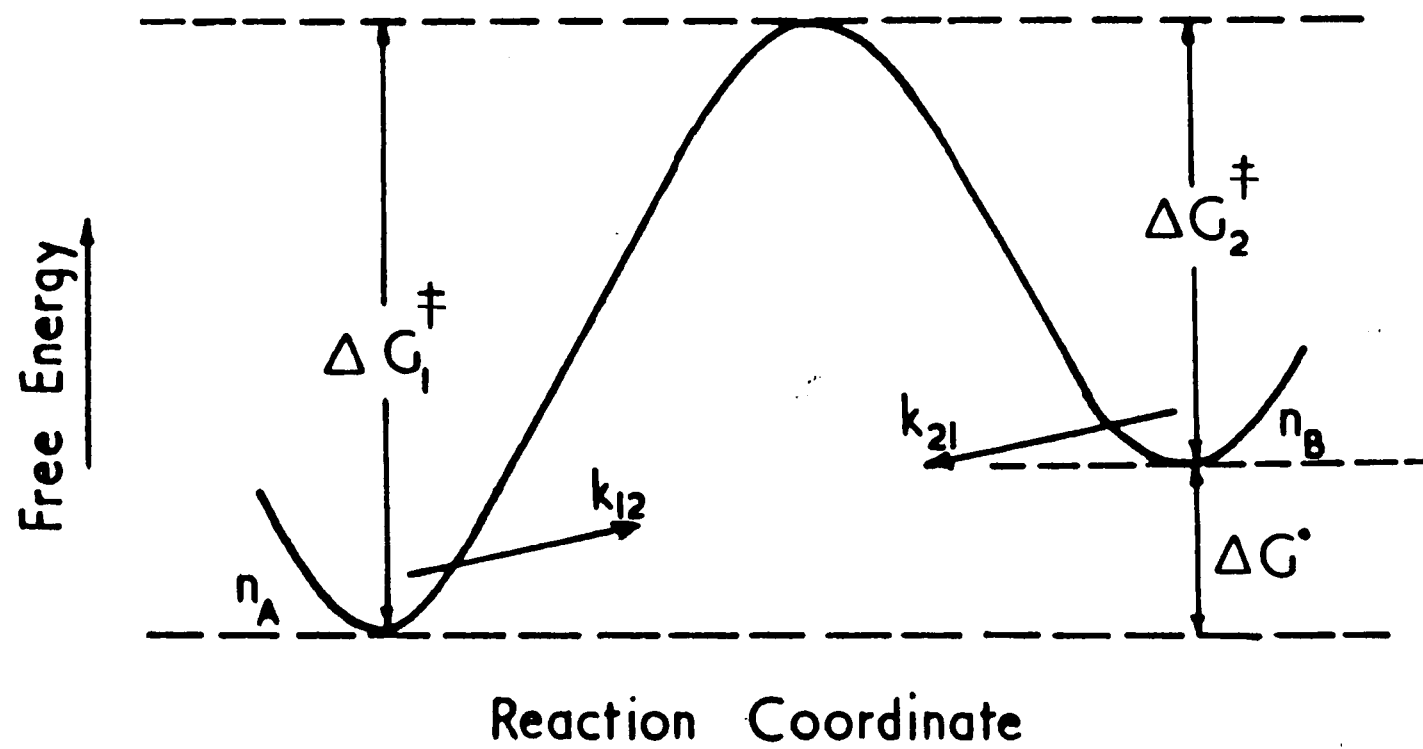


Figure 2.4. Energy profile for a two-state equilibrium.

where  $\tau$  is the relaxation time of the equilibrium,  $k_{12}$  is the forward rate constant and  $k_{21}$  is the backward rate constant. The theory of rate processes<sup>84</sup> expresses the rate constant  $k_{21}$  of a reaction in terms of the increase in free energy  $\Delta G^\ddagger$  on moving from the initial state to an intermediate activated state.

$$k_{21} = (kT/h) \exp\left(\frac{-\Delta G^\ddagger}{RT}\right) \quad 2.14$$

Hence

$$f_c = \left(\frac{1}{2\pi}\right) (kT/h) \left\{ \exp\left(\frac{-\Delta G_1^\ddagger}{RT}\right) + \exp\left(\frac{-\Delta G_2^\ddagger}{RT}\right) \right\} \quad 2.15$$

where  $\Delta G_1^\ddagger$  and  $\Delta G_2^\ddagger$  are the activation free energies of the forward and backward reactions and  $k$  and  $h$  are the Boltzmann and Planck constants. The theoretical analysis of ultrasonic relaxation and the evaluation of the energy parameters associated with the equilibrium has been described adequately elsewhere<sup>85,86</sup>. If conditions are such that  $\Delta G_2^\ddagger \ll \Delta G_1^\ddagger$ , then  $k_{12}$  would be neglected in comparison with  $k_{21}$ . In such a case

$$f_c = \frac{1}{2\pi} \left[\frac{kT}{h}\right] \left[ \exp\left(\frac{\Delta S_2^\ddagger}{R}\right) \exp\left(\frac{-\Delta H_2^\ddagger}{RT}\right) \right] \quad 2.16$$

since

$$\Delta G = \Delta H - T\Delta S$$

where  $\Delta S_2^\ddagger$  and  $\Delta H_2^\ddagger$  are the activation entropy and energy of the backward reaction respectively. An increase of the potential barrier,  $\Delta G_2^\ddagger$ , will result in a decrease of the characteristic frequency,  $f_c$ . Experimentally,  $f_c$  is obtained over as wide a range of temperatures as possible

and  $\Delta H_2^\ddagger$  can be obtained from the slope of the plot of  $\log f_c$  against  $1/T$  following which  $\Delta S_2^\ddagger$  can be calculated by insertion in equation 2.16.

(ii) Thermodynamic

The energy difference between the two assumed equilibrium states can be evaluated from the ultrasonic data if it is assumed that no change in volume occurs when the molecule passes from one state to another. It has been shown by Heasell and Lamb<sup>85</sup>

$$2\mu_{\max}/\pi = (\gamma-1)\Delta C_p/(C_p - \Delta C_p) [1 - \Delta V^\ominus C_p/V^\ominus \Delta H^\ominus \sigma]^2 \quad 2.17$$

$$\Delta C_p = R \left( \frac{\Delta H^\ominus}{RT} \right)^2 \left\{ \exp\left( \frac{-\Delta G^\ominus}{RT} \right) / \left( 1 + \exp\left( \frac{-\Delta G^\ominus}{RT} \right) \right)^2 \right\} \quad 2.18$$

where  $\mu_m$  is the acoustic loss at the characteristic frequency,  $C_p$  and  $\Delta C_p$  are the specific heat at constant pressure and the relaxing specific heat respectively,  $\Delta H^\ominus$ ,  $\Delta V^\ominus$ ,  $\Delta G^\ominus$  and  $\Delta S^\ominus$  are the standard state enthalpy, volume, free energy and entropy differences respectively associated with the equilibrium,  $\sigma$  is the expansion coefficient and

$$(\gamma-1) = c^2 \sigma^2 T/JC_p \quad 2.19$$

where  $c$  is the sound velocity of the ultrasonic wave at temperature  $T^\circ\text{K}$  and  $J$ , the mechanical equivalent of heat. The detailed derivation of the above relationships and discussion of the associated approximations are presented elsewhere<sup>82</sup>.

Very often there is no experimental information available over a range of pressures and it has to be

assumed that  $C_p \Delta V^\ominus \ll \Delta H^\ominus V^\ominus \sigma$  and that  $\Delta V^\ominus / V^\ominus$  is small.

Then combination of equations 2.17 and 2.18 gives

$$\mu_{\max} = \frac{\pi(\gamma-1)R}{2C_p} \left(\frac{\Delta H^\ominus}{RT}\right)^2 \left\{ \frac{\exp(-\Delta G^\ominus/RT)}{[1 + \exp(-\Delta G^\ominus/RT)]^2} \right\} \quad 2.20$$

Another assumption is made  $\Delta G^\ominus > 3RT$  to yield unique solutions for  $\Delta H^\ominus$  and  $\Delta G^\ominus$ , then equation 2.20 can be simplified to yield

$$\mu_{\max} = \frac{\pi(\gamma-1)}{2C_p} \left(\frac{\Delta H^\ominus}{RT}\right)^2 \left\{ \exp(-\Delta H^\ominus/RT) \exp(\Delta S^\ominus/R) \right\} \quad 2.21$$

By substituting equation 2.19 into 2.21

$$\mu_{\max} = \left[ \frac{\pi\sigma^2}{2JRC_p} (\Delta H^\ominus)^2 \exp\left(\frac{\Delta S^\ominus}{R}\right) \right] \frac{c^2}{T} \exp\left(-\frac{\Delta H^\ominus}{RT}\right) \quad 2.22$$

Making a further assumption<sup>87</sup> that the expansion coefficient and the specific heat of the liquid remain fairly constant over the temperature range under consideration

$$\mu_{\max} = \text{constant} \times \frac{c^2}{T} \exp\left(-\frac{\Delta H^\ominus}{RT}\right) \quad 2.23$$

A plot of  $\log(T\mu_m/c^2)$  against  $\frac{1}{T}$  is thus linear and its slope gives  $\Delta H^\ominus/R$  and hence  $\Delta H^\ominus$ , the energy difference between the two isomeric forms of the molecule.

This procedure is inaccurate when  $\Delta G^\ominus < 3RT$  and an alternative assumption is then required about the magnitude of  $\Delta S^\ominus$ . If  $\Delta S^\ominus = 0$ ,

$$\Delta C_p = R \left[ \frac{\Delta H^\ominus}{RT} \right]^2 \frac{\exp(-\Delta H^\ominus/RT)}{[1 + \exp(-\Delta H^\ominus/RT)]^2} \quad 2.24$$

and

$$\mu_{\max} = \frac{\pi(\gamma-1)R}{2C_p} \cdot \frac{(\Delta H^\ominus)^2}{RT} \cdot \frac{\exp(-\Delta H^\ominus/RT)}{[1+\exp(-\Delta H^\ominus/RT)]^2} \quad 2.25$$

$\Delta H^\ominus$  can be evaluated here from a series of values of  $\mu_{\max}$  by an iterative process. The variation of  $\Delta C_p$  with  $\Delta H^\ominus/RT$  (the Schottky function) is shown in Figure 2.5. It may be noted that the maximum, whilst being a function of  $\Delta S^\ominus$ , is located at approximately  $\Delta H^\ominus \simeq 2.4 RT$ . Information about the equilibrium thermodynamic parameter  $\Delta H^\ominus$  can now be obtained by comparing the experimental variation of  $(\mu_{\max}/Tc^2)^{1/2}$  with the curves shown in Figure 2.5. Three cases can be distinguished:

- (a) If  $(\mu_{\max}/Tc^2)^{1/2}$  increased with increasing temperature, then it is evident from Figure 2.5 that  $\Delta H^\ominus > (2.3-3.2) RT$ , and thus it is safe to assume that  $\Delta G^\ominus$  is so large that the term  $\exp(-\Delta G^\ominus/RT)$  is small compared with unity. In this case an approximate value of  $(\Delta H^\ominus/R)$  can be obtained from the slope of the plot  $\log(T\mu_{\max}/c^2)$  against  $\frac{1}{T}$ .
- (b) If the plot of  $(\mu_m/Tc^2)^{1/2}$  against temperature reaches a maximum, then it is evident that  $\Delta H^\ominus = (2.3-3.2) RT$  where  $T$  is the temperature at the maximum. The exact value of  $\Delta H^\ominus$  can be determined if  $\Delta S^\ominus$  is known.
- (c) If  $(\mu_m/Tc^2)^{1/2}$  decreases with increasing temperature, then from Figure 2.5 it allows that

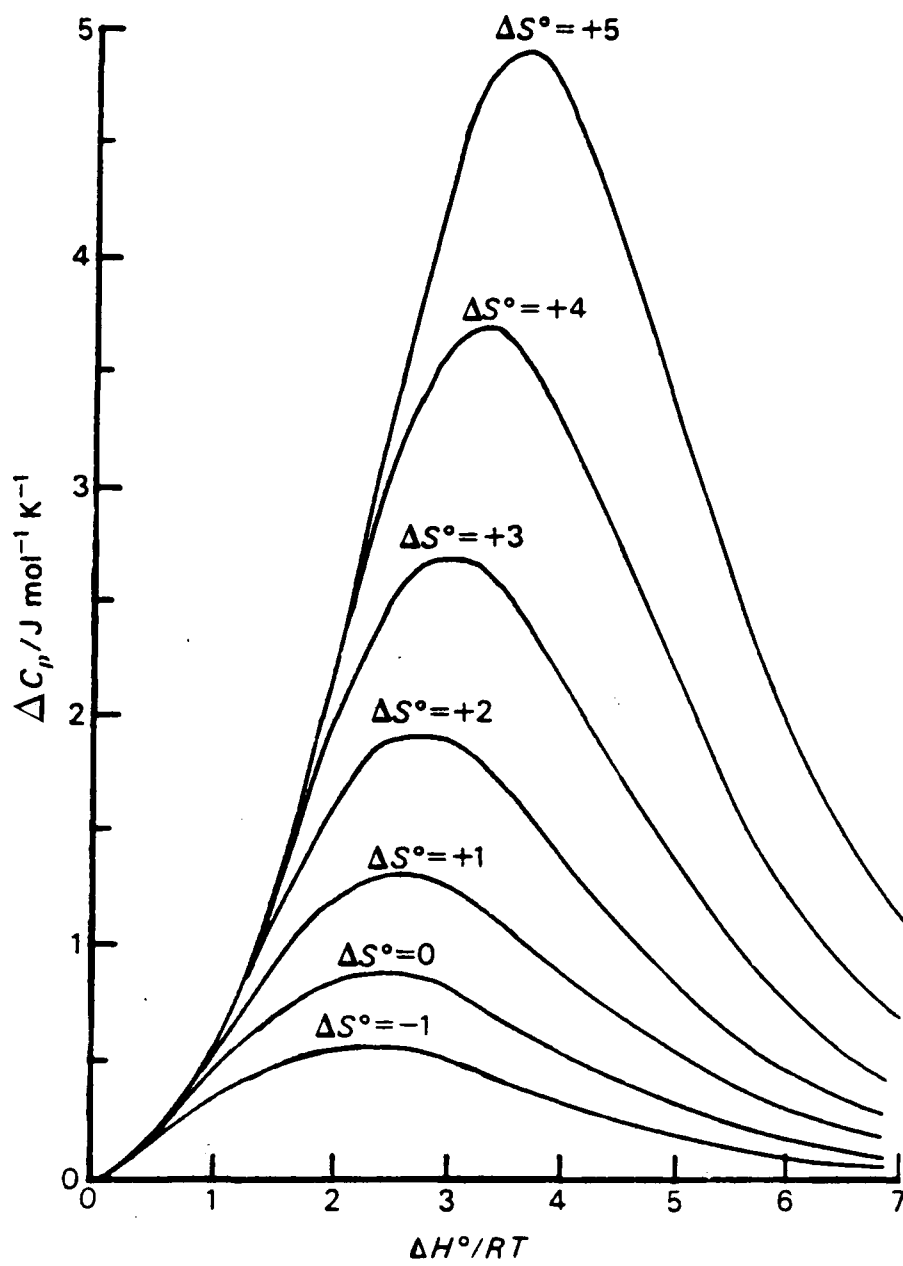


Figure 2.5. Variation of  $\Delta H^\circ / RT$  with  $\Delta C_p$ .

$\Delta H^\ominus < (2.3-3.2) RT$  where T corresponds to the lowest temperature measured experimentally.

## 2.5 Thermodynamic Functions of Binary Mixtures

### (i) Introduction

There are two principal reasons for the considerable amount of experimental and theoretical research which has been performed on the properties of liquid mixtures. The first is that it provides one way of studying the physical forces acting between molecules of different species. The second reason is the appearance of new phenomena which are not present in pure substances. The most interesting of these are new types of phase equilibrium which arise from the extra degrees of freedom introduced by the possibility of varying the proportions of the components. The number of degrees of freedom may be calculated from the phase rule of Gibbs. A system of one phase has two degrees of freedom, i.e. the two intensive properties, pressure and temperature, may both be changed without causing any new phase to appear. A two-component system of one phase has three degrees of freedom, for the composition may also be freely varied. A one-component system of two phases has one degree of freedom. If the temperature is fixed arbitrarily, then there is only one value of the pressure for which the two phases can exist together in equilibrium.

The basic thermodynamic relationships which are applicable to simple and binary liquid mixtures are derived adequately elsewhere<sup>88,89</sup>.

(ii) Ideal mixture

The ideal mixture is a hypothetical one whose properties are introduced into the thermodynamic description of real mixtures as convenient standards of normal behaviour.

There are several definitions of an ideal liquid mixture; one of the most convenient is that it is a mixture in which the chemical potentials of all components are given the equation

$$\mu_i(P, T, x) = \mu_i^{\circ}(P, T) + RT \ln x_i \quad 2.26$$

$$i = 1, 2, \dots$$

where  $\mu_i^{\circ}(P, T)$  is the potential of pure component,  $i$ , at the same pressure and temperature as the mixture being studied.

For an ideal mixture the molar functions of mixing are given by

$$\Delta_{\text{mix}} G_m^{\text{id}} = RT \{ (1-x) \ln(1-x) + x \ln x \} \quad 2.27$$

$$\Delta_{\text{mix}} S_m^{\text{id}} = -R \{ (1-x) \ln(1-x) + x \ln x \} \quad 2.28$$

$$\Delta_{\text{mix}} H_m^{\text{id}} = 0 \quad 2.29$$

$$\Delta_{\text{mix}} V_m^{\text{id}} = 0 \quad 2.30$$

For an ideal mixture the molar Gibbs function of mixing is negative and the molar entropy of mixing is positive for any value of  $x$ .

(iii) Molar mixing functions

The molar functions of mixing for a binary mixture  $[(1-x)A + xB]$ , where  $x$  denotes the mole fraction of B, are defined by

$$\Delta_{\text{mix}} X_m = X_m - (1-x)X_A^* - x X_B^* \quad 2.31$$

where  $X_m$  is the molar quantity of a binary mixture  $[(1-x)A + xB]$  at the temperature  $T$  and pressure  $P$  and where  $X_A^*$  and  $X_B^*$  are the molar quantities of the pure substances A and B at the same temperature and pressure.  $X$  denotes any extensive quantity such as  $G$ ,  $H$ ,  $S$ , or  $V$ .

(iv) Excess functions

The principal excess partial molar quantities can be written as the difference between the partial molar quantities for the non-ideal mixture and those of an ideal mixture.

It has become customary to use instead of the molar function of mixing,  $\Delta_{\text{mix}} X_m$ , the excess molar function,  $X_m^E$ , which is defined as follows:

$$X_m^E = \Delta_{\text{mix}} X_m - \Delta_{\text{mix}} X_m^{\text{id}} \quad 2.32$$

so that 'excess' means 'excess over ideal'.

For a binary mixture, the excess molar volume of mixing can be calculated from measurements of the density,  $\rho$ , of liquid mixtures by the following relation:

$$V_m^E = \left[ \frac{(1-x)M_A + xM_B}{\rho} \right] - \left[ \frac{(1-x)M_A}{\rho_A^*} + \frac{xM_B}{\rho_B^*} \right] \quad 2.33$$

where  $M_A$  and  $M_B$  are the molar masses of components A and B

and  $\rho$ ,  $\rho_A^*$  and  $\rho_B^*$  are respectively the densities of a mixture having mole fraction  $x$  of B, of pure A and B. To measure the excess volume in this case, it is necessary to measure the densities of pure liquids and the binary mixture with the highest possible accuracy in order to achieve even a modest accuracy in  $V_m^E$ . Direct dilatometer measurement of  $V_m^E$  gives the highest possible accuracy of determination of this quantity.

The excess isentropic compressibility,  $\kappa_s^E$ , for a binary mixture can be calculated from measurements of the density and sound velocity of liquid mixtures by the following equation

$$\kappa_s^E = \kappa_{s(\text{obs})} - [x_1 V_1 \kappa_{s(1)} + x_2 V_2 \kappa_{s(2)}] [x_1 V_1 + x_2 V_2]^{-1} \quad 2.34$$

where  $x_1$ ,  $x_2$ ,  $V_1$ ,  $V_2$ ,  $\kappa_{s(1)}$  and  $\kappa_{s(2)}$  are the mole fractions, molar volumes and isentropic compressibilities respectively of the pure components designated 1 and 2.  $\kappa_{s(\text{obs})}$  is the measured isentropic compressibility of the binary mixture. The isentropic compressibility of the pure components and binary mixtures were calculated using the Laplace relation

$$\kappa_s = (\rho c)^{-1} \quad 2.35$$

where  $\rho$  and  $c$  are the measured density and sound velocity of the medium respectively.

In the case of molar enthalpy of mixing  $H_m^E$  there is no alternative to direct measurements since  $H_m$  cannot be measured. Neither molar Gibbs function  $G_m$  nor molar

entropy  $S_m$  can be measured. Various techniques have been described adequately<sup>90-95</sup> for measurement of excess molar functions.

CHAPTER 3  
EXPERIMENTAL

## CHAPTER 3

### EXPERIMENTAL

#### 3.1 Generation and Detection of Ultrasonic Waves

Sound waves are generated or received by a device called a transducer; this converts energy from one form to another. The acoustic transducers are used to convert acoustical energy into electrical, mechanical, or thermal energy.

The most widely used transducers for the conversion of electrical energy to acoustical energy and vice versa are based on the piezoelectric effect<sup>96-98</sup>. A solid is said to be piezoelectric if electric charges are produced on its surface when it is subjected to a mechanical stress. Equal and opposite electric charges appear on the parallel surfaces. Provided that the solid is not strained beyond its elastic limit, the magnitude of the charge density or dielectric polarization is directly proportional to the applied stress. Piezoelectric substances also exhibit the converse piezoelectric effect: the substance changes in size when an electric field is applied to it, the sign of this change being reversed when the direction of the field is reversed. These effects were shown to exist in crystals which lack a centre of symmetry<sup>99</sup>.

One of the most widely used piezoelectric crystals is quartz on account of its chemical and mechanical stability. Quartz belongs to the trigonal crystallographic system, and a typical simplified section through part of a quartz

crystal is shown in Figure 3.1. The Z-optic axis runs along the crystal, the crystal section at right angles to the Z-axis being hexagonal in shape. The three axes joining opposite corners of this hexagon are known as the X-axes, while the three axes joining the opposite faces, perpendicular to the X-axes, are called Y-axes. X-cut crystals with faces normal to the X-axis are normally used in the generation and detection of ultrasonic longitudinal waves.

Consider an X-cut quartz crystal in the shape of a rectangular prism, as shown in Figure 3.1, is silvered on opposite faces and an alternating voltage of frequency  $f$  is applied across them. Electric field direction across the crystal will be compressed in the X direction and expanded in the normal Y direction. When the electric field is reversed, expansion will occur along the X-axis and interaction along the Y-axis. Thus the crystal dimensions will oscillate at the frequency  $f$ . These oscillations will be of small amplitude unless  $f$  coincides with one of the natural frequencies of mechanical vibration of the quartz disc.

The fundamental resonance frequency of a quartz disc is inversely proportional to its thickness. For an X-cut crystal of 2.8 mm thickness the fundamental resonance frequency is 1 MHz. For frequencies above 10 MHz, crystals vibrating in their fundamental mode become so thin and fragile that it is preferable to operate at a harmonic of a crystal with a lower fundamental resonance

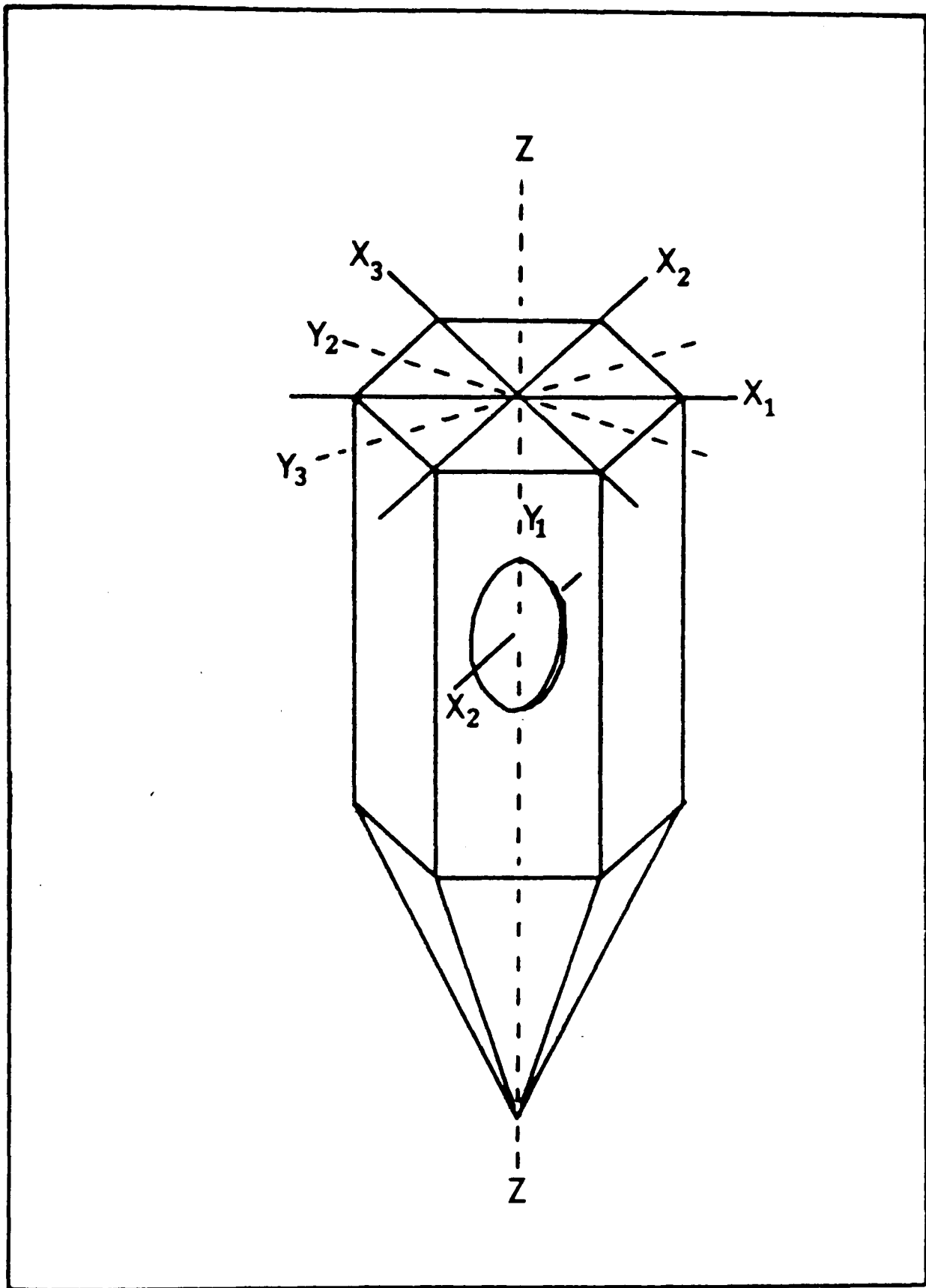


Figure 3.1. Simplified diagram of part of a quartz crystal, showing the X, Y and Z axes. The cylindrical disc represents an X-cut transducer.

frequency. Operation of quartz crystal transducers bonded to delay lines is limited to below 200MHz because of a significant loss in the piezoelectric efficiency of the crystal and attenuation due to losses in transducer-delay line bond above this frequency. These can be reduced, however, by using a crystalline delay rod made of Z-cut quartz activated by surface activation, a technique developed by Baranskii<sup>100</sup> and Lamb and Richter<sup>101</sup> for frequencies above 100MHz, but the transducer efficiency is still low.

Other types of transducers have been developed in order to overcome the difficulties encountered in the use of quartz crystals. These include the vapour-deposited, thin film, insulating, piezoelectric transducers such as Cdsm GaAS, ZnS, and ZnO<sup>102-109</sup>. Polycrystalline ceramic transducers<sup>110-113</sup> such as barium titanate, lead zirconate-titanate, lithium tantate and lithium niobate are now in common use to produce sound waves of high intensity and sensitivity or for operation at high frequency. Polyvinylidene fluoride (PVDF<sub>2</sub>) thin film transducers<sup>114-117</sup> are also being developed for wide band use.

### 3.2 General Review of Experimental Techniques

The various experimental techniques available for measurement of sound propagation has been extensively discussed<sup>78,118-128</sup>. A brief summary of the techniques available and an indication of their limitations are presented in Table 3.1.

### 3.3 Techniques of Specific Relevance to this Study

In this thesis all ultrasonic longitudinal investigations have been made using X-cut quartz and lithium

TABLE 3.1. Various experimental techniques available for measurement of sound propagation.

Technique	Frequency Range (MHz)	Volume required (ml)	Comments
Spherical reverberation technique	0.01 - 1	2000	Large quantities of liquid sample required. Absolute value of attenuation cannot be obtained.
Swept frequency acoustic resonator	0.1 - 10	2 - 10	Accurate determination of sound velocity and attenuation provided matching of reference liquid is carefully performed.
Low frequency pulse technique	5 - 100	5 - 20	Precise measurement of sound velocity and attenuation - precision 2%
High frequency pulse technique	100-2000	1 - 5	Precise measurement of attenuation - 2% using lithium niobate or zinc oxide transducers.
Acousto-optic techniques	5 - 1000	5 - 20	Precise measurements of sound velocity and attenuation, 3-5%.

niobate ( $\text{LiNbO}_3$ ) transducers. The frequency range available is nominally 1-1000 MHz and employs three techniques, namely a swept frequency acoustic resonator<sup>122</sup> from 1-10 MHz, the conventional pulse technique<sup>131</sup> from 15-75 MHz and ultra-high-frequency pulse technique<sup>127</sup> from 100-1000 MHz. Each of these is discussed below.

### 3.4 Swept Frequency Acoustic Resonator

#### (i) Principals of technique

This technique has been devised by Eggers<sup>121</sup> for studying liquids in the frequency range 200 KHz - 10 MHz. The major advantage of this technique is that only a small quantity of sample liquid is required - about 10 ml.

The resonator is shown in Figure 3.2 constructed from two X-cut quartz crystals with the liquid sample introduced between them. One crystal acts as the transmitter and the second as receiver with the liquid sample forming the coupling medium for the elastic displacements produced by the sound waves. The transmitting crystal is continuously excited and the resulting sound waves produced are propagated through the liquid sample and are partially reflected and detected by the receiver crystal and recorded as voltage against frequency on a display oscillograph. The ratio of the amount of energy transmitted to that reflected is determined by the relative magnitudes of the acoustic impedances of the two media involved. The observed electrical signal generated at the receiver crystal is the sum of all in-phase displacements generated by the time average of the transmitted

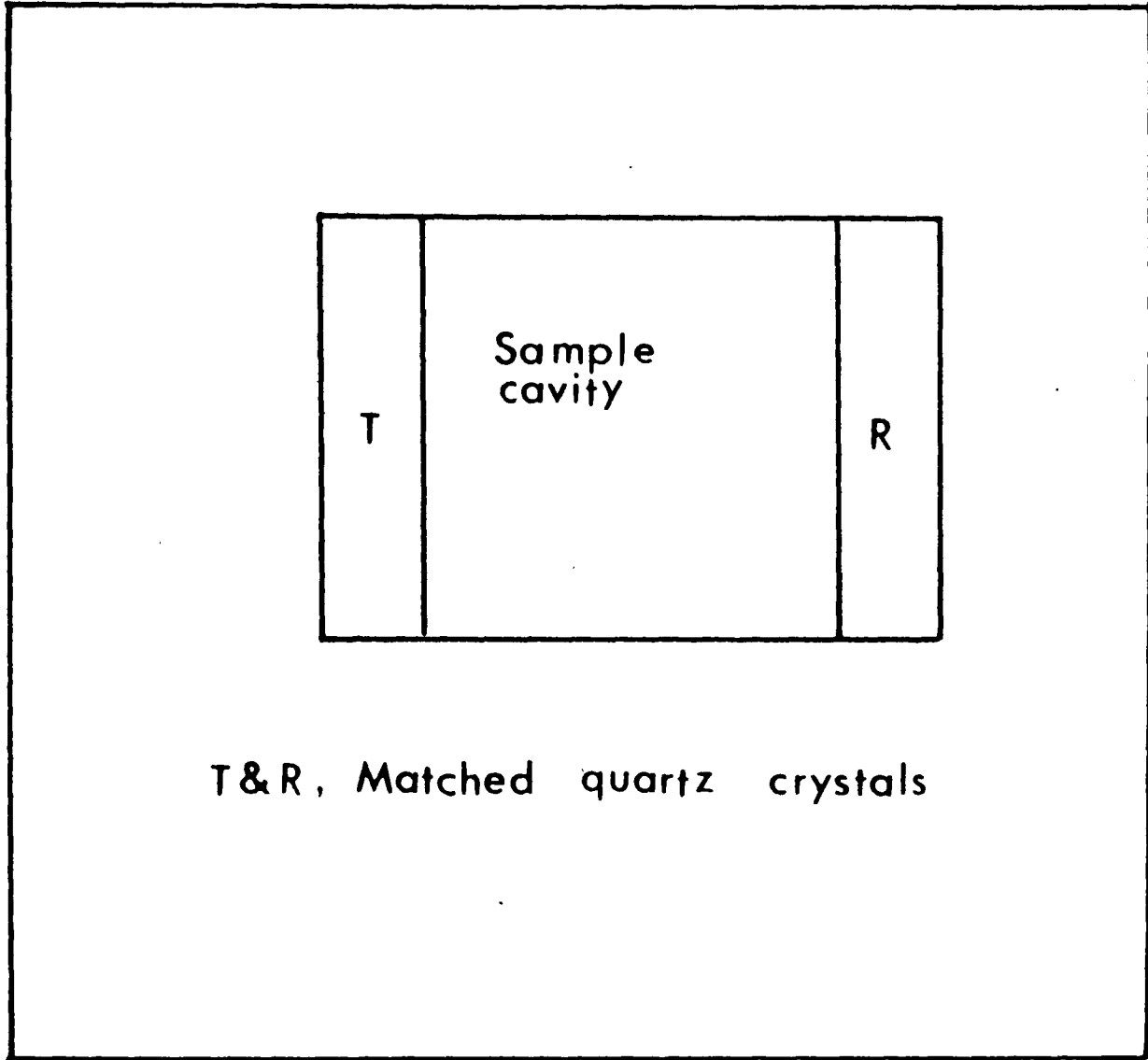


Figure 3.2. Simplified diagram of a cavity resonance cell.

waves.

(ii) Experimental system

A block diagram of the resonance apparatus is shown in Figure 3.3. The essential components of the acoustic cell are shown in Figure 3.4. It comprises two matched, 1 MHz, X-cut quartz crystals mounted on teflon rings. The cavity is completed by a teflon cylinder separating the two crystals. This material has a low acoustic reflectivity and so lowers the effect of diffraction and radial mode interference on plane wave propagation.

The two crystals' mountings are in thermal contact with a water jacket and their relative alignment is adjustable via high pitched micrometer screws. The electrical contacts to the crystals, which are gold plated on both flat faces, are through silver plated copper spirals. The highly mechanical compliance of these spirals minimise damping of the crystal resonances. The reverse faces of the crystals are earthed to the water jacket to complete the electrical circuit.

The liquid sample, typically 3 ml, is introduced into the cavity with the aid of a syringe through one of two holes drilled in the teflon waveguide. A Lauda thermostat unit, alcohol bath, and a cooling machine (Cryocool CC-80II) are incorporated in the cell system in order to maintain a constant temperature with a precision of  $\pm 0.01\text{K}$ .

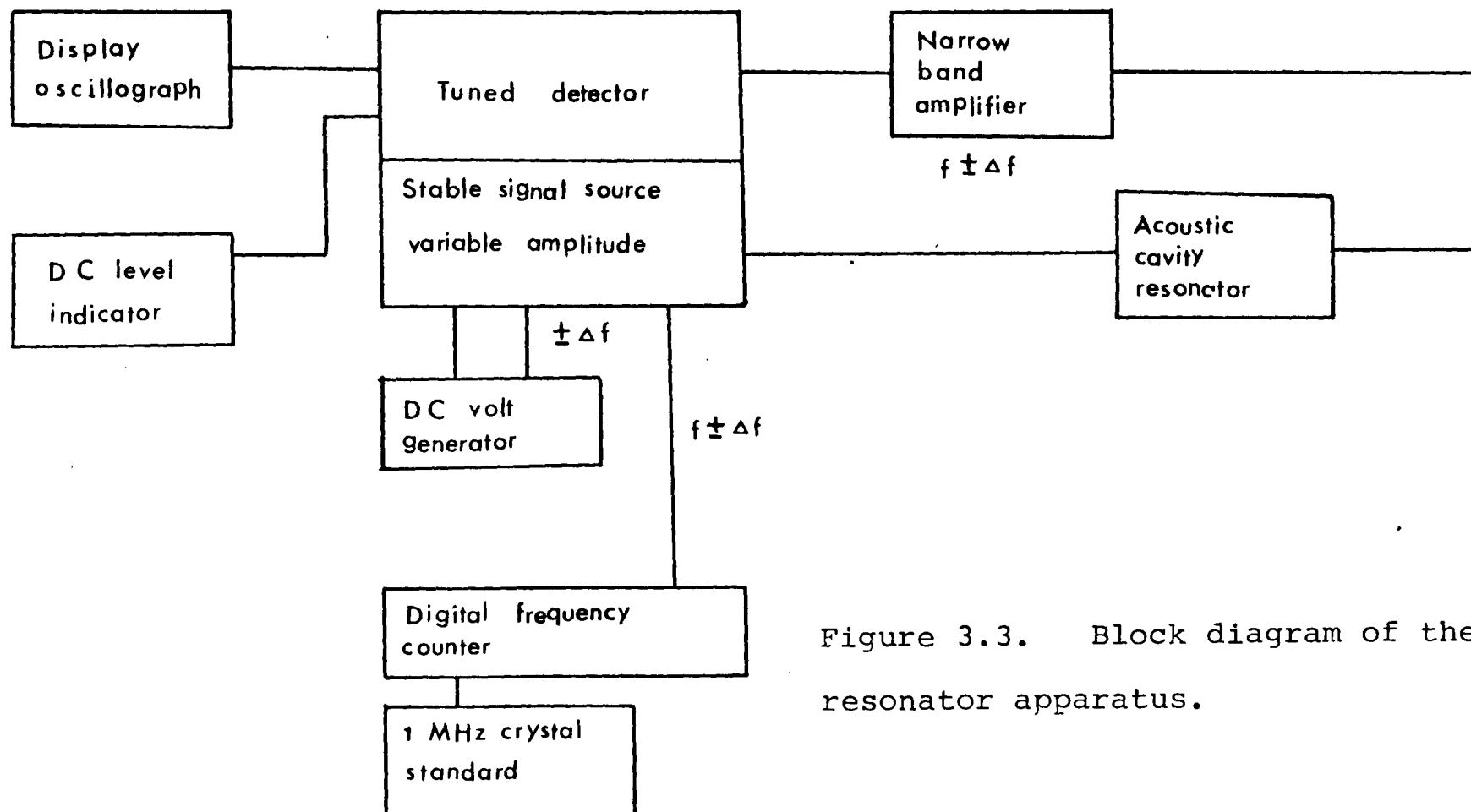


Figure 3.3. Block diagram of the acoustic resonator apparatus.

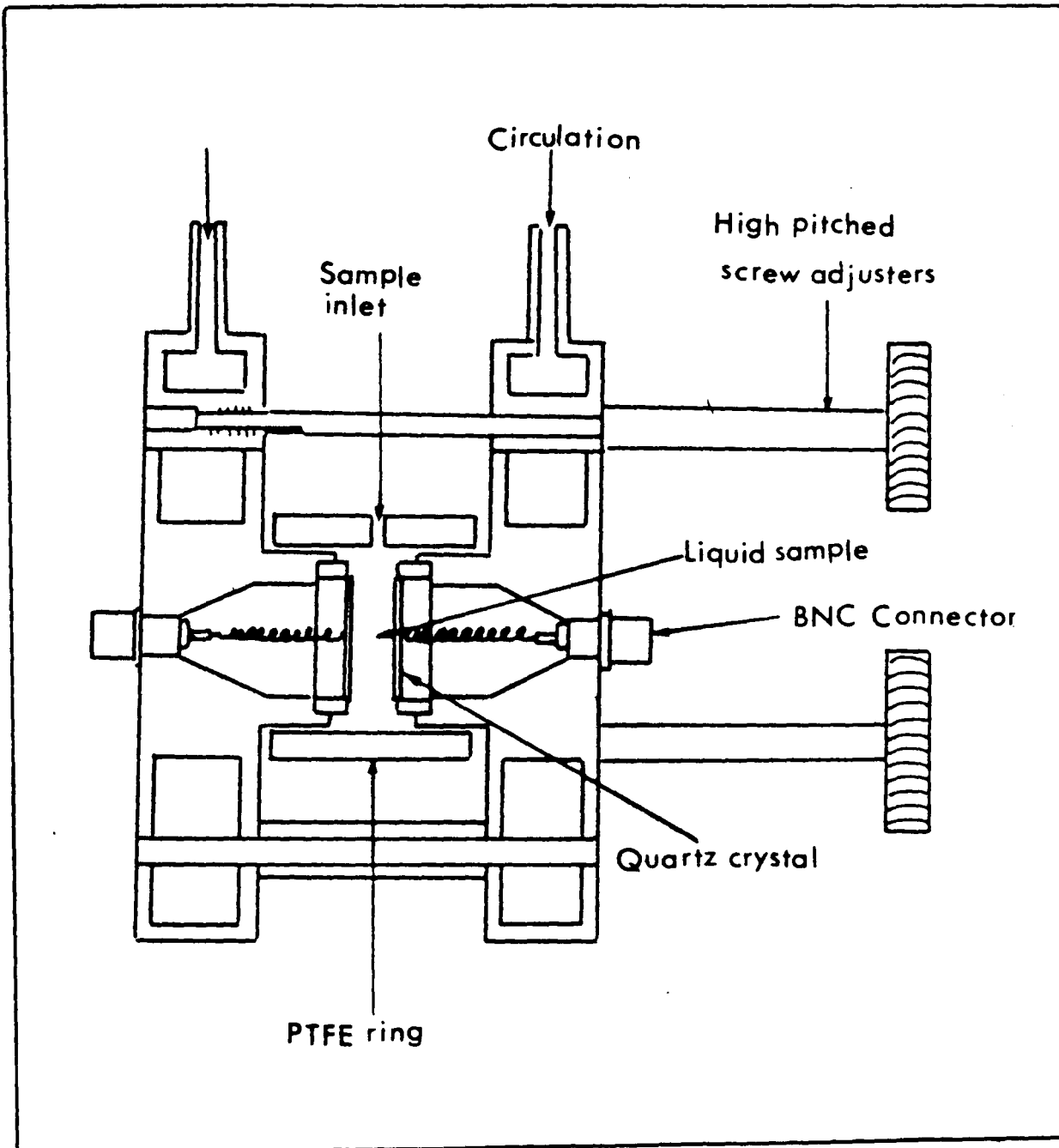


Figure 3.4. Essential features of an acoustic resonator cell.

(iii) Experimental procedure

A liquid sample, 3 ml for 1 MHz cell is introduced into the acoustic cavity slowly with the aid of a syringe to avoid air bubbles. The acoustic cell is first aligned at 298.15K and 7 MHz by using n-octane as the reference liquid sample. Alignment is achieved by adjusting the three micrometers as shown in Figure 3.4. When the cell is perfectly aligned, a sharp resonance peak with a satellite peak at the right hand side is observed, Figure 3.5. The minimum half-peak width occurs at 2 MHz and for n-octane will give a value of approximately 140 Hz.

The experiment, therefore, comprises sweeping through the resonance peaks of the cavity from 1.5-3 MHz, measuring the frequency of each peak at max-0dB,  $f_n$  and the half-peak width  $\Delta f$  in Hz at the 3dB point. A typical plot of  $\Delta f_n$  against  $f_n$  is shown in Figure 3.6 for n-octane and 1-octanol.

(iv) Analysis of data

The two ultrasonic parameters are obtained from the resonance technique, namely the sound velocity ( $c/\text{ms}^{-1}$ ) and the ultrasonic absorption coefficient ( $\alpha/f^2 \times 10^{15}/\text{s}^2\text{m}^{-1}$ ). Two sets of data, one of which is obtained for a standard reference (n-octane), are needed to calculate the sound velocity and ultrasonic absorption coefficient of the unknown liquid sample.

Eggers<sup>121</sup> has shown that the sound velocity in an unknown medium  $c_s$  may be related to that of some reference medium,

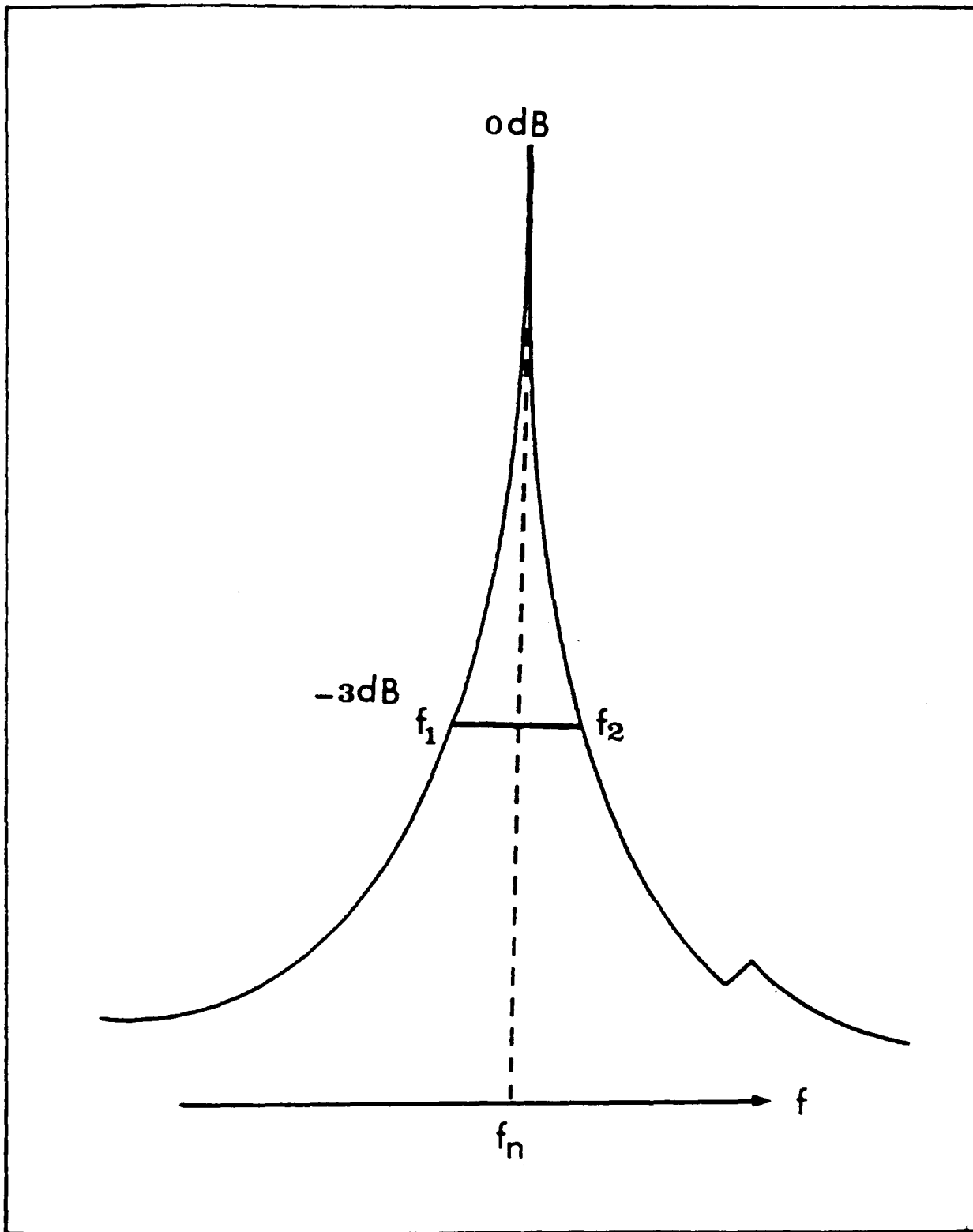


Figure 3.5. A typical resonance peak,  $\Delta f_n \approx 140\text{Hz}$  at  $f_n \approx 2\text{ MHz}$  when n-octane is the sample.

$c_r$ , through the following equation:

$$\frac{c_s}{c_r} = \frac{D_s}{D_r} \left[ 1 + \frac{2(D_s Z_s - D_r Z_r)}{f_q Z_q} \right] \quad 3.1$$

where  $D_s$ ,  $D_r$  are separation between adjacent resonances for unknown and reference samples respectively, and  $Z_s$ ,  $Z_r$  are the acoustic impedances of the unknown and reference samples respectively, and  $f_q$ ,  $Z_q$  are the resonance frequency and acoustic impedance of the quartz crystal respectively.

If the impedances of the unknown and reference samples are comparable, that is  $Z \approx Z_0$ , then equation 3.1 reduces to:

$$\frac{c_s}{c_r} = \frac{D_s}{D_r} \quad 3.2$$

Thus

$$c_s = \frac{D_s \times c_r}{D_r} \quad 3.3$$

In this study an average value of six consecutive separations of adjacent resonance peaks, in the frequency range 1.5-3 MHz, for unknown and reference samples were taken in obtaining the  $D_s$ ,  $D_r$  values. The sound velocity of the unknown sample can then be calculated from equation 3.3.

The ultrasonic absorption is obtained by using a graphical plot. The half-peak width ( $\Delta f$ ) values are plotted against frequency ( $f$ ) as shown in Figure 3.6 for both the unknown sample and the reference standard

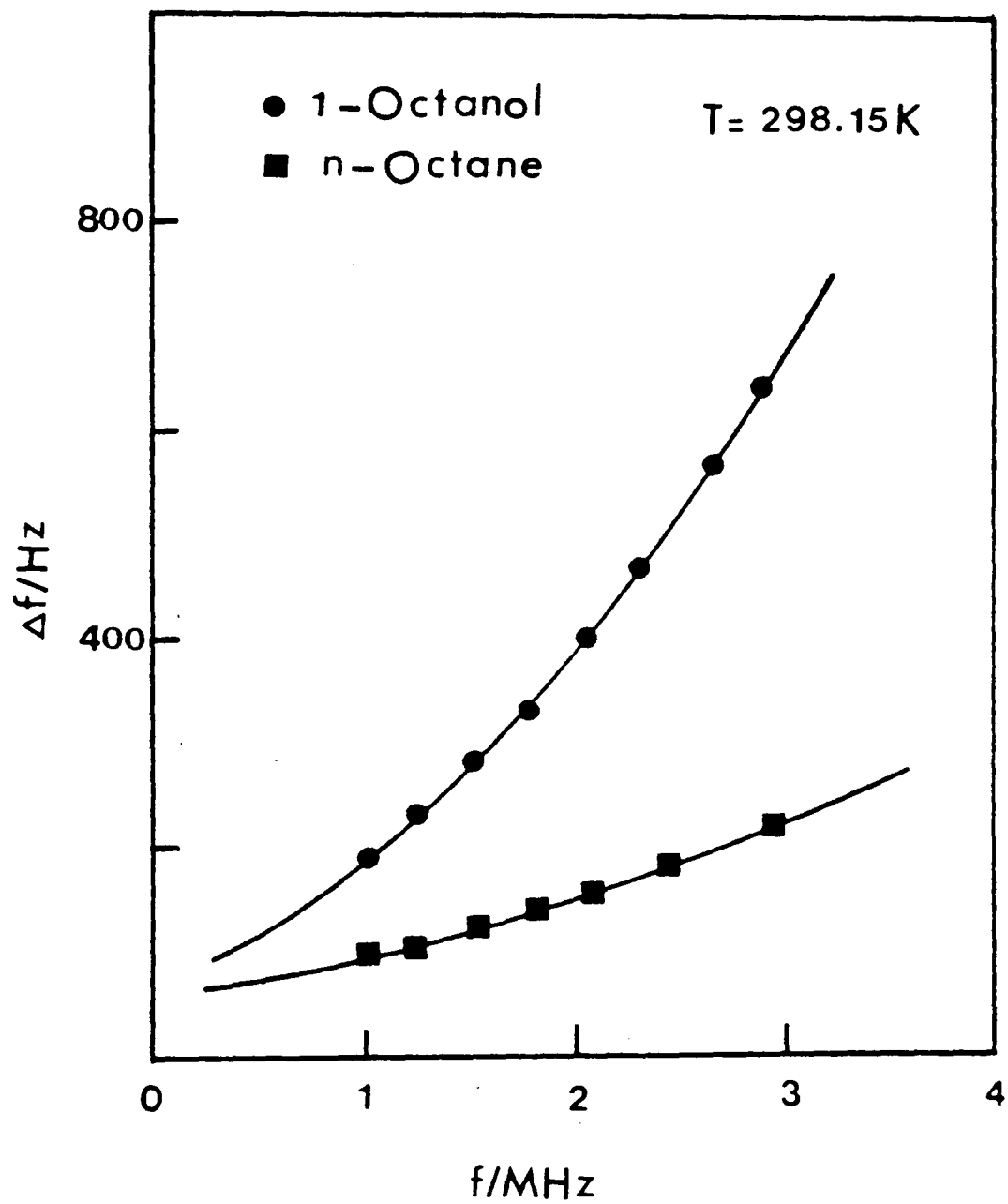


Figure 3.6. A typical plot of half-peak width  $\Delta f$  against frequency  $f$ .

(n-octane in this case). A smooth curve is drawn passing through the maximum number of points in both cases. Then the difference of the half-peak widths for the unknown and reference samples are taken at each regular frequency intervals, say, 1.5 MHz, 1.75 MHz, 2 MHz, and so on.

The ratio of the half-peak width and the resonance peak position is related to the quality factor  $Q_T$  of the resonator and is given by:

$$Q_T = \frac{f}{\Delta f}$$

or

$$Q_T^{-1} = \frac{\Delta f}{f}$$

The total measured quality factor  $Q_T$  is given by:

$$Q_T^{-1} = Q_L^{-1} + Q_M^{-1} \quad 3.4$$

where  $Q_L$  and  $Q_M$  are the quality factors due to the liquid sample and mechanical damping and electrical losses respectively.

But

$$Q_T^{-1} = \frac{\Delta f}{f} \quad 3.5$$

$$Q_L^{-1} = \frac{\alpha \lambda}{\pi} \quad 3.6$$

and

$$Q_M^{-1} = \text{constant} \quad 3.7$$

Equations 3.4, 3.5, 3.6 and 3.7 give:

$$\left(\frac{\Delta f}{f}\right) = \frac{\alpha \lambda}{\pi} + \text{constant}$$

If we denote s and r respectively for the unknown and reference standard, then we have:

$$\left(\frac{\Delta f}{f}\right)_s = \left(\frac{\alpha \lambda}{\pi}\right)_s + \text{constant} \quad 3.8$$

$$\left(\frac{\Delta f}{f}\right)_r = \left(\frac{\alpha \lambda}{\pi}\right)_r + \text{constant} \quad 3.9$$

By manipulating equations 3.8 and 3.9 and using the relationship  $c = f\lambda$ , a standard equation of ultrasonic absorption coefficient is derived as shown in equation 3.10:

$$\left(\frac{\alpha}{f^2}\right)_s = \left(\frac{\alpha}{f^2}\right)_r \left(\frac{c_r}{c_s}\right) + \frac{\pi}{c_s} \frac{\delta \Delta f}{f^2} \quad 3.10$$

where  $\delta \Delta f$  indicates the difference in half-peak widths,  $\delta \Delta f = (\Delta f_s - \Delta f_r)$ .

#### (v) Accuracy

Sound velocity measurements obtained using the resonator technique are reproducible within an error of +1%. The precision of measurements is determined by the precision to which the sound velocity of the reference sample is known.

The absorption coefficient can be estimated with a precision of +2%. In this case, the accuracy is determined by the alignment of the acoustic cell.

### 3.5 Conventional Pulse Equipment (15-75 MHz)

#### (i) Principle of technique

The general principle of this technique is to excite a piezoelectric crystal and its fundamental or an odd harmonic with a high voltage radio frequency (RF) pulse. The resultant mechanical oscillation passes along a delay line (in this work both crystal and delay lines

are quartz) and propagates through the liquid sample and is detected by a receiving transducer upon passage along a second delay line. As in the swept frequency resonator, the transmitting and receiving crystals are a matched pair to give maximum mechanico-electrical coupling.

The received electrical signal is demodulated and displayed on an oscilloscope together with a comparison pulse of the same frequency. The electronic and mechanical systems have been discussed previously<sup>131-132</sup>.

(ii) Experimental system

A block diagram of the apparatus is shown in Figure 3.7. A separate diagram showing the various components of the acoustic cell are illustrated in Figure 3.8. Basically, the requirements for conventional pulse technique cells are (a) a stable holder for one crystal delay/line system, (b) a precise mechanical drive for moving the second crystal/delay line relative to the first one, (c) an accurate micrometer screw coupled to this drive for measuring relative distance to  $2.5 \times 10^{-5} \text{m}$ , (d) a goniometer which comprises the base of the cell and moves the fixed crystal laterally with respect to the other thus allowing the two crystals to be aligned, and finally (e) a thermostated jacket which fits around the fixed delay line and thus completes the cell cavity. The two quartz crystals are coated on each side with a gold electrode  $1 \mu\text{m}$  thick. These are then bonded to the polished delay line.

A Lauda temperature water bath proportional temperature controller was linked to thermostating jacket of the

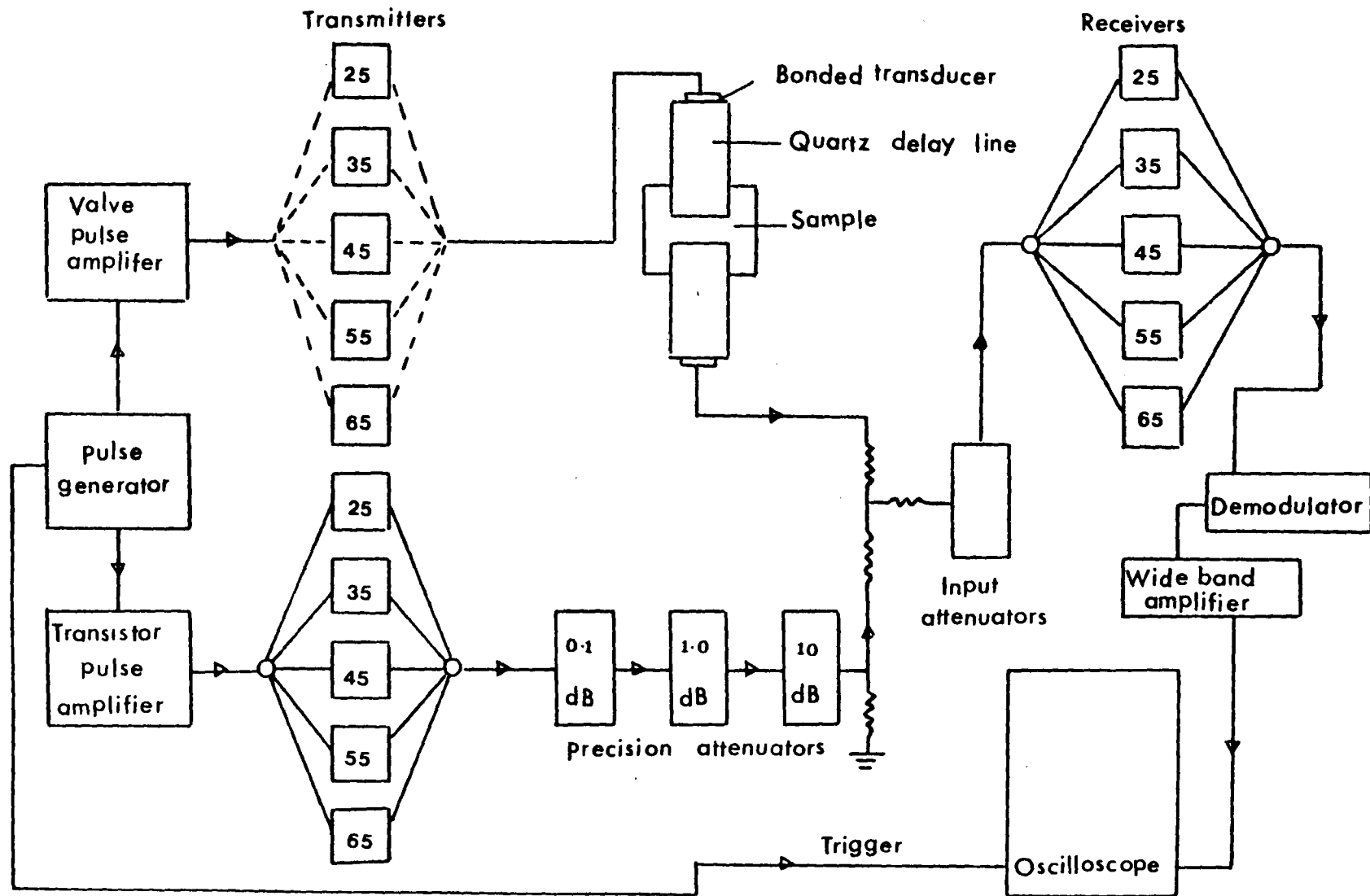


Figure 3.7. Block diagram of the conventional pulse equipment.

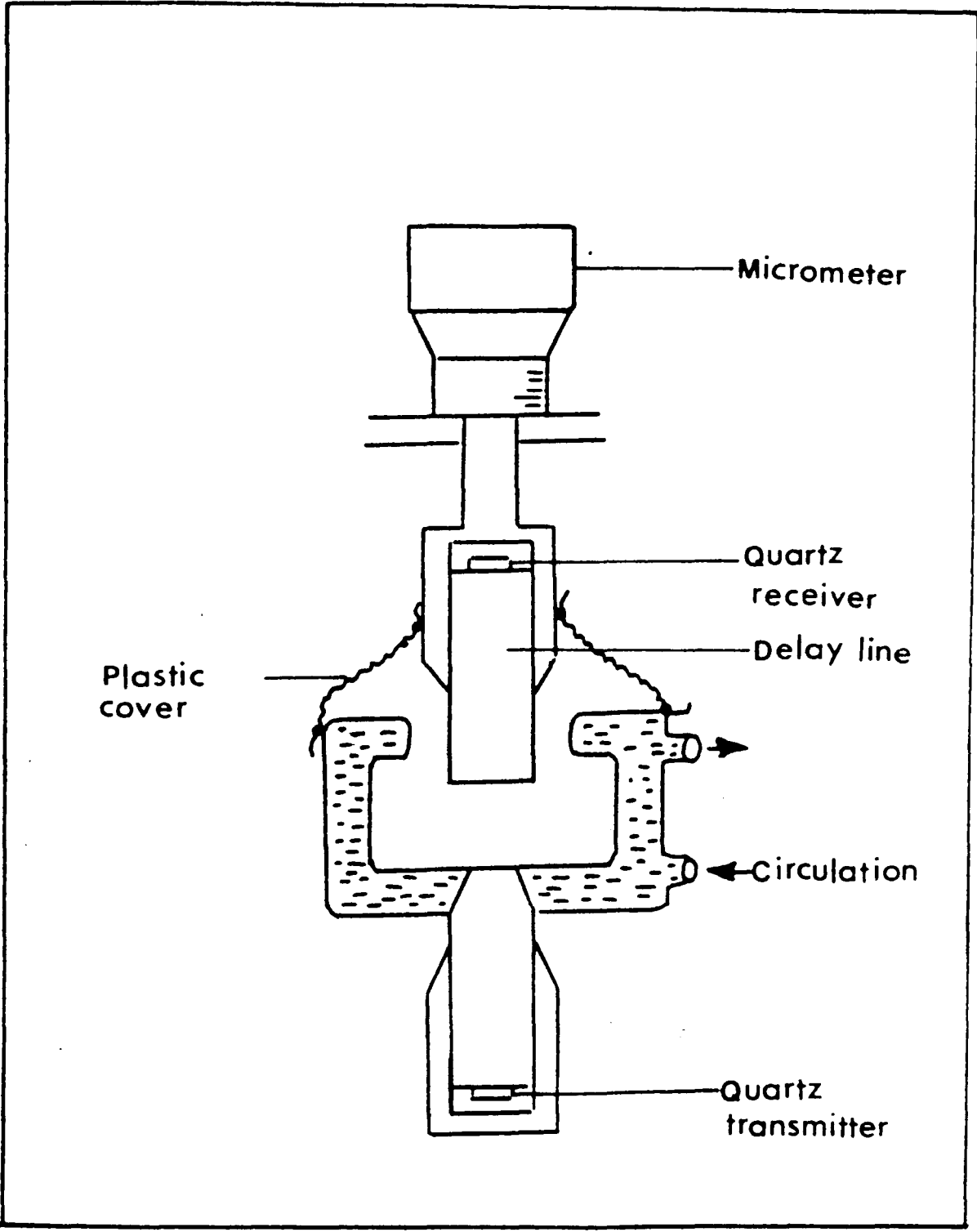


Figure 3.8. Essential features of the cell for the conventional pulse equipment.

cell for measurements at temperatures above 298.15 K, and Townson and Mercer 'Minus Seventy' alcohol bath and a cooling unit (Cryocool CC-80II) were used for measurements at very low temperatures.

(iii) Experimental procedure

Measurements using this technique give information on the ultrasonic absorption and sound velocity of the liquid sample. For a particular frequency of operation, the acoustic signal is tuned to give a maximum amplitude. The comparison pulse is superimposed on the ultrasonic pulse by the use of a variable time delay. The comparison and acoustic pulses are subsequently tuned to the common frequency by the 'zero beat' method<sup>125</sup>. The comparison signal is then moved to a convenient place for measurement. It is now possible to measure the attenuation,  $\alpha$ . This was done by varying the distance of separation between the two delay lines, relative distances being accurately measured by the micrometer drive. At each setting of the micrometer the comparison pulse was adjusted to the level of the first pulse by means of the variable attenuators, a procedure accurate to 0.1 dB. Attenuation of the comparison pulse was recorded as the separation of the delay line was both increased and decreased. From the gradient of the plot of relative attenuation in dB against the distance between the two delay lines in m, an absolute value of  $\alpha$  in dB/m is obtained.

(iv) Analysis of data

A typical plot of attenuation against the distance displaced is shown in Figure 3.9. The slope of the smooth straight line plot gives the ultrasonic attenuation,  $\alpha$ , in dB/mm.

By definition, attenuation in sound waves is given by:

$$\alpha \text{ (Nepers/m)} = \frac{\ln(P_1/P_2)}{x}$$
$$\alpha \text{ (Nepers/m)} = \frac{2.303 \log(P_1/P_2)}{x} \quad 3.11$$

However, from the definition of dB<sup>75</sup>, and the observed attenuation of  $\alpha$  in dB/m, then

$$\alpha_{\text{obs}} \text{ (dB/m)} = \frac{20 \log(V_1/V_2)}{x}$$
$$\alpha_{\text{obs}} \text{ (dB/m)} = \frac{20 \log(P_1/P_2)}{x} \quad 3.12$$

Equations 3.11 and 3.12 give

$$\frac{\alpha}{\alpha_{\text{obs}}} = \frac{2.303}{20}$$
$$= 0.115$$

or  $\alpha \text{ (Nepers/m)} = 0.115 \alpha_{\text{obs}} \text{ (dB/m)}$

Generally, acoustic absorption is expressed as  $(\alpha/f^2)$ , the absorption coefficient. Throughout this work, the absorption coefficient is quoted as  $(\alpha/f^2) \times 10^{15}/\text{s}^2 \text{ m}^{-1}$ .

(v) Accuracy

The accuracy of measurements is determined by

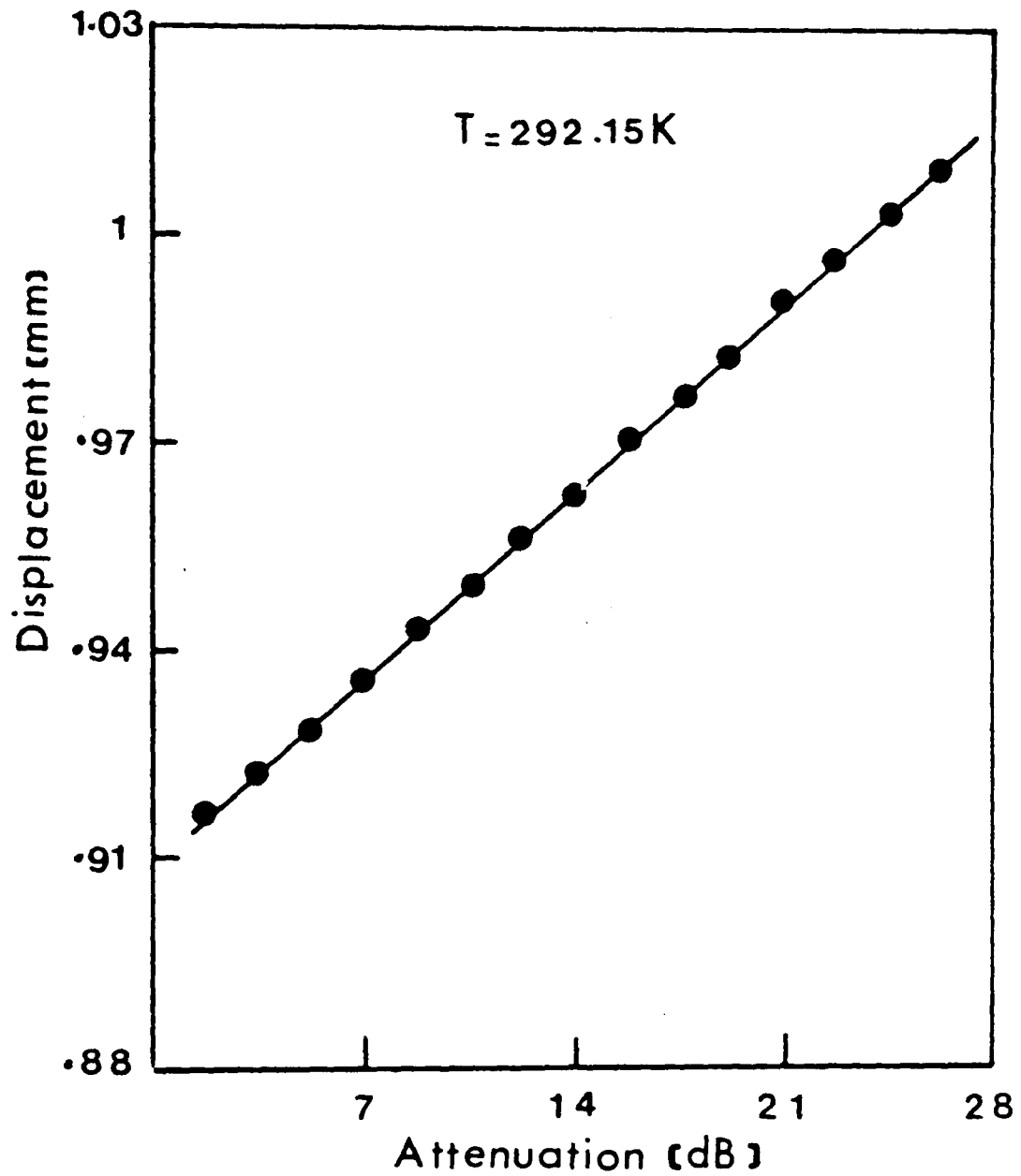


Figure 3.9. A typical plot of distance displaced against attenuation at 35 MHz.

the volatility of the liquid sample, operating frequency, stability of the electronic components of the system and temperature under investigation. A maximum error of +2% is estimated in all measurements.

### 3.6 Ultra-High Frequency Pulse Equipment (100-1000 MHz)

#### (i) Principle of technique

The production of ultrasonic waves above 300 MHz by the use of conventional techniques using quartz transducers bonded to delay lines gives rise to problems associated mainly with the quartz delay line bond and losses in the fused quartz delay line. These can be eliminated by using a crystalline delay rod made of Z-cut quartz<sup>101</sup> activated by surface excitation, but the transducer efficiency is still low. With the introduction of lithium niobate<sup>133-135</sup> as a transducer material with its attendant high efficiency, this has simplified operation at 1 GHz and just above.

The principle of operation of this equipment is similar to that used for studies below 100 MHz. A 2 microsecond pulse of 3 kilovolts in amplitude is produced by a pulse generator with a repetition frequency of 1 KHz. The RF pulse of a few hundred watts generated by the transmitter is applied to the transmitting crystal. The resulting acoustic pulse passes through the liquid sample and the electrical energy is reconverted to an electrical signal by a second transducer before amplification and displayed on an oscilloscope together with a comparison pulse.

## (ii) Experimental system

A block diagram of the whole equipment is shown in Figure 3.10. In this equipment, two 50 cm stub tuners separated by a 20 cm air line are used to replace the conventionally tuned system. A linear voltage differential transformer is incorporated into the electronic system, thus facilitating the detection of small displacements, typically a few microns of separation. The electrical and mechanical systems are discussed in more detail by Wright and Campbell<sup>127</sup>.

The essential components of the acoustic cell are clearly illustrated in Figure 3.11. The lithium niobate transducer is a Z-cut cylindrical crystal, polished to optical standards and the surface excited by VHF electric fields of strengths up to  $5 \text{ KV mm}^{-1}$ . The crystal is shown in Figure 3.12. The mechanical system was enclosed in a Perspex box and the temperature controlled using ducted air which was either heated or cooled by means of a proportional temperature controller. The temperature of the test liquid was measured by a platinum resistance thermometer element inserted in the liquid. The cell had a built-in water jacket through which water or alcohol could be circulated as an alternative to the ducted air system. To overcome the evaporation of the test liquid at high temperatures, a polythene seal was used to surround the two crystal holders.

## (iii) Experimental procedure

Before ultrasonic absorption measurements, it is

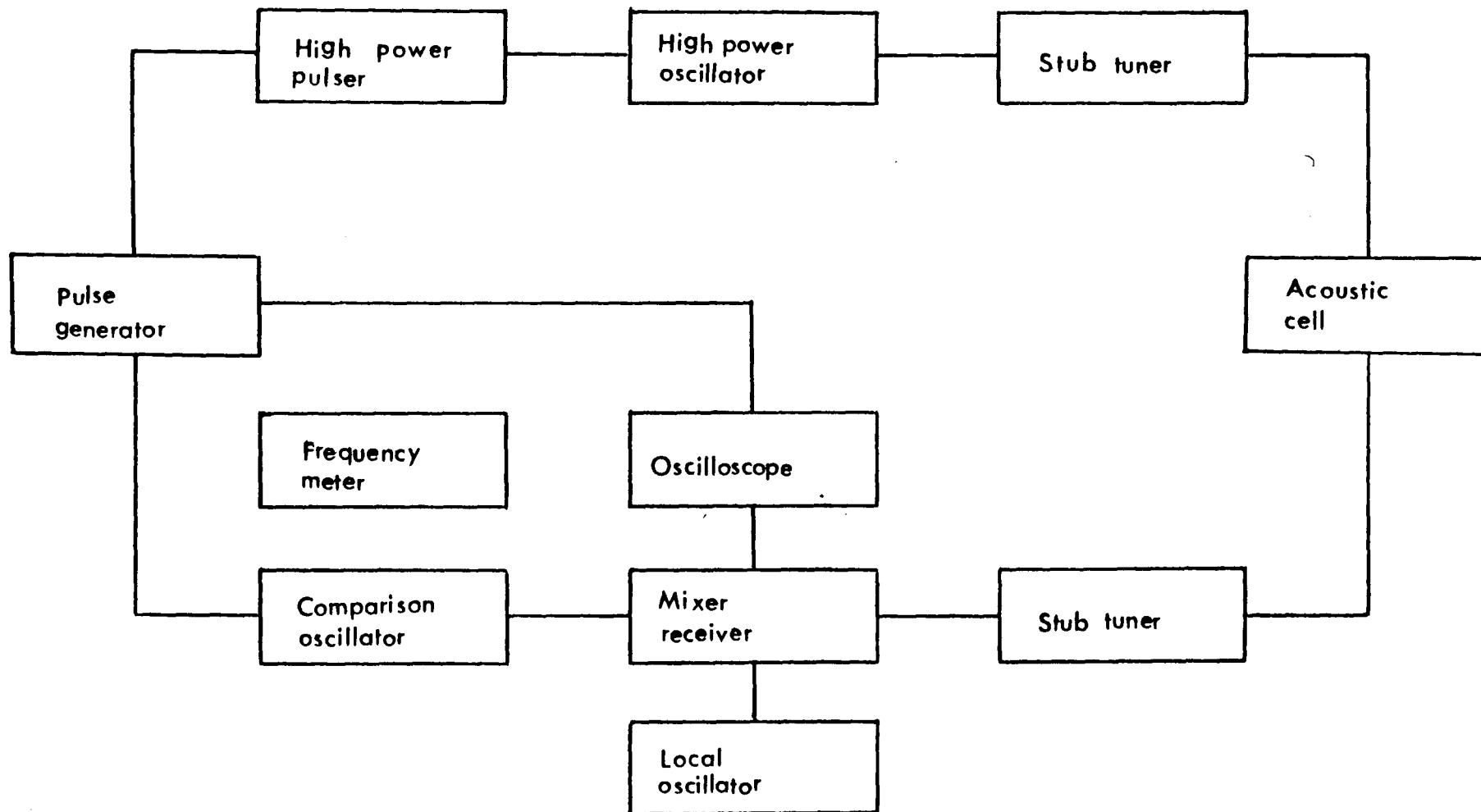


Figure 3.10. Block diagram of the ultra-high-frequency pulse equipment.

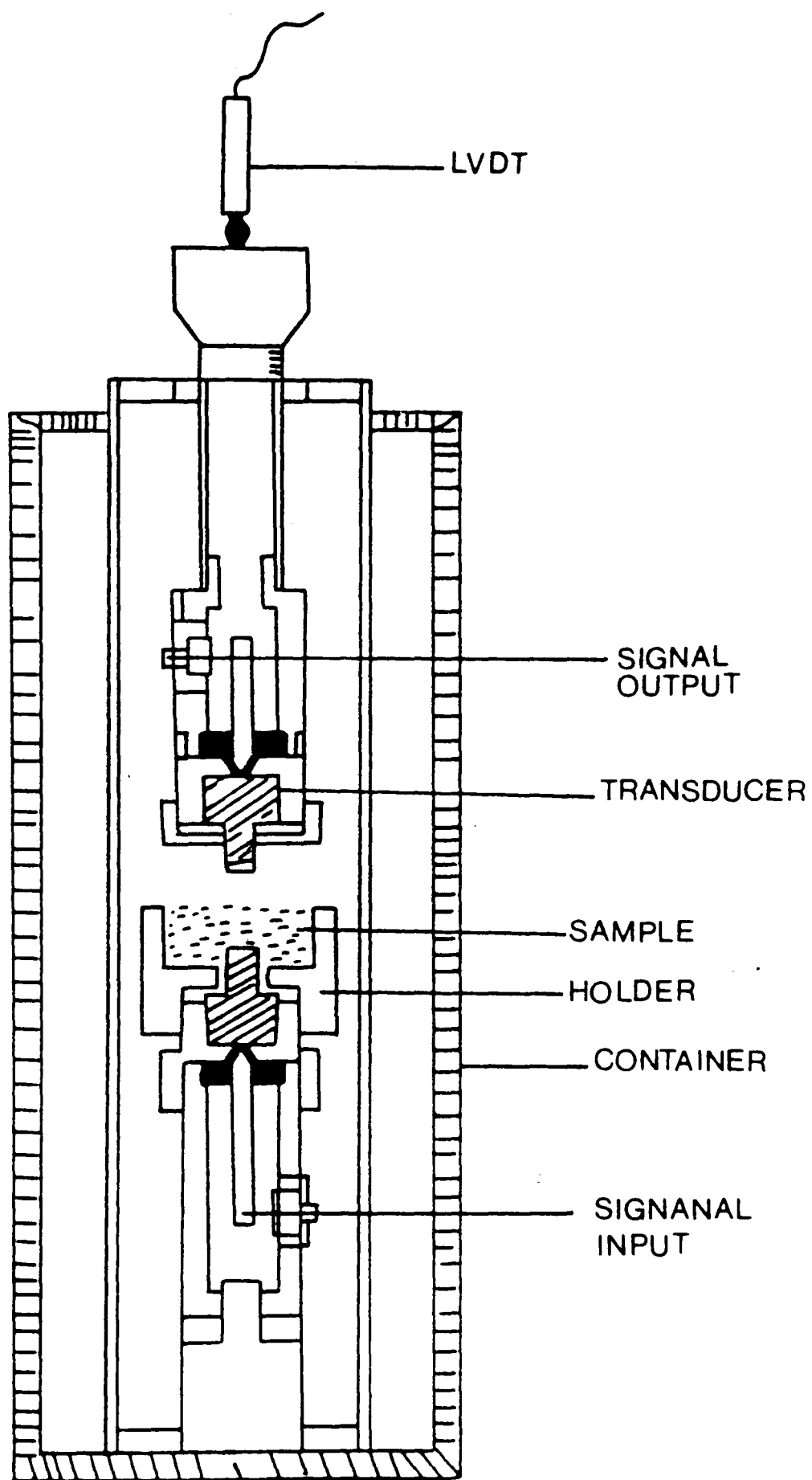


Figure 3.11. Essential features of the acoustic cell of the ultra-high-frequency pulse equipment.

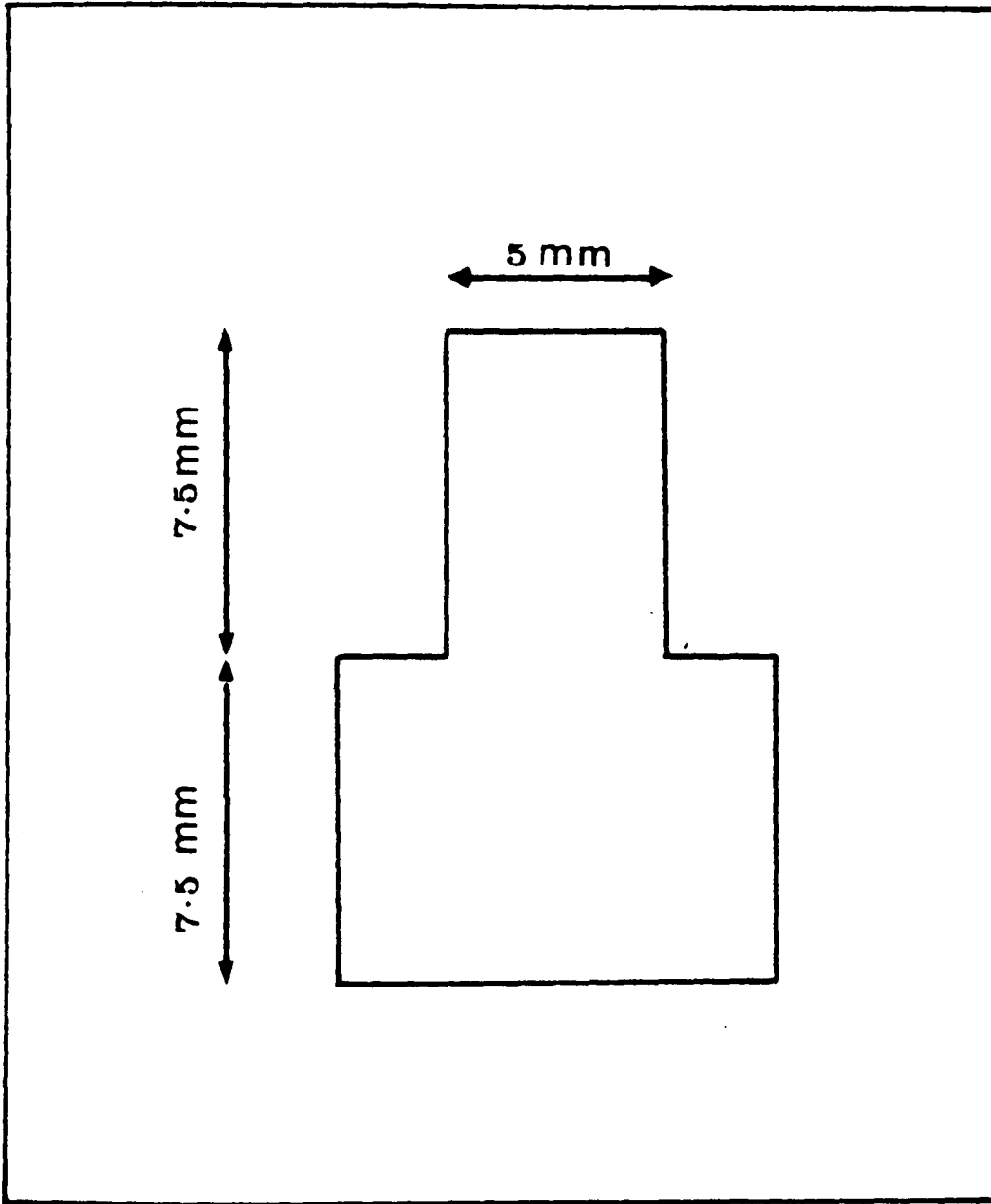


Figure 3.12. High frequency lithium niobate transducer.

necessary to calibrate the linear voltage differential transformer against the displacement between the two transducers. A plot of such a calibration is shown in Figure 3.13. The acoustic cell is aligned by adjusting the micrometers on the goniometer at 300 MHz and checked at 1GHz. Pure deionized water is used for the purpose of alignment because it has a low absorption coefficient.

The method of measurement is quite similar to that of the conventional pulse technique described previously. A typical plot of signal level (dB) against displacement (mm) for water at 450 MHz is shown in Figure 3.14. A smooth line is drawn through the maximum number of points.

(iv) Analysis of data

From the analysis developed by Musa<sup>136</sup>, the pressure  $P_x$  at a distance  $x$  from the transmitting crystal is given by:

$$P_x = P_0 (1 - \phi) \exp(i\omega t) \frac{\exp[-(\alpha + i\beta)x] + \phi \exp[-(\alpha + i\beta)(2r - x)]}{1 - \phi^2 \exp[-\alpha + (i\beta) 2r]}$$

3.13

where

$\alpha$  = amplitude

$\beta$  = phase propagation

$P_0$  = incident wave pressure

$r$  = distance between the crystals

$\omega$  = angular frequency of signal

$\phi$  = reflection coefficient at each liquid/crystal interface

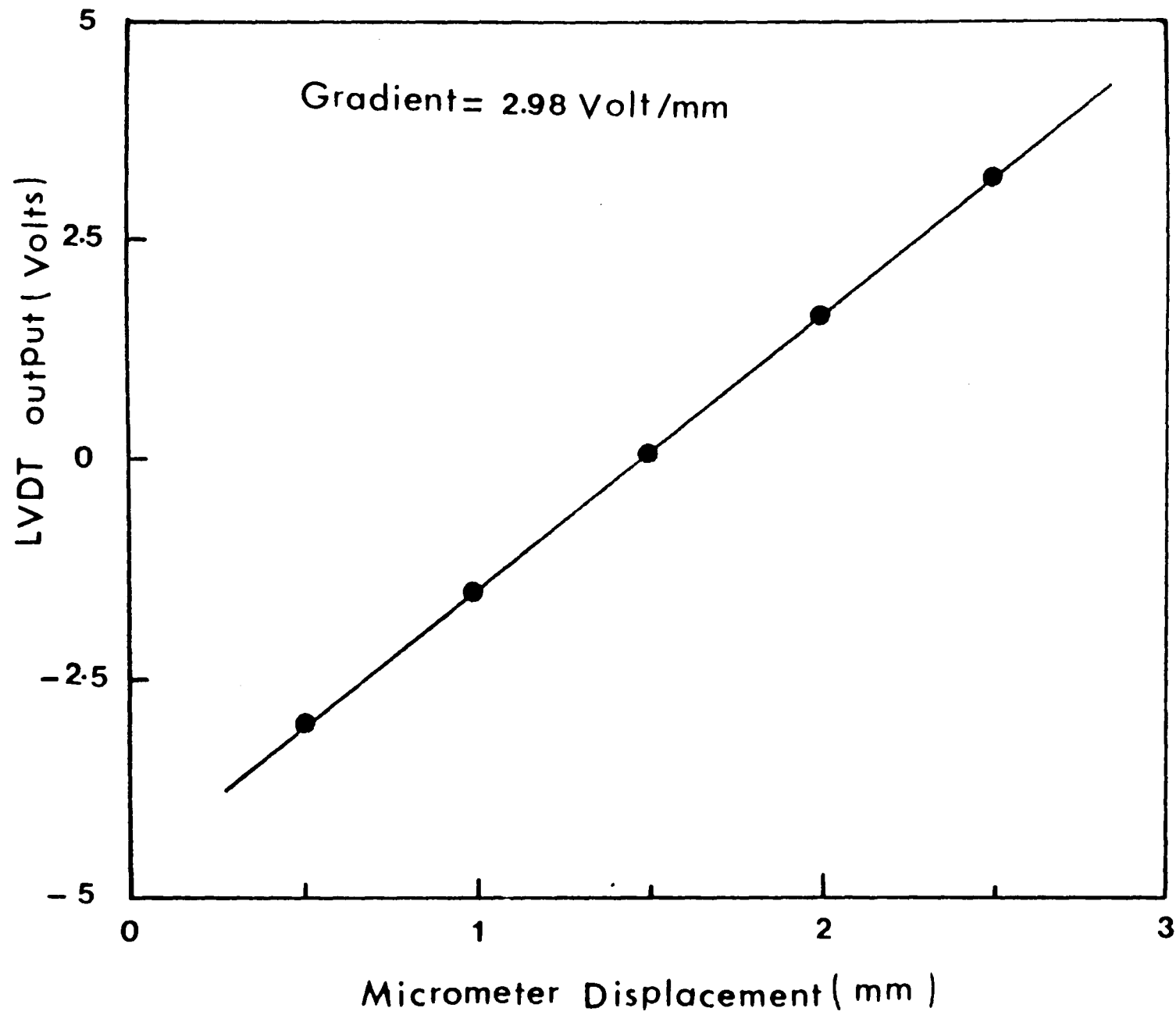


Figure 3.13. Calibration of LVDT.

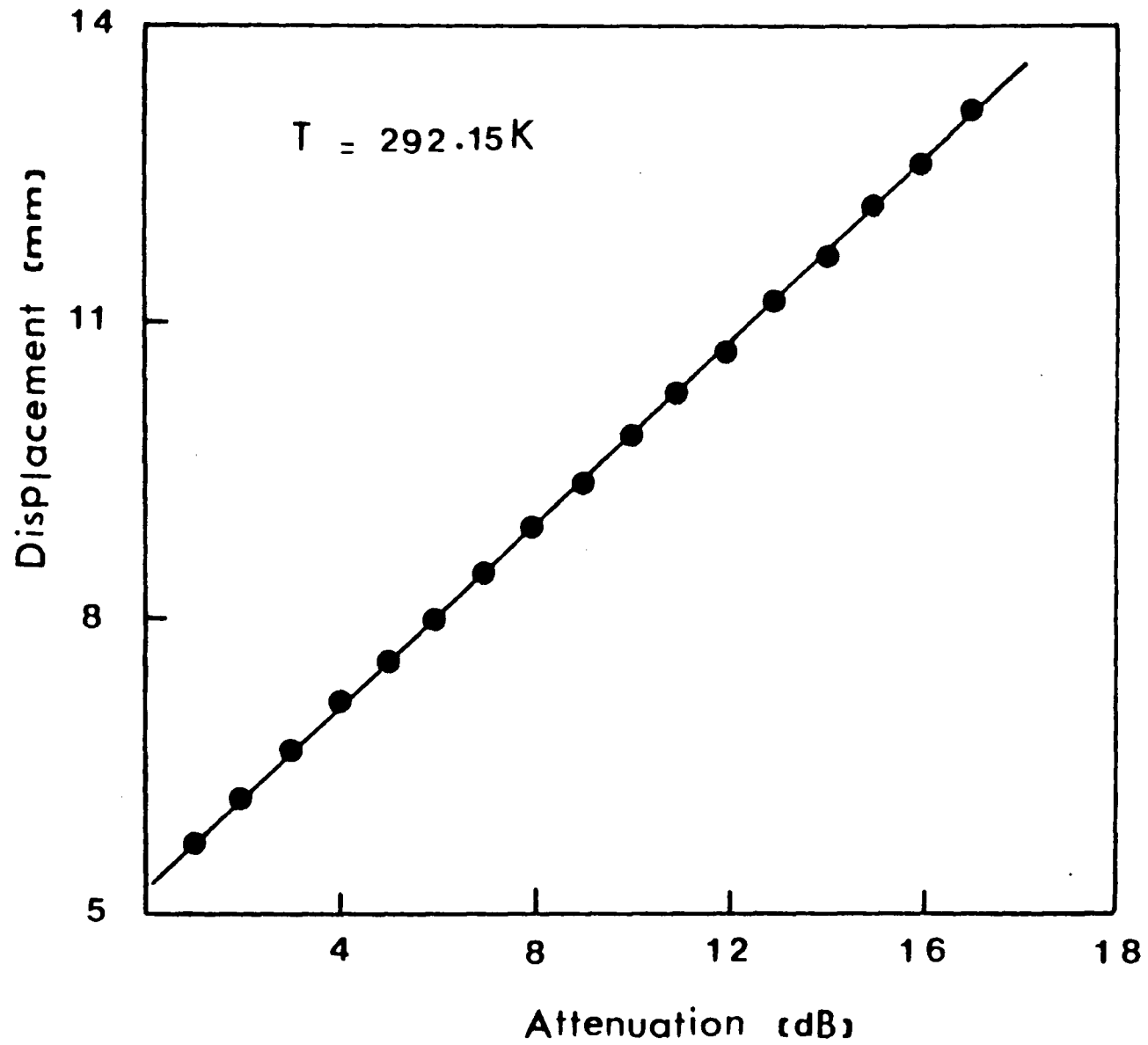


Figure 3.14. Signal level against distance displaced for water at 450 MHz.

For a given system the received signal voltage,  $V_r$ , is proportional to the magnitude of  $P_x$ ; hence setting  $x=r$ , equation 3.13 gives:

$$V_r = V_o \frac{(1-\phi^2) \exp(-\alpha r)}{[1-2\phi^2 \exp(-2\alpha r) \cos(2\beta r) + \phi^4 \exp(-4\alpha r)]^{1/2}} \quad 3.14$$

From equation 3.14  $V_r$  is maximum when  $r = \frac{n\pi}{\beta}$  and  $V_r$  is minimum when  $r = \frac{(2n+1)\pi}{2\beta}$  where  $n$  is a positive integer.

For an even number of quarter-wavelengths

$$V_{\max} = V_o \frac{(1-\phi^2) \exp(-\alpha r)}{(1-\phi^2) \exp(-2\alpha r)} \quad 3.15$$

and for an odd number of quarter-wavelengths

$$V_{\min} = V_o \frac{(1-\phi^2) \exp(-\alpha r)}{(1+\phi^2) \exp(-2\alpha r)} \quad 3.16$$

Three alternative methods<sup>127,136</sup> for determining the absorption coefficient of the liquid sample can be used, depending on the value of the quantity,  $\alpha r$ .

In this study, the third method was used as the most convenient giving a linear plot for dB against the distance. Since  $\alpha r > 1.5$   $V_{\max} \exp^{-\alpha r} \rightarrow 0$  as  $\alpha r \gg 1$ , equations 3.15 and 3.16 approach a common equation given by:

$$V_r = V_o (1-\phi^2) \exp(-\alpha r) \quad 3.17$$

and this equation can be expressed by:

$$20 \log(V_r/V_o) = 20 \log(1-\phi^2) - (20\alpha/2.303)r \quad 3.18$$

or attenuation (dB) = constant - (slope)(column length).

Hence a plot of attenuation (dB) against the column length ( $r$ ) would give a slope of  $20\alpha/2.303$  or:

$$\alpha(\text{Nepers/m}) = \text{slope} \times 0.115 \quad 3.19$$

### (v) Accuracy

Accuracy has a similar magnitude as in the conventional pulse technique. A maximum error of  $\pm 2\%$  is estimated in all measurements.

### 3.7 $^{13}\text{C}$ nmr Spectra

$^{13}\text{C}$  nmr spectra were obtained at 306K in deuterio-benzene using a Bruker WM250 MHz Fourier transform spectrometer operated at 62.9 MHz with tetramethylsilane as reference. The spectra were obtained with and without proton decoupling.

### 3.8 Density Measurements

Densities of all sample liquids in this study were measured using an Anton Paar (DMA 601) digital densimeter.

The principle of operation is that a hollow, flexible, glass vessel be excited to an undamped oscillation by electronic means. The resonant frequency of the oscillator is determined by its mass and thence by the density of liquid filling the vessel.

Air and pure distilled water were used to calibrate the cell constant (K) at each temperature according to the following equation:

$$K = \frac{\rho_{\text{H}_2\text{O}} - \rho_{\text{air}}}{T_{\text{H}_2\text{O}}^2 - T_{\text{air}}^2} \quad 3.20$$

where  $\rho$  and T are the density and the time required for  $5 \times 10^3$  periods of oscillation respectively. Then the density of the unknown liquid sample is calculated from the following equation:

$$\rho_{\text{unknown}} = \rho_{\text{H}_2\text{O}} + K(T_{\text{unknown}}^2 - T_{\text{H}_2\text{O}}^2) \quad 3.21$$

The temperature of the sample vessel is controlled to  $\pm 0.01\text{K}$  by a Lauda thermostat unit.

The overall precision of the densities measured were estimated to be better than  $\pm 3 \times 10^{-6} \text{ kg/m}^3$ .

### 3.9 Viscosity Measurements

The viscosities of all liquid samples in this study were determined using a suspended level Ubbelohde viscometer. The flow times were determined electronically using an electronic stopwatch with a precision of  $\pm 0.5\text{s}$ . The temperature of the thermostat bath was controlled to be better than  $\pm 0.01\text{K}$ . The viscosity values obtained are estimated to be accurate to  $\pm 0.5\%$ .

The viscosity of the liquid samples can be calculated from the following equation:

$$\eta = Ct \tag{3.22}$$

where C is the calibration constant of the viscometer (cSt) and t is the flow time (s).

CHAPTER 4

ULTRASONIC STUDIES OF ROTATIONAL ISOMERISM  
IN VARIOUS METHYLPENTANES

## CHAPTER 4

### ULTRASONIC STUDIES OF ROTATIONAL ISOMERISM IN VARIOUS METHYLPENTANES

#### 4.1 Introduction

The saturated hydrocarbons have been regarded for a number of years as a group of molecules, the study of which might form a useful precursor to the understanding of the dynamics of polymer molecules<sup>137</sup>. Of particular interest is the way in which the two-state rotational isomeric change of single covalent bonds in very short chains contribute to 'polymeric' modes of motion in long chains.

Molecular rearrangement in normal alkanes has been investigated by ultrasonic relaxation<sup>39,42</sup>, nuclear magnetic resonance<sup>138</sup>, neutron scattering<sup>139</sup>, vibrational spectroscopy<sup>140-141</sup> and X-ray diffraction<sup>142,143</sup> and interpreted in terms of trans-gauche isomerism of carbon-carbon covalent bonds.

The ultrasonic relaxation technique is ideally suited to the investigations of rotational isomerism in molecules possessing relatively low activation energies and finite energy differences associated with the internal rotation process<sup>144-147</sup>. The normal and branched-chain alkanes fall into this class having activation energies typically 12-80 kJ mol<sup>-1</sup>. Ultrasonic measurements of the rotational isomerism in normal alkanes have been reported by Piercy and Rao<sup>39</sup> and by Cochran et al<sup>42</sup>. It was found that in the longer chain alkanes the activation energy

exhibits a molecular weight dependence indicative of some degree of co-operative motion of units in the chain backbone.

Branched-chain hydrocarbons have been used in recent years to test the validity of various theories of the liquid state<sup>148-151,30</sup>. However, detailed quantitative observations of the rotational isomerism in branched chain hydrocarbons are very limited. To correct this deficiency, a systematic evaluation of internal rotational energies in common branched chain alkanes, using ultrasonic relaxation was carried out and is the substance of this chapter. Young and Petrauskas<sup>41</sup>, Chen and Petrauskas<sup>40</sup>, have reported the ultrasonic studies of 2-methylpentane, 3-methylpentane and 2,3-dimethylbutane at low temperatures using a limited frequency range 5 to 35 MHz.

In this study the influence of methyl group substitution on certain alkanes with a five carbon atom main chain is explored. An extended frequency range of 1-1000 MHz has been used, allowing the relaxation to be measured precisely and at ambient temperatures. The systems which were studied earlier by Petrauskas are re-measured, so allowing both comparison with the earlier data and extension of the temperature and frequency range. The systems studied are of particular interest to thermodynamicists since they have been widely studied as mixtures with linear hydrocarbons.

## 4.2 Materials

The branched-chain alkanes, 2-methylpentane, 3-methylpentane, 2,3-dimethylpentane, 2,4-dimethylpentane, 2,2,4-trimethylpentane and 2,3,4-trimethylpentane were obtained from Aldrich Chemical Company Ltd. and were dried over molecular sieves Type 4A (BDH) before use. Their purity was better than 99.5%. The densities, refractive indices and ultrasonic velocities are presented in Table 4.1. The data obtained are in good agreement with those published in the literature<sup>152-156</sup>.

## 4.3 Results

### (i) Viscosities

The variation of viscosity with temperature was measured, Figure 4.1. It was found that the data over the whole temperature range of 293 to 233K can be fitted to an empirical equation suggested by Barlow et al<sup>157</sup> having the form:

$$\ln \eta = A + B / [T(^{\circ}\text{C}) + 273.15) - T_0] \quad 4.1$$

where  $T_0$  is a reference temperature and A and B are two adjustable parameters. Values of the parameters obtained by fitting this equation to the observed viscosities are presented in Table 4.2.

### (ii) Densities

The variation of density with temperature was found to be linear over the whole temperature range of 263 to 313K and could be fitted by:

$$\rho / \text{gcm}^{-3} = A_d + B_d T(^{\circ}\text{C}) \quad 4.2$$

TABLE 4.1. Densities,  $\rho$ , Refractive Indices,  $n_D$ , and Ultrasonic Velocities,  $c$ , of Liquids Studied at 293.15K

Component	$\rho / \text{gcm}^{-3}$		$n_D$		$c / \text{ms}^{-1}$	
	obs.	lit.	obs.	lit.	obs.	lit.
2-methylpentane	0.65343	0.6356	1.37182	1.3722	1070	-
3-methylpentane	0.66443	0.6642	1.37581	1.37662	1099	-
2,2,4-trimethylpentane	0.69201	0.6918	1.39148	1.39151	1107	1105
	-	0.6919	-	1.39145	-	1103
2,3,4-trimethylpentane	0.71905	0.71903	1.40398	1.40422	1180	1181
	-	0.7191	-	-	-	1191
2,3-dimethylpentane	0.69505	0.6952	1.39224	1.39210	1150	1148.50
	-	0.6942	-	-	-	-
2,4-dimethylpentane	0.67298	0.6731	1.38121	1.38153	1087	1083.50
	-	0.6745	-	-	-	-

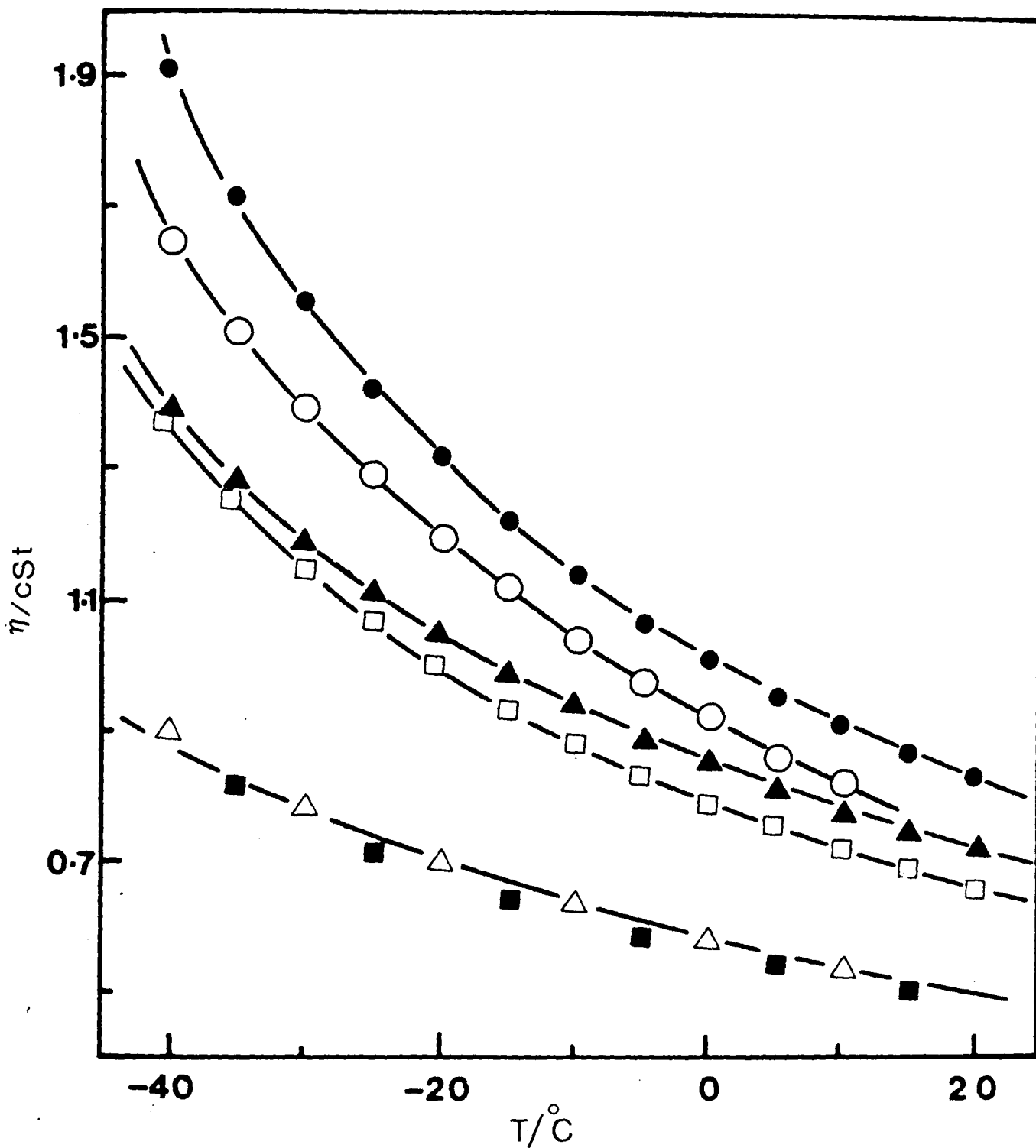


Figure 4.1. Variation of viscosity as a function of temperature for:

- , 2-methylpentane;  $\triangle$ , 3-methylpentane;
- $\square$ , 2,3-dimethylpentane;  $\blacktriangle$ , 2,4-dimethylpentane;
- $\circ$ , 2,2,4-trimethylpentane;  $\bullet$ , 2,3,4-trimethylpentane.

TABLE 4.2. Viscosity and Density Temperature Dependence Parameters

	2-methyl- pentane	3-methyl- pentane	2,4-dimethyl- pentane	2,3-dimethyl- pentane	2,2,4-tri- methyl- pentane	2,3,4-tri- methyl- pentane
$A_V$	-1.542	-1.737	-1.736	-1.602	-3.049	-1.5341
$B_V$	124.7	178.1	223.6	228.9	720.0	211.1
$T_O$	144.9	124.2	124.2	114.3	30.17	136.4
$A_d$	0.6717	0.6822	0.6898	0.7116	0.7082	0.7345
$B_d \times 10^4$	-9.136	-8.900	-8.422	-8.317	-8.137	-7.755

Values of the empirical parameters  $A_d$  and  $B_d$  are also listed in Table 4.2.

(iii) Isoentropic (adiabatic) compressibilities

The sound velocities and hence the isoentropic compressibilities defined in section 2.5(iv) were measured as a function of temperature and the data will be discussed later.

(iv) Ultrasonic relaxation

The ultrasonic absorption coefficient as a function of temperature and frequency is presented in Figures 4.2-4.7. The variation of absorption attenuation with frequency is fitted to the equation 2.8. Computer fits to the observed data for each compound yielded the parameters summarised in Table 4.3.

Energy parameters associated with internal rotation can be derived from the temperature dependence of the relaxation frequency and its amplitude, equation 2.16. The logarithm of the relaxation frequency was observed to vary linearly with inverse temperature, Figure 4.8, indicating the validity of the simple kinetic analysis in which the equilibrium constant,  $K = \frac{k_{12}}{k_{21}} \ll 1$  where  $k_{12}$ ,  $k_{21}$  are the rate constants for passage across the conformational energy barrier. Values of the Arrhenius activation energy,  $\Delta E^\ddagger$ , so obtained are presented in Table 4.4. If it is further assumed that the change in volume associated with the rotational isomeric process is small, then a plot of  $\log(T\mu_{\max}/c^2)$  versus  $\frac{1}{T}$ ; equation 2.23, is linear

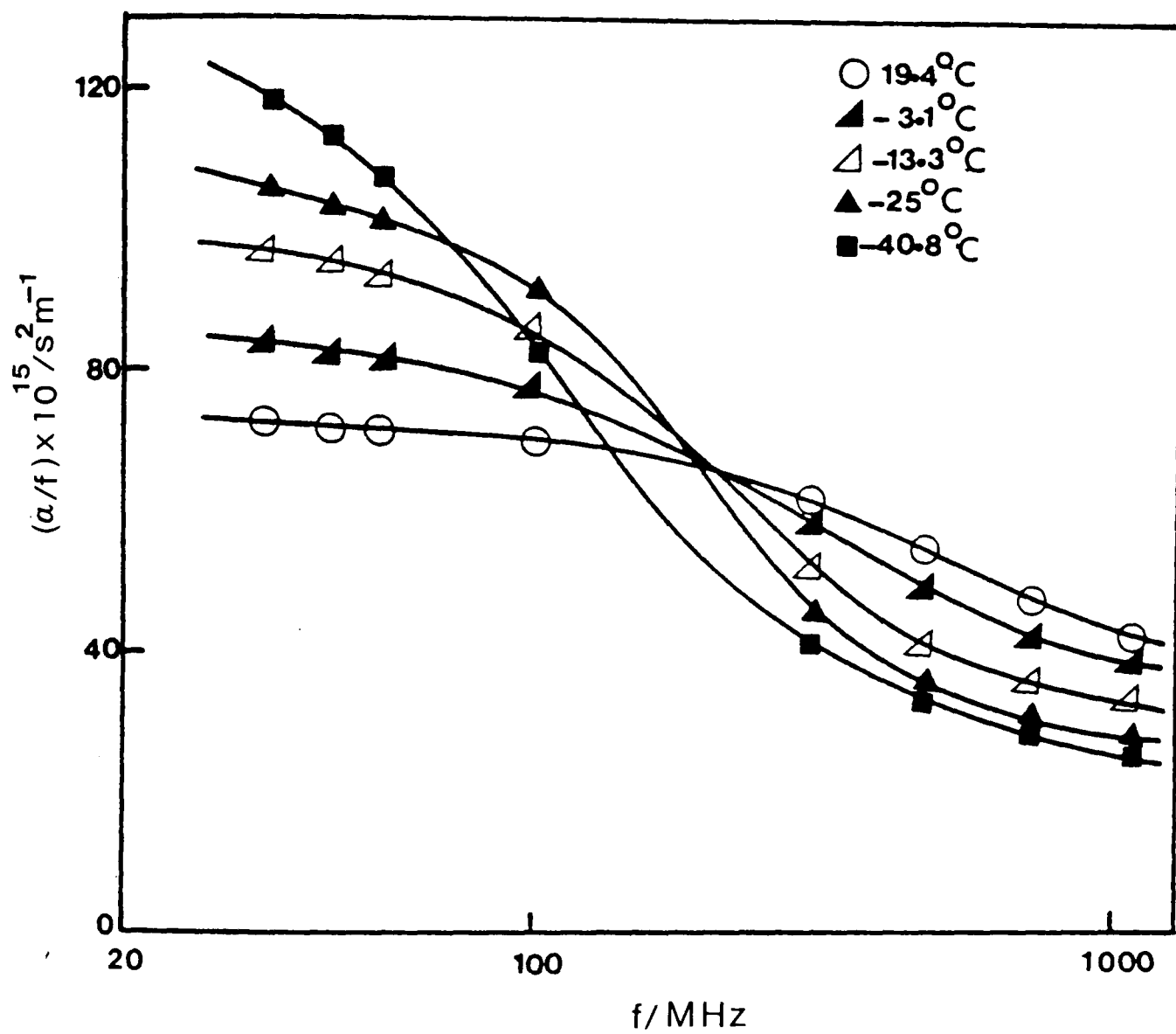


Figure 4.2. Variation of the ultrasonic absorption coefficient with frequency at various temperatures for 2-methylpentane.

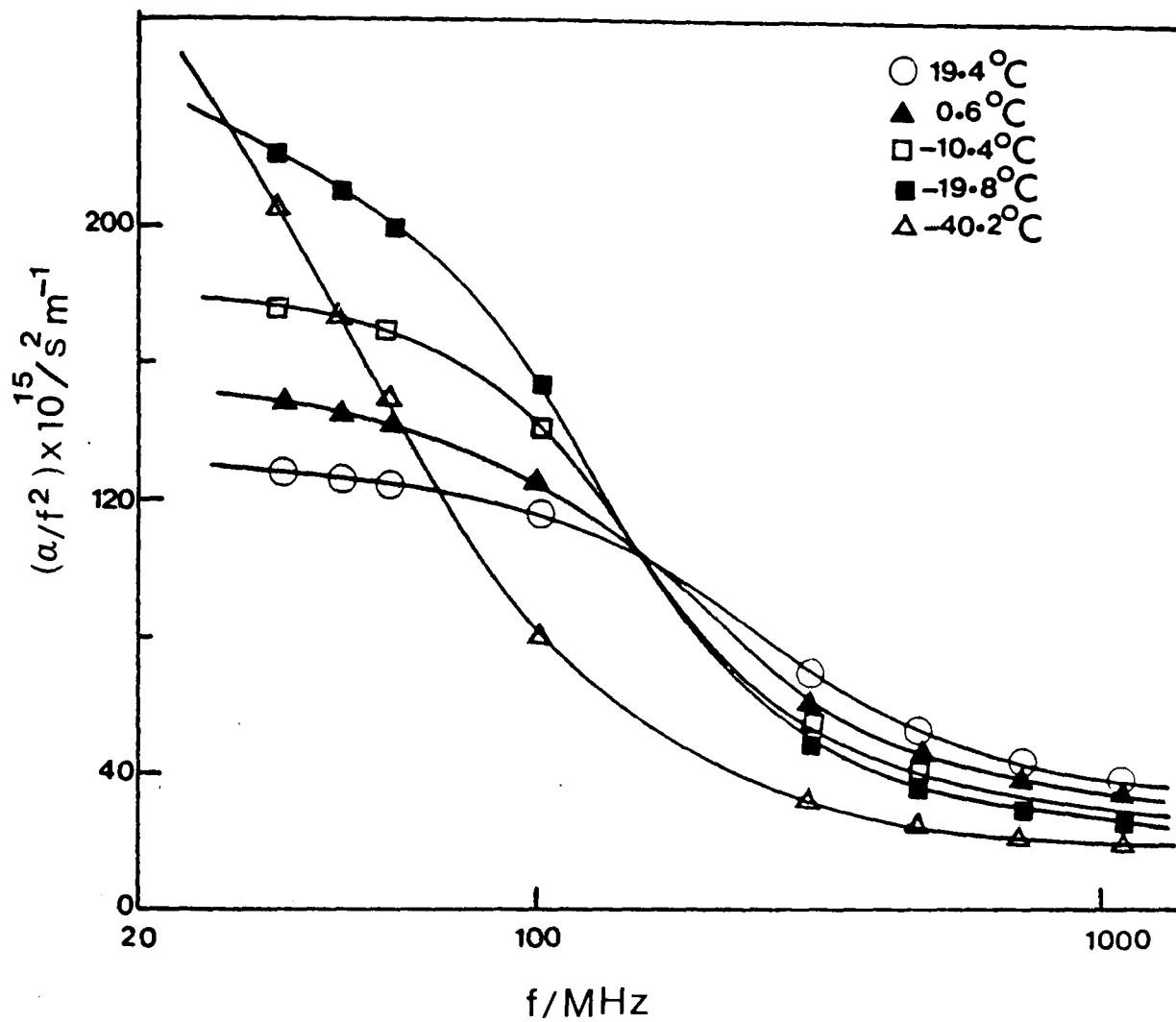


Figure 4.3. Variation of the ultrasonic absorption coefficient with frequency at various temperatures for 3-methylpentane.

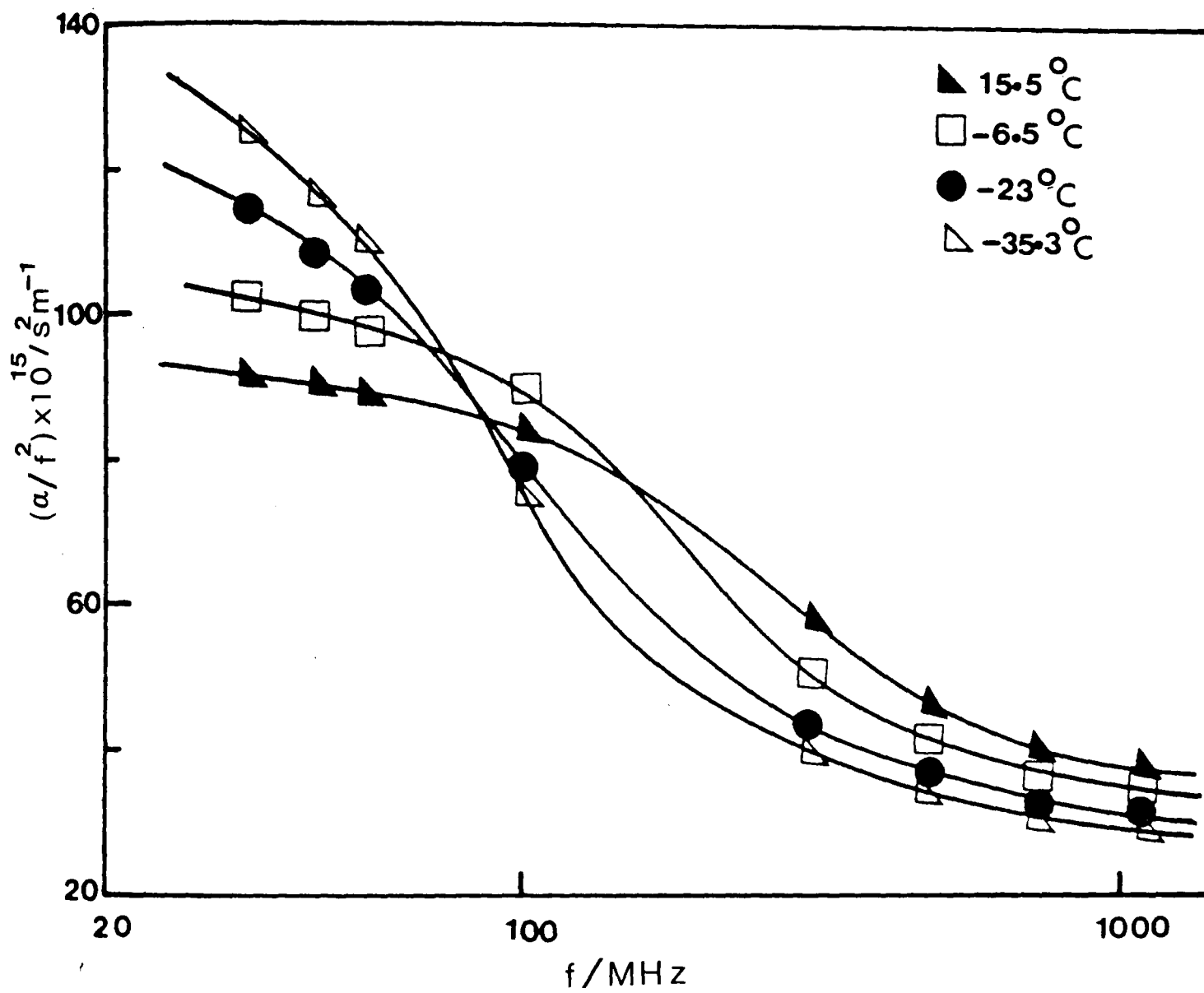


Figure 4.4. Variation of the ultrasonic absorption coefficient with frequency at various temperatures for 2,3-dimethylpentane.

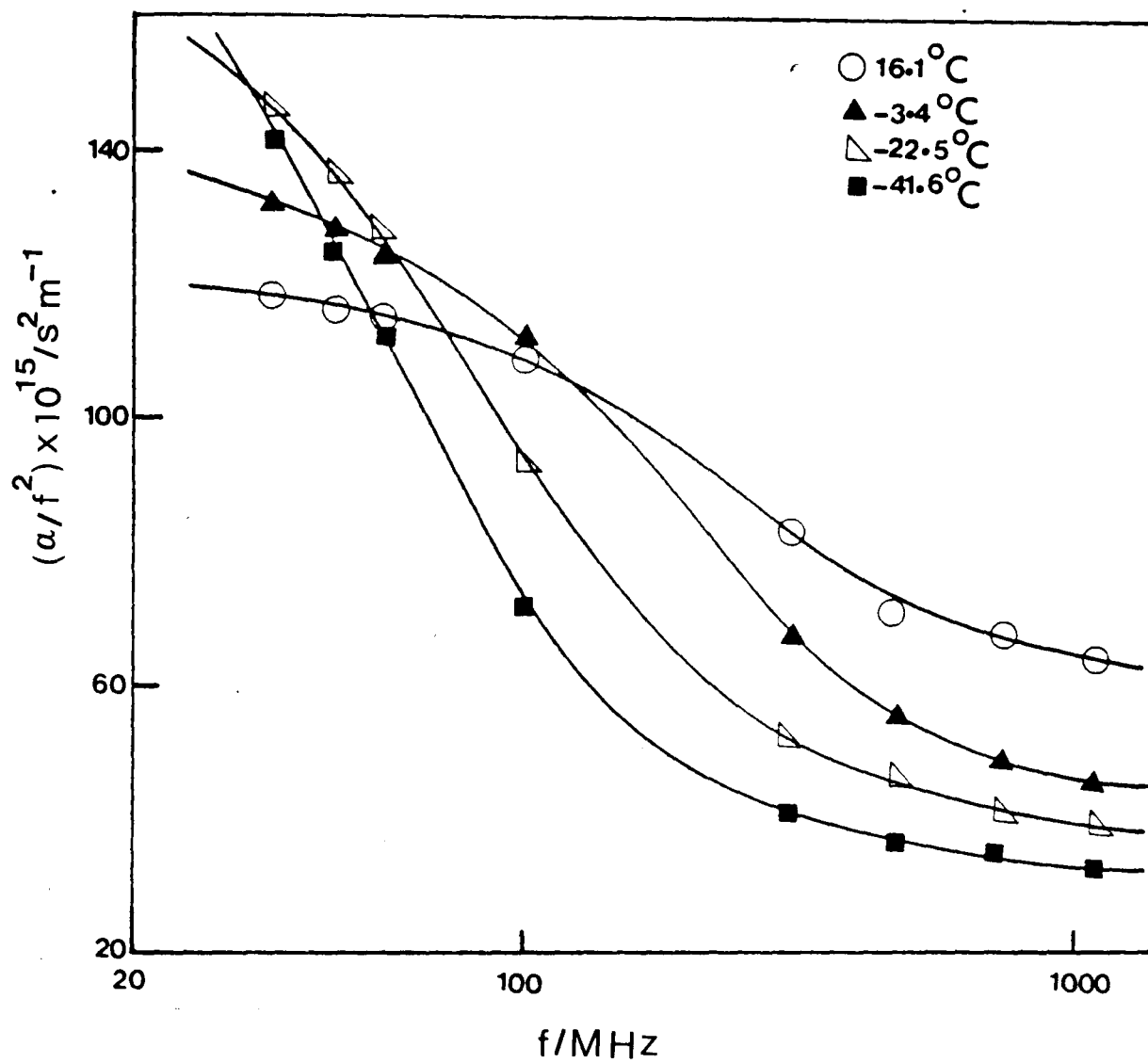


Figure 4.5. Variation of the ultrasonic absorption coefficient with frequency at various temperatures for 2,4-dimethylpentane.

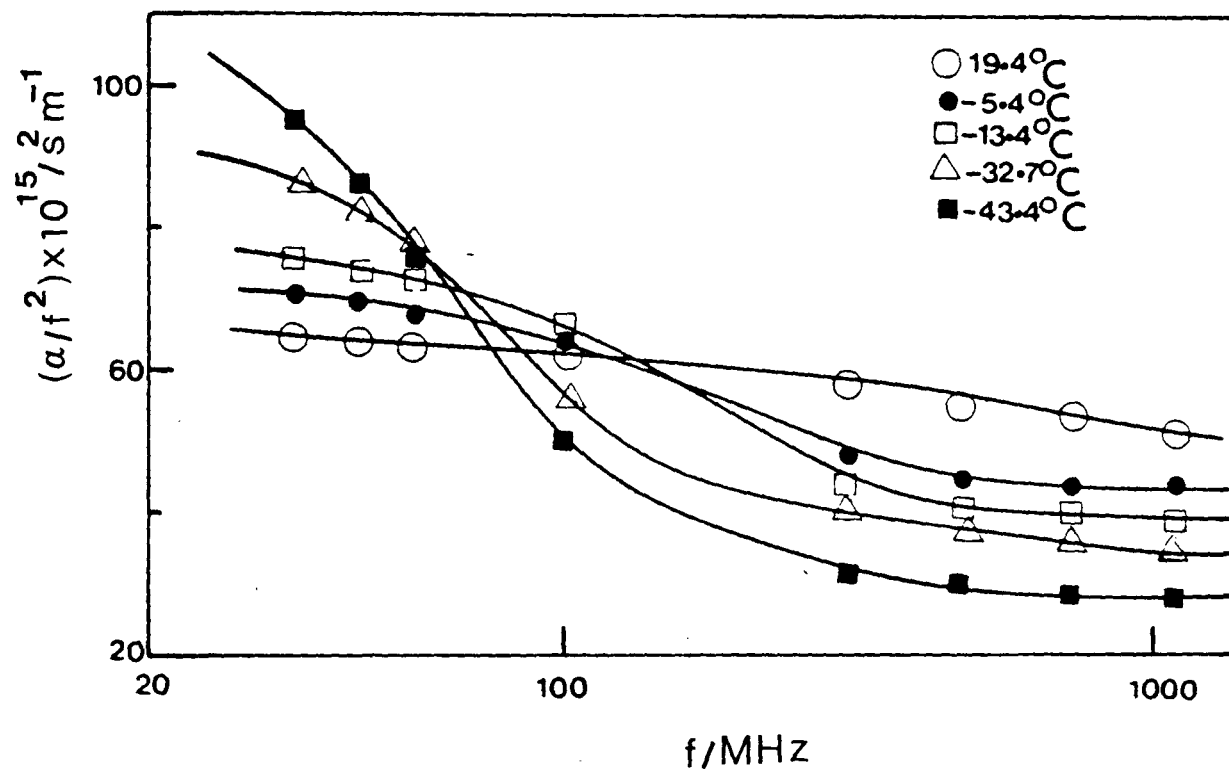


Figure 4.6. Variation of the ultrasonic absorption coefficient with frequency at various temperatures for 2,2,4-trimethylpentane.

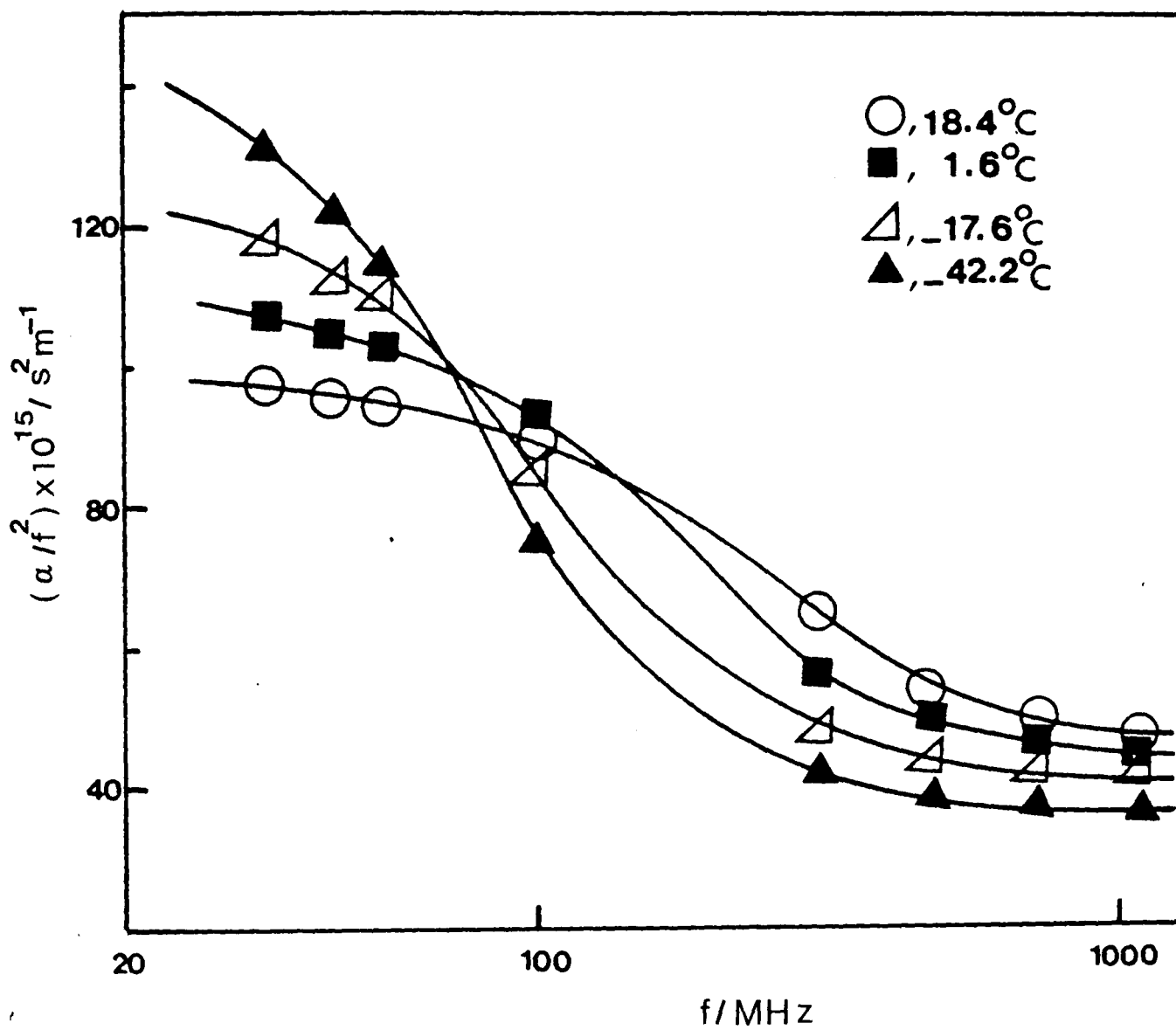


Figure 4.7. Variation of the ultrasonic absorption coefficient with frequency at various temperatures for 2,3,4-trimethylpentane.

TABLE 4.3. Ultrasonic Relaxation Parameters

Molecule	T/°C	Ax10 <sup>15</sup> /s <sup>2</sup> m <sup>-1</sup>	Bx10 <sup>15</sup> /s <sup>2</sup> m <sup>-1</sup>	f <sub>c</sub> /MHz
2-methylpentane	19.40	30	42	364
	-3.10	47	37	270
	-13.30	66	31	218
	-25.00	86	25	172
	-40.80	98	25	131
3-methylpentane	19.40	100	29	268
	0.60	124	30	174
	-10.40	162	28	135
	-19.80	221	24	110
	-40.20	261	20	55
2,3,4-trimethylpentane	19.40	53	43	275
	-1.60	68	41	183
	-17.60	82	39	132
	-42.20	115	36	80
2,2,4-trimethylpentane	19.40	12	52	265
	15.40	30	42	160
	-13.90	40	38	133
	-32.70	62	35	78
	-43.40	88	28	60
2,3-dimethylpentane	15.50	59	33	263
	-6.50	73	32	180
	-23.00	87	32	122
	-35.00	105	30	94

TABLE 4.3 (cont.)

Molecule	T/°C	$A \times 10^{15} / \text{s}^2 \text{m}^{-1}$	$B \times 10^{15} / \text{s}^2 \text{m}^{-1}$	$f_c / \text{MHz}$
2,4-dimethylpentane	16.10	55	64	202
	-3.40	90	43	150
	-22.50	116	40	103
	-41.60	138	33	66

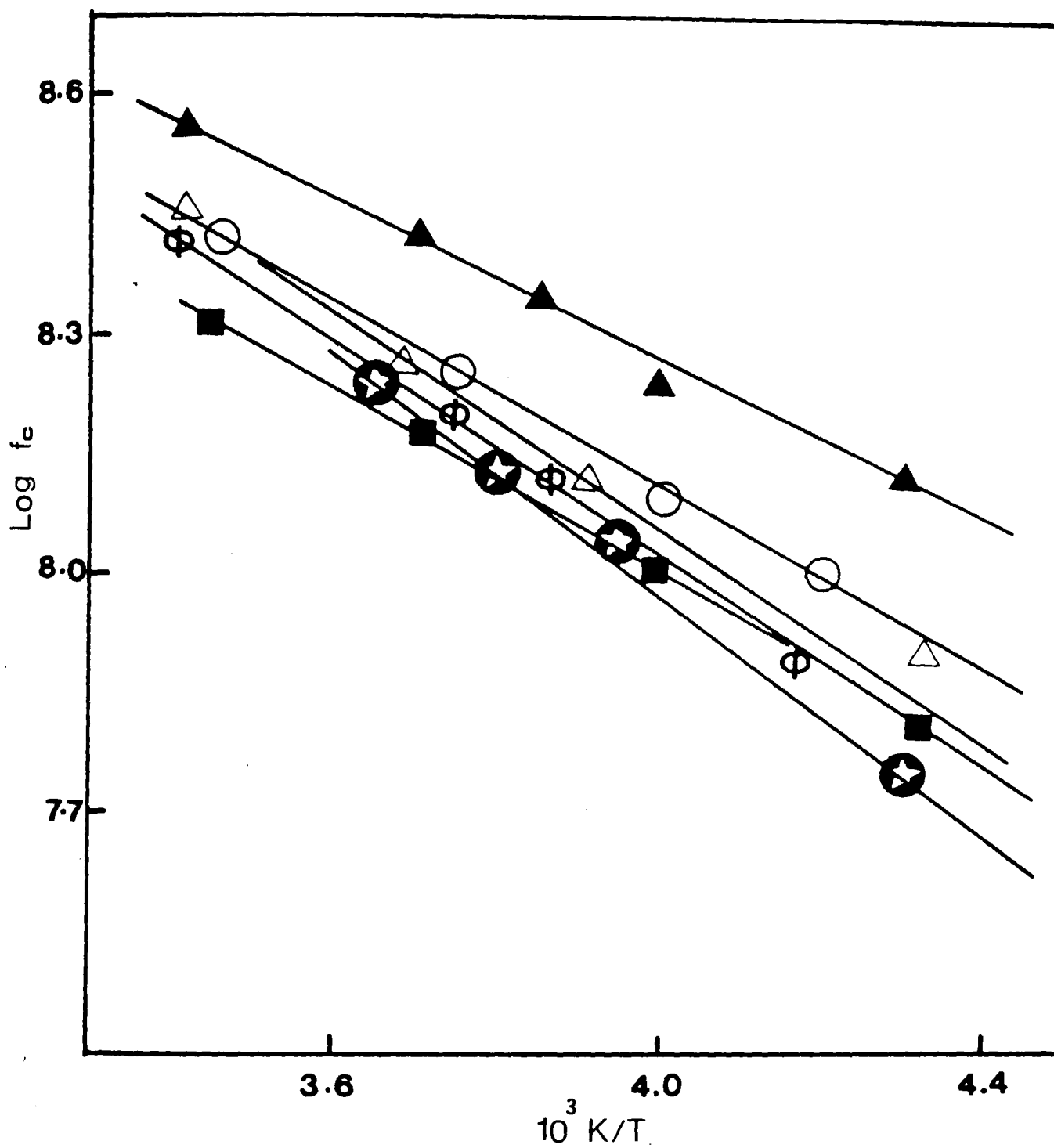


Figure 4.8. Arrhenius plot of relaxation frequencies for:

- ▲, 2-methylpentane; ○, 3-methylpentane;
- , 2,3-dimethylpentane; ⊙, 2,4-dimethylpentane
- △, 2,2,4-trimethylpentane; ⊛, 2,3,4-trimethylpentane.

TABLE 4.4. Rotational Energy Values

Molecule	$\Delta E^\ddagger/\text{kJ mol}^{-1}$	$\Delta S^\ominus/\text{J K}^{-1} \text{mol}^{-1}$	$\Delta H^\ominus/\text{kJ mol}^{-1}$
2-methylpentane	9.8	-65.6	2.6
3-methylpentane	14.9	-68.1	4.1
2,3-dimethylpentane	11.7	-68.2	4.1
2,4-dimethylpentane	10.2	-70.4	3.7
2,2,4-trimethylpentane	13.4	-68.2	1.4
2,3,4-trimethylpentane	11.2	-67.9	3.6

and its slope gives  $\Delta H^\ominus/R$ . The validity of this analysis is supported by the linearity of the plots shown in Figure 4.9, although neglect of  $\Delta V^\ominus$  must contribute an uncertainty to the values of  $\Delta H^\ominus$  and particularly  $\Delta S^\ominus$  presented in Table 4.4.

(v) Theoretical prediction of rotational energy parameters

Among the simplest phenomena caused by interactions between non-bonded atoms in molecules are the potential barriers to internal rotation about single bonds. Since these barriers have been known to exist for some time and a considerable body of experimental evidence pertaining to their size has been accumulated, they provide a convenient body of data on which to test proposed methods of calculating such interactions.

There have been a number of empirical attempts to explain the origin of a potential barrier to internal rotation<sup>158-160</sup>, none of which appears to have been entirely successful. More empirical approaches have been made by Aston et al<sup>161</sup> and French and Rasmussen<sup>162</sup> who adopted the idea of simple van der Waals' repulsion between atoms, but had to use values of known barriers to determine the repulsions, rather than calculate barriers from known repulsions. Later, the approach proposed by Mason and Kreevoy<sup>163,164</sup> showed a successful calculation of potential barriers caused by van der Waals' repulsions between non-bonded atoms or groups of atoms in

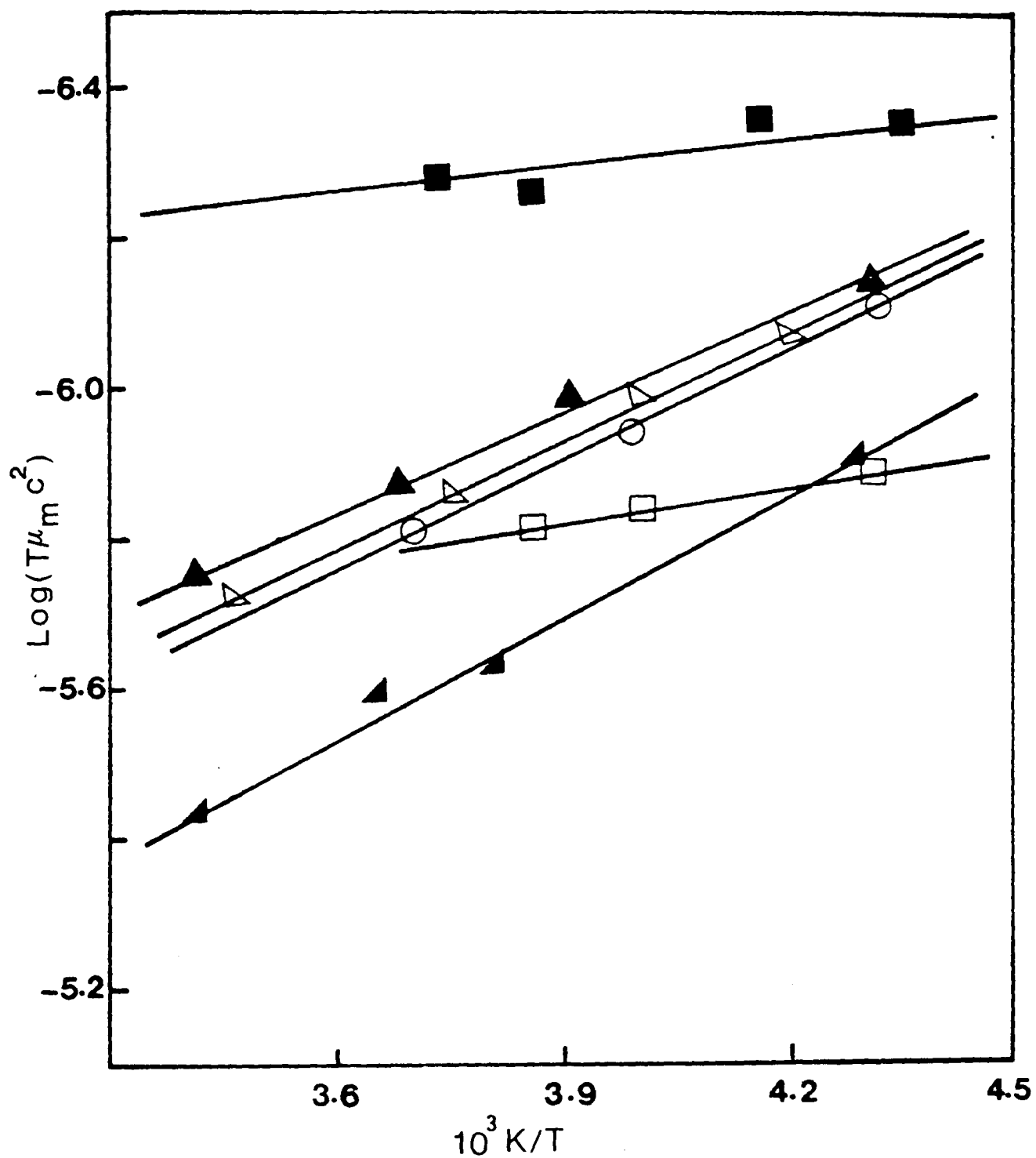


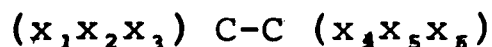
Figure 4.9. Plot of  $\log (T\mu_m/c^2)$  versus  $1/T$  for:

- , 2-methylpentane; ▲, 3-methylpentane;
- △, 2,3-dimethylpentane; ○, 2,4-dimethylpentane;
- , 2,2,4-trimethylpentane; ▲, 2,3,4-trimethylpentane.

the molecules. They have proposed that the repulsions are the same as those between similar fragments existing as free particles. For example, the force law governing the interactions between two fluorine atoms bonded to different parts of a larger molecule have been assumed to be the same as the force law governing the interactions between two isolated neon atoms and the interactions between two chlorine atoms to those between argon atoms. The form of the potential energy function proposed by Kreevoy and Mason<sup>164</sup> used a Lennard-Jones (6:12) interaction potential<sup>165</sup> to define the short range interactions, and Buckingham exponential -6 function<sup>166,167</sup> to determine the longer range interactions. Scott and Scheraga<sup>168</sup> proposed another approach for calculating potential barriers for internal rotation which includes two effects, namely non-bonded interactions and exchange interactions of the electrons in bonds adjacent to the bond about which internal rotation occurs (e.g. C-H bonds in ethane). A modified Buckingham or '6-exp' potential is used to calculate non-bonded interactions and a method is developed for obtaining the constants in the '6-exp' potential for any pair of atoms based on the experimentally available parameters for the inert gases. This approach uses an equation which is basically the same as that used by Mason and Kreevoy<sup>163</sup> and combines this with the effects of exchange interactions as proposed by Pauling<sup>169,170</sup>.

The model proposed by Scott and Scheraga is as

follows: A molecule of type



where in general all of atoms  $x_i$  could be different and where some of them may in certain cases be missing. For example, for ethane  $x_1, x_2, x_3, x_4, x_5$  and  $x_6$  are hydrogens and C is carbon. The bond between C-C is the one about which rotation occurs, the dihedral angle of internal rotation being  $\phi$ . All the bond distances and bond angles are considered fixed, thus making the molecule a rigid structure except for the one degree of rotational freedom about the C-C bond. The internal rotation angle,  $\phi$ , is considered zero in the eclipsed configuration and the minima occur at  $60^\circ, 180^\circ$  and  $300^\circ$ , the maxima occurring at  $0^\circ, 120^\circ$  and  $240^\circ$ . As mentioned before, the potential barrier includes two effects, the exchange interactions of electrons in orbitals  $x_1\text{-C}, x_2\text{-C}$  and  $x_3\text{-C}$  with orbitals  $\text{C-}x_4, \text{C-}x_5$  and  $\text{C-}x_6$  and non-bonded interactions between atoms  $x_1, x_2$  and  $x_3$  with atoms  $x_4, x_5$  and  $x_6$  and this could be expressed mathematically:

$$(V)\phi = \frac{1}{2}V_0(1+\cos\phi) + \sum_{k=1}^m \{a_k \exp(-b_k r_k) - [c_k / (r_k)^6] + (d_k / r_k)\} \quad 4.3$$

The first term on the right hand side of equation 4.3 takes account of the exchange interactions and the second term, involving the summation, the non-bonded interactions. The first term contains the parameter

$V_0$  which would be the barrier height in the absence of non-bonded interactions. According to Pauling's theory<sup>169</sup> it should be a constant for each class of molecules having the same atoms C-C, regardless of the substituent atoms. The second term which takes account of the non-bonded interactions, consists of a sum of modified Buckingham or '6-exp' functions,  $m$  is an integer. For example,  $m=9$  for  $\text{CH}_3\text{-CH}_3$  and  $m=3$  for  $\text{CH}_3\text{OH}$ . Since the molecule is considered to be rigid except for the internal rotational degree of freedom, it is necessary to calculate non-bonded interactions only of the type  $(x_1, x_2, x_3)\dots(x_4, x_5, x_6)$  and not such interactions as  $x_1 \dots x_3, x_5 \dots x_6$ . The parameters  $a_k, b_k$  and  $c_k$  are the usual ones for the '6-exp' potential but  $d_k/r_k$  is an additional term necessary for a few cases and has therefore been included<sup>163,168</sup>. The parameter  $c_k$  in equation 4.3 is obtained by using the Slater-Kirkwood equation<sup>171</sup> but replacing  $N$  by an 'effective'  $N$  as suggested by Pitzer<sup>172</sup> and therefore calculated from the Slater-Kirkwood equation:

$$c_k = \frac{3/2e(h/m^{1/2})\alpha_1\alpha_2}{(\alpha_1/N_1)^{1/2} + (\alpha_2/N_2)^{1/2}} \quad 4.4$$

where  $\alpha_1$  and  $\alpha_2$  are the atomic polarizabilities,  $e$  and  $m$  are the electronic charge and mass, and  $N_1$  and  $N_2$  are the 'effective' values for atoms 1 and 2. Values of the parameters discussed above are summarised in Table 4.5. The potential barrier for molecules of the ethane type  $V(\phi)$  was computed from equation 4.3 using the values of

parameters listed in Table 4.5.

In this study, the intramolecular potential governing internal rotation of methylpentanes was estimated using the approach proposed by Scott and Scheraga<sup>168</sup>. The same coefficients published by Scott and Scheraga<sup>168</sup> are used in this study; the only modification introduced was for the methyl group which was treated as suggested by Overend and Scherer<sup>173</sup>. A recent review by Smith<sup>174</sup> has indicated that the above combination does represent the interaction potential between non-polar groups, at least for semi-quantitative comparison with experiment and for prediction of stable rotational states. The total steric potential contribution between atoms and groups used in this study are presented in Table 4.6. In these calculations, the non-bonded intramolecular interaction is assumed to be similar to that for the intermolecular interaction between similar isoelectric species. Also the effects of polarization changes due to non-valence electrons have been neglected. The inclusion of these interactions is unlikely to change the energy differences between the states involved. It has been further assumed that the electrostatic contributions are negligible and that the geometry of the staggered state is retained in eclipsed conformations. This latter assumption probably leads to predicted rotational barriers which are artificially high, since bond angle distortion and bond lengthening

TABLE 4.5. Parameters for Non-bonded Potential Functions using 6-exp Potential Function

Interaction	$r = r_{w_1} + r_{w_2}$	$a_k$	$b_k$	$c_k$	$d_k$
H - H	2.8	$9.17 \times 10^3$	4.54	42.5	0
F - F	2.94	$6.62 \times 10^4$	4.60	118	14.4 (C-F bonds)
Cl-Cl	3.50	$3.14 \times 10^5$	3.75	2520	1.16 (C-Cl bonds)
Br - Br	3.70	$3.46 \times 10^7$	2.78	5180	0
O - O	3.04	$1.35 \times 10^5$	4.59	217	0
H - F	2.67	$1.69 \times 10^4$	4.57	62.7	0
H - Cl	2.95	$3.90 \times 10^4$	4.15	321	0
H - Br	3.05	$2.18 \times 10^4$	3.66	465	0
H - O	2.72	$2.68 \times 10^4$	4.57	90.4	0

TABLE 4.6. Total Steric Potential Contribution

Potential Between	$\phi =$	0	60	120	180
		60	300	240	360
H - H		3.03	1.48	0.42	0.21
H - Cl		4.39	1.33	0.09	-.01
H - Br		4.39	1.47	0.14	0.01
H - I		4.93	1.54	0.14	0.02
CH <sub>3</sub> - H		10.86	3.99	0.59	0.21
CH <sub>3</sub> - CH <sub>3</sub>		24.62	8.65	-.43	-.17
CH <sub>3</sub> - Cl		11.40	3.60	-.21	-.27
CH <sub>3</sub> - Br		16.96	6.26	-.16	-.3
CH <sub>3</sub> - I		24.26	7.06	-.24	-.38

will allow minimization of the energy of the eclipsed state.

In this way simplified energy-angle diagrams were obtained as illustrated in Figures 4.10 to 4.16.

#### 4.4 Discussion

Comparison of the observed values of the energy differences and activation energies to internal rotation with the potential energy profiles predicted by theory indicate that certain of the possible rotational isomeric processes can be eliminated. For instance, in 2-methylpentane, if the C(5) is eclipsed with the C(2) the profile predicts for C(2) - C(3) bond rotation an energy difference and an activation energy which are much larger than those observed. The process responsible for the acoustic relaxation is therefore interchange between the singly degenerate upper state ( $300^\circ$ ) and the doubly degenerate lower ( $60^\circ$  and  $180^\circ$ ) state of the staggered C(3) - C(4) geometry. The predicted activation energy is rather higher than that observed. However, this is partly a consequence of bond angle distortion and bond length changes. A further effect which would lead to a lowering of the activation energy when a pair of methyl rotors is involved is the so-called 'cogwheel' effect. If in forming the eclipsed state the rotation of the methyl group on C(2) is synchronized with the motion of the ethyl group a meshing of the two rotors can occur leading to a lowering of the interactions in the eclipsed state. Both the measurements and the predictions are in fair agreement

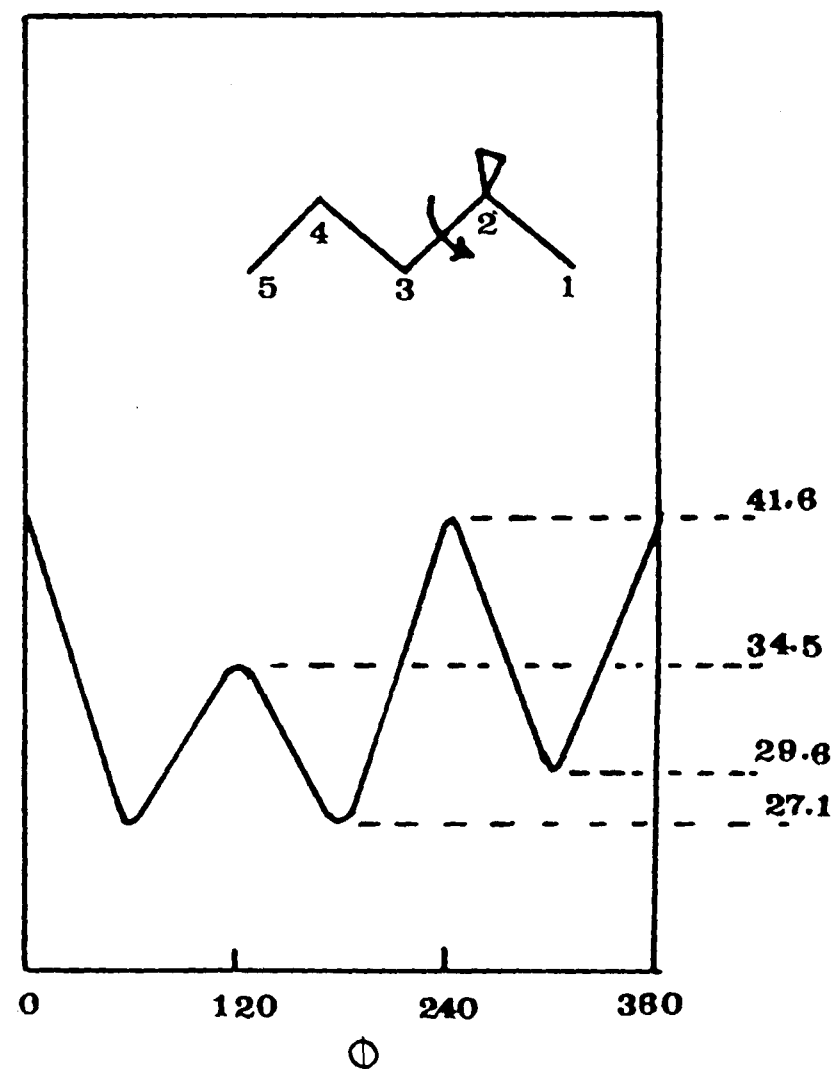
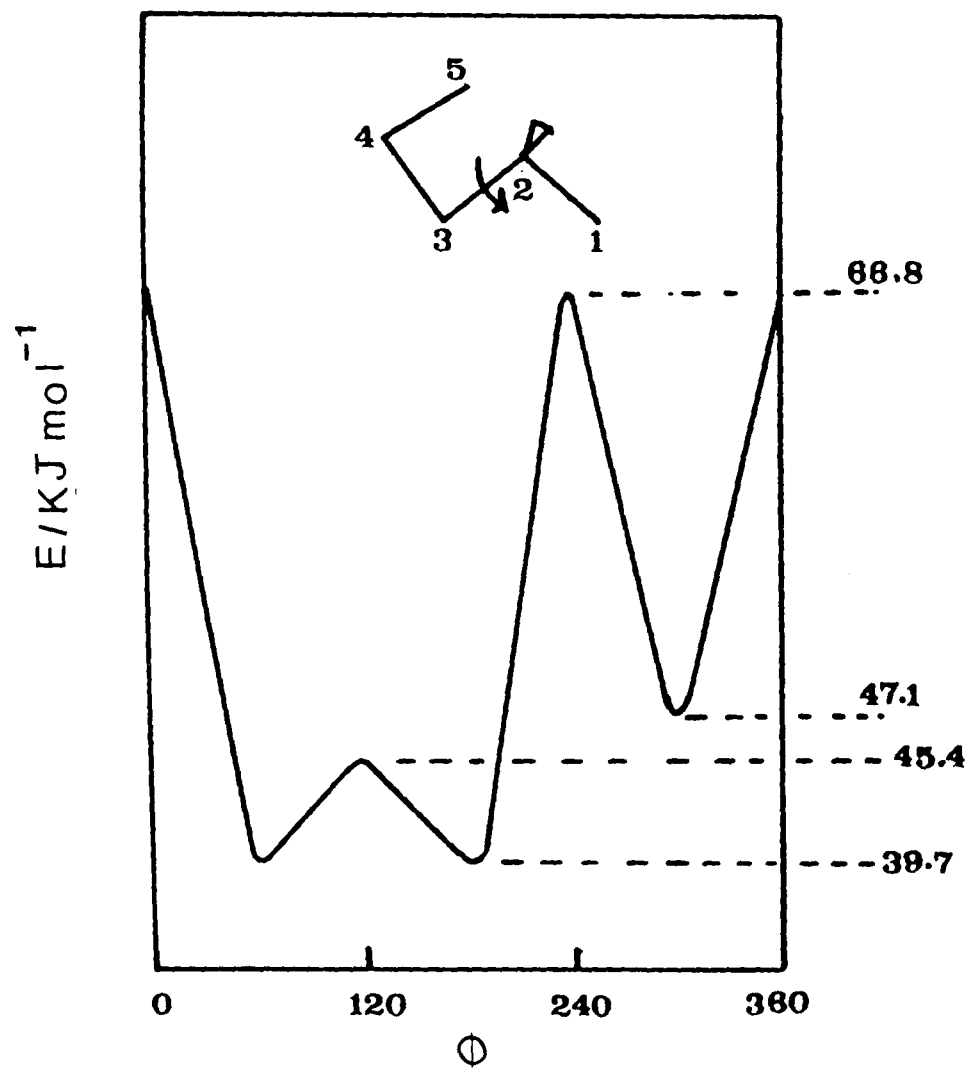


Figure 4.10. Energy-angle relationship for 2-methylpentane.

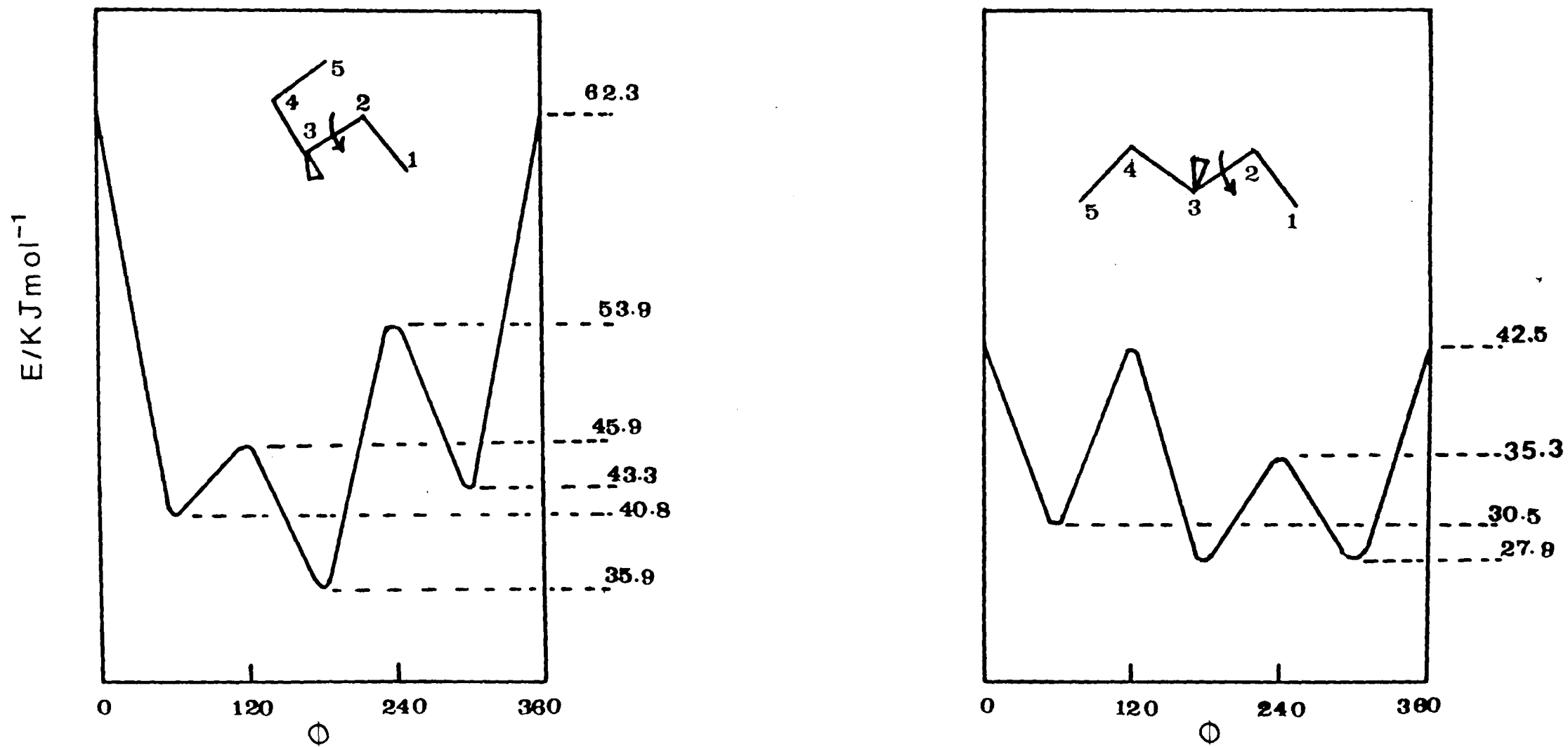


Figure 4.11. Energy-angle relationship for 3-methylpentane.

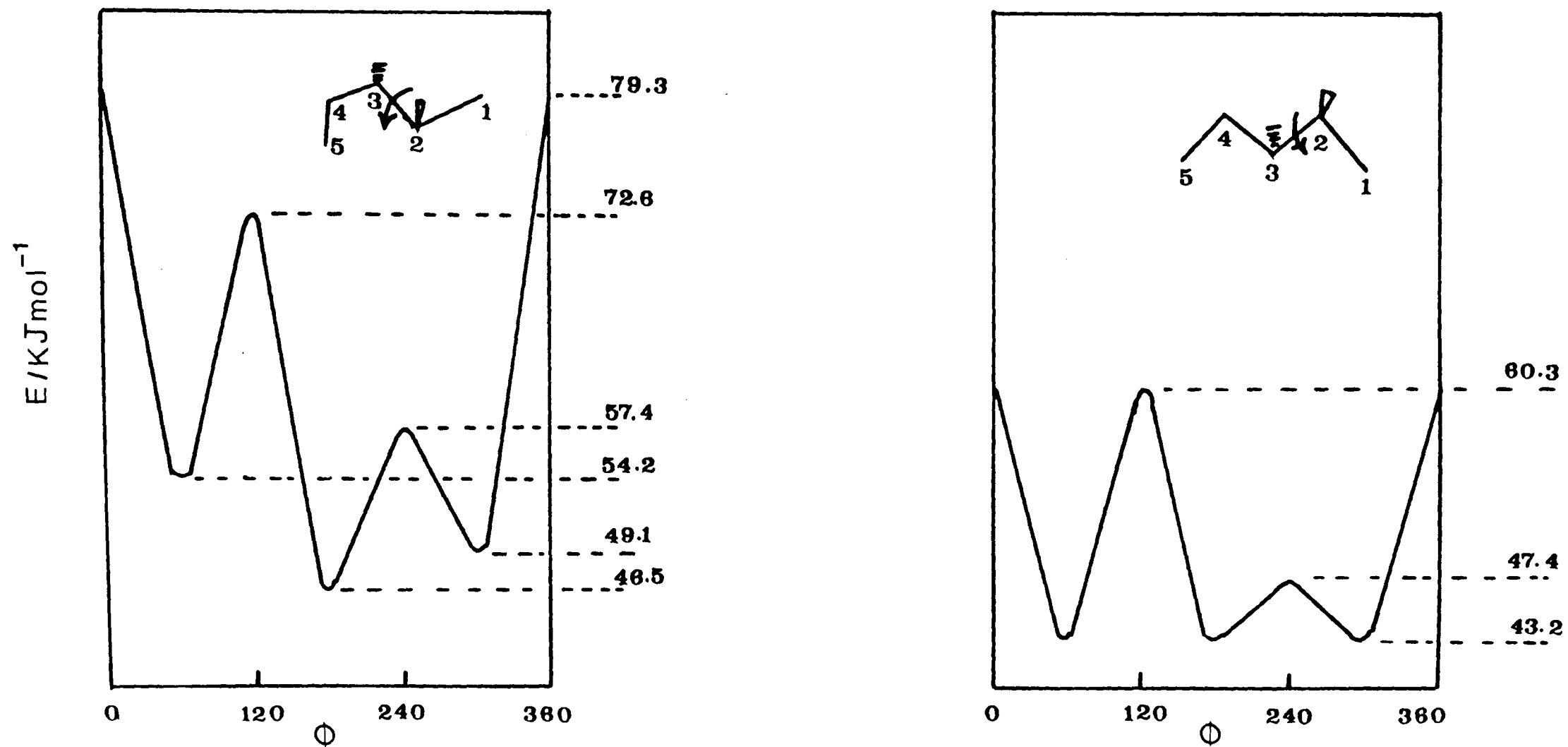


Figure 4.12. Energy-angle relationship for 2,3-dimethylpentane.

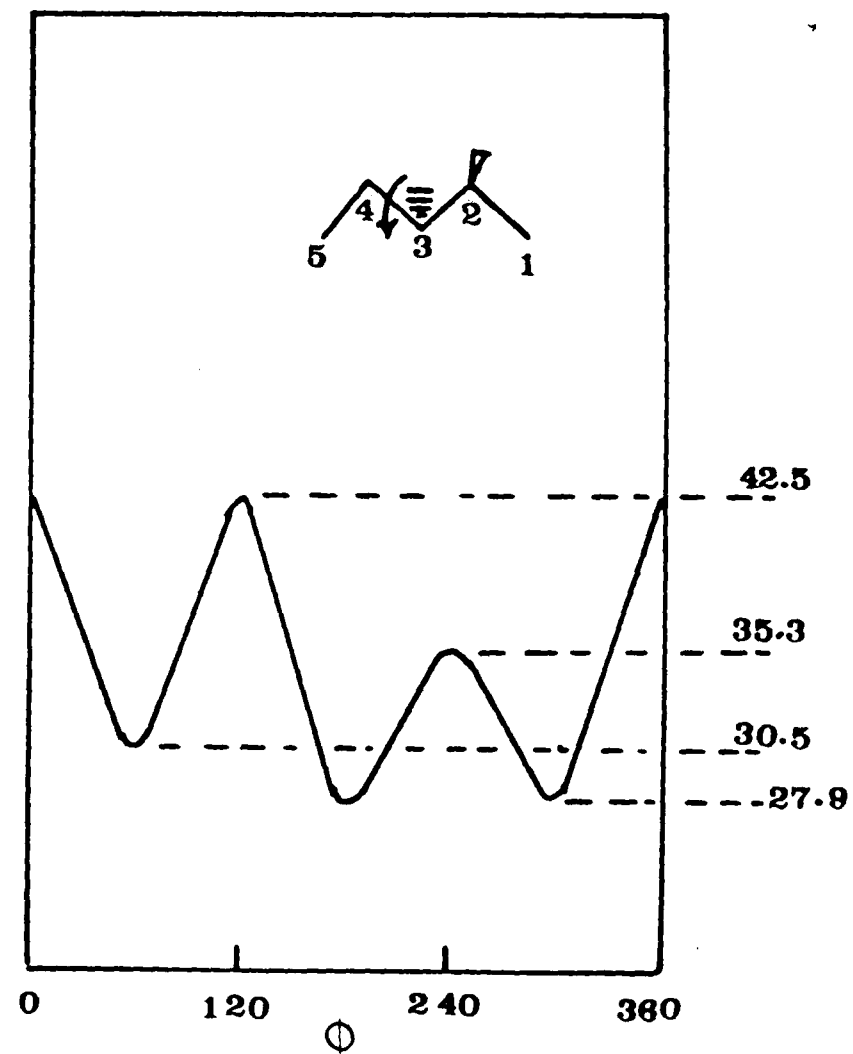
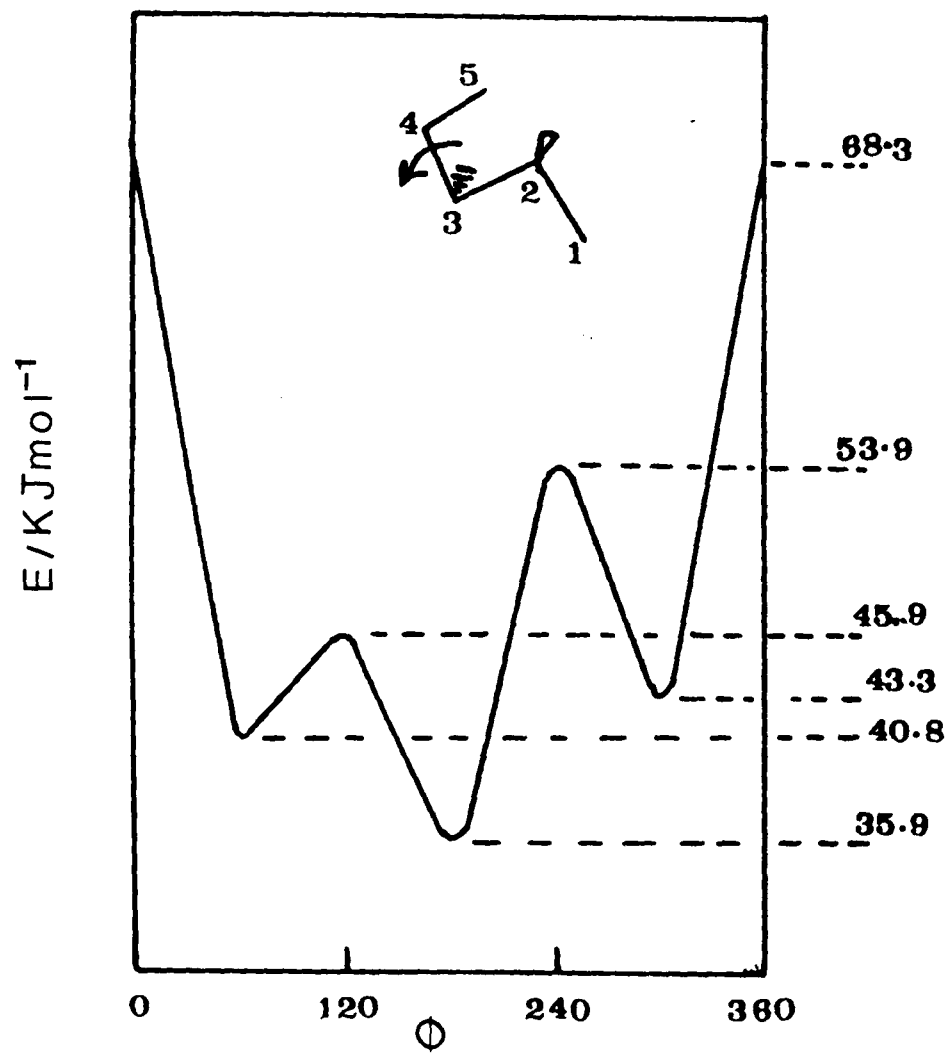


Figure 4.13. Energy-angle relationship for 2,3-dimethylpentane.

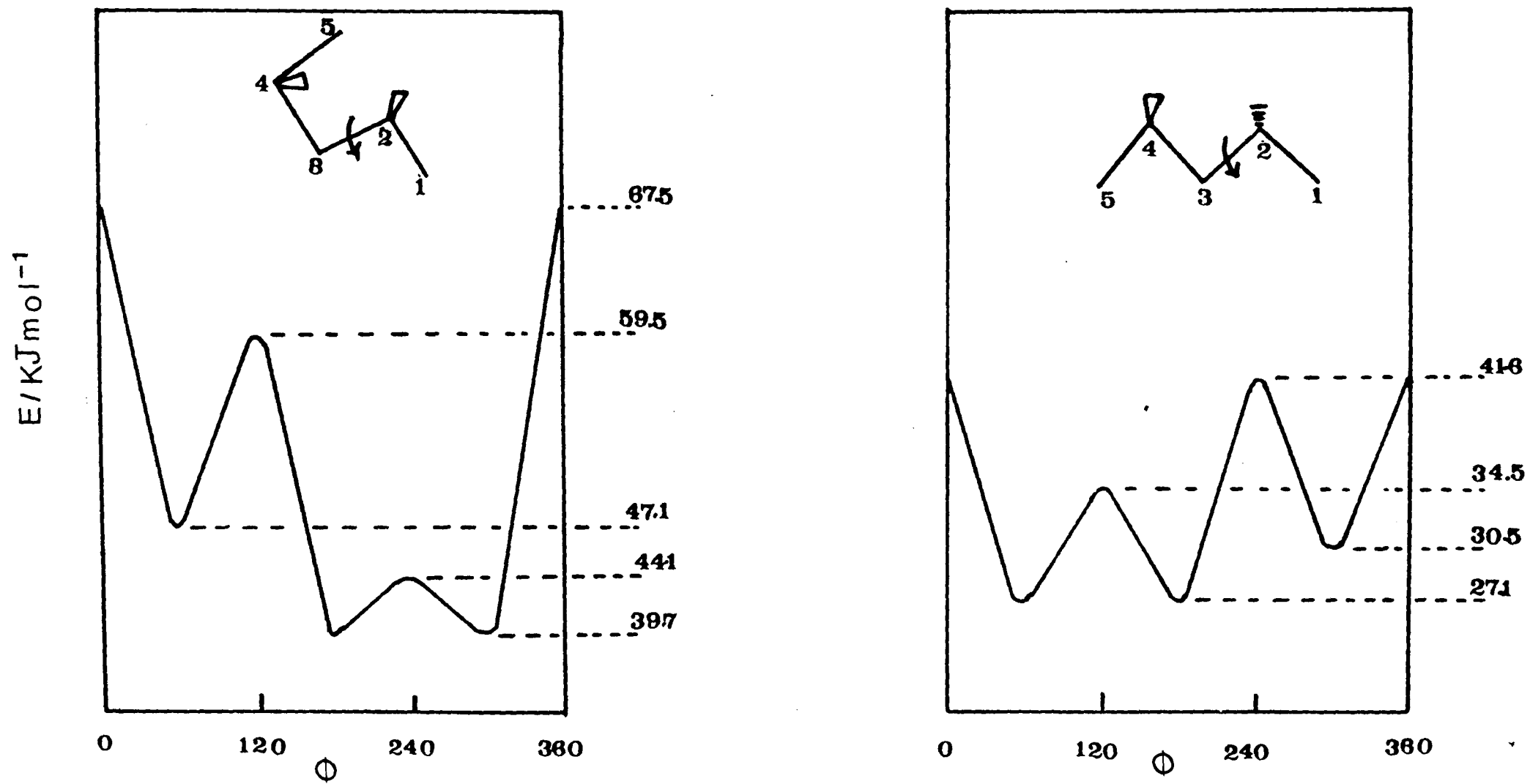


Figure 4.14. Energy-angle relationship for 2,4-dimethylpentane.

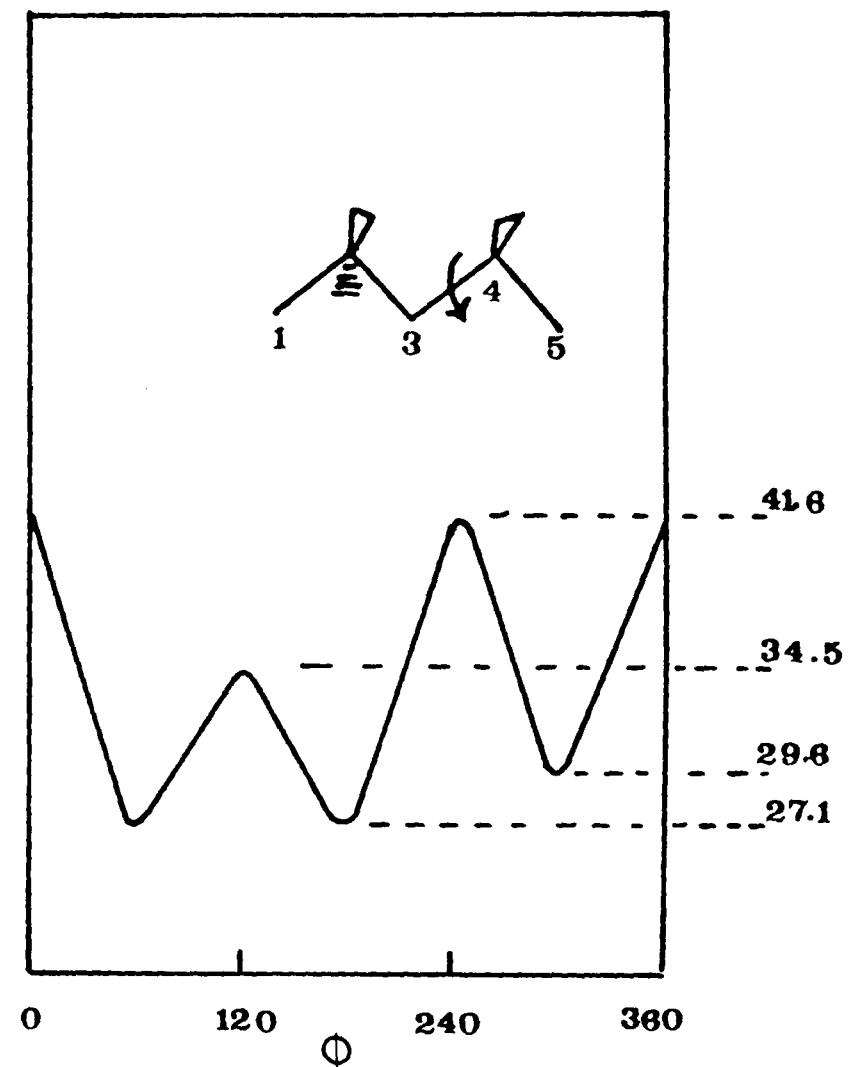
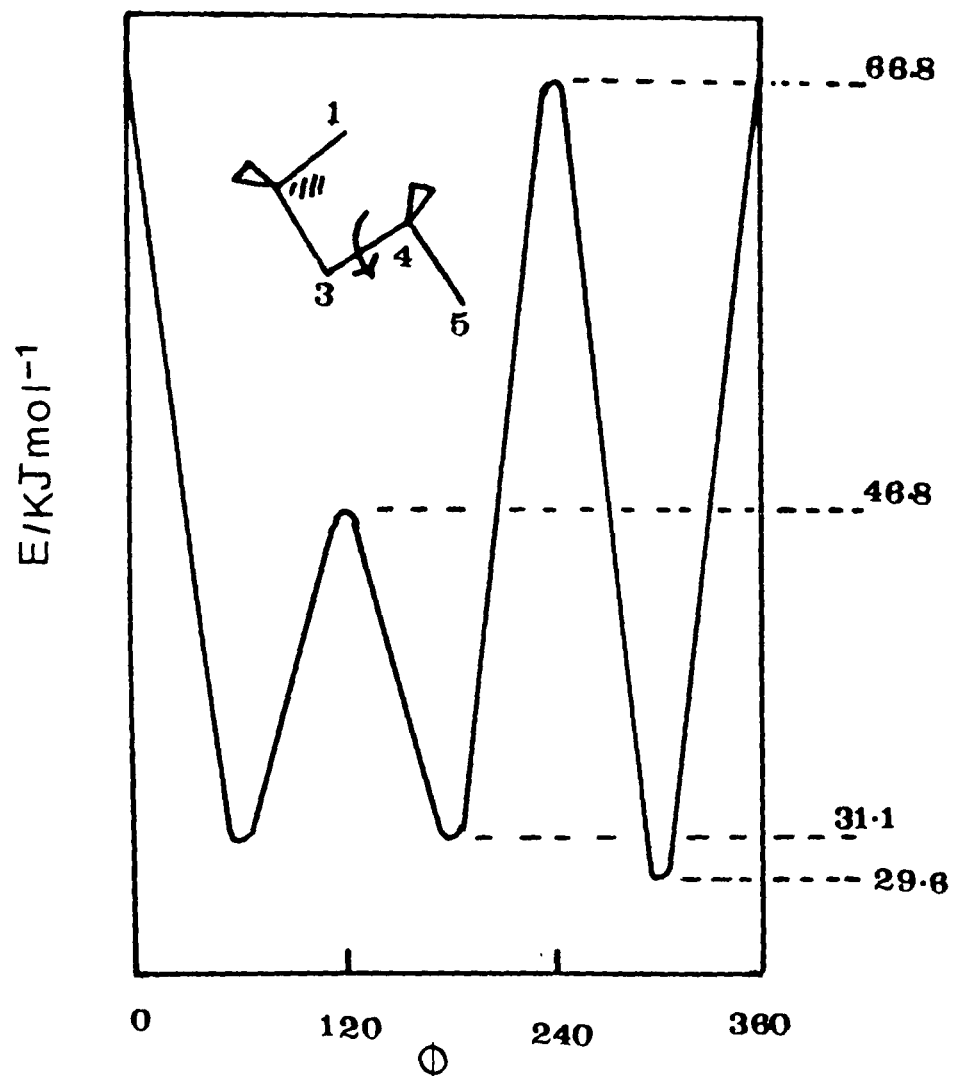


Figure 4.15. Energy-angle relationship for 2,2,4-trimethylpentane.

OGI

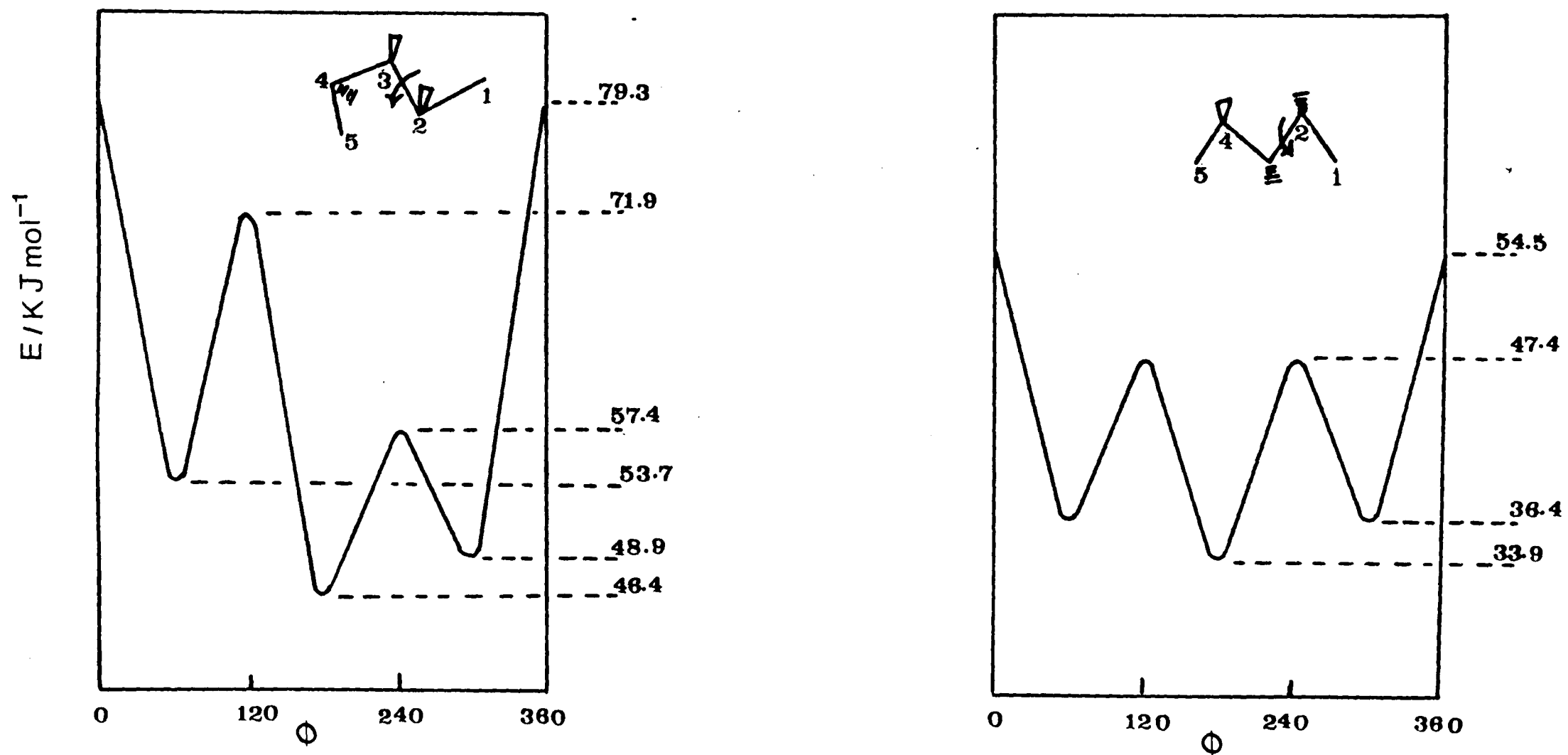


Figure 4.16. Energy-angle relationship for 2,3,4-trimethylpentane.

with the earlier studies of Chen and Petrauskas<sup>40</sup> and Cochran et al<sup>42</sup>. The earlier studies<sup>40,41</sup> were performed at low temperatures and over a limited frequency range and hence are of lower precision than these data.

In a similar way, 3-methylpentane can exhibit both gauche and trans structures of the C(5) carbon with respect to the C(3) carbon. In this case, we find that the rotation around the C(2) - C(3) bond is easier when the terminal methyl group is trans to the C(2) atom. However, the predicted energy levels show poor agreement with the experimental observation. It is probable that in this system there is a relatively high degree of coupling or meshing of the rotation of neighbouring methyl groups.

In 2,3-dimethylpentane, rotation around the C(2) - C(3) leads to the energy level diagram shown in Figure 4.12. Here the predictions are significantly greater than the experimentally observed values. Alternative calculations based on rotation about the C(3) - C(4) bond yields the alternative diagram shown in Figure 4.13. This structure is less sterically hindered and the energetics appear to be more consistent with the acoustic observations.

In 2,4-dimethylpentane there are two identical rotational energy potentials for motion about the C(3) - C(4) and C(2) - C(3) bonds. In this case the agreement between experiment and theory is good;  $\Delta H^\ominus(\text{theory}) = 3.4 \text{ kJ mol}^{-1}$  and  $\Delta H^\ominus(\text{experiment}) = 3.7 \text{ kJ mol}^{-1}$ ,  $\Delta E^\ddagger(\text{theory}) = 11.1 \text{ kJ mol}^{-1}$  and  $\Delta E^\ddagger(\text{experiment}) = 10.2 \text{ kJ mol}^{-1}$ . This appears to imply that the rotation about the

backbone occurs as two independent relaxations which are not significantly influencing one another, although intuitively it is probable that there is some synchronization of neighbouring groups during the process.

Similarly, 2,2,4-trimethylpentane, which has a plane of symmetry, exhibits good agreement between experiment and theory  $\Delta E^\ddagger(\text{theory}) = 12 \text{ kJ mol}^{-1}$  and  $\Delta E^\ddagger(\text{experiment}) = 13.4 \text{ kJ mol}^{-1}$ ,  $\Delta H^\ominus(\text{theory}) = 2.5 \text{ kJ mol}^{-1}$  and  $\Delta H^\ominus(\text{experiment}) = 1.4 \text{ kJ mol}^{-1}$ . Likewise in the case of the 2,3,4-trimethylpentane there is good agreement with the predictions of theory  $\Delta E^\ddagger(\text{theory}) = 11 \text{ kJ mol}^{-1}$ ,  $\Delta E^\ddagger(\text{experiment}) = 11.2 \text{ kJ mol}^{-1}$ ,  $\Delta H^\ominus(\text{theory}) = 2.5 \text{ kJ mol}^{-1}$  and  $\Delta H^\ominus(\text{experiment}) = 3.6 \text{ kJ mol}^{-1}$ . In both of these cases a higher value is observed in the experiment than in theory, implying that coupled rotation of the methyl rotors may contribute to the activation energy. Recent calculations<sup>175</sup> using the additivity scheme of Benson<sup>176</sup> (based on enthalpies of formation) have supported the assignment of the most stable state presented in this study.

A summary of the states contributing to the acoustically active conformation changes, together with the appropriate energetics, is provided in Table 4.7. This study of the rotational isomerism of branched chain pentanes indicates that the activation energy to internal rotation increases with the extent of steric hindrance, although the increase is less than might be expected on the basis of simple additivity of pair interactions.

TABLE 4.7. Comparison of Experimentally Determined Activation Energies and Energy Differences with the Values Predicted Theoretically.

Molecule	$\phi$	$\frac{\Delta E^\ddagger(\text{exp})}{k \text{ J mol}^{-1}}$	$\frac{\Delta E^\ddagger(\text{theor})}{k \text{ J mol}^{-1}}$	$\frac{\Delta H^\ominus(\text{exp})}{k \text{ J mol}^{-1}}$	$\frac{\Delta H^\ominus(\text{theor})}{k \text{ J mol}^{-1}}$
2-methylpentane	60,180 → 300	9.8	12	2.6	2.5
3-methylpentane	60 → 180, 300	14.9	12	4.0	2.5
2,3-dimethylpentane	C(3) - C(4)				
	60 → 180, 300	11.7	12	4.1	2.6
	180 → 300	11.7	10.6	4.1	4.9
2,4-dimethylpentane	60 → 180, 300	10.2	11.1	3.7	3.4
2,2,4-trimethylpentane	60, 180 → 300	13.4	12	1.4	2.5
	60, 180 → 300	13.4	15.7	1.4	1.5
2,3,4-trimethylpentane	60, 300 → 180	11.2	11	3.6	2.5

Surprisingly good agreement is observed for the energy differences between calculated and observed stable rotational states. However, the high negative  $\Delta S^\ominus$  values are difficult to explain on statistical grounds. Possibly the assumptions in the analysis of the acoustic data create a larger uncertainty in  $\Delta G^\ominus$  than in its temperature dependence ( $\Delta H^\ominus$ ). For this reason we emphasise the energy rather than the entropy aspects of the measurements and their analysis.

#### 4.5 Conclusions

1. The observed relaxational behaviour is attributed to perturbation by the sound wave of an equilibrium between stable rotational states.
2. The potential energy barrier restricting internal rotation and the energy difference between stable isomers is due to a single relaxation process.
3. The single relaxation process confirms the intramolecular nature of internal rotation about carbon-carbon bonds.
4. The activation energy to internal rotation increases with the extent of steric hindrance.
5. Good agreement is observed for the activation energy and energy differences between calculated and observed stable rotational states.

CHAPTER 5

ULTRASONIC STUDIES OF ROTATIONAL  
ISOMERISM IN VARIOUS METHYLHEXANES

## CHAPTER 5

### ULTRASONIC STUDIES OF ROTATIONAL ISOMERISM

#### IN VARIOUS METHYLHEXANES

##### 5.1 Introduction

In the previous chapter, ultrasonic relaxation arising from the perturbation of a chemical equilibrium by a sound wave has been observed in methylpentane. Investigations of this type provide an extension of conventional methods of studying reaction kinetics to the range of very short reaction times in the range of  $10^{-5}$  to  $10^{-9}$ s. A particular advantage of the ultrasonic technique is that if the experiments are conducted over a sufficiently wide range of temperature and frequency, it is possible to obtain directly the energy differences between stable rotational states and the activation energy associated with the reaction.

The conformational energetics obtained from ultrasonic relaxation study of six methylpentanes are compared with those predicted on the basis of non-bonded van der Waals' interactions between neighbouring groups. In general, there is agreement between the theoretical and experimental activation energy for rotation. In this chapter, experiments extending the study of conformational energetics of five methyl substituted hexanes are reported. A possible explanation for the anomalous behaviour of branched-chain hydrocarbons is due to the rotation of methyl groups about carbon-carbon bonds and

the extent of steric interaction between adjacent groups.

## 5.2 Materials

The branched-chain alkanes, 2-methylhexane, 3-methylhexane, 2,2-dimethylhexane, 2,5-dimethylhexane and 2,2,4-trimethylhexane were obtained from Fluorochem (UK) Ltd and dried over molecular sieves (BDH type 4A) before use.

Their purity was better than 99%. The densities, refractive indices and ultrasonic velocities are presented in Table 5.1. The data obtained are in good agreement with those published in the literature<sup>152-156,177,178</sup>.

## 5.3 Results

### (i) Viscosities and Densities

The measured viscosities, Figure 5.1, and densities over the whole temperature range of 253 to 313K were fitted to the empirical equations 4.1 and 4.2 and the adjustable parameters are listed in Table 5.2.

### (ii) Isoentropic (Adiabatic) Compressibilities

The sound velocities and hence the isoentropic compressibilities were measured as a function of temperature and the data will be discussed later.

### (iii) Ultrasonic Relaxation

The ultrasonic absorption coefficient as a function of temperature and frequency is presented in Figures 5.2 to 5.6. The variation of the absorption coefficient with frequency can be expressed by equation 2.8. Computer fits to the experimental data for each compound yielded the adjustable parameters summarised in

TABLE 5.1. Densities,  $\rho$ , refractive indices,  $n_D$ , and ultrasonic velocities,  $c$ , of liquids studied at 293K.

Component	$\rho/\text{g cm}^{-3}$		$n_D$		$c/\text{ms}^{-1}$	
	obs.	lit.	obs.	lit.	obs.	lit.
2-methylhexane	0.67888	0.6785 0.6789	1.38487	1.38485	1126.9	1120 1121
3-methylhexane	0.68739	0.6870	1.38867	1.38864	1148.2	1136 1141 1145
2,2-dimethyl- hexane	0.69538	0.6953 0.6952	1.39352	1.39349	1138.2	1135
2,5-dimethyl- hexane	0.69384	0.6930 0.6935	1.39249	1.39246	1141.8	1137 1133
2,2,4-trimethyl- hexane	0.71567	0.7156	1.40335	1.4033	1164.9	-

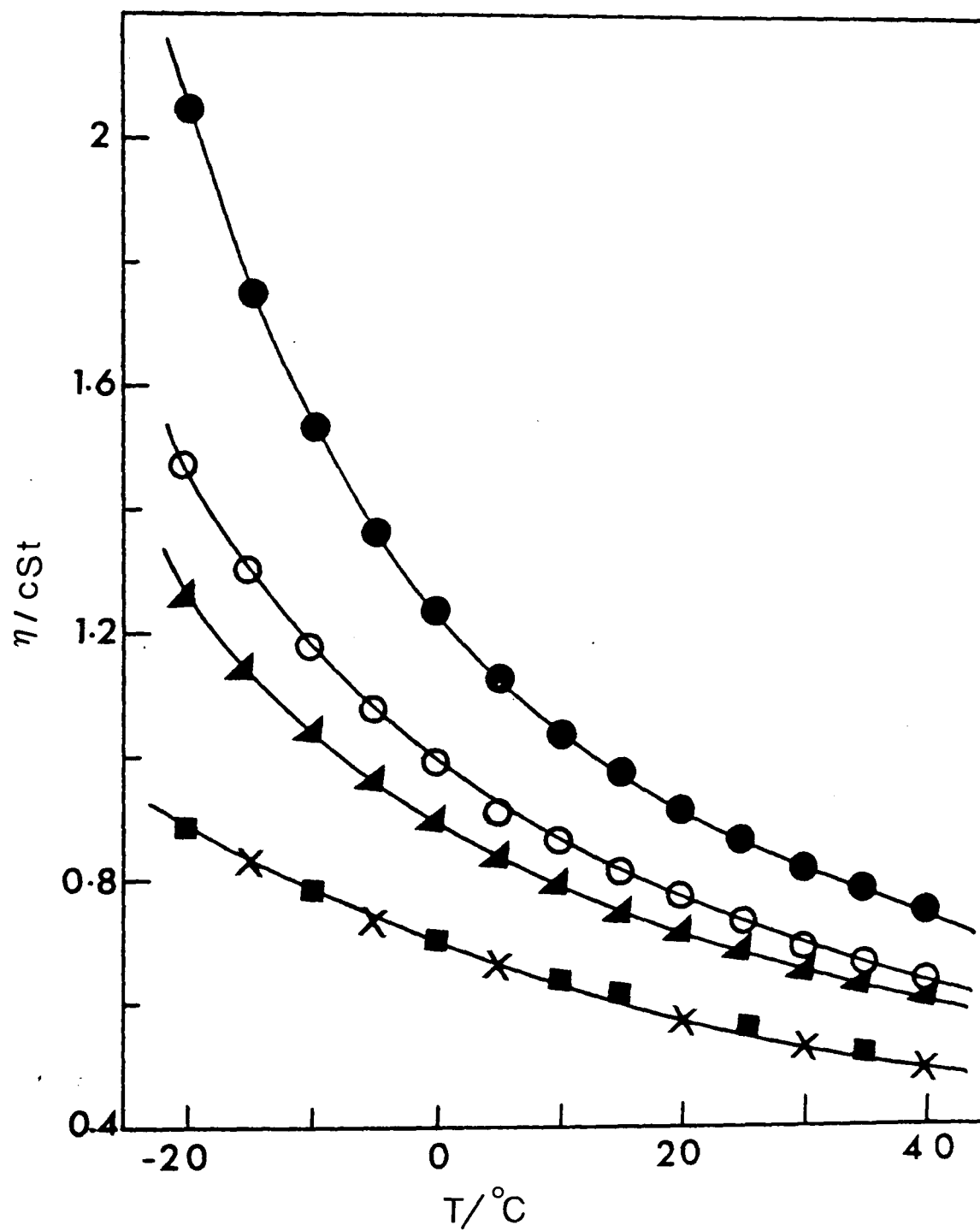


Figure 5.1. Variation of viscosity with temperature for:  
 ■, 2-methylhexane ; ×, 3-methylhexane ; ○, 2,2-dimethylhexane; ▲, 2,5-dimethylhexane; ●, 2,2,4-trimethylhexane.

TABLE 5.2. Viscosity and density temperature dependence parameters.

	2-methyl- hexane	3-methyl- hexane	2,2-dimethyl- hexane	2,5-dimethyl- hexane	2,2,4-trimethyl- hexane
$A_V$	-2.04	-1.98	-1.42	-1.53	-1.24
$B_V$	274	243	127	167	112
$T_O$	111	123	182	150	195
$A_d$	0.696	0.704	0.712	0.710	0.730
$B_d \times 10^4$	-8.52	-8.53	-8.37	-8.18	-7.56

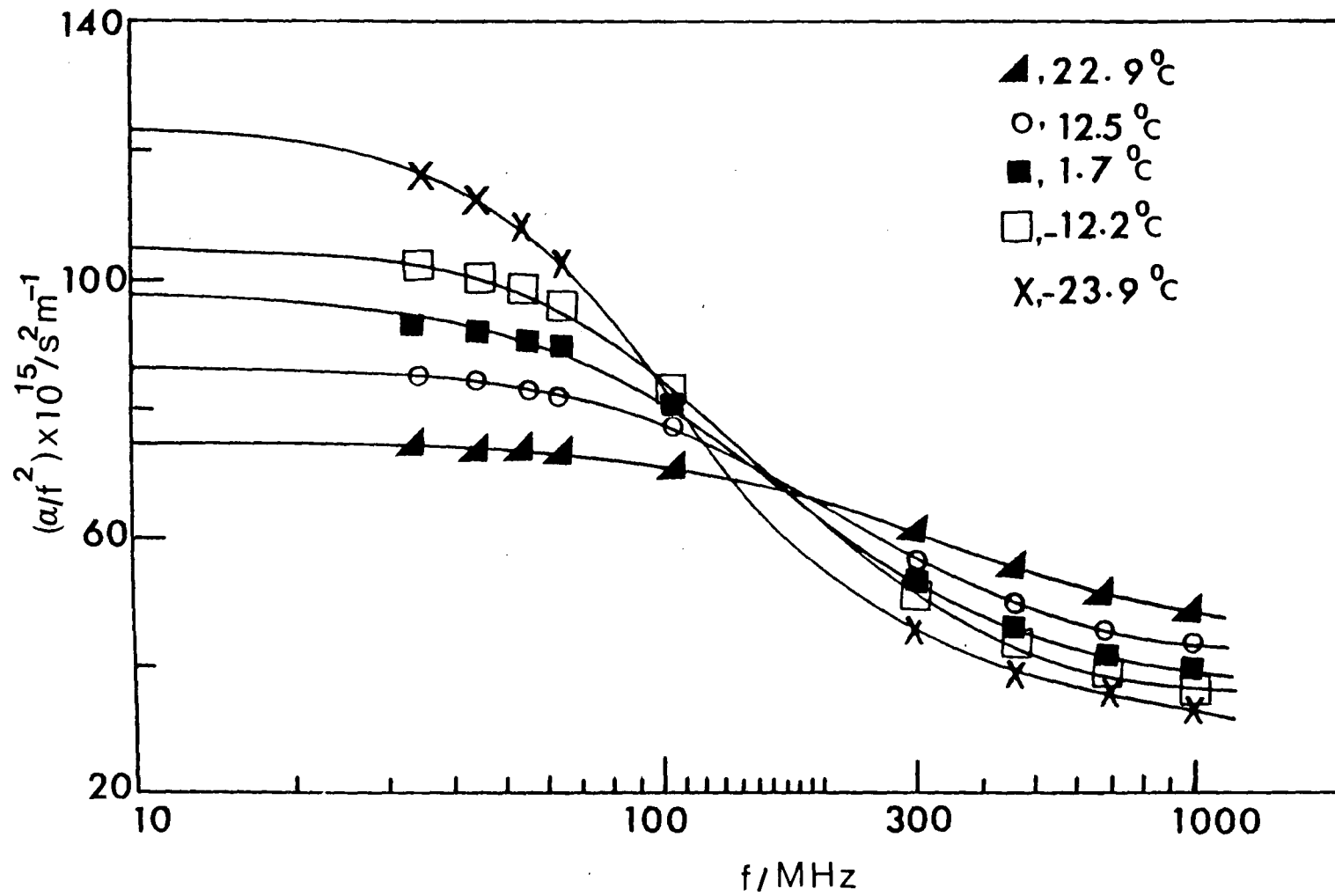


Figure 5.2. Variation of the ultrasonic absorption coefficient with frequency at various temperatures for 2-methylhexane.

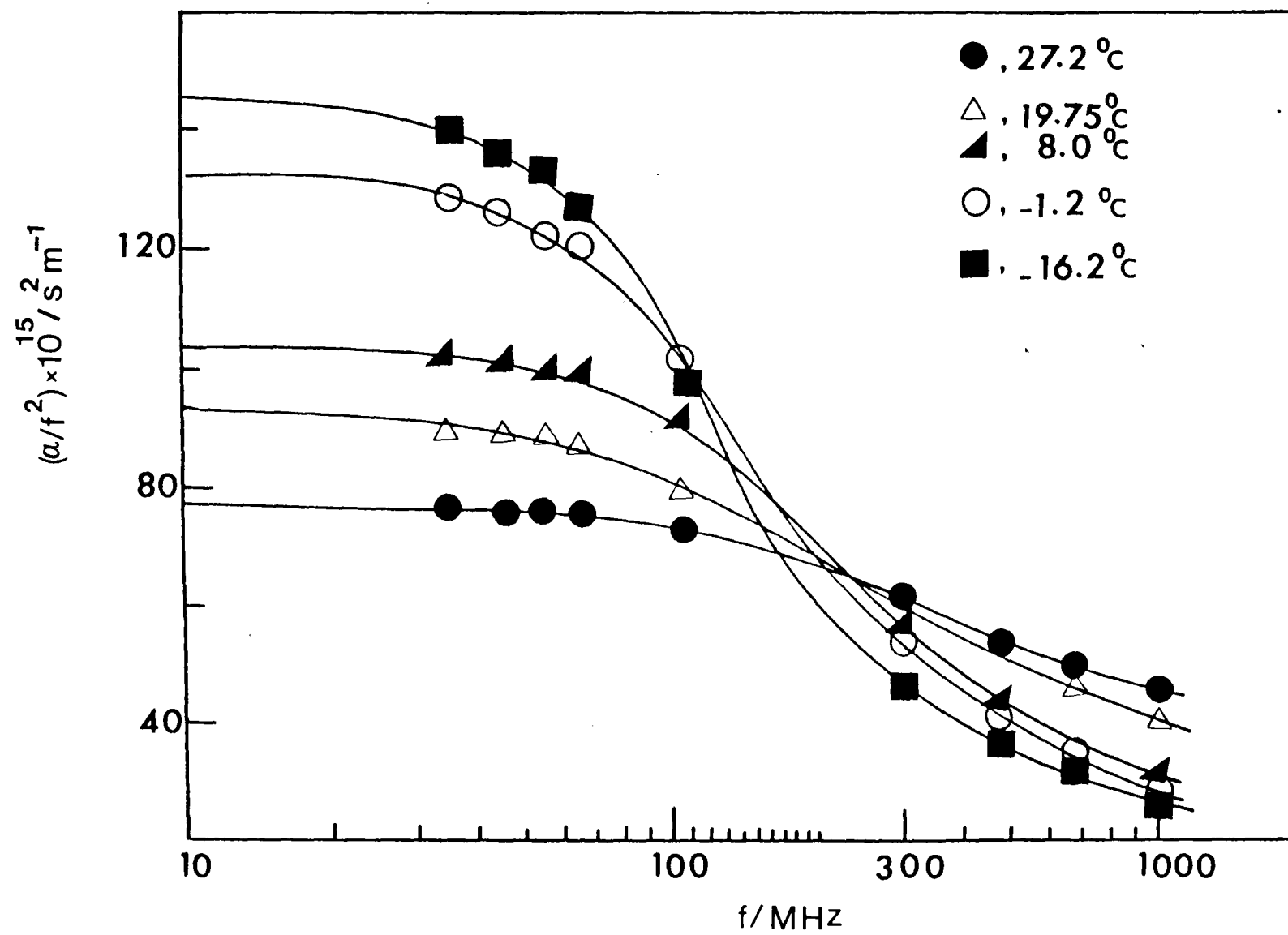


Figure 5.3. Variation of the ultrasonic absorption coefficient with frequency at various temperatures for 3-methylhexane.

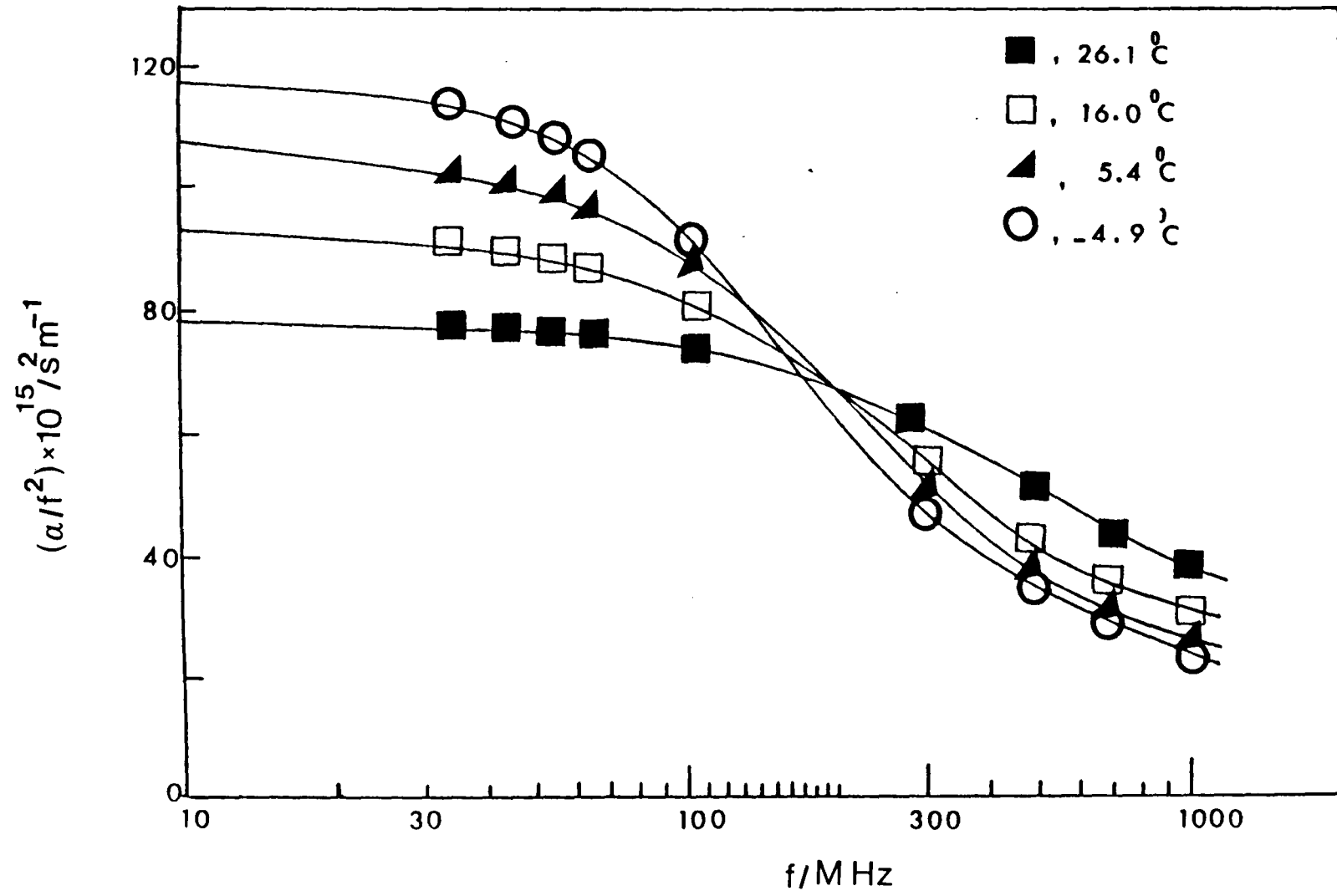


Figure 5.4. Variation of the ultrasonic absorption coefficient with frequency at various temperatures for 2,2-dimethylhexane.

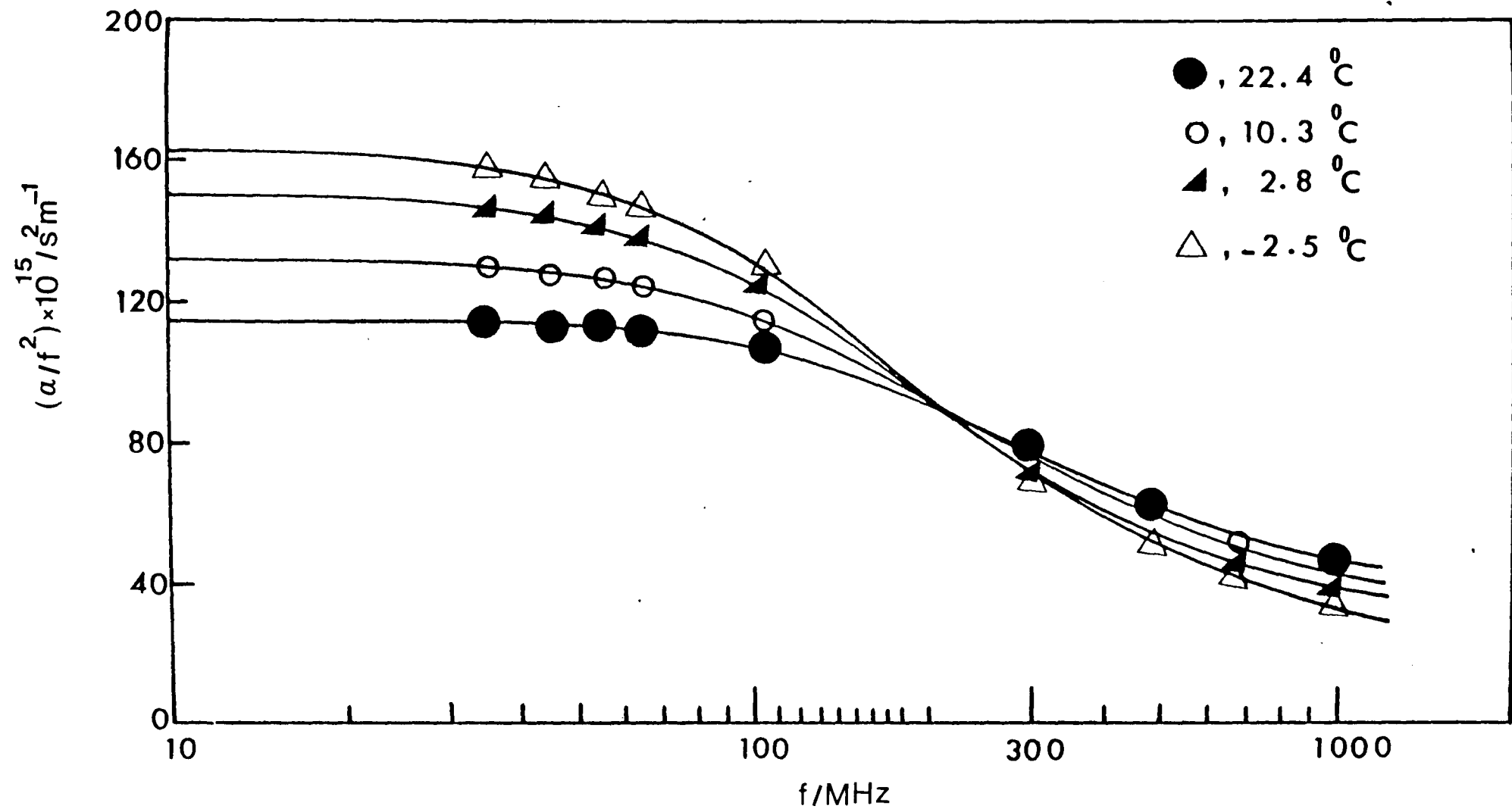


Figure 5.5. Variation of the ultrasonic absorption coefficient with frequency at various temperatures for 2,5-dimethylhexane.

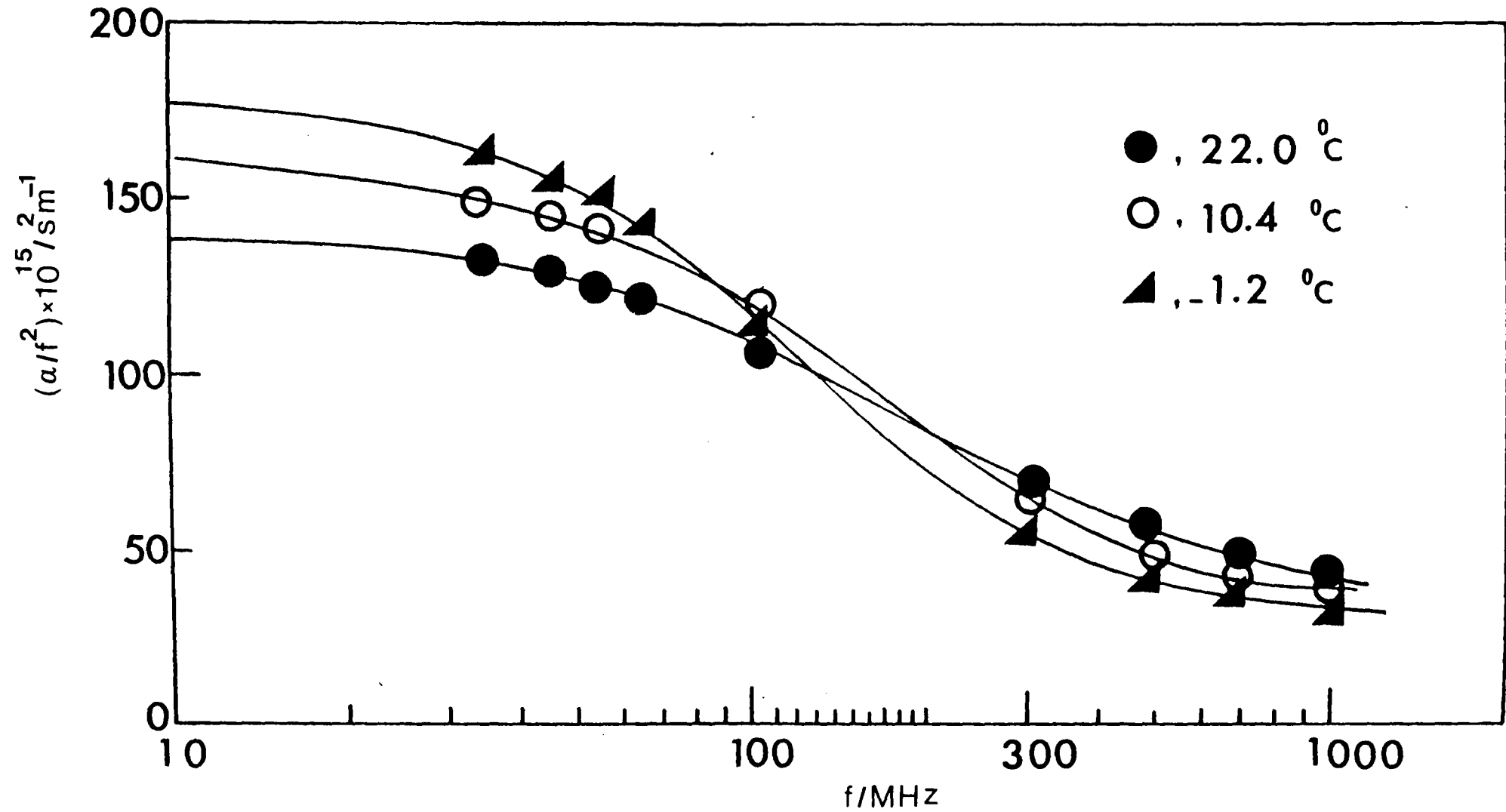


Figure 5.6. Variation of the ultrasonic absorption coefficient with frequency at various temperatures for 2,2,4-trimethylhexane .

Table 5.3.

Continuing the analysis as discussed in section 4.3(iv), the required linear dependence of log relaxation frequency ( $\log f_c$ ) and of  $\log(T\mu_{\max}/c^2)$  on  $T^{-1}$  are illustrated in Figures 5.7 and 5.8 respectively and the derived energy parameters are summarised in Table 5.4. The above analysis assumes that the volume changes,  $\Delta V^\ominus$  associated with the rotational isomeric process are negligible. This need not necessarily be the case and hence the values of  $\Delta H^\ominus$  and  $\Delta S^\ominus$  are subject to some uncertainty.

(iv) Theoretical Prediction of Rotational Energy Parameters

Unlike the previous systems, methylpentanes investigated, rotations about more than two bonds have to be considered to include all possible isomeric states. However, the linear portion of the hydrocarbon chain will exhibit a rotational isomeric potential closely resembling that of the unbranched hydrocarbons, with  $\Delta E^\ddagger$  and  $\Delta H^\ominus$  known to be considerably lower than those associated with rotation about the more hindered methyl-substituted bonds. In the hexanes, in all but one case, the problem thus reduced to consideration of rotational motion about the two bonds C(2) - C(3) and C(3) - C(4).

The inter-group potentials used in the calculations, their applicability and their deficiencies are discussed in the previous chapter. These calculations are believed to provide a useful basis for the representation of the changes in the potential energy as a function of azimuthal

TABLE 5.3. Ultrasonic relaxation parameters

Molecule	T/°C	$A \times 10^{15} / \text{s}^2 \text{m}^{-1}$	$B \times 10^{15} / \text{s}^2 \text{m}^{-1}$	$f_c / \text{MHz}$
2-methylhexane	22.9	28	46.5	300
	12.5	45	40	240
	1.7	56.5	37.5	200
	-12.2	70	35	170
	-23.9	89	33	120
3-methylhexane	27.2	33	43	330
	19.75	48	37	295
	8.0	77	27	255
	-1.2	107	25	180
	-16.2	124	26	140
2,2,4-trimethylhexane	22.0	90	42	200
	10.4	118	36	160
	-1.2	138	36	120
2,5-dimethylhexane	22.4	71	43	300
	10.3	90	39.5	250
	2.8	111	38	200
	-2.5	129	33	180
2,2-dimethylhexane	26.10	43	34	370
	16.00	63	27	270
	5.4	79	25	220
	-5.9	94	22	190

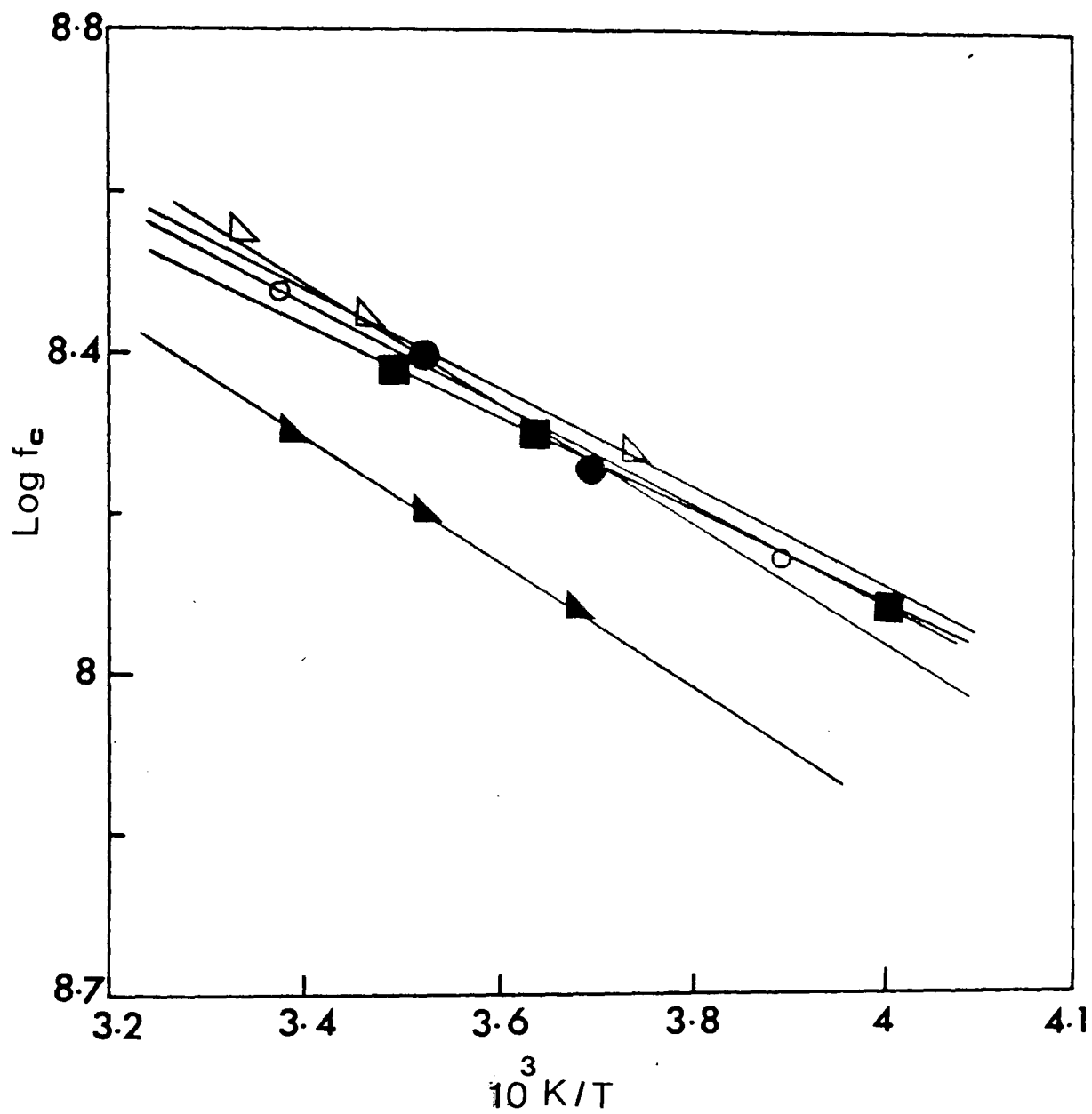


Figure 5.7. Arrhenius plot of relaxation frequencies for: ■, 2-methylhexane; ○, 3-methylhexane; △, 2,2-dimethylhexane; ●, 2,5-dimethylhexane; ▲, 2,2,4-trimethylhexane.

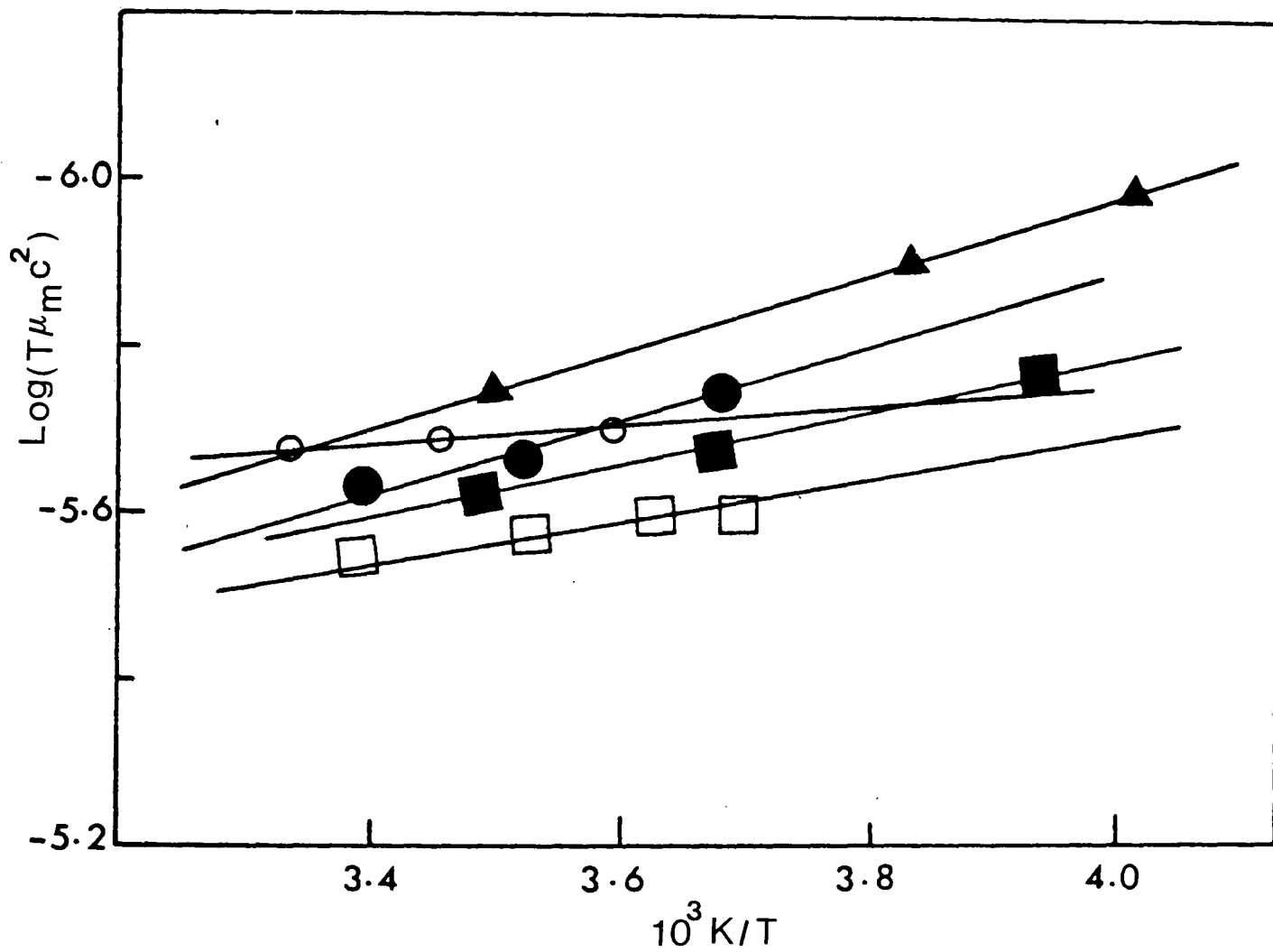


Figure 5.8. Plot of  $\log (T\mu_m/c^2)$  against  $\frac{1}{T}$  for:  
 ▲, 2-methylhexane; ■, 3-methylhexane; ○, 2,2-dimethylhexane; □, 2,5-dimethylhexane; ●, 2,2,4-trimethylhexane.

TABLE 5.4. Rotational Energy Values

Molecule	$\Delta E^\ddagger$ /KJ mol <sup>-1</sup>	$\Delta S^\ominus$ /JK <sup>-1</sup> mol <sup>-1</sup>	$\Delta H^\ominus$ /KJ mol <sup>-1</sup>
2-methylhexane	11.3	-105.5	3.6
3-methylhexane	13.2	-110.6	2.9
2,2-dimethylhexane	13.6	-114.8	0.8
2,5-dimethylhexane	14	-114.7	1.2
2,2,4-trimethylhexane	14.7	-116.7	3

angle although since they are derived from inert gas fields they may not be considered to be absolute. Preliminary quantum mechanical calculations have indicated that these semi-empirical calculations are quantitatively correct.

The resulting energy profiles are presented in Figures 5.9 to 5.13 and  $\Delta E^\ddagger$  and  $\Delta H^\ominus$  values compared with experimental quantities in Table 5.5.

#### 5.4 Discussion

In the calculations presented in Figures 5.9 to 5.13 it has been assumed that the linear 'tails' of the molecules adopt an all-trans structure. Clearly, since the activation energy for the rotational isomerism of this part of the molecule is relatively low, ca. 8 kJ mol<sup>-1</sup>, the minimum energy structure can be rapidly achieved when rotations occur about the more hindered C(2) - C(3) or C(3) - C(4) bonds. In support of this assumption, ultrasonic studies of linear hydrocarbons have indicated that conformational changes at room temperature occur at rates greater than 10<sup>8</sup> sec<sup>-1</sup> and contribute only a small increment to the observed attenuation.

2-methylhexane. Reasonable agreement between theory and experiment is obtained for  $\Delta E^\ddagger$  by assuming that the process corresponds to rotation about the C(2) - C(3) bond, involves the doubly degenerate 60°, 180° states and the 300° state. The discrepancy between experiment and theory for the rather small  $\Delta H^\ominus$  probably reflects inadequacies in the form of the potential function used

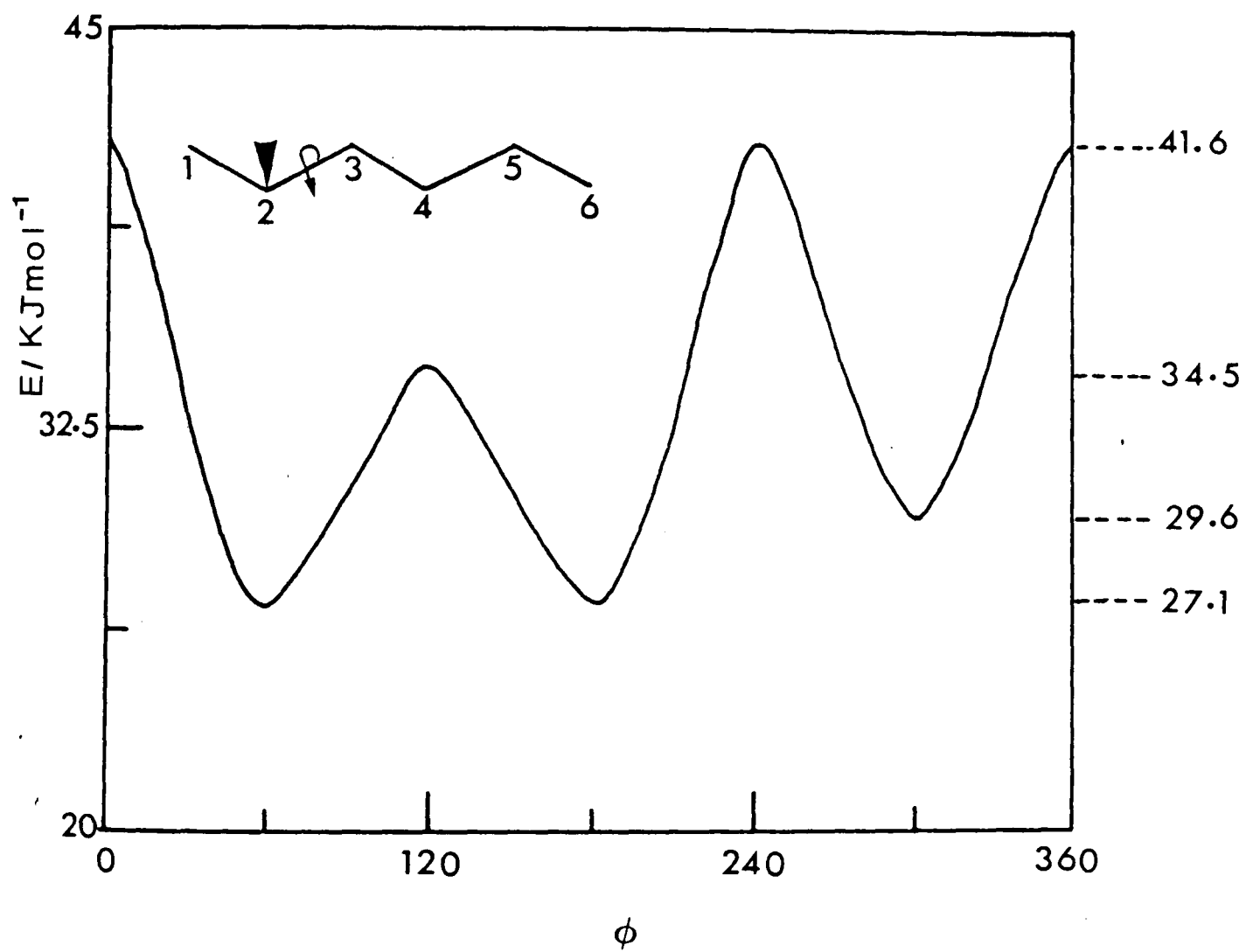


Figure 5.9. Energy-angle relationship for 2-methylhexane.

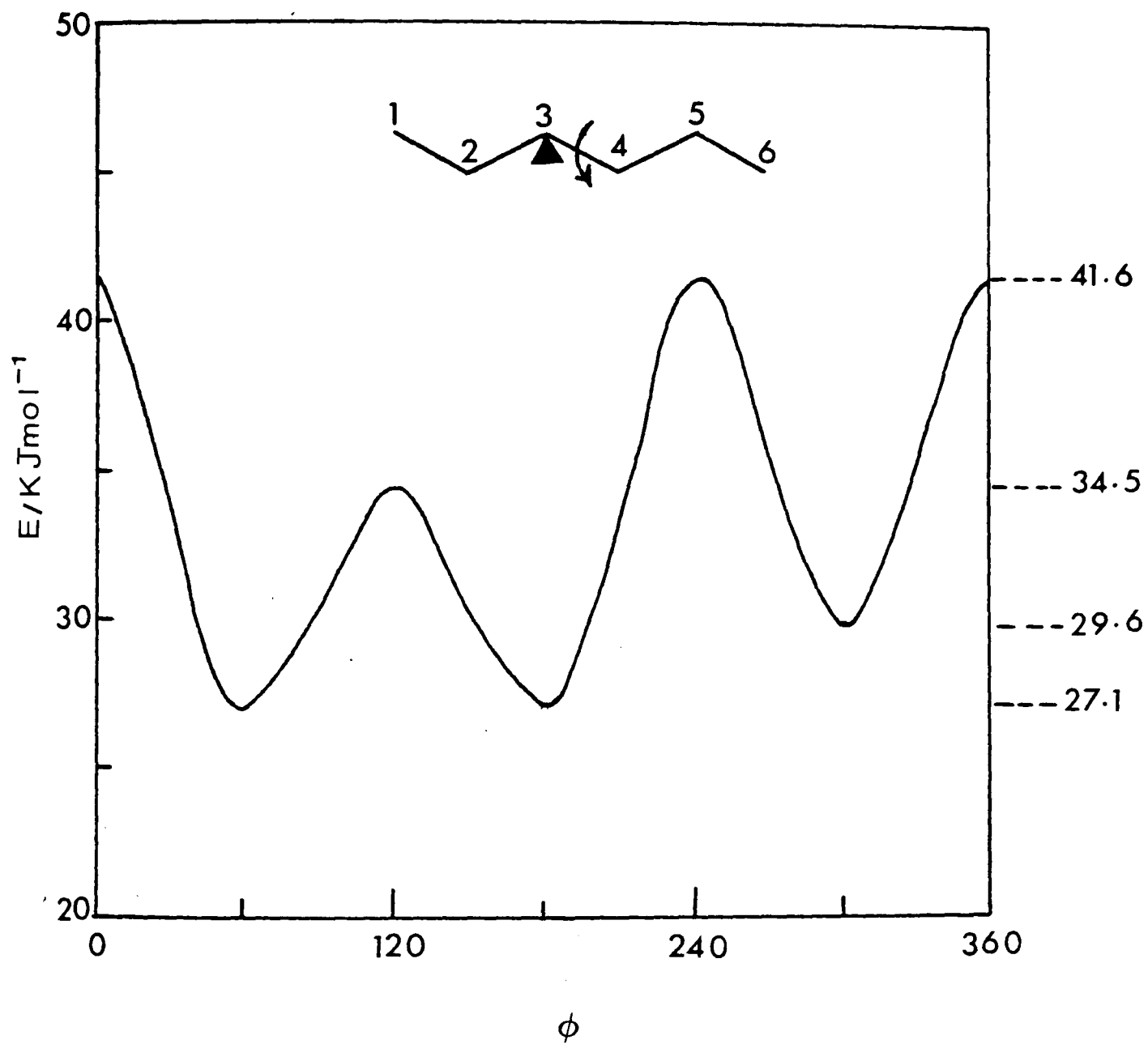


Figure 5.10a. Energy-angle relationship for 3-methylhexane.

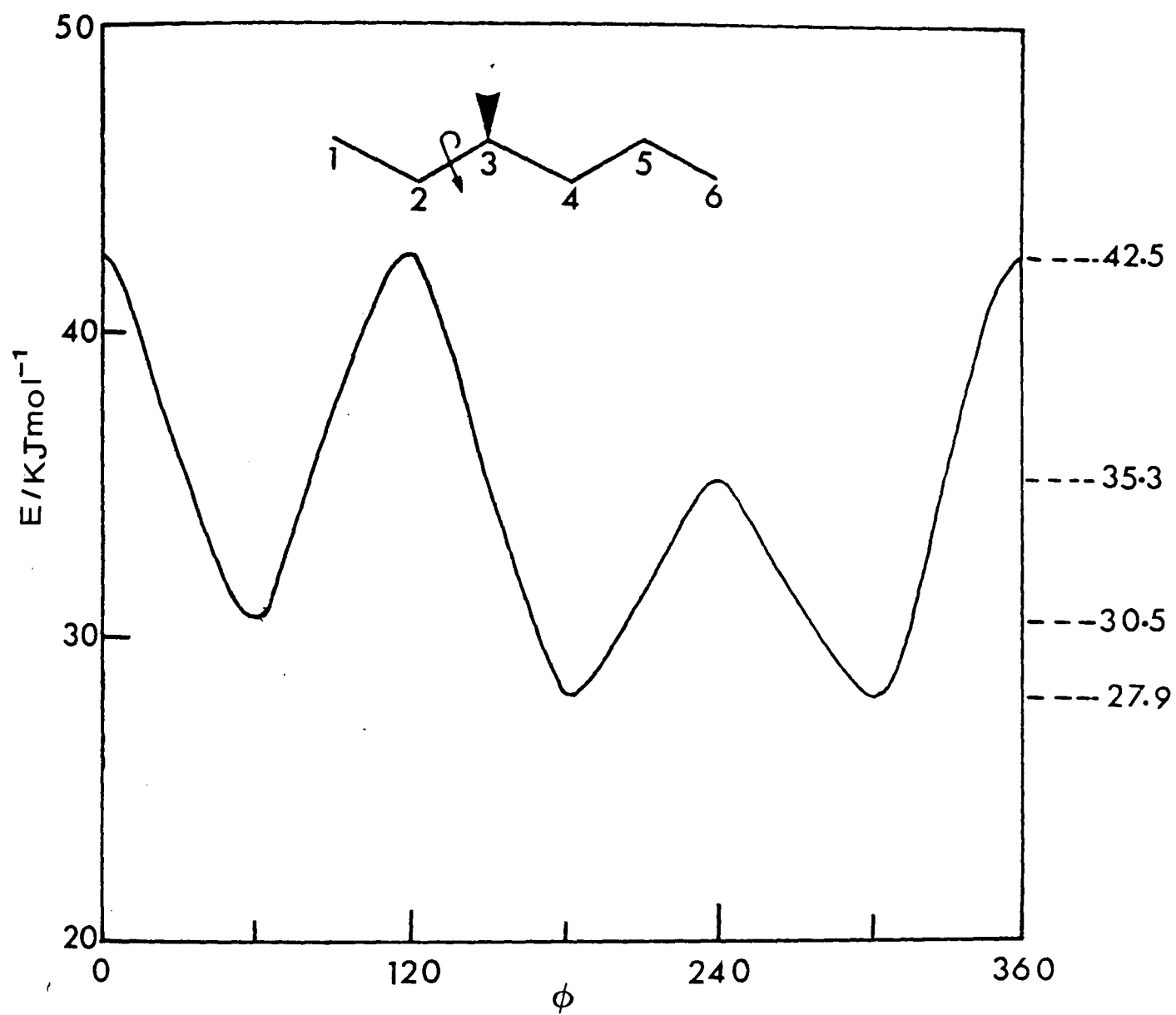


Figure 5.10b. Energy-angle relationship for 3-methylhexane.

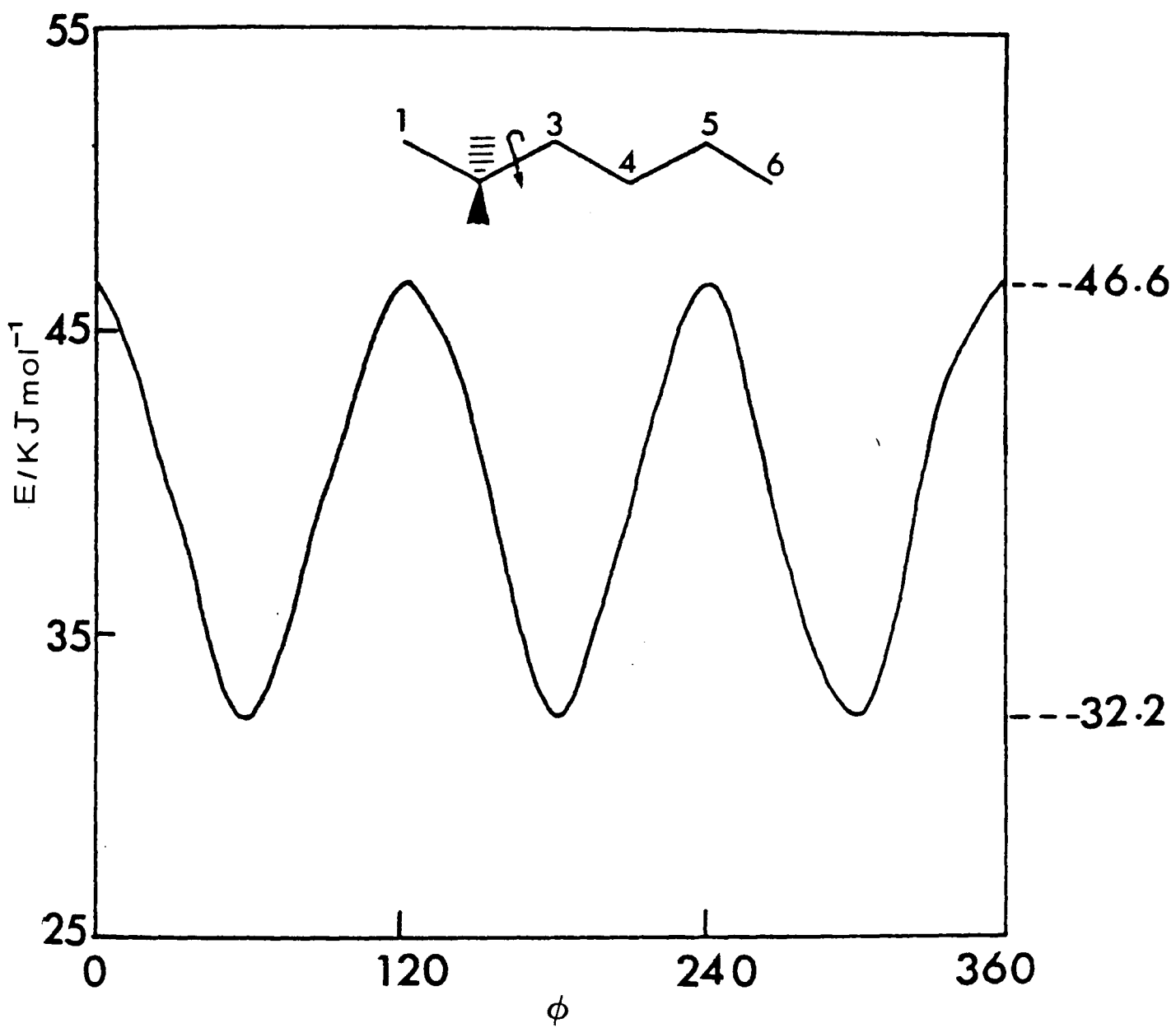


Figure 5.11a. Energy-angle relationship for 2,2-dimethylhexane.

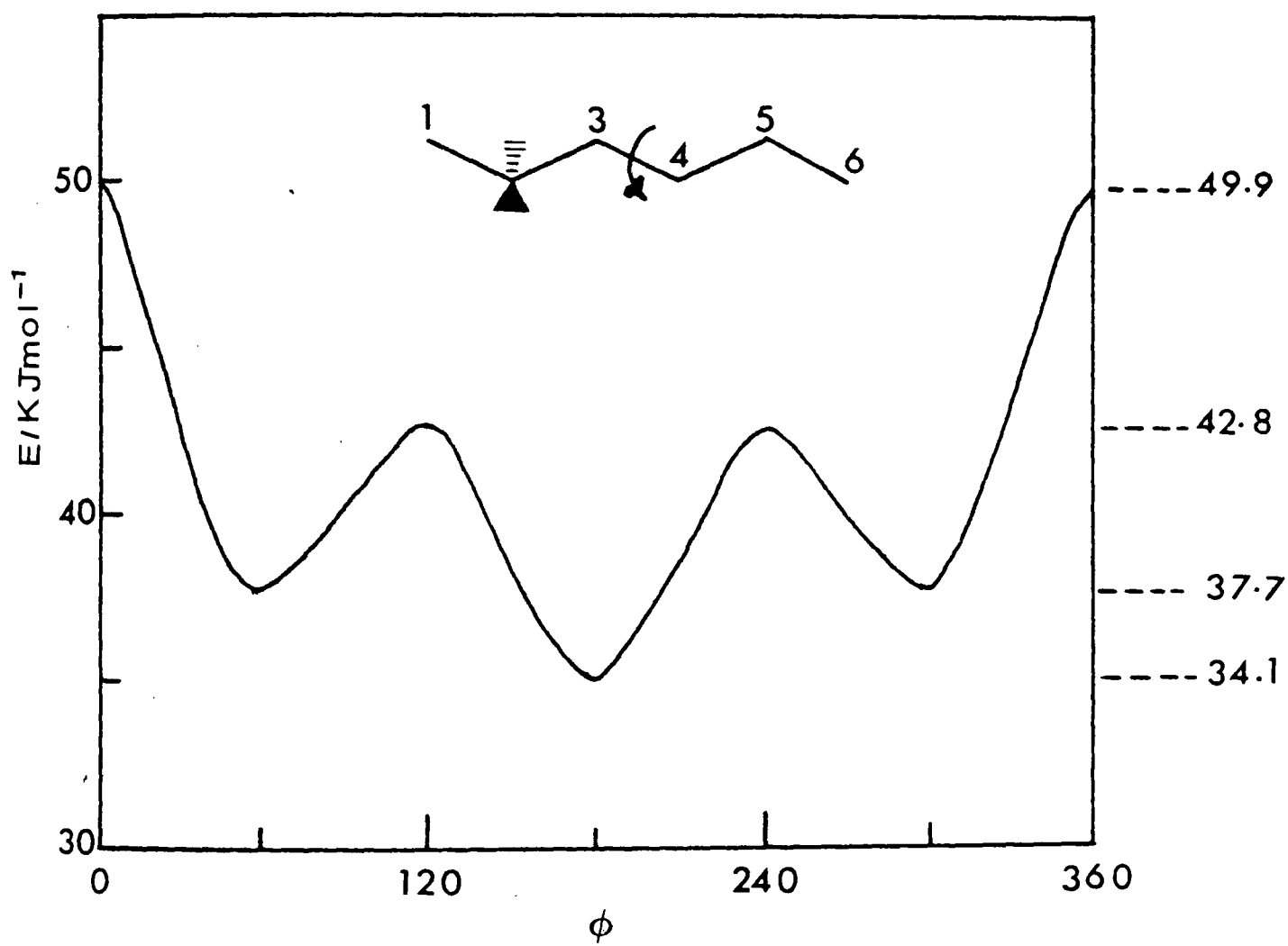


Figure 5.11b. Energy-angle relationship for 2,2-dimethylhexane.

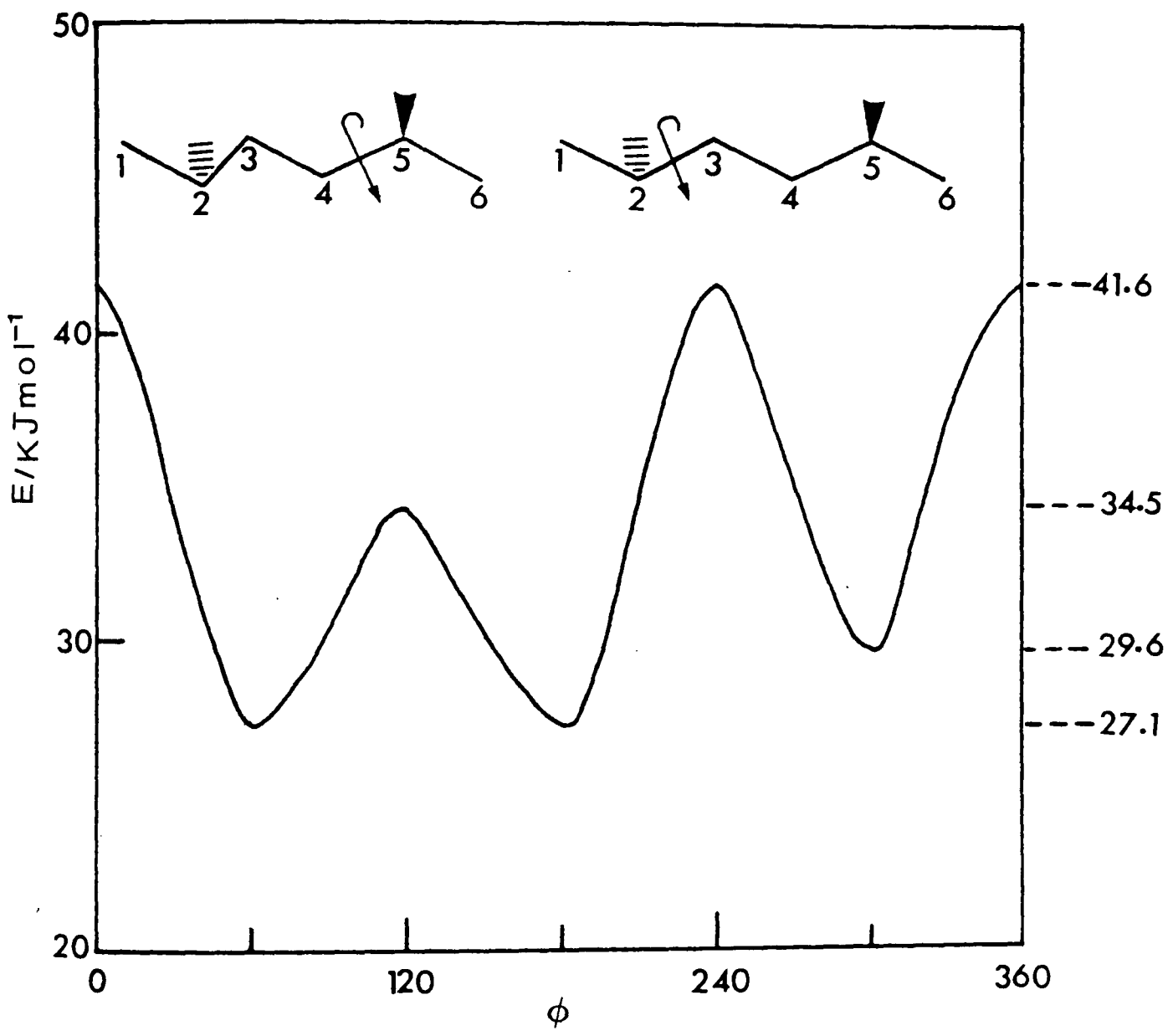


Figure 5.12. Energy-angle relationship for 2,5-dimethylhexane.

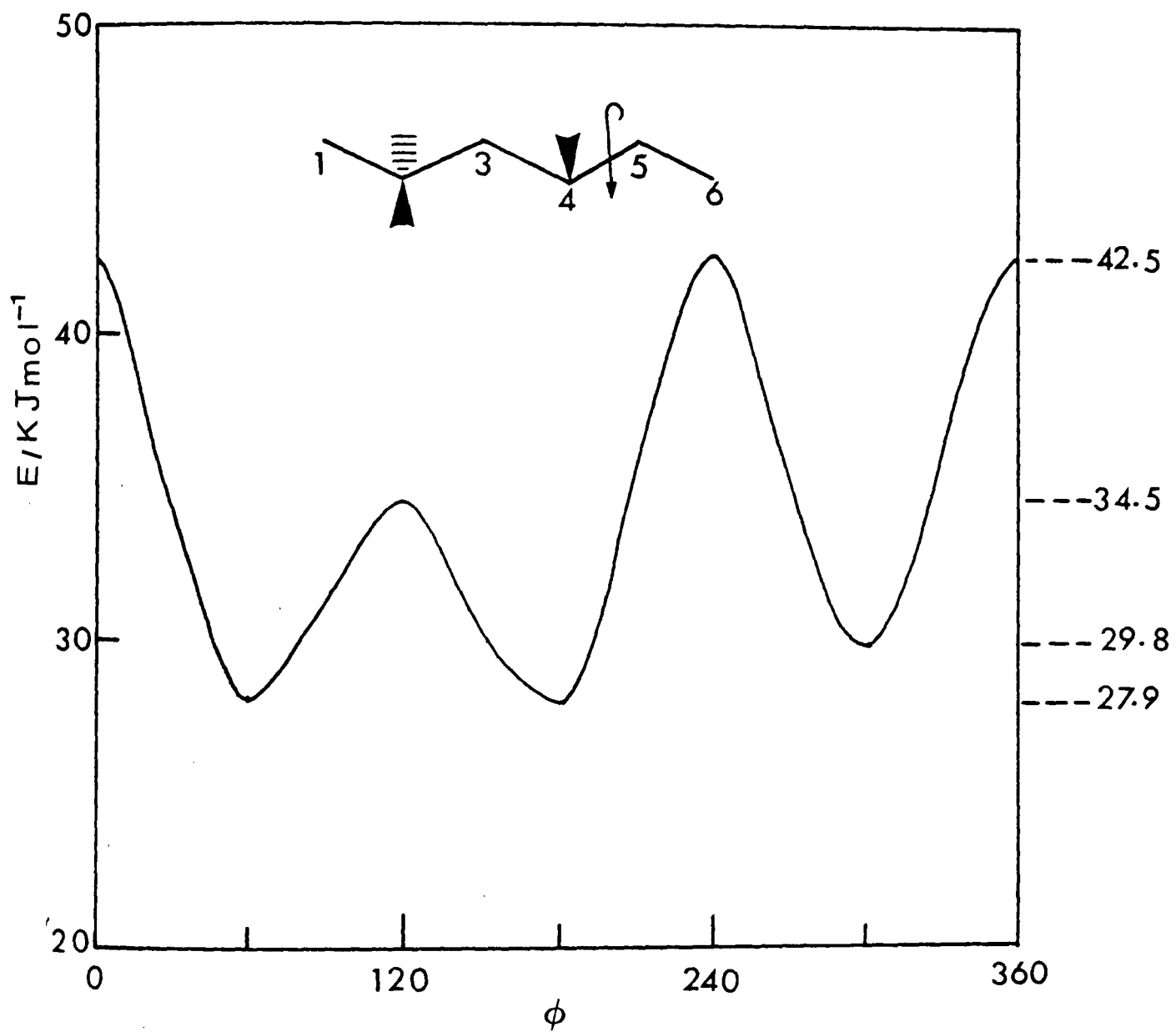


Figure 5.13a. Energy-angle relationship for 2,2,4-trimethylhexane.

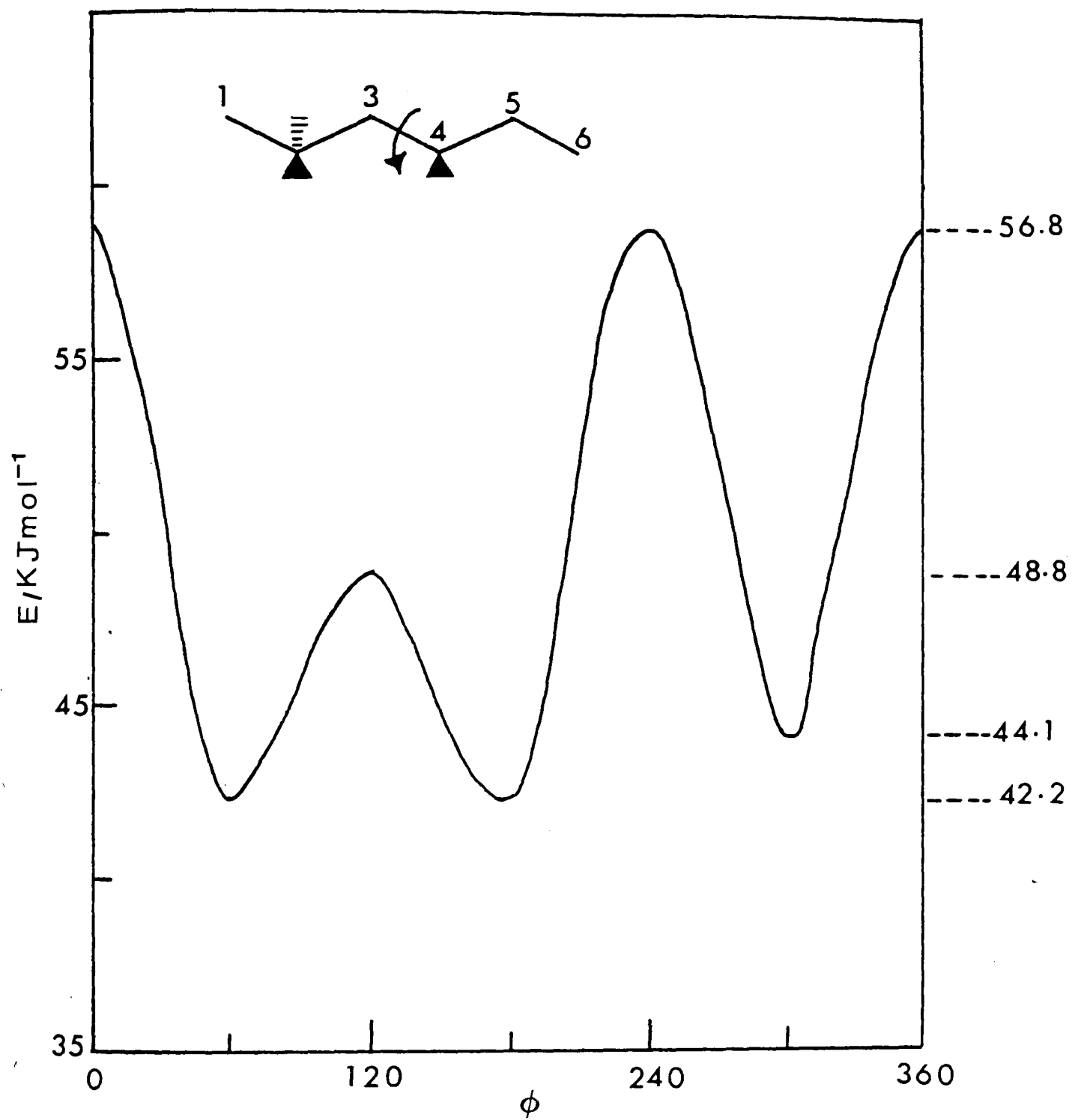


Figure 5.13b. Energy-angle relationship for 2,2,4-trimethylhexane.

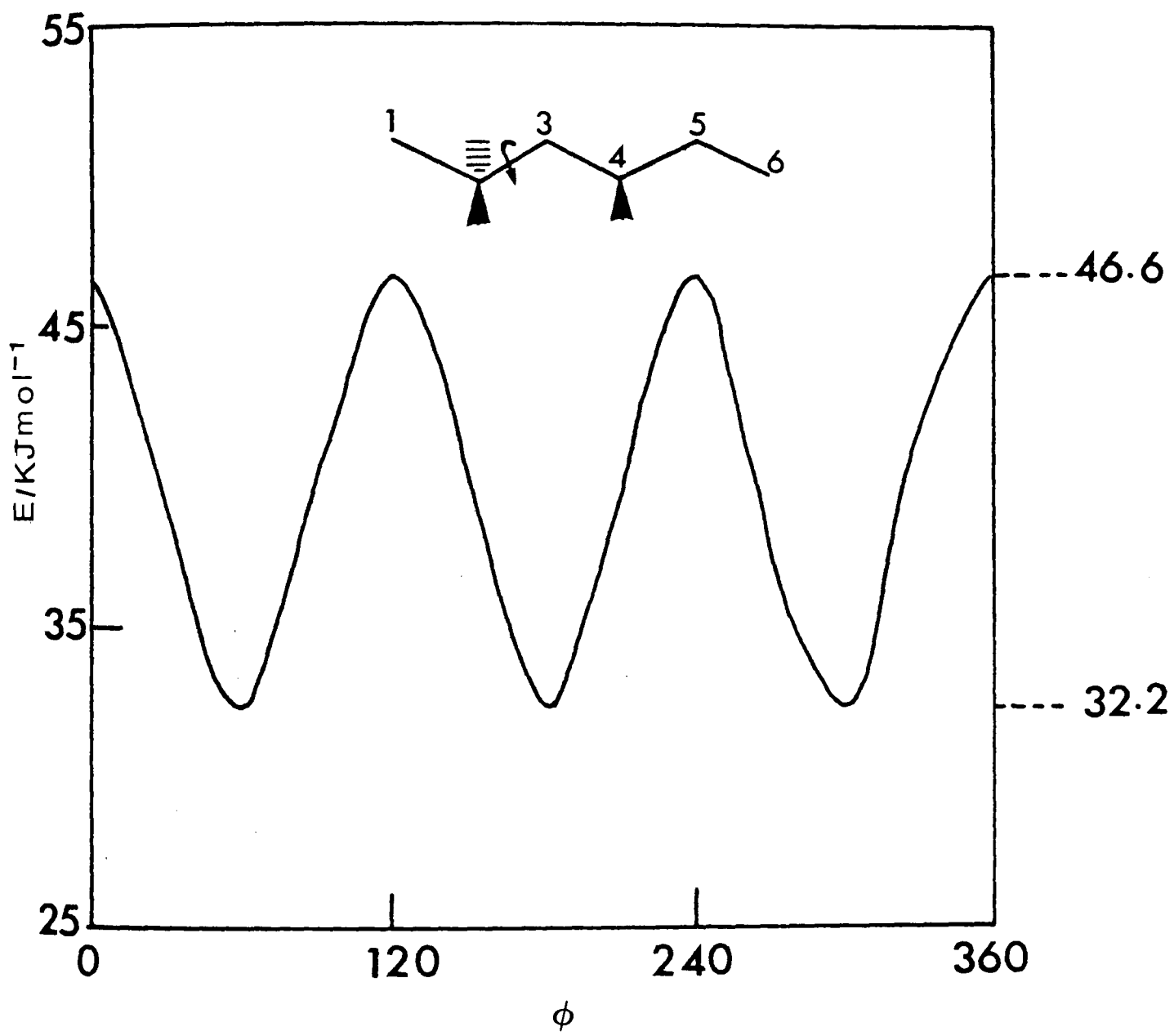


Figure 5.13c. Energy-angle relationship for 2,2,4-trimethylhexane.

TABLE 5.5. Comparison of experimentally determined and theoretically predicted activation energies.

Molecule	$\phi$	$\Delta E^\ddagger$ (exp) / kJ mol <sup>-1</sup>	$\Delta E^\ddagger$ (theor) / kJ mol <sup>-1</sup>	$\Delta H^\ominus$ (exp) / kJ mol <sup>-1</sup>	$\Delta H^\ominus$ (theor) / kJ mol <sup>-1</sup>
2-methylhexane	C(2)-C(3) 60,180→300	11.3	12	3.6	2.5
3-methylhexane	C(2)-C(3) 60→180,300	13.2	12	2.9	2.6
	C(3)-C(4) 60,180→300		12		2.5
2,2,7-dimethylhexane	C(2)-C(3) 60,180,300	inactive	14.4	inactive	0
	C(3)-C(4) 60,300→180	13.6	5.1	0.8	3.6
2,5-dimethylhexane	C(2)-C(3) and C(4)-C(5) 60,180→300	14	12	1.2	2.5
2,2,4-trimethylhexane	C(2)-C(3) 60,180,300	inactive	14.4	inactive	0
	C(3)-C(4) 60,180→300	14.7	12.7	3	1.9
	C(4)-C(5) 60,180→300		12.7		1.7

and we feel that the acoustic value is a more dependable quantity for use in conformational equilibrium considerations.

3-methylhexane. Considering the rotation about either the C(2) - C(3) or C(3) - C(4) bonds, the energy differences and activation energies are very similar and it is not possible from these experiments to differentiate between these processes. It therefore seems likely that the observed relaxation is the result of both. However, since agreement between theory and experiment appears based on a single profile, we suggest that isomerism involves two asynchronous motions rather than one coordinated process.

2,2-dimethylhexane. Rotation about the C(2) - C(3) bond is an isoenergetic process, and so is acoustically inactive. However, rotation about C(3) - C(4) leads to the generation of states with a profile which might be expected to reflect the observed relaxation. Comparison with theory indicates a poor agreement and this probably reflects inadequacies of the potential for interactions of the t-butyl group. Again we suggest that the acoustic data form a more reliable base for conformational equilibrium calculations.

2,5-dimethylhexane. Rotations about C(2) - C(3) and C(4) - C(5) are identical. In this case the theoretical energy difference for exchange between the degenerate  $60^\circ$  and  $180^\circ$  positions and the  $300^\circ$  position is larger than that observed experimentally, although the activation

parameters are in reasonable agreement.

2,2,4-trimethylhexane. Rotations about C(2) - C(3) lead to isoenergetic states which will not be observed acoustically. There are two other possible isomeric processes which must be considered. First rotation about C(3) - C(4) leads to a doubly degenerate lower energy state and a single upper state. Rotation about C(4) - C(5) leads to a similar situation. Again from the acoustic data we are unable to decide between these two possibilities, and presumably both occur with possibly some degree of coordination.

The entropy difference,  $\Delta S^\ominus$ , associated with the internal rotational process in these systems is observed to be high. This reflects the complexity of the processes being observed and is probably a consequence of the 'cogwheeling' effect of neighbouring methyl groups in formation of the eclipsed transition state form.

### 5.5 Conclusion

(i) Study of the rotational isomerism of branched chain hexanes indicates that the activation energy to internal rotation increases with the extent of steric hindrance, although the increase is less than might be expected on the basis of simple additivity of pair interactions and probably reflects the effects of long range interactions on the rotational isomeric exchange processes observed by ultrasonics.

(ii) In general, there is a reasonable agreement between the theoretical and experimental conformational energetics.

CHAPTER 6

ULTRASONIC STUDIES OF MIXTURES OF n-HEXADECANE  
WITH DIMETHYLPENTANES

## CHAPTER 6

### ULTRASONIC STUDIES OF MIXTURES OF n-HEXADECANE WITH DIMETHYLPENTANES

#### 6.1 Introduction

The study of the thermodynamic properties of hydrocarbon mixtures and attempts to interpret the excess volume, enthalpy, free energy and entropy have a long history, starting with binary mixtures of n-alkanes<sup>179-182</sup>, later extending to linear and branched chain alkanes<sup>32,183-185</sup> and still more recently to cyclo-alkanes and n-alkanes<sup>186-189</sup>.

The binary mixtures of linear and branched chain hydrocarbons have been subjects of some of the most painstaking experiments on binary mixtures of non-polar liquids. These studies have been concerned with the excess volume of mixing<sup>190-194</sup>, excess enthalpy of mixing<sup>195-197,30,31</sup>, excess heat capacity of mixing<sup>198,199</sup> and excess Gibbs free energy and entropy of mixing<sup>148</sup>. Three contributions to the excess functions of liquid mixtures were recognised by Prigogine-Flory theory<sup>22,9</sup>.

1. The Combinatorial or configurational part of  $\Delta S_m$  as predicted for chain-molecule mixtures by Flory<sup>9</sup> and Huggins<sup>28</sup>. Using the excess of the experimental mixing function, in this case  $\Delta S_m$ , over the ideal value, then the combinatorial excess entropy is positive and increases with the difference in molecular size of the two components.

2. An interactional contribution represented by

the  $\chi_{12}$  parameter which arises because of any difference in chemical nature of the components leading to a difference in contact energies between the molecules.

3. A free volume contribution due to volume changes taking place during the mixing process.

Recently two contributions to the mixing functions have been distinguished by Patterson et al<sup>30,149,150,200</sup>, both involving molecular ordering.

4. Thermodynamic effects associated with the presence of short-range orientational order in one of the component liquids, e.g. a long-chain normal-alkane such as n-hexadecane. The orientational order is thought of as a partial alignment of neighbouring segments or possibly of whole molecules. On mixing with another liquid whose molecules are more globular in shape, e.g. n-hexane or 2,2-dimethylhexane, the order between n-hexadecane molecules is destroyed or replaced by weaker correlations, giving positive contributions to  $H^E$ ,  $G^E$  and  $TS^E$ .

5. A condensation effect associated with creation of order during the mixing process. With order-creation one finds negative contributions to  $H^E$  and  $S^E$  which decrease with increase of T, the signs therefore being opposite to those which characterize destruction of order.

Various attempts have been made to understand the phenomena of excess volumes of n-alkane mixtures. The theory of Orwoll and Flory<sup>201</sup> has been used extensively, for the prediction of excess volumes of n-alkane mixtures at different temperatures. This model predicts the

volume of mixing from differences in the expansion of the components, and the heat of mixing from a pair interaction energy parameter  $\chi_{12}$  itself obtained from the excess enthalpies. Currently there is considerable disagreement as to whether  $\chi_{12}$  derives solely from an interaction energy (as proposed by Flory<sup>201</sup>), or contains geometrical packing terms (as pointed out by Patterson<sup>150</sup>). Further, time-averaged thermodynamic measurements seem unable to resolve the relative significance of intramolecular conformational isomerism and intermolecular short range order in any such geometrical contributions.

Comparison of theory and experiment based on mixtures of n-alkanes are inconclusive because disturbance of order in one n-alkane by another is very small. Both molecules are linear, have the same cross section and can easily correlate their molecular orientations. However, introduction of a branched alkane into a linear alkane could lead to significant changes in short range correlations in the liquid. A study of branched and linear alkanes has suggested<sup>149,150,30,202</sup> that the influence of order perturbation on excess thermodynamic quantities is, (i) proportional to  $m/n$  where  $m$  is the number of methyl groups and  $n$  is the number of carbon atoms in the longest chain of the order-breaking branched molecule, (ii) proportional to the number of carbon atoms in the linear ordered component, and (iii) inversely proportional to temperature. Thus mixtures such as n-hexadecane-dimethylpentane should be suitable for examination of

conflicting theories.

Barbe and Patterson<sup>148</sup> have reported the thermodynamic studies on binary mixtures of n-hexadecane-dimethylpentanes. Molar excess mixing enthalpies,  $H^E$ , Gibbs free energies,  $G^E$ , and entropies  $S^E$ . Values of  $H^E$  and  $TS^E$  are strongly positive, while those of  $G^E$  are only slightly less negative.. The values are explained by the contributions suggested by Prigogine-Flory theory<sup>9,22</sup> and Patterson et al<sup>148,150</sup>.

The technique of ultrasonic relaxation, by the introduction of frequency/time dependence, can in principle separate conformational effects (contributing to the relaxing specific heat) and packing characteristics (determining the bulk viscosity which contributes to the non-relaxing visco-thermal absorption). The method does not seem to have been applied before to a test of solution theories in this way and also the study of ultrasonic relaxation of such binary mixtures.

## 6.2 Materials

The branched-chain hydrocarbons 2,2-dimethylpentane, 2,3-dimethylpentane, 2,4-dimethylpentane, 3,3-dimethylpentane and n-hexadecane were obtained from Aldrich Chemical Company Ltd and were dried over molecular sieves Type 4A (BDH) before use. Their purity was better than 99%. The densities, refractive indices and ultrasonic velocities are presented in Table 6.1. The data obtained are in good agreement with those published in the literature<sup>203-206</sup>.

TABLE 6.1. Densities,  $\rho$ , refractive indices,  $n_D$ , and sound velocities,  $c$ , of pure liquids studies at 298.15K.

Compound	$\rho/\text{gcm}^{-3}$		$n_D$		$c/\text{ms}^{-1}$	
	obs.	Lit.	obs.	Lit.	obs.	Lit.
2,2-dimethylpentane	0.6696	0.66953	1.37958	1.37955	1065	-
2,3-dimethylpentane	0.69089	0.69091	1.38931	1.38945	1130	-
2,4-dimethylpentane	0.66877	0.66832	1.37881	1.37882	1068	-
3,3-dimethylpentane	0.68915	0.68908	1.38846	1.38842	1115	-
n-hexadecane	0.77006	0.7703	1.43249	1.4325	1341	1337.88
		0.76998	-	-	-	1340.5

### 6.3 Theory

The rotational isomeric process is an intramolecular effect and it is additive. Hence the contribution to the total attenuation in a mixture can be expressed as:

$$(\alpha/f^2)_{\text{total}} = x_1 (\alpha/f^2)_{x_1}^{\text{rot}} + x_2 (\alpha/f^2)_{x_2}^{\text{rot}} + B \quad 6.1$$

where  $x_1$  and  $x_2$  are the mole fractions of components 1 and 2 which make rotational isomeric contributions  $(\alpha/f^2)_{x_1}^{\text{rot}}$ . Each rotational isomeric contribution will have the form:-

$$(\alpha/f^2)_{x_i}^{\text{rot}} = A_i / (1 + (f/f_{c,i})^2) \quad 6.2$$

where  $A_i$  is the amplitude of the relaxation measured in the pure component  $i$  and  $f_{c,i}$  is its relaxation time. Equation 6.2 makes the assumption that each relaxation conforms to a simple Debye process. In practice, this is justified for rotational isomerism in the methyl pentanes and lower  $n$ -alkanes, although it is inappropriate for much longer chains. Although the addition of two Debye relaxations will lead to a total observed process which is broader than ideal, in this case the dispersion is very small and does not justify an equation more sophisticated than 6.1.

The classical contribution,  $B$ , in equation 6.1 contains three components. A viscous term arises from isovolumetric shear, and a volume viscosity and thermal term is associated with energy migration between the compression and rarefaction regions of the propagating wave. This last is negligible for most organic liquids, i.e.  $\alpha/f^2$  of

less than  $1 \times 10^{-15}/\text{s}^2 \text{ m}^{-1}$ . The shear contribution can be calculated from the macroscopic viscosity equation 2.3. The difference between the observed 'classical' attenuation,  $B$ , and that predicted, equation 2.3, gives the volume viscosity,  $\eta_v$ .

$$\left(\frac{\alpha}{f^2}\right)_{\text{vol}} = B - \left(\frac{\alpha}{f^2}\right)_{\text{shear}} = \frac{2\pi^2}{\rho c^3} \eta_v \quad 6.3$$

In time-averaged thermodynamic studies the phase 'volume viscosity' is associated with conformational, vibrational and structural relaxation in the liquid. However, the analysis outlined above separates out the contribution to the attenuation from rotational isomerism, so that equation 6.3 describes the contributions from structural and vibrational relaxation only. In normal alkanes and similar organic molecules low symmetry vibrational relaxation makes a minor contribution to the volume viscosity (ca.  $2 \times 10^{-15}$ )  $\text{s}^2 \text{ m}^{-1}$  and may be neglected<sup>215</sup>.

For many organic liquids the ratio<sup>215</sup>

$$K = \left(\frac{\alpha}{f^2}\right)_{\text{vol}} / \left(\frac{\alpha}{f^2}\right)_{\text{shear}} \quad 6.4$$

is characteristic of the intermolecular interactions which determine the liquid structure. So in real mixtures the way in which  $K$  varies with composition will reflect packing contributions to the intermolecular interaction terms such as  $\chi_{12}$ . Thus comparison of non-linearity in the composition dependences of  $K$  and  $\Delta V_{\text{mix}}^E$  should help decide whether  $\chi_{12}$  is purely energetic, or contains both energy

and packing components.

#### 6.4 Results

The measured density, sound velocity and viscosity for the binary mixtures of n-hexadecane and dimethylpentanes and pure n-hexadecane are presented in Table 6.2. The excess volumes of mixing computed by using equation 2.33 and the data fitted to an empirical equation of form

$$V^E = x(1-x) \sum_{n=1}^m a_n x^{n-1} \quad 6.5$$

where  $a_n$  is the fitting coefficient of order n obtained from a least-squares fit of the data presented in Table 6.3. The standard deviations associated with this analysis are also presented in Table 6.3, along with the coefficients for  $a_n$ . Comparison of the plots of the actual data and the predictions of equation 6.5 indicates that the deviation is in all cases  $< 0.1\%$ . The excess volumes for the binary mixtures of n-hexadecane with dimethylpentane are all negative over the whole mole fraction range, Figure 6.1 at 298.15K.

The variation of ultrasonic absorption coefficient for pure n-hexadecane as a function of frequency and temperature is presented in Figure 6.2. Figures 6.3-6.6 show the variation of ultrasonic absorption coefficient as a function of frequency and the mole fraction,  $x$ , of dimethylpentane for the binary mixtures of n-hexadecane-dimethylpentane at 298.15K.

The variation of absorption coefficient,  $(\alpha/f^2)$  with frequency is fitted to the empirical equation 2.8.

TABLE 6.2. Physical and Ultrasonic Parameters

Components Temp./K	x	$\rho/\text{gcm}^{-3}$	$c/\text{ms}^{-1}$	$\eta/\text{cSt}$	$A \times 10^{15}$ $/\text{m}^{-1}\text{s}^2$	$B \times 10^{15}$ $/\text{m}^{-1}\text{s}^2$	$f_c \times 10^9$ $/\text{Hz}$	K
Hexadecane								
298.15	0	0.7700	1341	4.2	21	62	0.9	0.35
305.15	0	0.7653	1314	3.4	20	58	1.01	0.47
315.15	0	0.7587	1281	2.8	18	54	1.06	0.54
321.15	0	0.7547	1260	2.6	16	51	1.08	0.50
Hexadecane and 2,2-dimethyl- pentane	0 0.24 0.52 0.74 0.90	0.7700 0.7577 0.7365 0.7129 0.6893	1341 1304 1244 1181 1117	4.2 3.0 1.7 1.1 0.8	21 20 20 20 20	62 53 43 42 40	0.9 0.75 0.45 0.41 0.36	0.35 0.49 0.85 1.36 1.65
298.15	1.00	0.6696	1065	0.5	20	39	0.32	2.58
Hexadecane and 2,3-dimethyl- pentane	0 0.24 0.41 0.64 0.84	0.7700 0.7603 0.7515 0.7357 0.7163	1341 1311 1287 1242 1190	4.2 2.9 2.3 1.5 0.9	21 19 19 18 19	62 57 51 49 43	0.9 0.82 0.71 0.4 0.37	0.35 0.68 0.80 1.38 2.05
298.15	1.00	0.6929	1133	0.6	19	42	0.3	2.85
Hexadecane and 2,4-dimethyl- pentane	0 0.24 0.41 0.64 0.85	0.7700 0.7571 0.7452 0.7237 0.6979	1341 1303 1271 1209 1142	4.2 2.9 2.2 1.3 0.8	21 20 18 16 15	62 56 53 50 49	0.9 0.75 0.61 0.54 0.48	0.35 0.62 0.88 1.58 2.48
298.15	1.0	0.6690	1068	0.5	14	49	0.4	3.54

TABLE 6.2 (cont.)

Components Temp./K	x	$\rho/\text{gcm}^{-3}$	$c/\text{ms}^{-1}$	$\eta/\text{cSt}$	$A \times 10^{15}$ $/\text{m}^{-1}\text{s}^2$	$B \times 10^{15}$ $/\text{m}^{-1}\text{s}^2$	$f_c \times 10^9$ $/\text{Hz}$	K
Hexadecane	0	0.7700	1341	4.2	21	62	0.9	0.35
and	0.24	0.7500	1309	3.0	19	59	0.7	0.68
3,3-dimethyl-	0.51	0.7440	1268	1.9	18	53	0.5	1.16
pentane	0.72	0.7258	1218	1.3	15	50	0.39	1.65
	0.89	0.7067	1158	0.8	15	49	0.36	2.65
	1.0	0.6890	1115	0.6	16	47	0.32	3.12

TABLE 6.3. Coefficients  $a_n$  and standard deviations  $\sigma V/\text{cm}^3 \text{ mol}^{-1}$  for least squares representations of excess volumes for  $[xC_7H_{16} + (1-x) \text{ n-hexadecane}]$  at 298.15K by equation 6.5.

$a_n$	2,2-dimethyl- pentane	2,3-dimethyl- pentane	2,4-dimethyl- pentane	3,3-dimethyl- pentane
$a_1$	$-8.7504 \times 10^{-5}$	-0.0003	$3.450 \times 10^{-6}$	-0.0001
$a_2$	-1.1334	-0.333	-0.606	-1.157
$a_3$	-10.536	-8.454	-18.114	-3.246
$a_4$	41.191	33.584	121.559	15.194
$a_5$	-54.300	-55.163	-368.357	-20.297
$a_6$	24.780	41.872	576.926	9.507
$\sigma V^E/\text{cm}^3 \text{ mol}^{-1}$	$9.76 \times 10^{-4}$	$4.58 \times 10^{-3}$	$1.59 \times 10^{-3}$	$1.48 \times 10^{-3}$

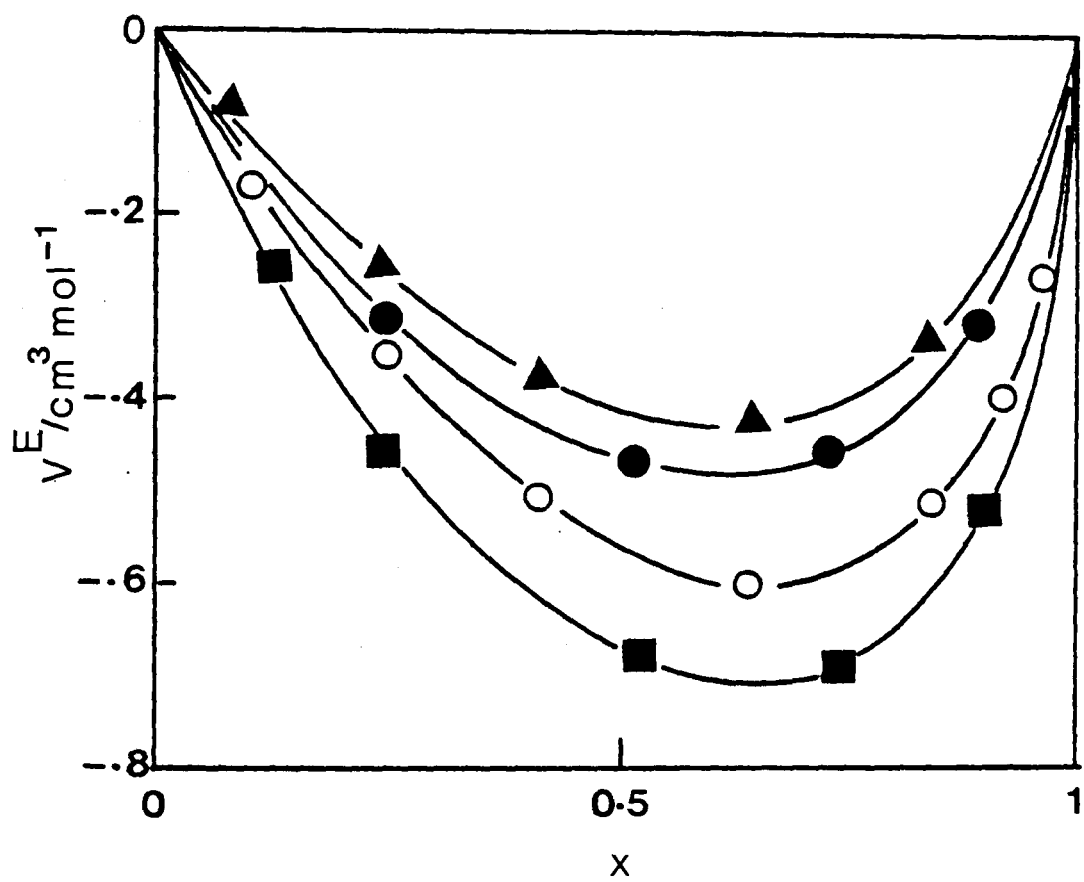


Figure 6.1. Excess volumes for  $[x\text{C}_7\text{H}_{16} + (1-x)n\text{-hexadecane}]$  at 298.15K: ■, 2,2-dimethylpentane; ○, 2,4-dimethylpentane; ●, 3,3-dimethylpentane; ▲, 2,3-dimethylpentane.

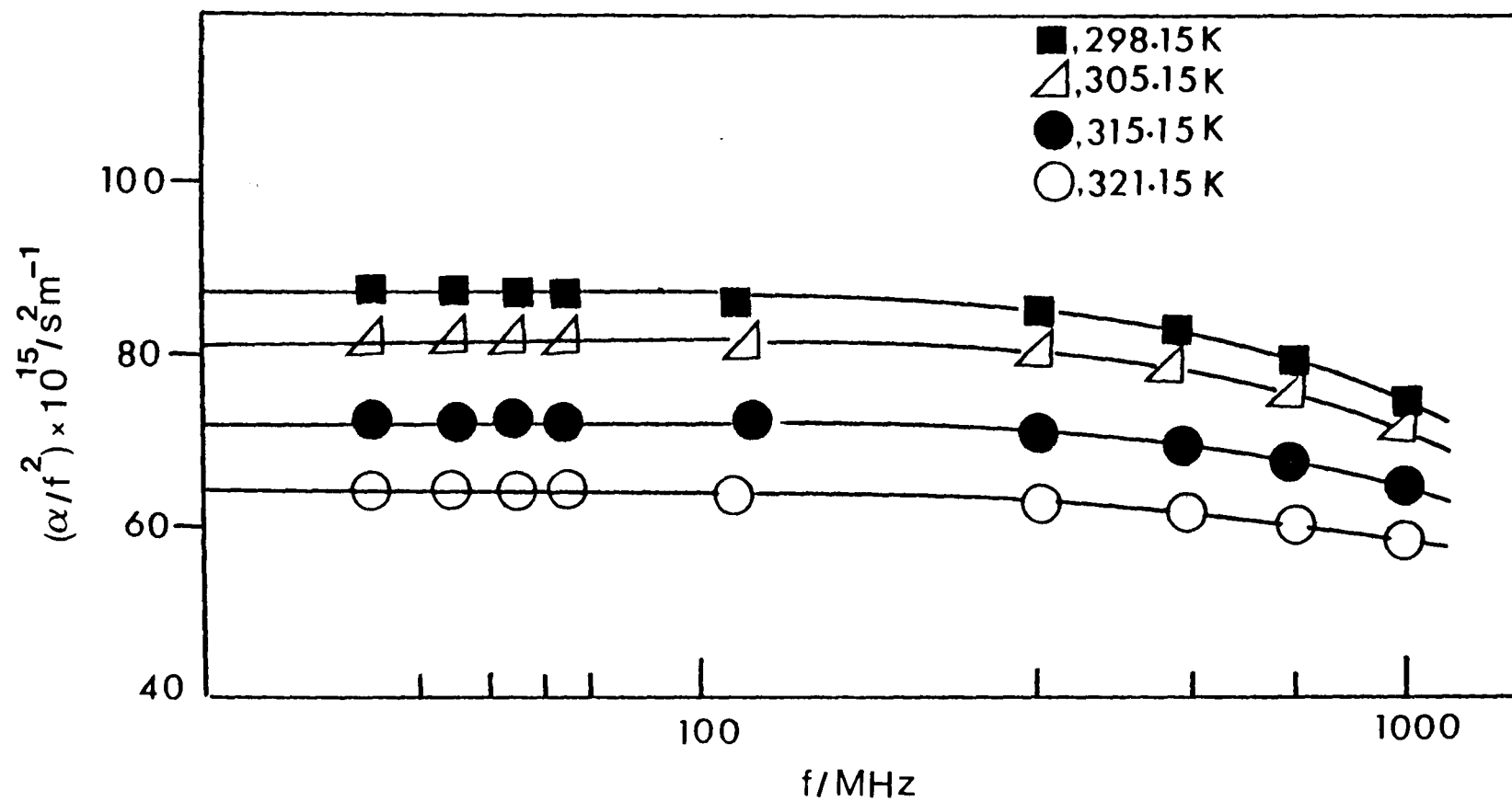


Figure 6.2. Variation of the ultrasonic absorption coefficient with frequency at various temperatures for n-hexadecane.

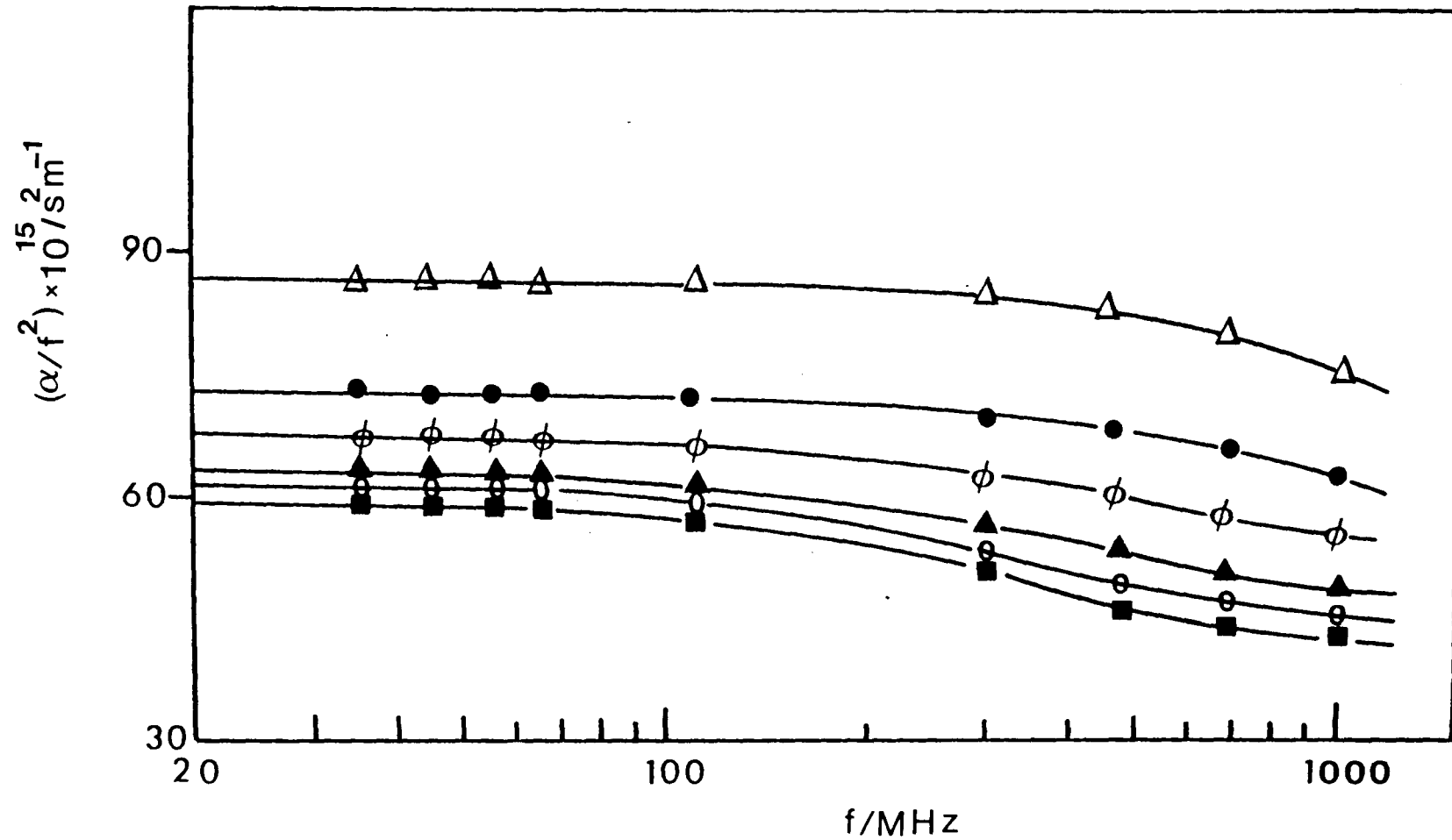


Figure 6.3. Variation of the ultrasonic absorption with frequency and mole fraction;  $x$  of 2,3-dimethylpentane for  $[xC_7H_{16} + (1-x) \text{ n-hexadecane}]$  at 298.15K:  $\Delta$ , 0;  $\bullet$ , 0.24;  $\phi$ , 0.41;  $\blacktriangle$ , 0.64;  $\circ$ , 0.84;  $\blacksquare$ , 1.

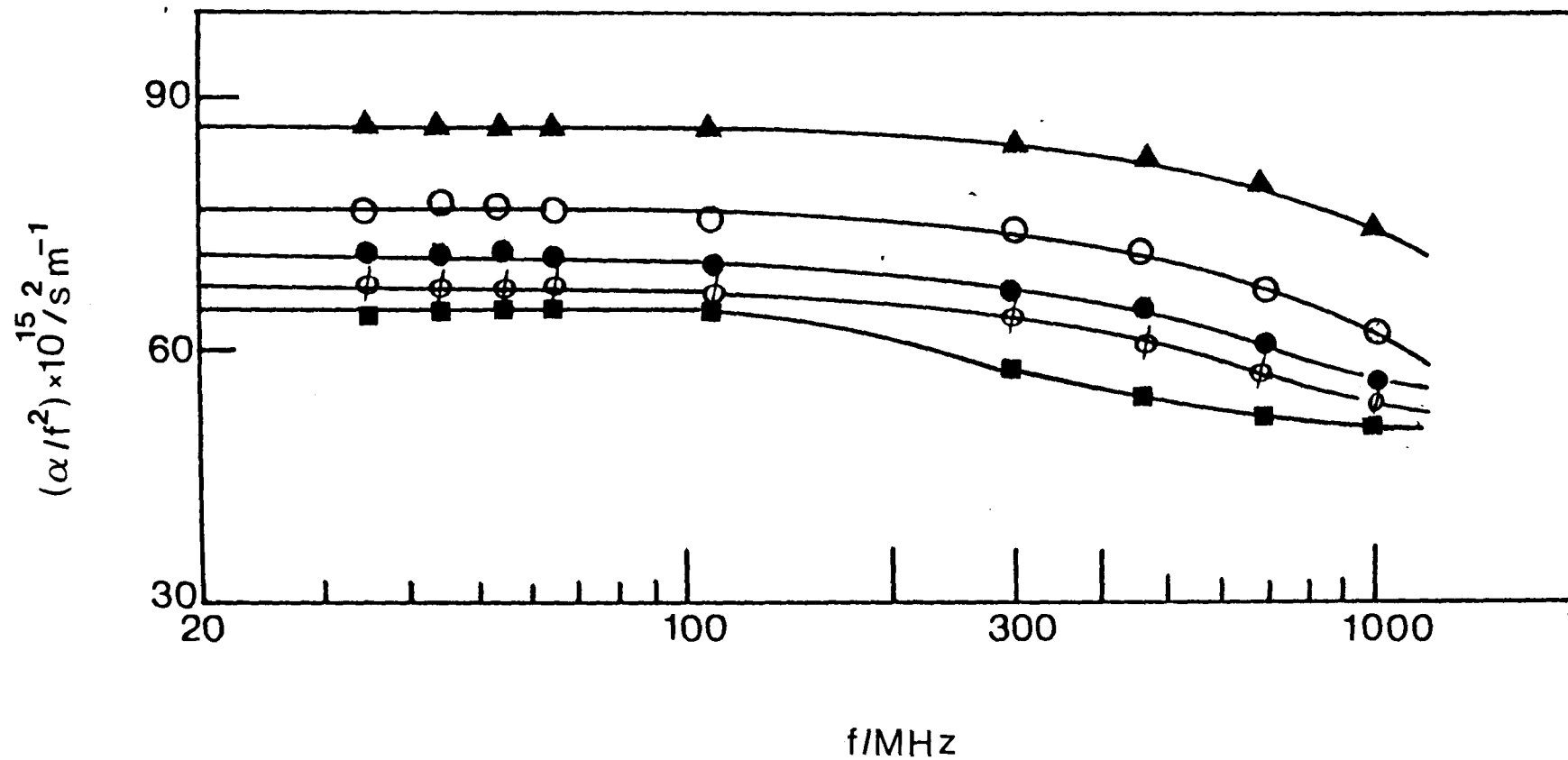


Figure 6.4. Variation of the ultrasonic absorption coefficient with frequency and mole fraction,  $x$ , of 3,3-dimethylpentane for  $[xC_7H_{16} + (1-x) \text{ n-hexadecane}]$  at 298.15K:

○, 0.24; ●, 0.51; ⊙, 0.72; ■, 1; ▲, 0.

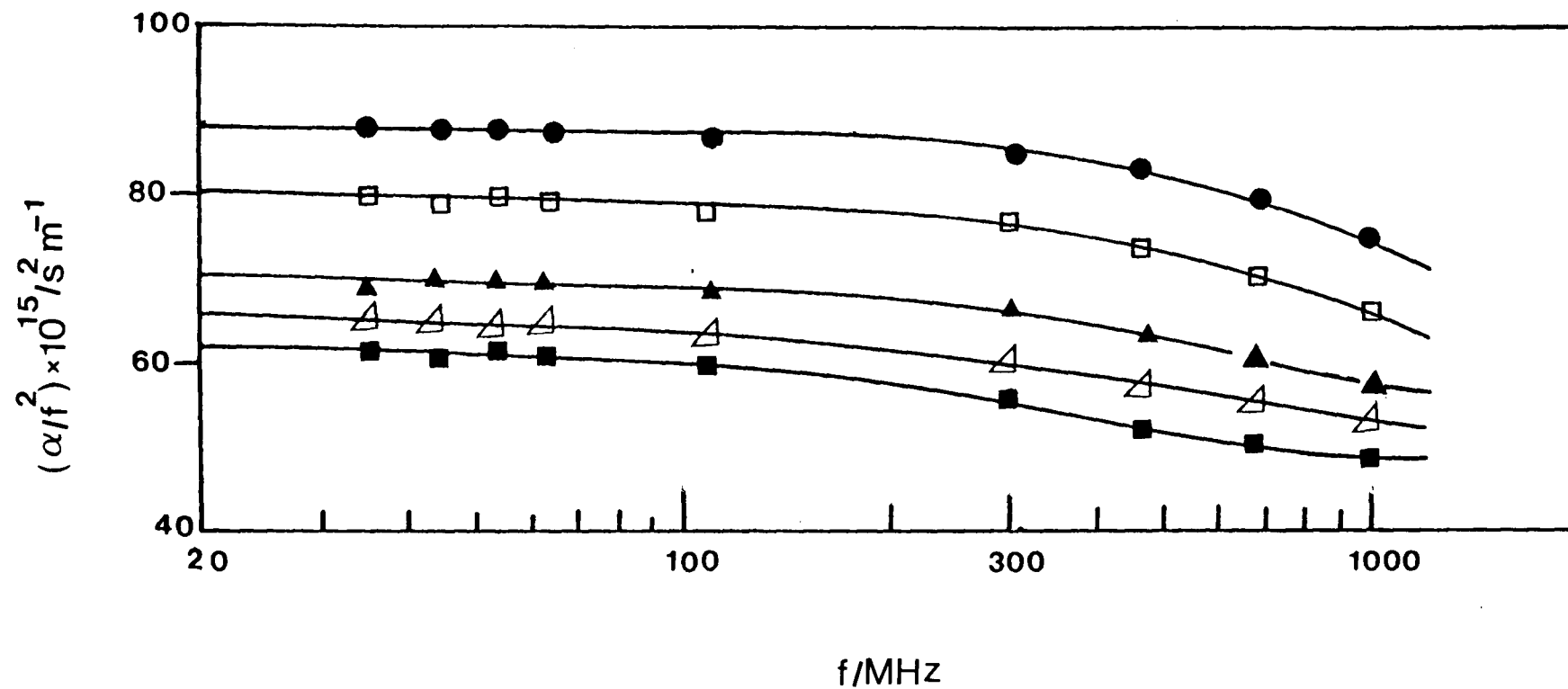


Figure 6.5. Variation of the ultrasonic absorption coefficient with frequency and mole fraction,  $x$ , of 2,4-dimethylpentane for  $(xC_7H_{16} + (1-x) \text{ n-hexadecane})$  at 298.15K.  
 □, 0.24; ▲, 0.41; △, 0.64; ■, 1; ●, 0.

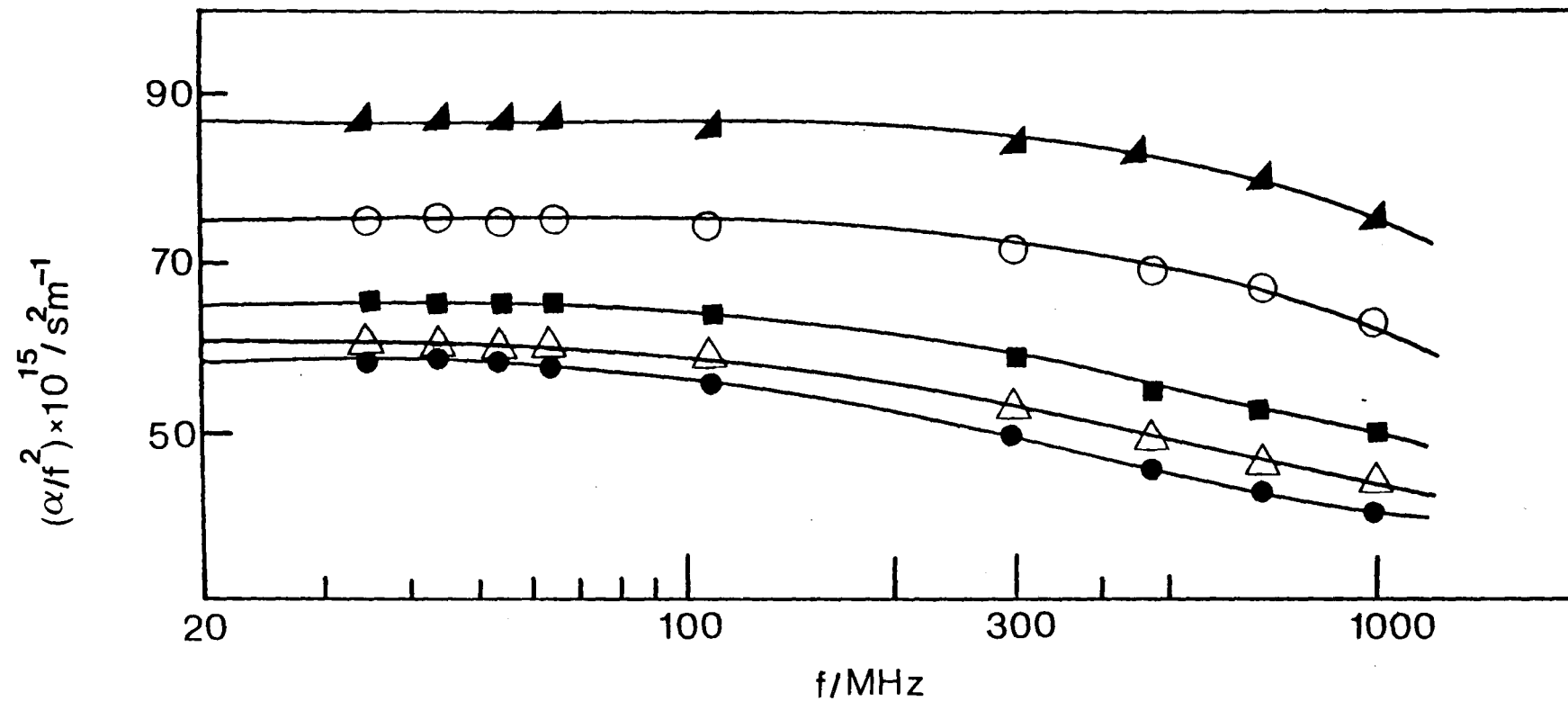


Figure 6.6. Variation of the ultrasonic absorption coefficient with frequency and mole fraction,  $x$ , of 2,2-dimethylpentane for  $[xC_7H_{16} + (1-x) \text{ n-hexadecane}]$  at 298.15K: ○, 0.24; ■, 0.52; △, 0.74; ●, 1; ▲, 0.

Computer fits to the observed data for pure n-hexadecane and binary mixtures of n-hexadecane and dimethylpentane yielded the parameters (A, the relaxing amplitude due to conformational changes; B, the classical viscothermal absorption; and  $f_c$ , the relaxation frequency), Table 6.2. Since this is the first recorded acoustic studies for n-hexadecane and so the temperature dependences are given in Table 6.2. These lead to conformational energies of  $25 \pm 2.5$  KJ/mole for  $\Delta E^\ddagger$  and  $9 \pm 2.4$  KJ/mole for  $\Delta H^\ominus$ .

Tests of the form of the dispersion in those cases where the full dispersion curve could be obtained indicated no significant deviation, within experimental error, from ideality. The discussion presented in the remainder of this study is critically dependent upon the value of B obtained from the analysis. A least squares computer fit of the data need not necessarily provide a unique value for this parameter and does not help with an indication of the associated uncertainty in its value. In view of the necessity to quantify precisely the error, two additional types of analysis have been applied to the data presented here. It should be pointed out at this stage that it is not possible to extend the observations to higher frequency or to lower temperature, the lowest accessible temperature being controlled by the melting point of hexadecane which is 291K.

Equations 6.1 and 6.2 can be written in the form<sup>57,207,208</sup>

$$(a/f^2) = A/(1 + (f/f_c)^2) + B \quad 6.6$$

Rearrangement of equation 6.6 will give

$$\left[ \frac{A}{(\alpha/f^2) - B} - 1 \right] = \frac{f^2}{f_c^2} \quad 6.7$$

and hence a plot of  $\left[ A/((\alpha/f^2) - B) - 1 \right]$  against  $f^2$  should pass through the origin and have slope  $f_c^2$ . These plots for the data obtained were found to be linear and checked the computer calculations.

An alternative method<sup>208</sup> of analysis is to plot  $((\alpha/f^2) - B)^{-1}$  versus  $f^2$  in which case the intercept is  $1/A$  and the slope is  $(f_c^2)^{-1}$ . The latter plot is extremely sensitive to the choice of  $B$ , Figure 6.7. It can clearly be seen that a variation of the value of  $B$  by  $\pm 2$  leads to a marked deviation from linearity of the plot and therefore allows determination of this quantity to the precision of measurement of the attenuation ca.  $\pm 2\%$ . Values of the constants obtained from the analysis are presented in Table 6.2.

### 6.5 Discussion

The magnitude of the relaxing absorption,  $A$ , vary linearly (within the  $\pm 2 \times 10^{15}/s^2 \text{ m}^{-1}$  experimental error) with composition, supporting the hypothesis that the intramolecular isomerism conforms to a simple additivity relationship.

From  $B$  and  $K$  we note that the volume viscosity contribution changes with composition, Figure 6.8. It is highest in the branched chain hydrocarbons and does not follow a simple additivity relation. A high value of the

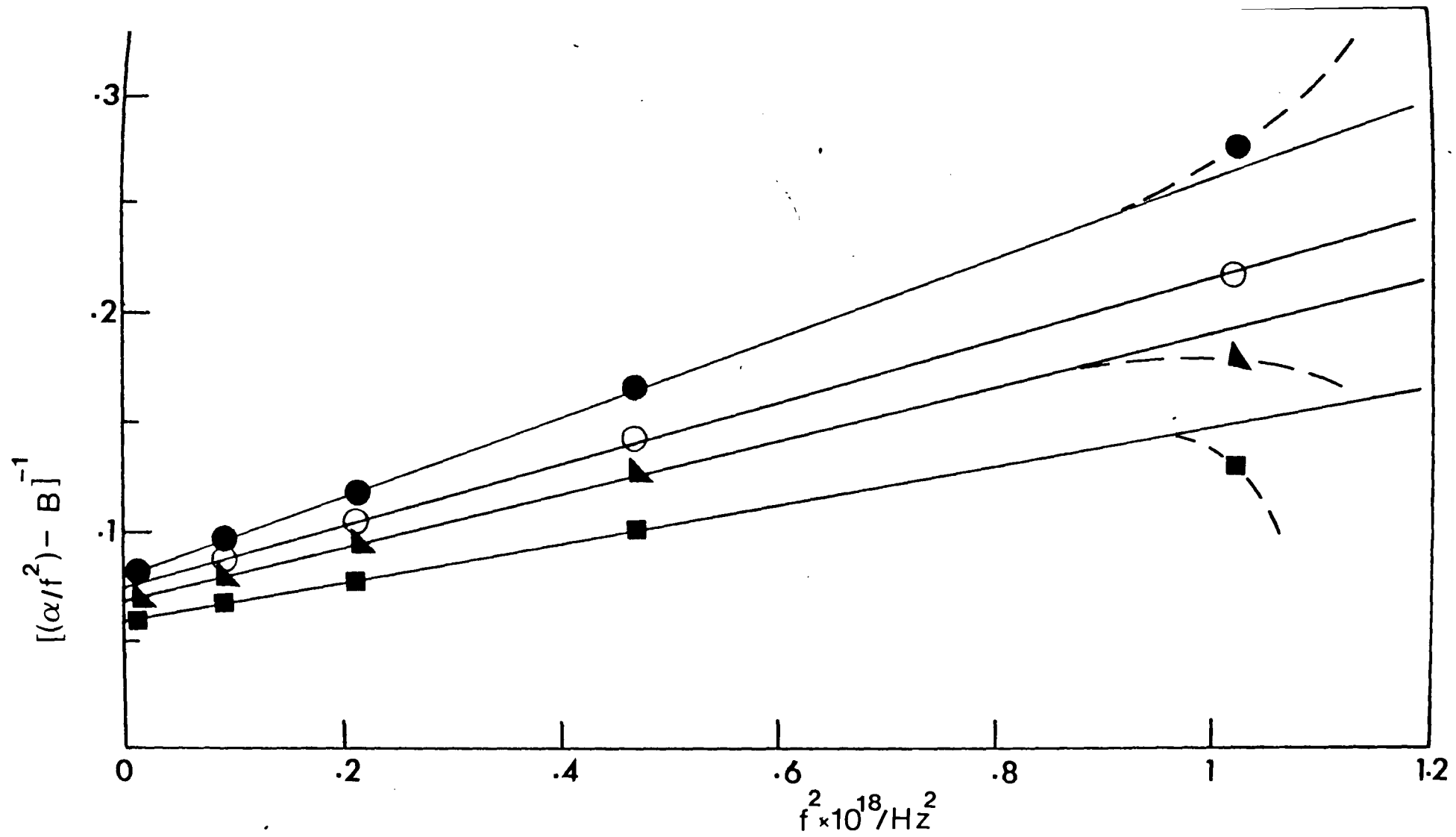


Figure 6.7. Typical plot of  $[(\alpha/f^2) - B]^{-1}$  against  $f^2$  for various values of B.

●, 52; ○, 51; ▲, 50; ■, 48.

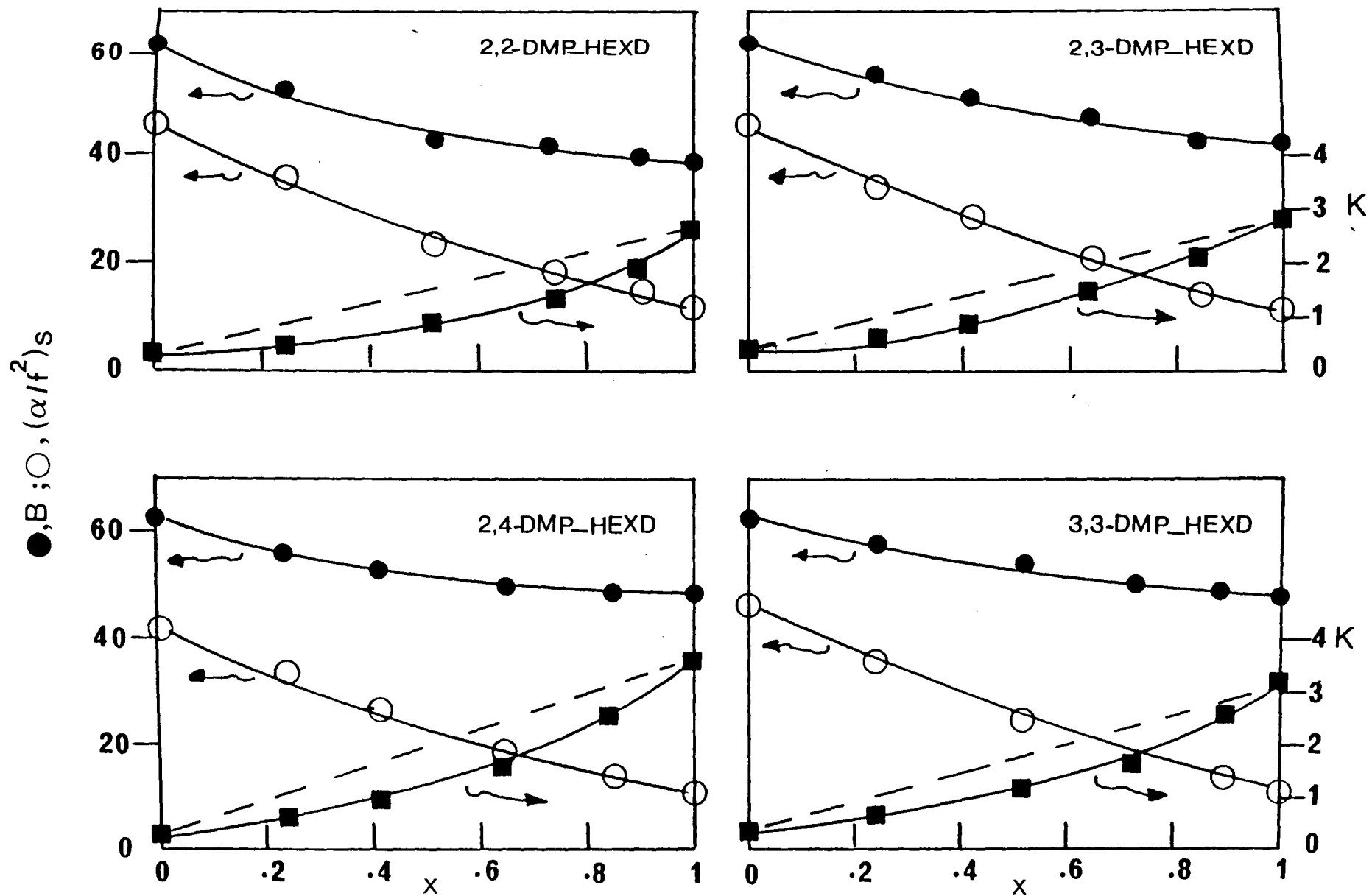


Figure 6.8. Variation of  $B$ , shear viscosity contribution and  $K$  with mole fraction,  $x$ , of dimethylpentane for  $[xC_7H_{16} + (1-x) n\text{-hexadecane}]$  at 298.15K.

unresolved volume viscosity is sometimes attributed to a high frequency rotational isomeric process, but in this study this possibility has been removed as the relaxation term A. Vibrational relaxation, too, cannot account for the values obtained and so this indicated that the assignment of structural compression as appropriate absorption phenomena.

The deviations from ideal mixing characterized by the variation of B with concentration, Figure 6.8, are in the case of 2,2- and 2,4-dimethylpentane an order of magnitude larger than the error involved in its determination. In the case of 2,3- and 3,3-dimethylpentane, the deviation from ideality is only slightly greater than experimental error. However, correction of the data for the shear contribution leads to an excess volume contribution that once more exhibits a deviation from ideality which is greater than the uncertainty in the experimental data. In all cases the variation of the volume contribution with concentration exhibits a negative deviation from ideal mixing behaviour.

Contributions to the acoustic attenuation, B, arising from dynamic fluctuations between transient strongly interacting forms have been successfully predicted for alcohol water mixtures and related systems from the measured thermodynamic excesses<sup>59</sup>. Using the approach outlined by Blandamer<sup>59</sup> and others<sup>209,210</sup>, the appropriate contributions to the acoustic absorption have been calculated. The

equations predict a positive excess absorption rather than the negative observed in practice. All manipulations of the basic relaxation equations lead to the same conclusions.

This apparent contradiction can be resolved by considering in more detail the process being affected by the sound wave. This is a perturbation of the distribution between various structural forms adopted by the molecules in the liquid. Unlike aqueous systems these structures are less well defined. However, the hydrocarbon is considered to exist in a compact pseudo solid-like structure having low attenuation and in a more disordered liquid-like structure. Various theories of liquids have been proposed on this basis; in fact the two state liquid model<sup>211</sup> has been used for the description of water itself<sup>212-214</sup>. Assuming that the fraction of the material in the more closely packed regions is  $x$  and the volume difference between states is  $\Delta V$ . A two state model would predict that the volume viscosity will have the form<sup>215</sup>:

$$\eta_v = \frac{(\Delta V)^2}{RT} \frac{\eta_s}{(\kappa_s)^2} (1 - x) x^2 \quad 6.8$$

where  $\eta_s$  is the shear viscosity,  $\kappa_s$  is the adiabatic compressibility defined as ( $\kappa_s = 1/\rho c^2$ ) and  $R$  and  $T$  have their usual meanings.

Application of equation 6.8 with  $\Delta V$  estimated from X-ray data leads to a value of  $x = 0.28$  for water at

298.15K<sup>215</sup>. In the present systems, the magnitude of  $\Delta V$  is unknown and therefore  $F(v,x)$  can be calculated defined as

$$F(v,x) = \frac{\eta_v}{\eta_s} (\kappa_s)^2 RT \quad 6.9$$

If the binary mixture is considered to be a simple combination of the structures found in the pure liquids then equation 6.9 should have a Raoult's Law form for the mixture. Plots of  $F(v,x)$  as a function of temperature for pure n-hexadecane and as a function of concentration in various binary mixtures are shown in Figures 6.9 and 6.10 respectively.

An increase of  $F(v,x)$  with temperature, Figure 6.9, would be consistent with a decrease in  $x$ , since  $(\Delta V)^2$  will always exhibit a positive temperature dependence. A reduction in  $x$  is associated with a loss of order in the liquid.

A negative deviation from Raoult's Law would imply an increase in  $x$  consistent with the creation of a larger proportion of close packed structure or a decrease in the  $(\Delta V)^2$  on mixing. Both possibilities are consistent with an observed negative volume of mixing and lead to the conclusion that the mixture has a more tightly packed structure than the component liquids. These observations may be directly related to the existence of a structural contribution to  $\chi_{12}$ , in the theory of liquid mixtures.

The creation of closely packed structures might be expected to lead to a reduction of the molecules undergoing internal rotation and hence to the observed values

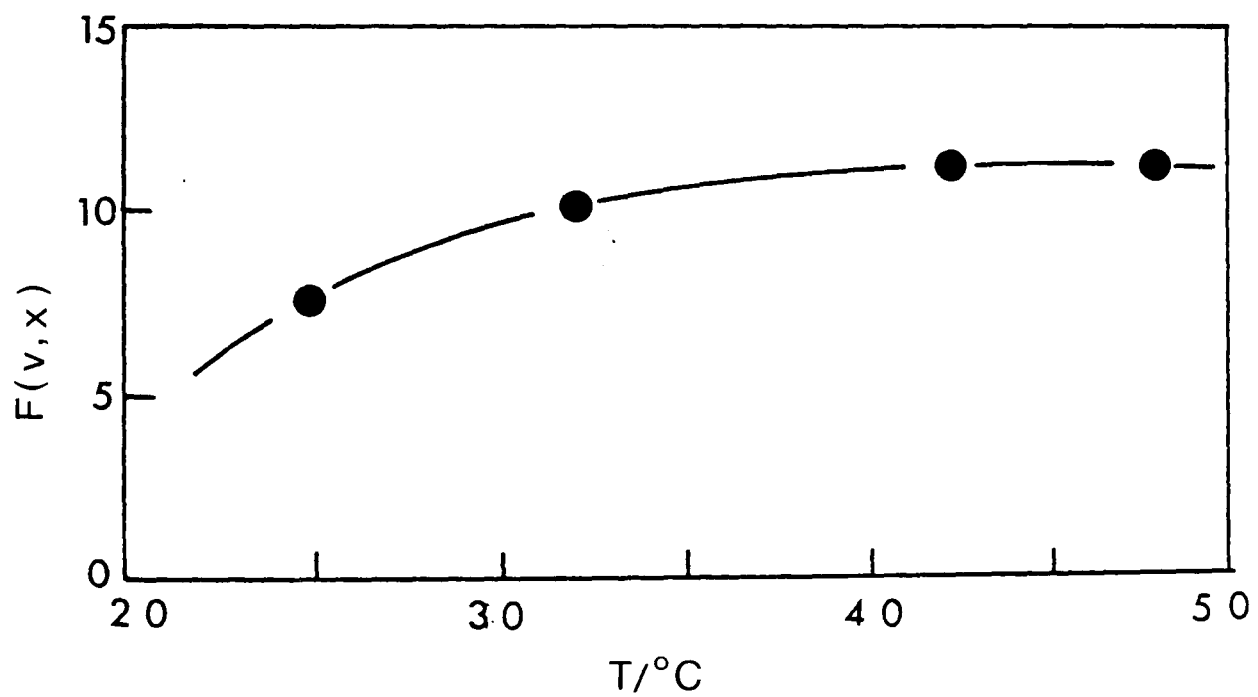


Figure 6.9. Variation of the function  $F(v,x)$  with temperature for pure n-hexadecane.

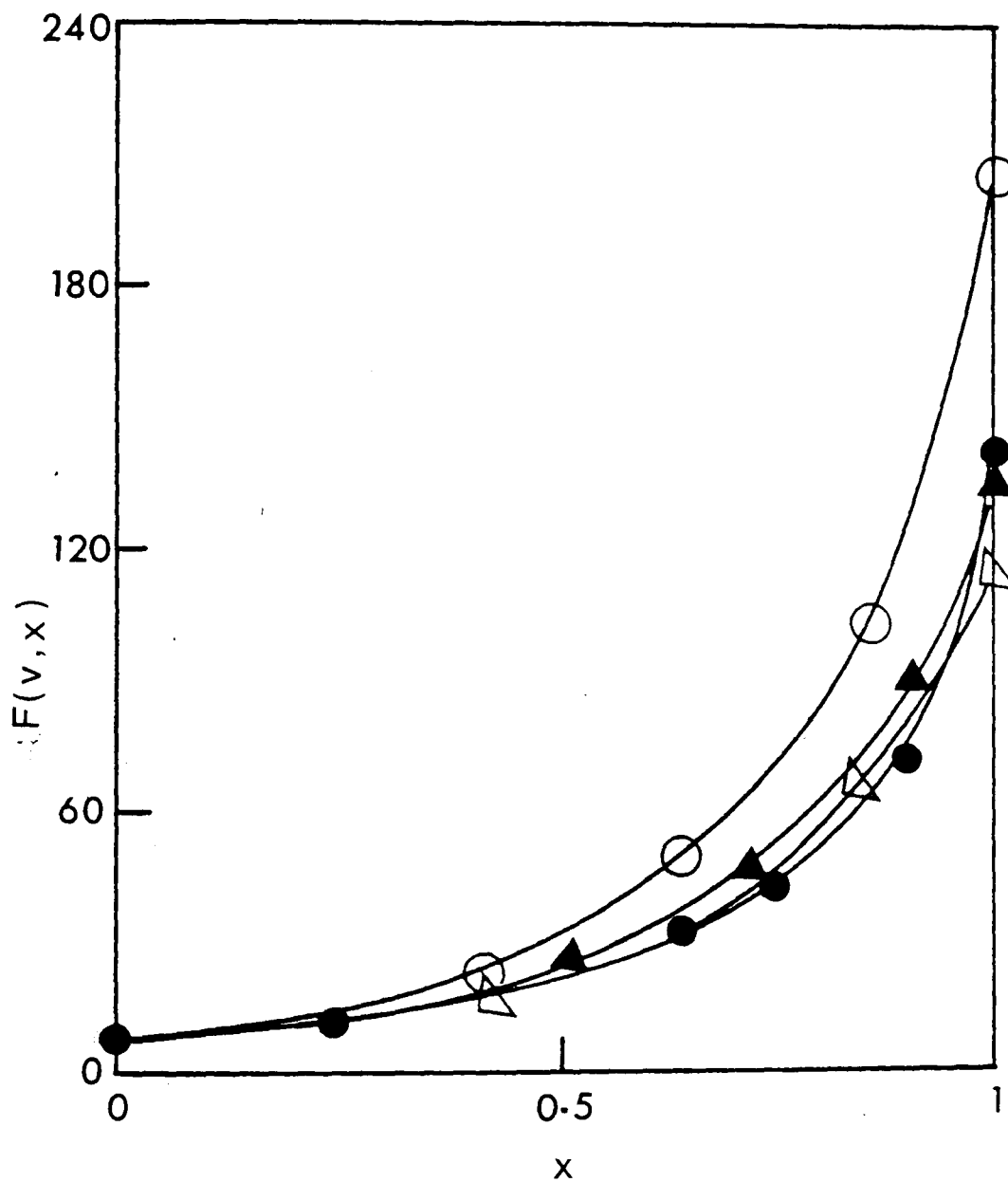


Figure 6.10. Variation of the function  $F(v,x)$  with mole fraction,  $x$ , of dimethylpentanes for  $[xC_7H_{16} + (1-x) \text{ n-hexadecane}]$  at 298.15K:

○, 2,4-dimethylpentane; ●, 2,2-dimethylpentane;  
 ▲, 3,3-dimethylpentane; △, 2,3-dimethylpentane.

of A. This is not observed. The explanation of this is that whilst a change of 5-10% in the concentration of close packed structures can significantly influence the value of B, it is barely detectable as a deviation from simple additivity of A because of the low amplitude of the relaxational contribution.

## 6.6 Conclusion

The behaviour in these mixtures is consistent with the observed acoustic attenuation being described by two contributions: a rotational isomeric process associated with hindered rotation and a clustering of the molecules in the mixture. The analysis of the data supports the hypothesis that the  $\chi_{12}$  value should contain a contribution from packing in the mixtures.

CHAPTER 7

ISOENTROPIC (ADIABATIC) COMPRESSIBILITY  
OF HYDROCARBONS AND THEIR MIXTURES

CHAPTER 7  
ISOENTROPIC (ADIABATIC) COMPRESSIBILITY  
OF HYDROCARBONS AND THEIR MIXTURES

7.1 Introduction

Ultrasonic velocity data have been obtained for a variety of liquids as a function of temperature<sup>177, 216-220</sup>. These studies showed that, with the exception of water,<sup>221,222</sup> the sound velocity of the pure liquids varies linearly with temperature.

It has been recognised for many years<sup>223-225</sup> that there exists a strong correlation between the magnitude of the ultrasonic propagation velocity and the chemical structure of its molecular entities. A major contribution in this direction was made by Rao<sup>226</sup> when he showed that a characteristic molecular sound velocity exists for each liquid, which is a function of the ultrasonic velocity, the density and the molecular weight. The Rao constant has been determined for the first few members of a number of homogeneous series. These results indicated that the Rao constant is additive and has an increment of about 195 units for each  $-\text{CH}_2-$  group in n-alkanes<sup>223</sup>, 190 for n-alkanols<sup>227</sup>, 189 for 1-olefins<sup>228</sup> and 188 for n-alkanes.<sup>229</sup> It appears that the size of the increment associated with a particular structural entity varies from homologous series to homologous series. The parachor increment is, however, often sufficiently small for doubt to exist as to whether the variation is larger than experimental error.

Ultrasonic velocity measurements have played an important role in the investigation of intermolecular interactions in liquid mixtures<sup>230-234</sup>. The strength of molecule-molecule interactions is characteristic of a particular class of liquids and is indicative of the strength of the structural interaction and extent of molecule-molecule correlations. Properties of a liquid are influenced, not only by the shape and size of the molecules, but also by the strength of dipolar interactions and/or the presence of hydrogen bonds.

This study and the previous ultrasonic studies of branched-chain hydrocarbons attempt to identify the nature of the molecule-molecule interactions in hydrocarbon mixtures, Chapters 4-6. The ultrasonic velocity and density were measured accurately over a wide range of temperature for a series of branched-chain hydrocarbons and for binary mixtures of dimethylpentanes with n-hexadecane at 298.15K. These data have been used to compute other parameters, Rao constant, van der Waals' b parameter, molecular radius and isoentropic compressibility.

The isoentropic compressibility of a liquid provides an extremely powerful tool for the investigation of deviations from ideal behaviour in liquids. Since the excess isoentropic compressibility is sensitive to any perturbation of liquid structure, it is influenced by changes in molecular shape and the form of the interaction potential. It can therefore be a more sensitive measure

of specific molecular interaction than the excess enthalpy or free energy.

The data obtained in this study are discussed in terms of the effects of stereochemistry and intermolecular interactions occurring in these liquids.

## 7.2 Materials

The purification, purity and physical properties of the materials have all been reported previously in sections 4.2, 5.2 and 6.2.

## 7.3 Results

### (i) Sound velocity and density data

The measured densities and sound velocities of pure methylpentanes, methylhexanes, pure n-hexadecane and the binary mixtures of dimethylpentane with n-hexadecane are listed in Tables 7.1-7.13. It was found that the sound velocity of pure hydrocarbons varies linearly with temperature over the whole temperature range studied, Figures 7.1 and 7.2. The variation of sound velocity of binary mixtures of dimethylpentanes and n-hexadecane with mole fraction,  $x$ , of dimethylpentane at 298.15K is presented in Figure 7.3.

### (ii) Isoentropic (adiabatic) compressibility data

Isoentropic compressibility,  $\kappa_s$ , of the pure components and the binary mixtures was calculated using equation 2.35. The data so obtained are listed in Tables 7.1 - 7.13 and plotted as a function of temperature for methylpentanes, Figure 7.4, and methylhexanes, Figure 7.5. The variation of the isoentropic compressibility with mole

TABLE 7.1. Densities, Ultrasonic Properties and other Parameters of 2-methylpentane.

T/°C	$\rho/\text{gcm}^{-3}$	$c/\text{ms}^{-1}$	$\kappa_S \times 10^{12} / \text{Pa}^{-1}$	$R/(\text{cm}^3\text{mol}^{-1})^{1/3} / (\text{ms}^{-1})^{1/3}$	$b \times 10^6 / \text{m}^3 \text{mol}^{-1}$	r/nm
40	0.63516	988	1613	1351	136	0.2378
35	0.63972	1009	1535	1351	135	0.2372
30	0.64429	1032	1457	1352	134	0.2367
25	0.64886	1054	1387	1352	133	0.2361
20	0.65343	1070	1337	1349	132	0.2356
15	0.65800	1097	1263	1351	131	0.2350
10	0.66256	1118	1207	1350	130	0.2345
5	0.66713	1139	1156	1349	129	0.2339
0	0.67170	1160	1106	1348	128	0.2334
-5	0.67627	1184	1054	1348	127	0.2329
-10	0.68084	1205	1011	1347	127	0.2324
-15	0.68540	1225	971	1346	126	0.2318
-20	0.68997	1247	931	1345	125	0.2313
-25	0.69454	1271	891	1349	124	0.2308
-30	0.69911	1300	846	1345	123	0.2303
-35	0.70368	1313	824	1341	123	0.2298
-40	0.70824	1334	793	1340	122	0.2293

TABLE 7.2. Densities, Ultrasonic Properties and other Parameters of 3-methylpentane.

T/°C	$\rho/\text{gcm}^{-3}$	$c/\text{ms}^{-1}$	$\kappa_S \times 10^{12} / \text{Pa}^{-1}$	$R/(\text{cm}^3\text{mol}^{-1})^{1/3} / (\text{ms}^{-1})^{1/3}$	$b \times 10^6 / \text{m}^3\text{mol}^{-1}$	r/nm
40	0.64658	1012	1510	1338	133	0.2364
35	0.65107	1034	1437	1338	132	0.2358
30	0.65555	1056	1368	1339	131	0.2353
25	0.66004	1079	1301	1339	131	0.2348
20	0.66453	1099	1246	1338	130	0.2342
15	0.66902	1124	1183	1340	129	0.2337
10	0.67351	1144	1135	1338	128	0.2332
5	0.67800	1167	1083	1338	127	0.2327
0	0.68249	1188	1038	1337	126	0.2322
-5	0.68687	1212	991	1338	126	0.2317
-10	0.69146	1231	954	1336	125	0.2312
-15	0.69595	1256	911	1336	124	0.2307
-20	0.70044	1278	874	1335	123	0.2302
-25	0.70493	1299	841	1331	122	0.2297
-30	0.70942	1322	807	1334	122	0.2292
-35	0.71390	1345	774	1333	121	0.2287
-40	0.71839	1364	748	1330	120	0.2282

TABLE 7.3. Densities, Ultrasonic Properties and other Parameters of  
2,3-dimethylpentane.

T/°C	$\rho/\text{gcm}^{-3}$	$c/\text{ms}^{-1}$	$\kappa_S \times 10^{12} / \text{Pa}^{-1}$	$R/(\text{cm}^3\text{mol}^{-1})^{1/3}$	$b \times 10^6 / \text{m}^3\text{mol}^{-1}$	r/nm
40	0.67841	1068	1292	1510	148	0.2446
35	0.68340	1088	1236	1508	147	0.2440
30	0.68673	1107	1186	1510	146	0.2436
25	0.69089	1130	1134	1511	145	0.2431
20	0.69505	1150	1088	1511	144	0.2427
15	0.69921	1169	1047	1510	143	0.2422
10	0.70336	1190	1004	1510	142	0.2417
5	0.70752	1211	964	1510	142	0.2412
0	0.71168	1232	926	1510	141	0.2408
-5	0.71584	1254	888	1510	140	0.2403
-10	0.71999	1272	858	1508	139	0.2398
-15	0.72416	1292	827	1507	138	0.2394
-20	0.72831	1312	798	1506	138	0.2389
-25	0.73247	1332	770	1505	137	0.2385
-30	0.73665	1353	742	1504	136	0.2380
-35	0.74079	1373	716	1503	135	0.2376
-40	0.74495	1393	692	1502	135	0.2371

TABLE 7.4. Densities, Ultrasonic Properties and other Parameters of 2,4-dimethylpentane.

T/°C	$\rho/\text{gcm}^{-3}$	$c/\text{ms}^{-1}$	$\kappa_S \times 10^{12} / \text{Pa}^{-1}$	$R/(\text{cm}^3\text{mol}^{-1})^{1/3}$ ( $\text{ms}^{-1}$ ) <sup>1/3</sup>	$b \times 10^6 / \text{m}^3\text{mol}^{-1}$	r/nm
40	0.65613	996	1633	1525	153	0.2474
35	0.66034	1019	1458	1527	152	0.2468
30	0.66455	1042	1386	1529	151	0.2463
25	0.66877	1068	1131	1524	150	0.2458
20	0.67298	1087	1258	1531	149	0.2453
15	0.67719	1118	1181	1536	148	0.2484
10	0.68140	1143	1123	1537	147	0.2443
5	0.68561	1162	1080	1537	146	0.2438
0	0.68982	1187	1029	1538	145	0.2433
-5	0.69403	1207	989	1537	144	0.2428
-10	0.69824	1226	953	1536	144	0.2423
-15	0.70245	1249	913	1536	143	0.2418
-20	0.70666	1272	875	1537	142	0.2413
-25	0.71088	1295	839	1537	141	0.2408
-30	0.71508	1318	805	1537	140	0.2404
-35	0.71930	1341	773	1536	139	0.2399
-40	0.72351	1364	743	1536	139	0.2394

TABLE 7.5. Densities, Ultrasonic Properties and other Parameters of  
2,2,4-trimethylpentane.

T/°C	$\rho/\text{gcm}^{-3}$	$c/\text{ms}^{-1}$	$\kappa_S \times 10^{12}/\text{Pa}^{-1}$	$R/(\text{cm}^3\text{mol}^{-1})^{1/3}$	$b \times 10^6/\text{m}^3\text{mol}^{-1}$	$r/\text{nm}$
40	0.67573	1016	1434	1700	169	0.2559
35	0.67980	1039	1363	1712	168	0.2554
30	0.68387	1068	1282	1718	167	0.2549
25	0.68794	1083	1239	1705	166	0.2544
20	0.69201	1108	1177	1708	165	0.2539
15	0.69608	1128	1129	1708	164	0.2534
10	0.70014	1148	1084	1709	163	0.2529
5	0.70420	1169	1039	1704	162	0.2524
0	0.70828	1188	1000	1708	161	0.2519
-5	0.71235	1214	953	1711	160	0.2514
-10	0.71642	1236	914	1711	159	0.2509
-15	0.72049	1259	876	1712	159	0.2505
-20	0.72456	1283	838	1713	158	0.2500
-25	0.72862	1306	805	1714	157	0.2495
-30	0.73269	1328	774	1714	156	0.2491
-35	0.73676	1384	747	1713	155	0.2486
-40	0.74083	1370	719	1712	154	0.2482

7.

TABLE 7.6. Densities, Ultrasonic Properties and other Parameters of  
2,3,4-trimethylpentane

T/°C	$\rho/\text{gcm}^{-3}$	$c/\text{ms}^{-1}$	$\kappa_S \times 10^{12}/\text{Pa}^{-1}$	$R/(\text{cm}^3\text{mol}^{-1})$ $(\text{ms}^{-1})^{1/3}$	$b \times 10^6/\text{m}^3\text{mol}^{-1}$	r/nm
40	0.70354	1091	1194	1671	162	0.2525
35	0.70742	1113	1141	1673	162	0.2520
30	0.71130	1135	1091	1675	161	0.2515
25	0.71517	1161	1037	1679	160	0.2511
20	0.71905	1180	999	1679	159	0.2506
15	0.72293	1198	964	1678	158	0.2502
10	0.72681	1225	917	1682	157	0.2497
5	0.73068	1249	877	1684	156	0.2493
0	0.73456	1269	845	1684	156	0.2488
-5	0.73844	1289	815	1684	155	0.2484
-10	0.74232	1311	784	1684	154	0.2480
-15	0.74619	1334	753	1685	153	0.2476
-20	0.75007	1356	725	1686	152	0.2471
-25	0.75395	1378	699	1686	152	0.2467
-30	0.75783	1400	673	1686	151	0.2463
-35	0.76170	1422	649	1686	150	0.2459
-40	0.76558	1444	626	1686	149	0.2455

TABLE 7.7. Densities, Ultrasonic Properties and other Parameters of 2-methylhexane.

$T/^{\circ}\text{C}$	$\rho/\text{gcm}^{-3}$	$c/\text{ms}^{-1}$	$\kappa_{\text{S}} \times 10^{12} / \text{Pa}^{-1}$	$R/(\text{cm}^3\text{mol}^{-1})$ $(\text{ms}^{-1})^{1/3}$	$b \times 10^6 / \text{m}^3\text{mol}^{-1}$	$r/\text{nm}$
40	0.66171	1048	1376	1538	151	0.2467
35	0.66600	1067	1319	1538	151	0.2461
30	0.67030	1087	1263	1537	150	0.2456
25	0.67457	1107	1210	1537	149	0.2451
20	0.67888	1127	1160	1536	148	0.2446
15	0.68318	1147	1113	1535	147	0.2441
10	0.68747	1167	1068	1535	146	0.2436
5	0.69177	1186	1028	1534	145	0.2430
0	0.69606	1206	988	1533	144	0.2425
-5	0.70028	1226	950	1532	142	0.2422
-10	0.70454	1246	914	1531	142	0.2416
-15	0.70880	1266	880	1529	141	0.2411
-20	0.71307	1286	848	1528	141	0.2405
-25	0.71733	1306	817	1527	140	0.2401
-30	0.72160	1325	789	1525	139	0.2396

TABLE 7.8. Densities, Ultrasonic Properties and other Parameters of  
3-methylhexane.

T/°C	$\rho/\text{gcm}^{-3}$	$c/\text{ms}^{-1}$	$\kappa_S \times 10^{12} / \text{Pa}^{-1}$	$R/(\text{cm}^3\text{mol}^{-1})$ $(\text{ms}^{-1})^{1/3}$	$b \times 10^6 / \text{m}^3\text{mol}^{-1}$	r/nm
40	0.67032	1069	1306	1529	150	0.2456
35	0.67459	1089	1250	1528	149	0.2451
30	0.67886	1109	1198	1528	148	0.2446
25	0.68312	1128	1151	1527	147	0.2441
20	0.68739	1148	1104	1527	146	0.2436
15	0.69165	1168	1060	1526	145	0.2431
10	0.69592	1187	1020	1525	144	0.2426
5	0.70019	1207	980	1524	143	0.2421
0	0.70445	1227	943	1523	142	0.2416
-5	0.70872	1246	909	1522	141	0.2411
-10	0.71298	1266	875	1520	141	0.2406
-15	0.71725	1286	843	1519	140	0.2401
-20	0.72151	1305	814	1518	139	0.2397
-25	0.72578	1325	785	1516	138	0.2392
-30	0.73005	1344	758	1515	137	0.2387

TABLE 7.9. Densities, Ultrasonic Properties and other Parameters of  
2,2-dimethylhexane.

T/°C	$\rho/\text{gcm}^{-3}$	$c/\text{ms}^{-1}$	$\kappa_S \times 10^{12}/\text{Pa}^{-1}$	$R/(\text{cm}^3\text{mol}^{-1})$ $(\text{ms}^{-1})^{1/3}$	$b \times 10^6/\text{m}^3\text{mol}^{-1}$	r/nm
40	0.67865	1063	1304	1718	168	0.2555
35	0.68284	1083	1249	1718	167	0.2550
30	0.68702	1101	1201	1717	166	0.2545
25	0.69101	1119	1156	1716	165	0.2540
20	0.69538	1139	1109	1715	164	0.2534
15	0.69958	1157	1068	1714	163	0.2529
10	0.70377	1176	1027	1713	162	0.2524
5	0.70796	1195	989	1712	161	0.2519
0	0.71214	1213	954	1711	160	0.2514
-5	0.71633	1232	920	1710	160	0.2509
-10	0.72051	1251	887	1708	159	0.2505
-15	0.72470	1270	856	1707	158	0.2501
-20	0.72889	1288	827	1705	157	0.2495
-25	0.73308	1307	799	1704	156	0.2490
-30	0.73726	1326	771	1702	155	0.2486

TABLE 7.10. Densities, Ultrasonic Properties and other Parameters of  
2,5-dimethylhexane.

T/°C	$\rho/\text{gcm}^{-3}$	$c/\text{ms}^{-1}$	$\kappa_s \times 10^{12} / \text{Pa}^{-1}$	$R/(\text{cm}^3\text{mol}^{-1})^{1/3}$ $(\text{ms}^{-1})^{1/3}$	$b \times 10^6 / \text{m}^3\text{mol}^{-1}$	r/nm
40	0.67748	1066	1299	1723	169	0.2557
35	0.68157	1085	1246	1722	168	0.2551
30	0.68566	1104	1197	1722	167	0.2546
25	0.68975	1123	1150	1721	166	0.2541
20	0.69384	1142	1105	1721	165	0.2536
15	0.69793	1161	1063	1720	164	0.2531
10	0.70202	1180	1023	1719	163	0.2526
5	0.70611	1198	987	1718	162	0.2521
0	0.71020	1217	951	1717	161	0.2516
-5	0.71429	1236	916	1716	160	0.2511
-10	0.71838	1255	884	1715	159	0.2507
-15	0.72470	1247	850	1709	158	0.2502
-20	0.72656	1293	823	1713	157	0.2498
-25	0.73065	1312	795	1711	156	0.2493
-30	0.73474	1331	768	1710	156	0.2488

TABLE 7.11. Densities, Ultrasonic Properties and other Parameters of  
2,2,4-trimethylhexane.

T/°C	$\rho/\text{gcm}^{-3}$	$c/\text{ms}^{-1}$	$\kappa_S \times 10^{12} / \text{Pa}^{-1}$	$R/(\text{cm}^3\text{mol}^{-1})$ $(\text{ms}^{-1})^{1/3}$	$b \times 10^6 / \text{m}^3\text{mol}^{-1}$	r/nm
40	0.70056	1090	1201	1884	183	0.2628
35	0.70435	1108	1157	1885	182	0.2623
30	0.70813	1129	1108	1886	181	0.2618
25	0.71193	1146	1070	1885	180	0.2614
20	0.71567	1165	1030	1886	179	0.2609
15	0.71949	1184	992	1886	178	0.2604
10	0.72327	1202	957	1886	177	0.2600
5	0.72706	1221	923	1886	176	0.2595
0	0.73084	1240	890	1885	176	0.2591
-5	0.73464	1259	859	1885	175	0.2586
-10	0.73841	1277	831	1885	174	0.2581
-15	0.74220	1296	802	1884	173	0.2578
-20	0.74598	1315	775	1884	172	0.2573
-25	0.74976	1334	750	1883	171	0.2569
-30	0.75355	1352	726	1882	170	0.2564

TABLE 7.12. Densities, Ultrasonic Properties and other Parameters of n-hexadecane.

T/°C	$\rho/\text{gcm}^{-3}$	$c/\text{ms}^{-1}$	$\kappa_s \times 10^{12} / \text{Pa}^{-1}$	$R / (\text{cm}^3 \text{mol}^{-1}) (\text{ms}^{-1})^{1/3}$	$b \times 10^6 / \text{m}^3 \text{mol}^{-1}$	r/nm
25	0.77006	1341	722	3243	294	0.3077
30	0.76673	1323	745	3243	295	0.3082
35	0.76337	1306	768	3242	297	0.3086
40	0.75982	1288	793	3243	298	0.3091
45	0.75668	1271	818	3242	299	0.3095
50	0.75334	1253	846	3241	301	0.3100
55	0.74999	1236	873	3240	302	0.3105
60	0.74665	1218	903	3239	303	0.3109

TABLE 7.13. Density,  $\rho$ , sound velocity,  $c$ , isoentropic compressibility,  $\kappa_S$ , and excess isoentropic compressibility,  $\kappa_S^E$ , at 298.15K for  $[xC_7H_{16}+(1-x)n\text{-hexadecane}]$ .

x	$\rho/\text{gcm}^{-3}$	$c/\text{ms}^{-1}$	$\kappa_S \times 10^{12} / \text{Pa}^{-1}$	$\kappa_S^E \times 10^{12} / \text{Pa}^{-1}$
x,2,2-dimethylpentane + (1-x) n-hexadecane				
0.000	0.7700	1341	722	.....
0.130	0.7636	1323	748	-15.85
0.237	0.7576	1304	776	-27.56
0.521	0.7365	1245	876	-57.49
0.744	0.7127	1181	1006	-70.77
0.901	0.6893	1117	1163	-51.05
1.000	0.6696	1065	1317	.....
x,2,3-dimethylpentane + (1-x) n-hexadecane				
0.083	0.7669	1331	736	-2.97
0.241	0.7603	1311	765	-11.76
0.411	0.7514	1287	803	-21.27
0.638	0.7356	1242	881	-27.39
0.835	0.7163	1190	986	-23.25
0.942	0.7020	1154	1070	-9.04
1.000	0.6927	1134	1123	.....
x,3,3-dimethylpentane + (1-x) n-hexadecane				
0.102	0.7661	1328	740	-6.44
0.243	0.7598	1309	768	-15.60
0.512	0.7439	1268	836	-28.28
0.727	0.7258	1218	929	-46.05
0.890	0.7066	1158	1055	-23.49
1.000	0.6891	1115	1167	.....

TABLE 7.13 (cont.)

x	$\rho/\text{gcm}^{-3}$	c/ms <sup>-1</sup>	$\kappa_S \times 10^{12} / \text{Pa}^{-1}$	$\kappa_S^E \times 10^{12} / \text{Pa}^{-1}$
x, 2, 4-dimethylpentane + (1-x) n-hexadecane				
0.104	0.7648	1326	744	-11.11
0.239	0.7571	1303	778	-25.95
0.411	0.7451	1271	831	-45.89
0.645	0.7236	1209	945	-60.36
0.844	0.6979	1142	1089	-57.86
0.921	0.6851	1107	1191	-36.23
0.956	0.6784	1089	1243	-19.32
1.000	0.6689	1068	1311	.....

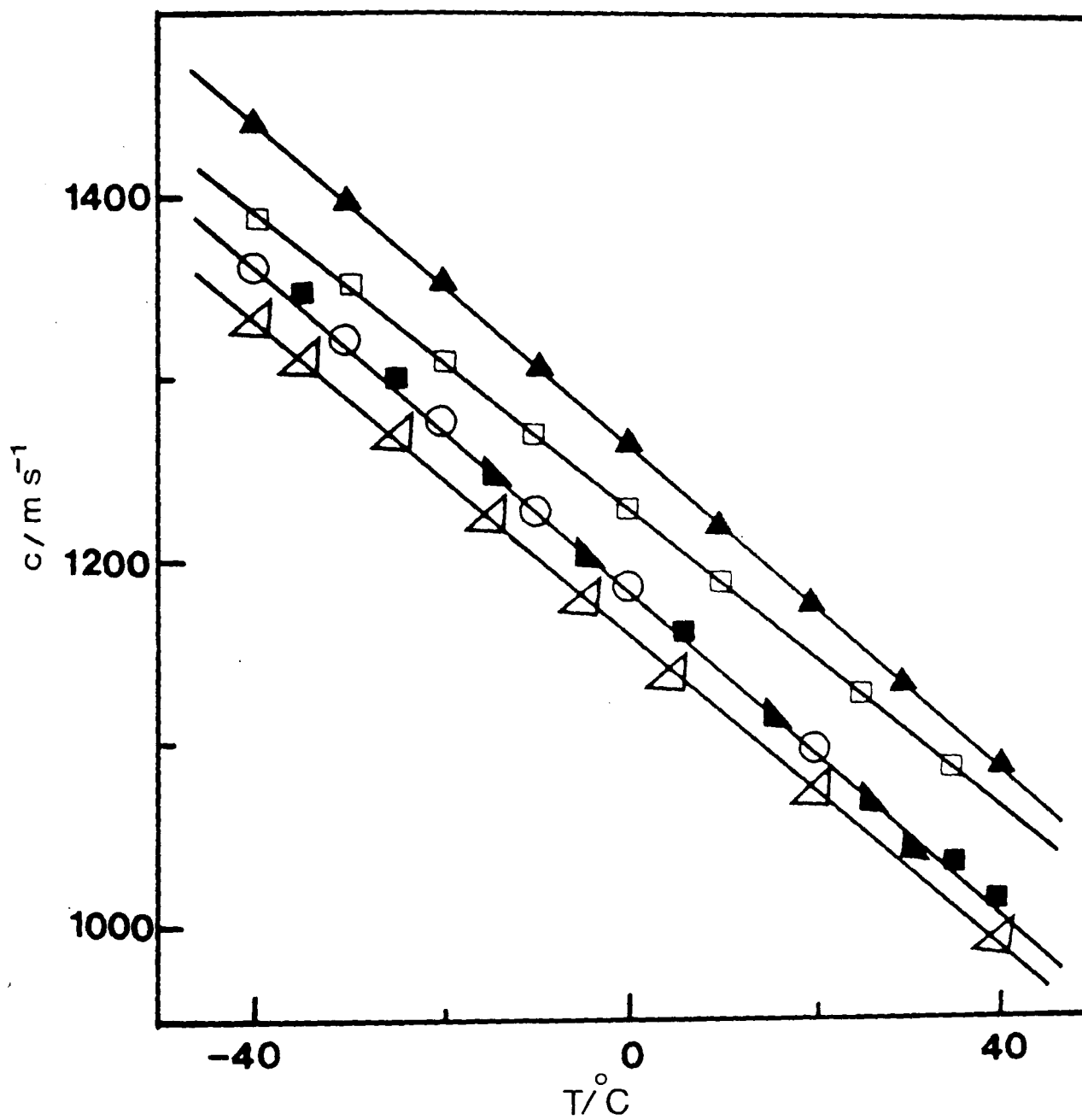


Figure 7.1. Variation of ultrasonic velocity with temperature for:  $\triangle$ , 2-methylpentane;  $\circ$ , 3-methylpentane;  $\square$ , 2,3-dimethylpentane;  $\blacktriangle$ , 2,4-dimethylpentane;  $\blacksquare$ , 2,2,4-trimethylpentane;  $\blacktriangle$ , 2,3,4-trimethylpentane.

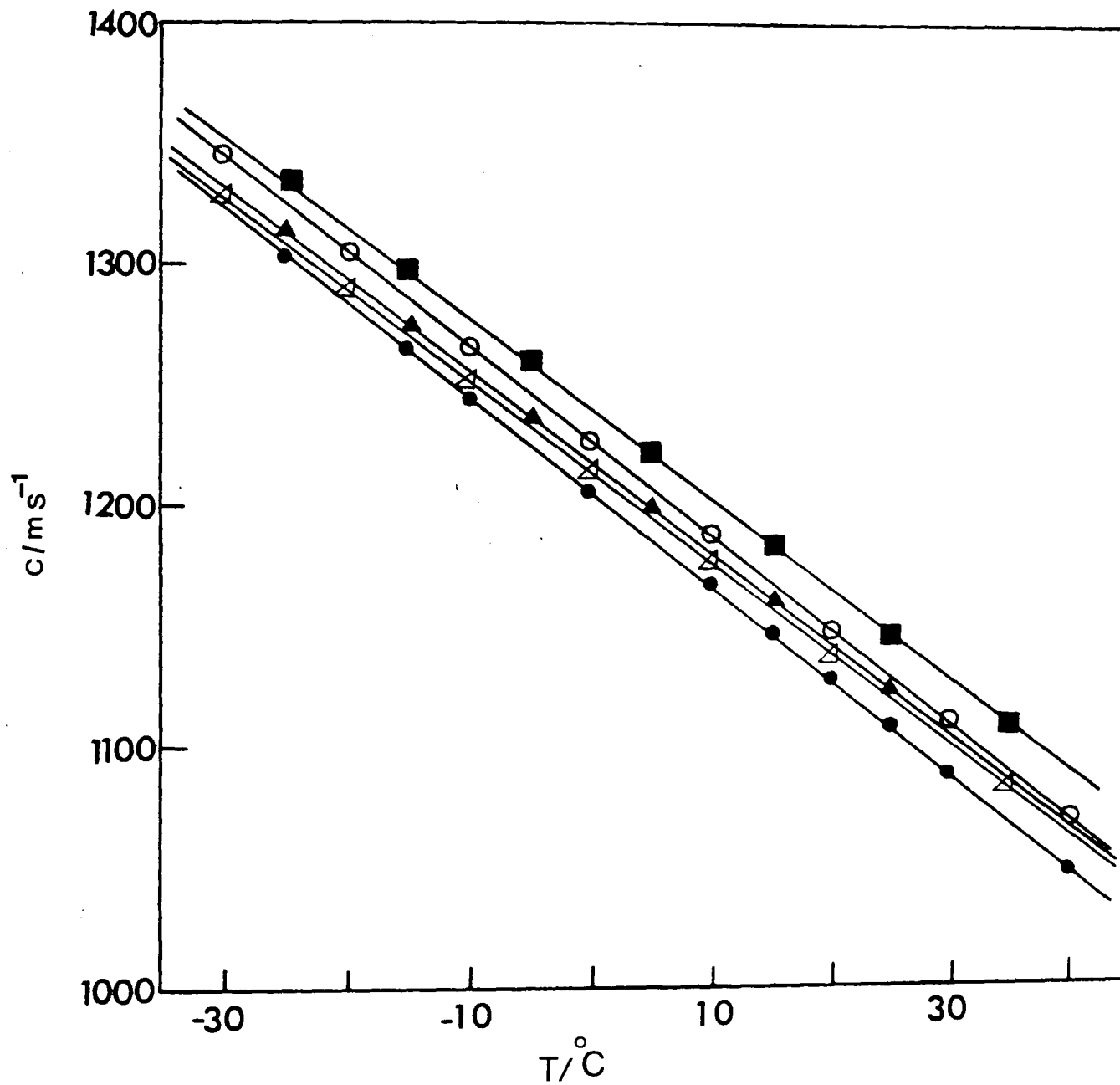


Figure 7.2. Variation of ultrasonic velocity with temperature for: ●, 2-methylhexane; ○, 3-methylhexane; △, 2,2,-dimethylhexane; ▲, 2,5-dimethylhexane; ■, 2,2,4-trimethylhexane.

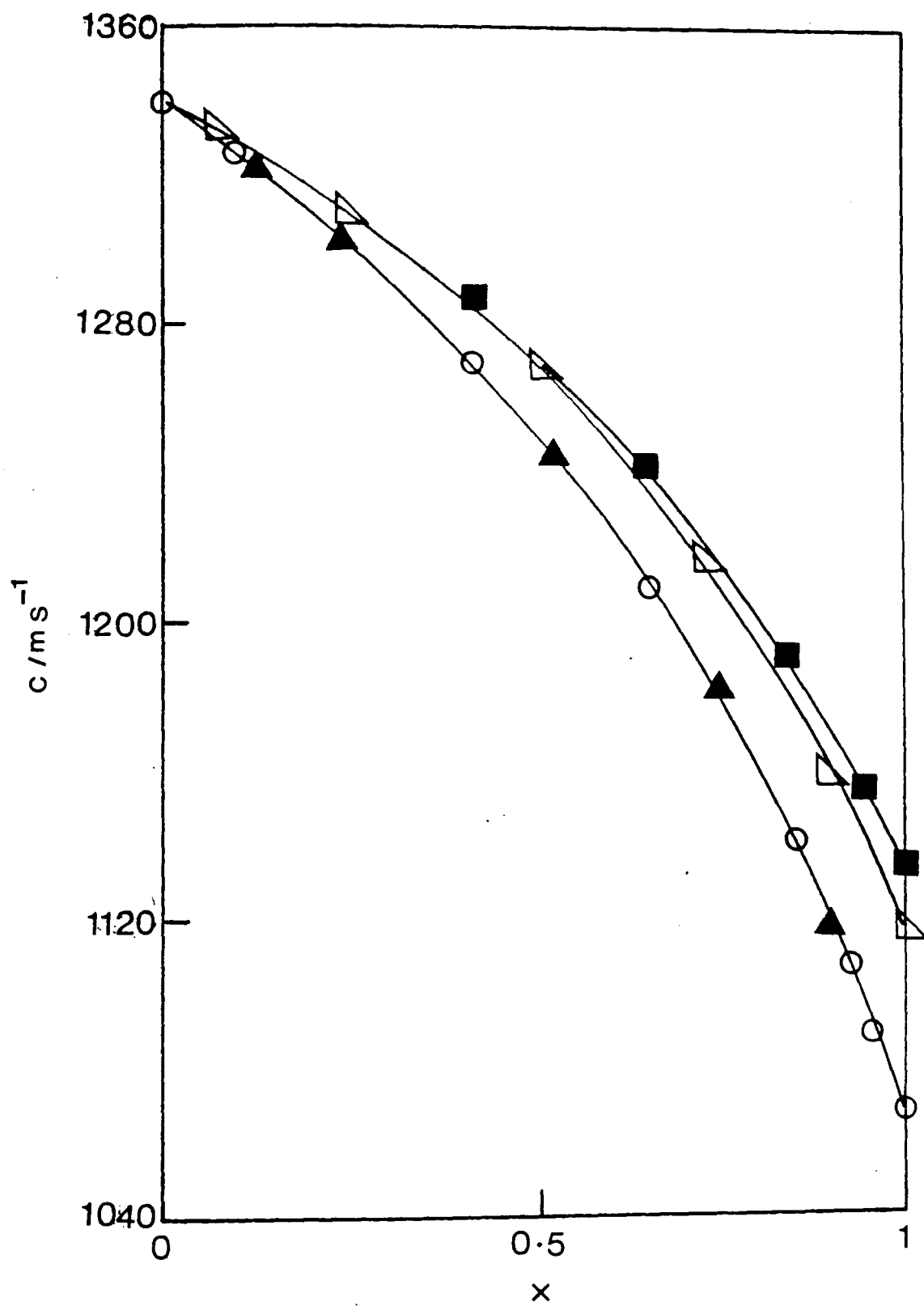


Figure 7.3. Variation of ultrasonic velocity with mole fraction,  $x$ , for  $[xC_7H_{16} + (1-x) \text{ n-hexadecane}]$  at 298.15K.

○, 2,2-dimethylpentane; ■, 2,3-dimethylpentane;  
 ▲, 2,4-dimethylpentane; △, 3,3-dimethylpentane.

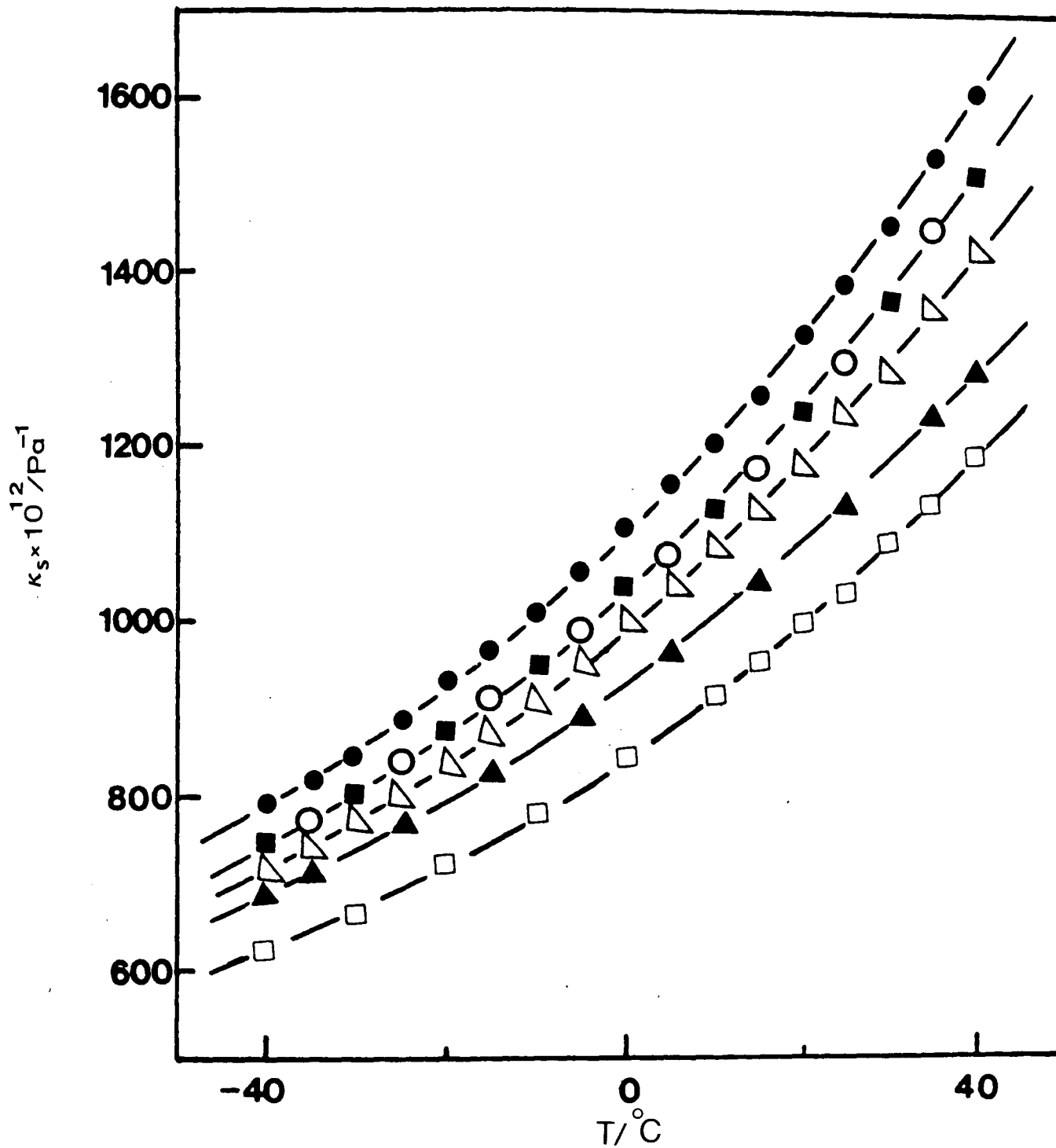


Figure 7.4. Variation of isoentropic compressibility as a function of temperature for:

●, 2-methylpentane; ■, 3-methylpentane; ▲, 2,3-dimethylpentane; ○, 2,4-dimethylpentane; △, 2,2,4-trimethylpentane; □, 2,3,4-trimethylpentane.

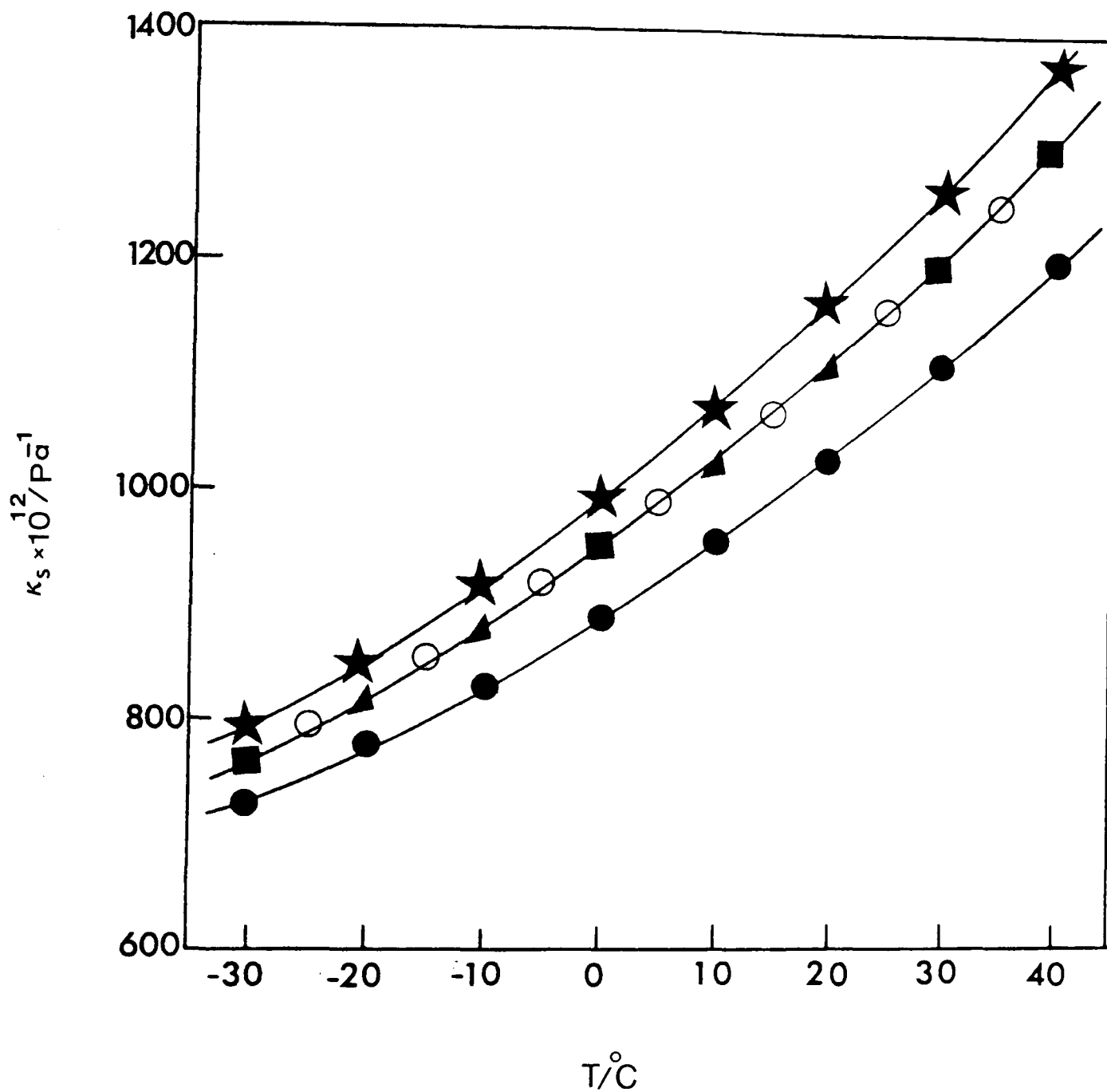


Figure 7.5. Variation of isentropic compressibility with temperature for: ★, 2-methylhexane; ▲, 3-methylhexane; ○, 2,2-dimethylhexane; ■, 2,5-dimethylhexane; ●, 2,2,4-trimethylhexane.

fraction,  $x$ , of dimethylpentane for binary mixtures of dimethylpentanes and n-hexadecane at 298.15K is illustrated in Figure 7.6.

The excess isentropic compressibility,  $\kappa_s^E$ , of binary mixtures of dimethylpentanes and n-hexadecane was calculated using equation 2.34. The data so obtained are listed in Table 7.13 and plotted as a function of mole fraction,  $x$ , of dimethylpentane at 298.15K, Figure 7.7.

#### 7.4 Discussion

##### (i) Pure liquids

It has been proposed that the velocity of sound propagation in a molecular liquid can be calculated on the basis of a simple additivity. The molar sound velocity (Rao constant)<sup>223</sup> can be calculated using the relation

$$R = Mc^{1/3}/\rho \quad 7.1$$

where  $M$  is the molecular weight,  $c$  is the sound velocity and  $\rho$  is the density. This equation would indicate that liquids of the same density should have the same sound velocities. A plot of  $R$  values for branched chain hydrocarbons at 298.15K, Figure 7.8, indicates the general validity of this hypothesis. However, it is clear that molecules with the same molecular weight do not necessarily have the same universal constants. Values for the molar velocity constant range between 188 and 195<sup>226-229</sup>. The values obtained by analysis of the data obtained in this study of branched chain hydrocarbons range from 167 to 187, Table 7.14. It is clear that, whilst this approach can

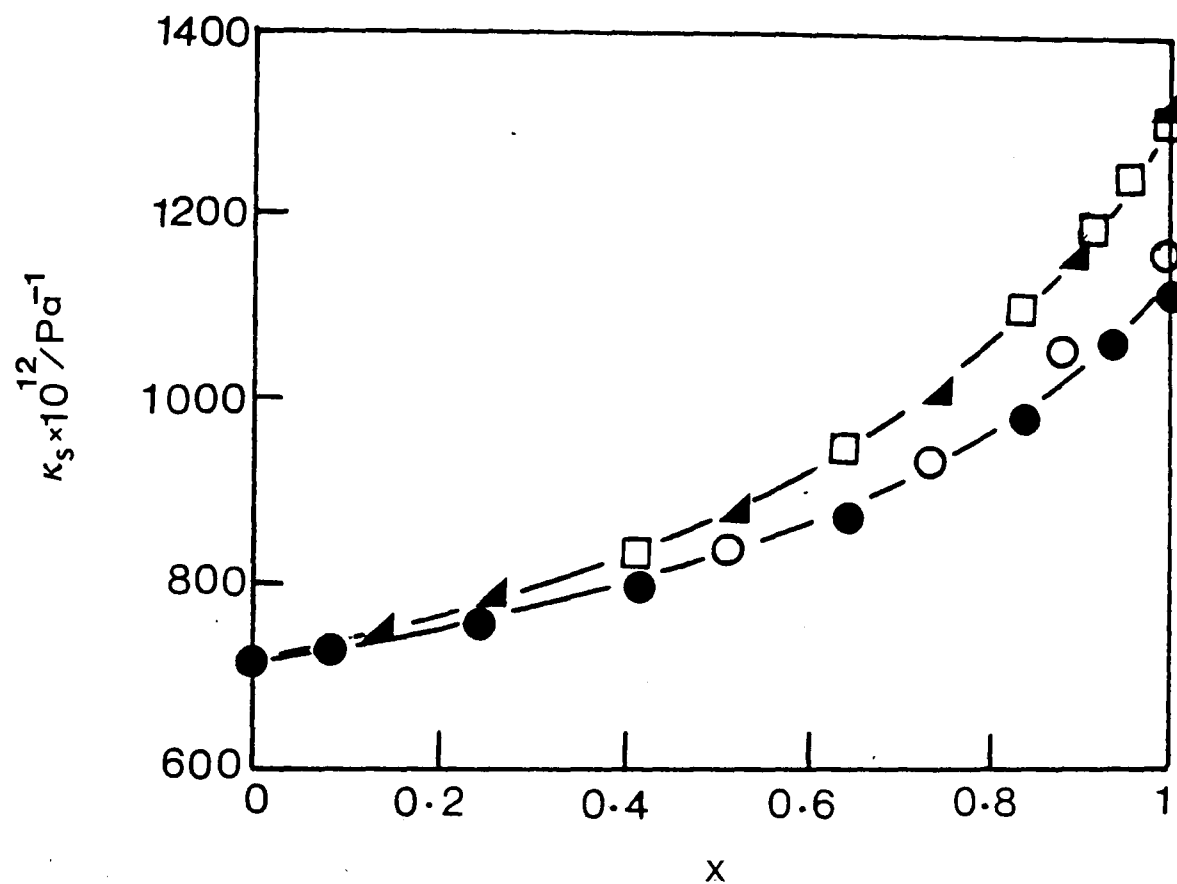


Figure 7.6. Variation of isoentropic compressibility as a function of mole fraction,  $x$ , for  $[xC_7H_{16} + (1-x) \text{ n-hexadecane}]$  at 298.15K.

▲, 2,2-dimethylpentane; ●, 2,3-dimethylpentane;  
 □, 2,4-dimethylpentane; ○, 3,3-dimethylpentane.

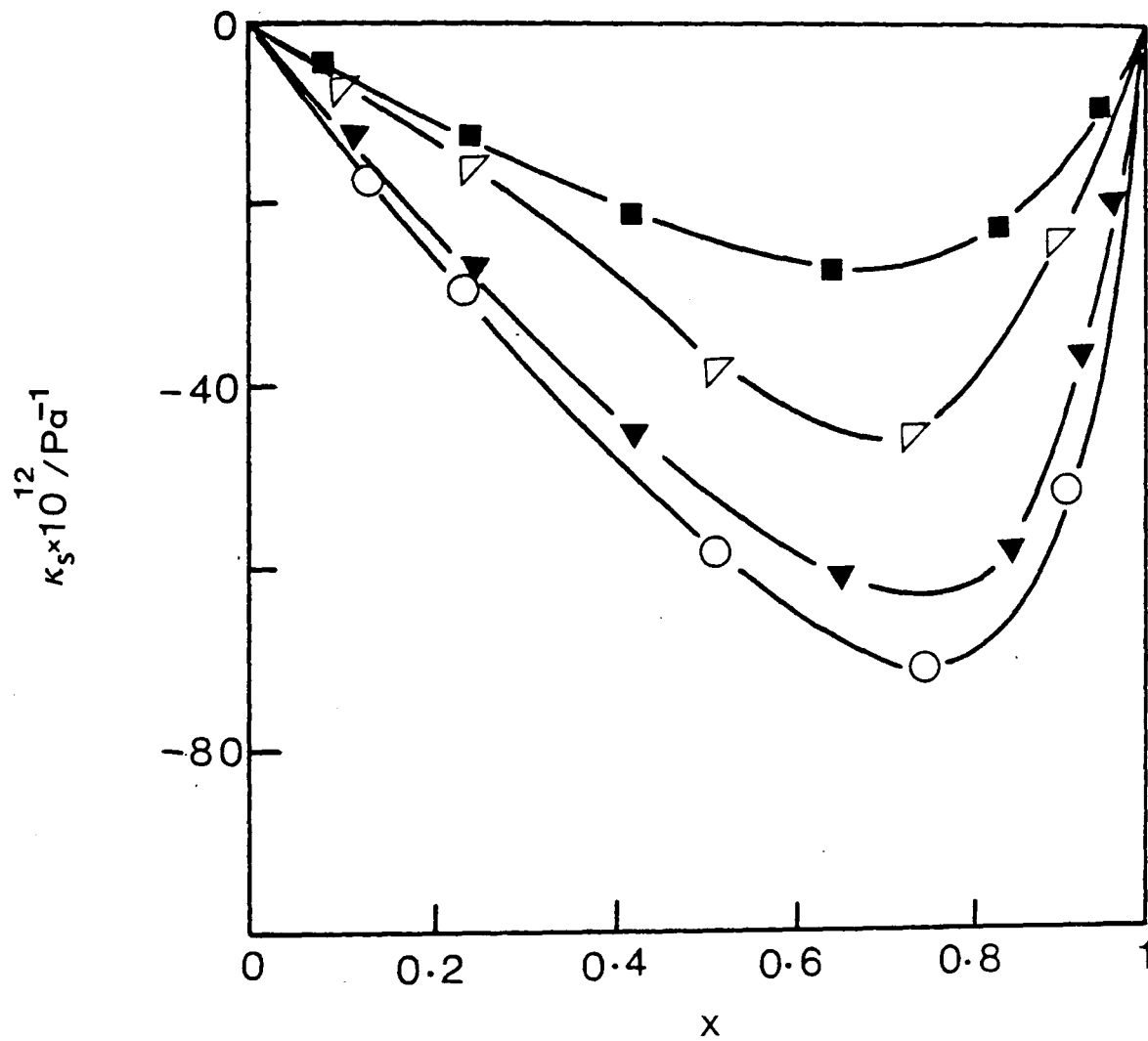


Figure 7.7. Excess isoentropic compressibility for  $[x\text{C}_7\text{H}_{16} + (1-x) \text{n-hexadecane}]$  at 298.15K.

○, 2,2-dimethylpentane; ◻, 2,3-dimethylpentane;  
 ▼, 2,4-dimethylpentane; ◁, 3,3-dimethylpentane.

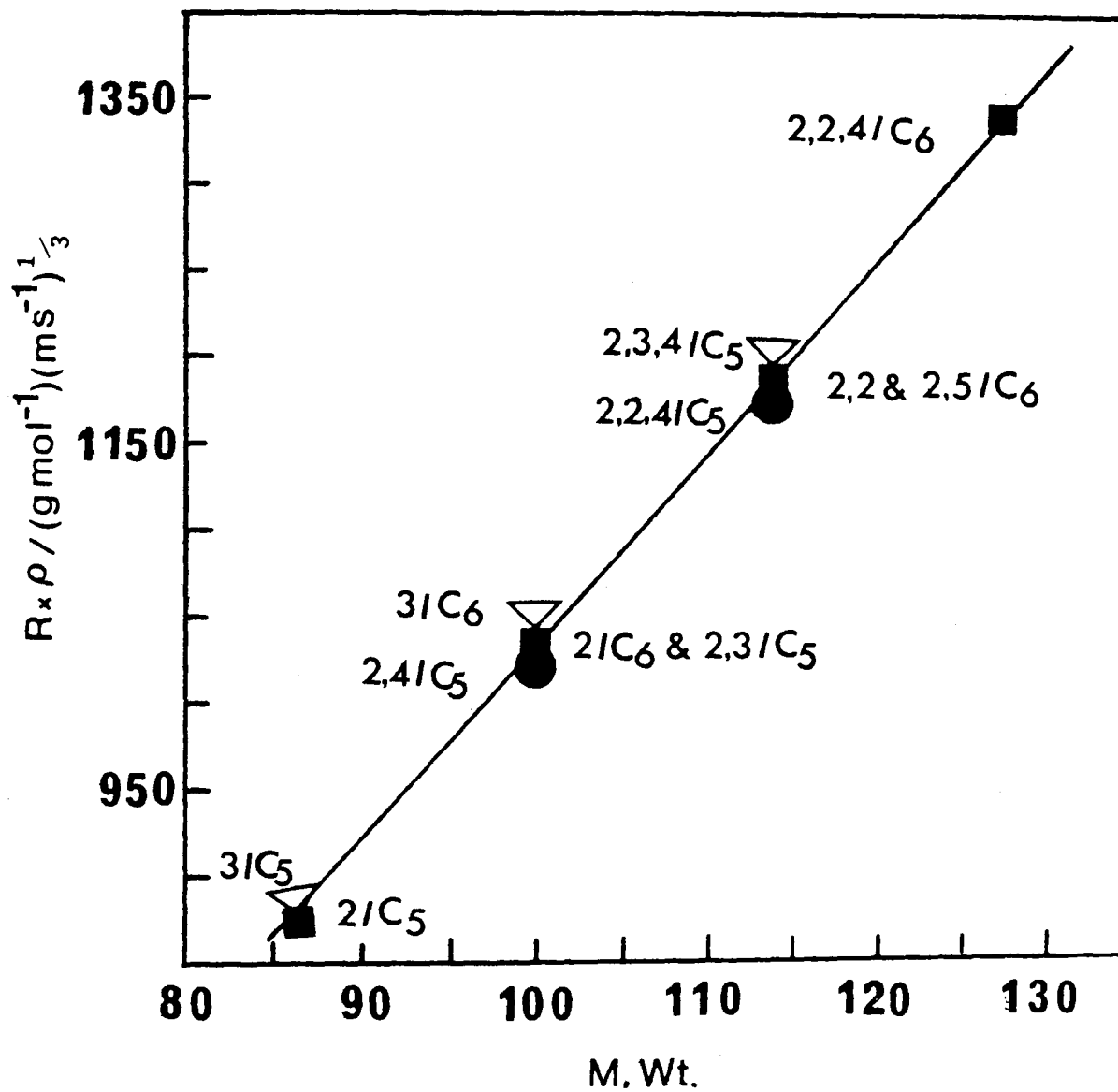


Figure 7.8. Molar sound velocity plotted as a function of molecular weight of methylpentanes and hexanes at 298.15K.

TABLE 7.14. Ultrasonic Properties of Branched Chain Hydrocarbons at 293K.

Molecule	$R / (\text{cm}^3 \text{mol}^{-1})$ $(\text{ms}^{-1})^{1/3}$	$-CH_3 / (\text{cm}^3 \text{mol}^{-1})$ $(\text{ms}^{-1})^{1/3}$
2-methylpentane	1349	
3-methylpentane	1388	
		177
2,3-dimethylpentane	1511	
2,4-dimethylpentane	1531	
		172
2,2,4-trimethylpentane	1708	
2,3,4-trimethylpentane	1679	
		188
2-methylhexane	1536	
3-methylhexane	1527	
		187
2,2-dimethylhexane	1715	
2,5-dimethylhexane	1721	
		167
2,2,4-trimethylhexane	1885	
		<u>Average</u> 178

provide an approximate guide as to the molar sound velocity, other factors occurring within the liquid will ultimately determine the observed values.

In an attempt to explore the nature of these interactions, the van der Waals' b parameter and the molecular radius were calculated. The van der Waals' b parameter is defined by Schaafs<sup>235-237</sup> in terms of

$$b = M/\rho - RT/\rho c^2 [(1 + M_c^2/3RT)^{1/2} - 1] \quad 7.2$$

where the constants have their definitions above. The molecular radius similarly can be defined as

$$r^3 = 3b/16\pi N \quad 7.3$$

where N is Avogadro's number.

The values of van der Waals' b parameter and the molecular radius so obtained are listed in Tables 7.1-7.12 and presented in Figures 7.9 and 7.10. It is clear from these plots that the values of the molar sound velocity and also b are sensitive to the molecular structure of the molecule being studied. The above equations illustrate that the properties of the fluid can be considered to arise predominantly from the repulsive non-bonding interactions between molecules. Molecules of a similar branched chain structure might be expected to exhibit similar intermolecular interactions. It has recently been shown by Chandler<sup>238-240</sup> that the thermodynamic properties of a liquid are dominated by the repulsive part of the non bonded interactions. The interpretation of the sonic propagation data in terms of Rao constants is in keeping with the views promoted by

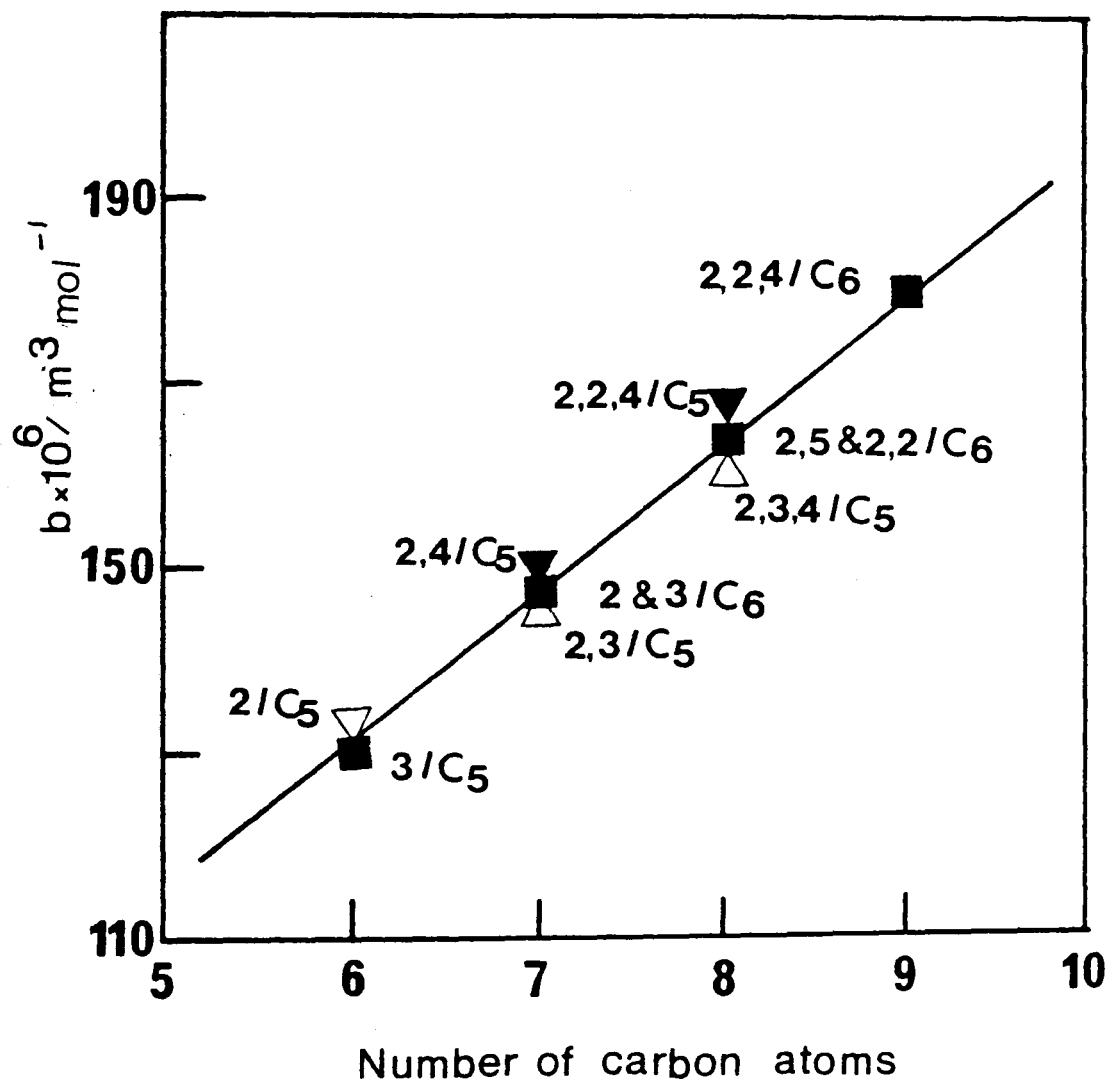


Figure 7.9. Van der Waals'  $b$  parameter plotted as a function of number of carbon atoms for methylpentanes and methylhexanes at 298.15K.

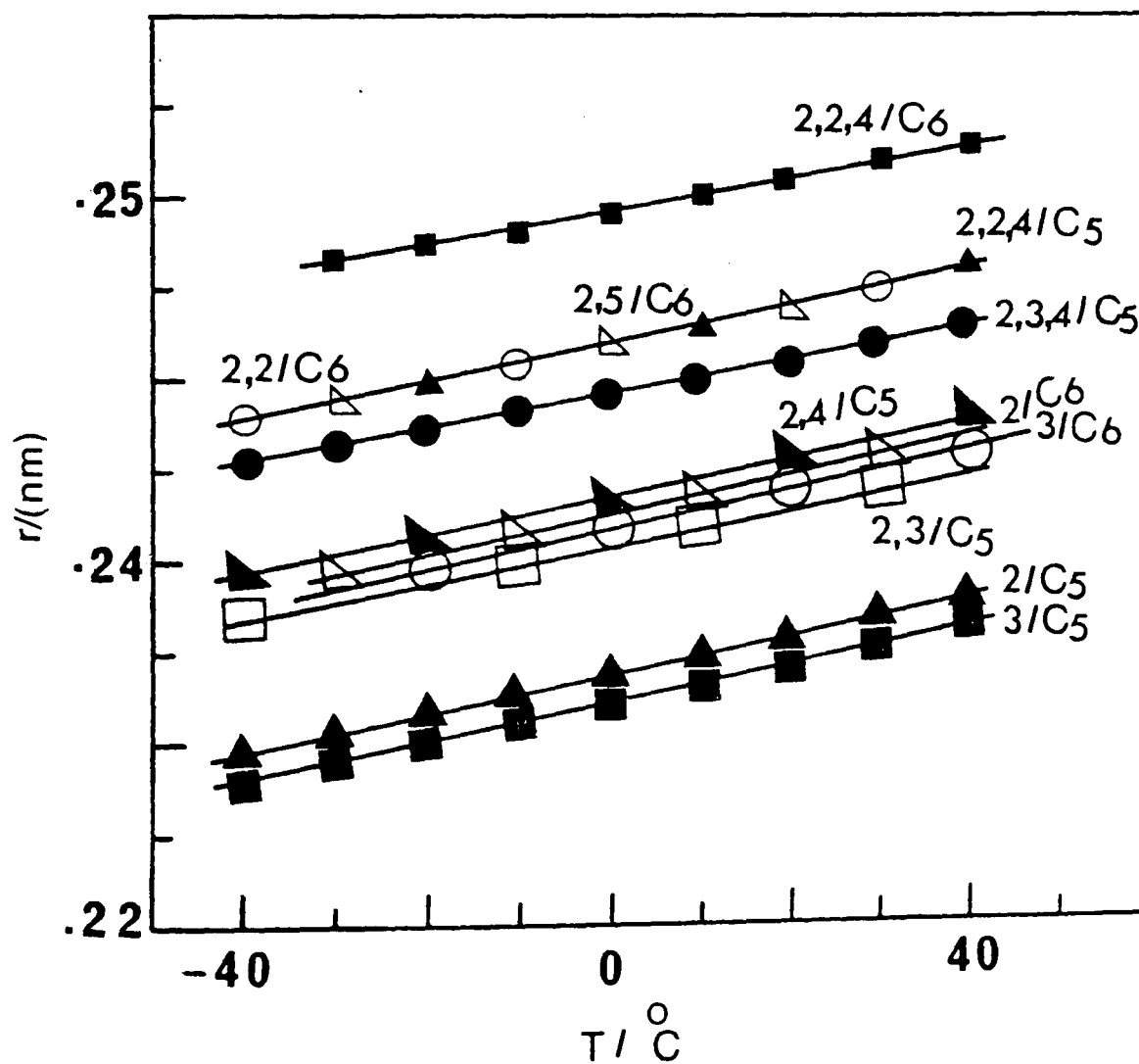
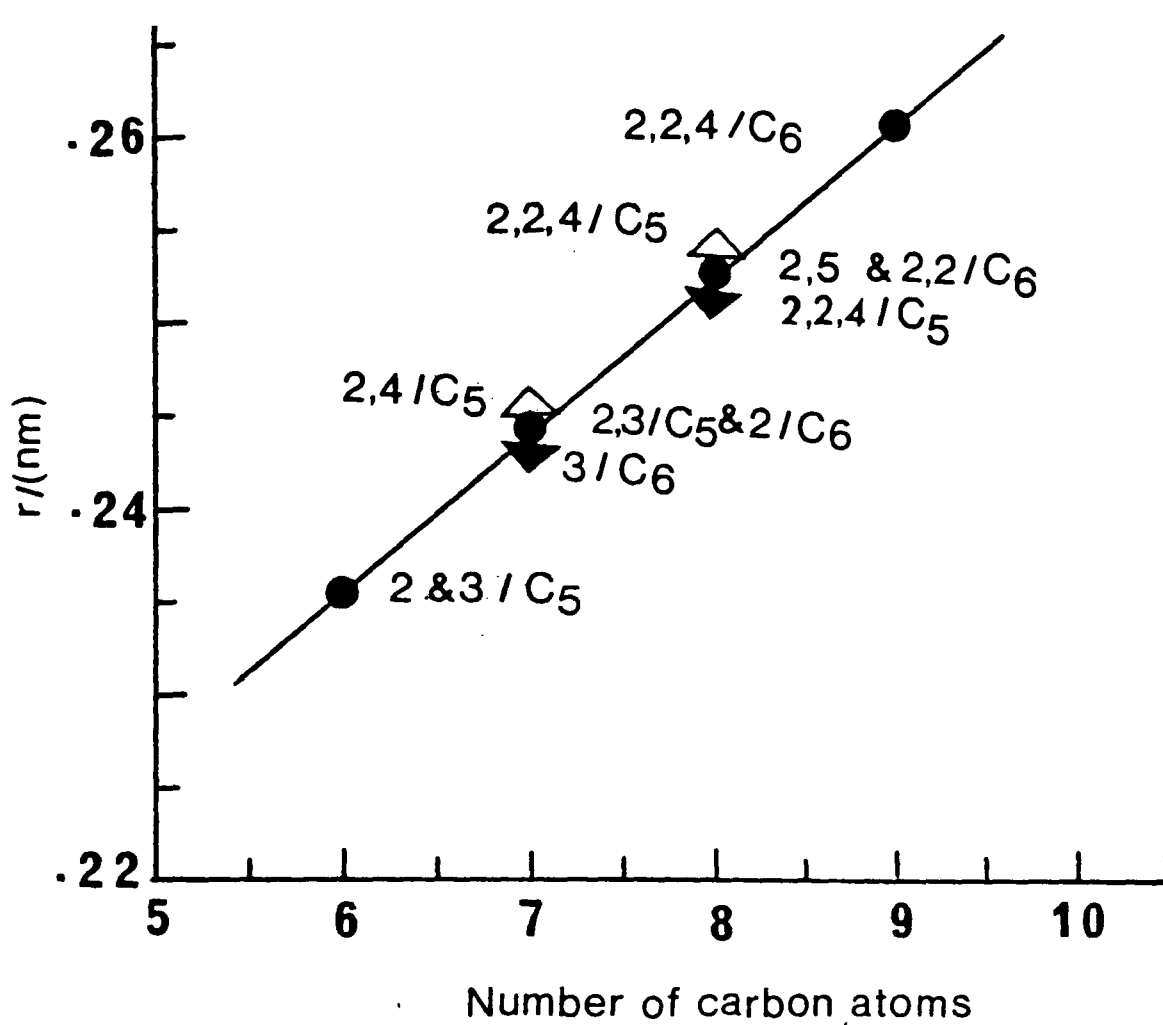


Figure 7.10. Molecular radius plotted as a function of number of carbon atoms and temperature for methylpentanes and methylhexanes.

Chandler. The differences observed must therefore reflect the differences in the shape of the molecules as a consequence of the differences in the stereochemical structure of the molecules. Jacobsen<sup>241, 242</sup> proposed a method of data analysis which proposes that for molecules having similar structures their properties can be scaled on the basis of an intermolecular free length. The intermolecular free length,  $L_f$ , was calculated for the above systems as a function of temperature from the following relation:<sup>235, 243, 244</sup>

$$L_f = 2 \left[ V \left( 1 - \frac{c}{c_\infty} \right) \right] / \left( \frac{9}{4} \pi N b^2 \right)^{1/3} \quad 7.4$$

where

$V$  = the molar volume

$c$  = the sound velocity

$c_\infty$  = 1600 ms<sup>-1</sup>

$N$  = Avogadro's number

$b$  = van der Waals' parameter

It was found that the theory and experiment are in disagreement contrary to the claims in the literature. The theory proposes that the isoentropic compressibility should be described by the relationship

$$\kappa_s = k L^p \quad 7.5$$

where  $p$  and  $k$  are temperature dependent constants and  $L$  is the free intermolecular length. Most probably the theory is failing to reflect the fact that within the hydrocarbon liquids clustering of the molecules can occur and this will

change significantly with temperature, Figure 7.11. The clustering may arise as a consequence of weak interactions or as a result of entropic considerations in binary mixtures or liquids capable of existing in more than one rotational isomeric form. As a consequence, heating the liquid will lead to a reduction of the number of interacting molecules and as a consequence the molecules will approach ideality.

The isothermal compressibility of these systems has been reported previously in the literature<sup>154</sup>. The calculations are based on the equation

$$\kappa_T = \kappa_S + \frac{T\alpha^2}{\rho C_p} \quad 7.6$$

where  $\alpha$  is the expansion coefficient,  $C_p$  is the specific heat of the liquid and the other terms have their usual meanings. The isothermal compressibilities were calculated from the measured velocity and density of the hydrocarbons which had been measured over an extended temperature range. In the earlier work<sup>154</sup> the API project data had been used for  $C_p$  and it was assumed that  $\alpha$  is independent of temperature. Subsequently  $C_p$  has been measured by Huffman et al<sup>245</sup> and Shaw<sup>246</sup> and they have shown that the API data are very low compared with experimental data. Examination of the temperature dependence of the densities for the hydrocarbons indicates that  $\alpha$  is not independent of temperature and is, in fact, markedly temperature dependent. Using the revised experimental

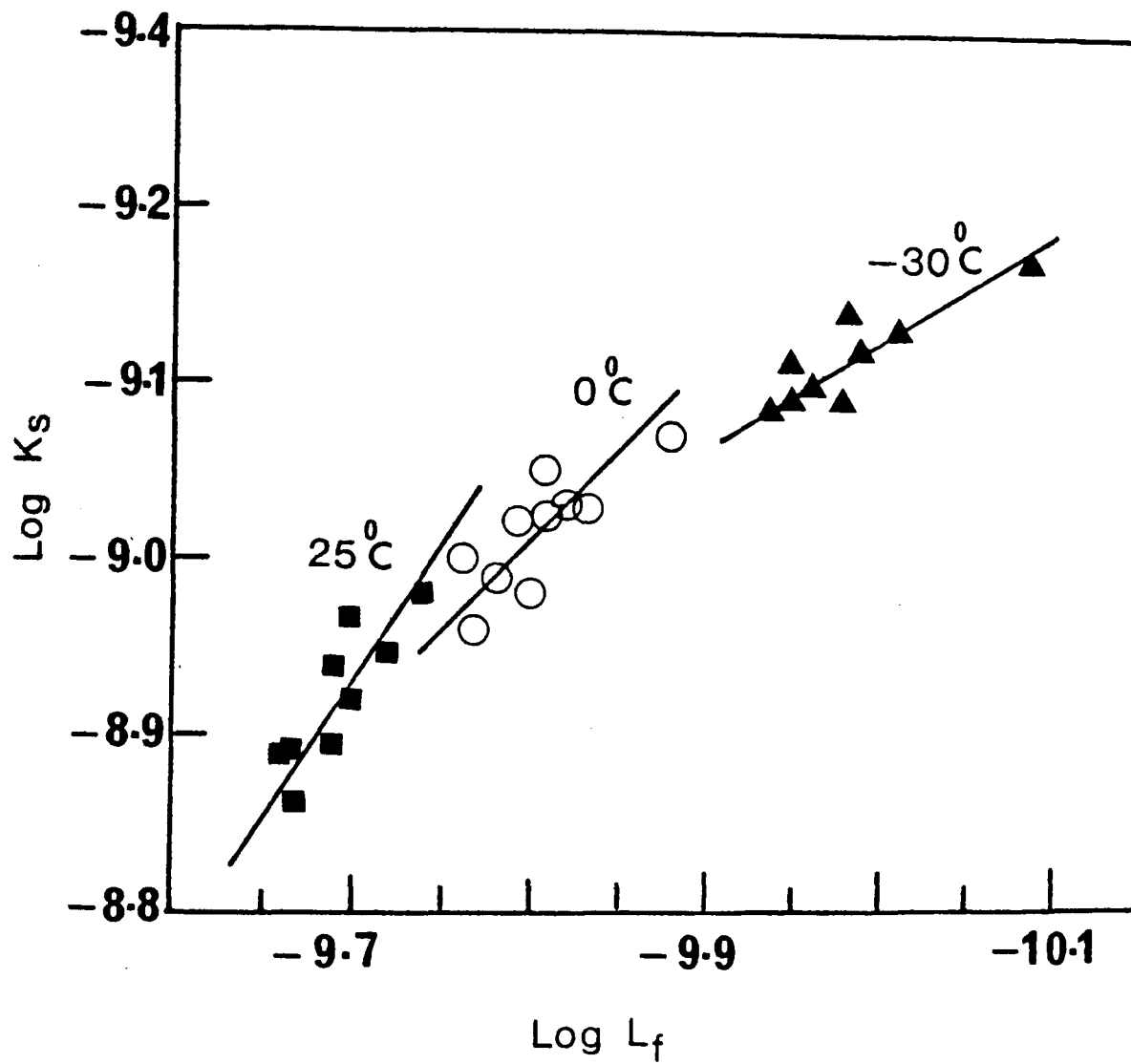


Figure 7.11. Adiabatic compressibility plotted as a function of intermolecular free length for methylpentanes and methylhexanes.

data isothermal compressibilities for 2,4-dimethylpentane and 2-methylhexane were calculated, Table 7.15. These data are significantly different from those reported previously which are considered to be in error.

The principal reason for the difference between the data presented in this study and those published previously<sup>154</sup> appears to be that the previous workers used the API project values for  $C_p$  (approximately  $143.0(\text{J/K}^{-1} \text{mol}^{-1})$ ) whereas the experimentally determined values (approximately  $220.5 (\text{J/K}^{-1} \text{mol}^{-1})$ ) have been used in this study. According to the API project data,<sup>155</sup> there is no difference in the  $C_p$  of the branched chain hydrocarbons and the same value is applicable to all. In practice, small differences are observed and these lead to differences between the 'theoretical' and experimental values.

(ii) Binary mixtures

In all binary mixtures of n-hexadecane with dimethylpentanes studied the excess isentropic compressibility exhibits a negative deviation from ideal behaviour, Figure 7.7, and this parallels the variation observed in the excess volume (section 6.4). These observations are consistent with the previous hypothesis (section 6.5) that the variation in the limiting high frequency ultrasonic attenuation B reflects the formation of aggregated more compact structure in the mixtures compared with that existing in the pure branched chain hydrocarbons. In the pure liquids, Rao constant has been used to predict

TABLE 7.15. Thermal Expansion Coefficient,  $\alpha$ , Isothermal Compressibility,  $\kappa_T$ , and Internal Pressure of 2-methylhexane and 2,4-dimethylpentane as a function of temperature.

T/°C	2-methylhexane			2,4-dimethylpentane		
	$\alpha \times 10^3 / \text{K}^{-1}$	$\kappa_T \times 10^9 / \text{Pa}^{-1}$	P/ $\text{Jcm}^{-3}$	$\alpha \times 10^3 / \text{K}^{-1}$	$\kappa_T \times 10^9 / \text{Pa}^{-1}$	P/ $\text{Jcm}^{-3}$
30	1.28	4.56	85.14	1.27	4.63	83.05
25	1.27	4.41	85.84	1.26	4.46	84.27
20	1.27	4.25	87.54	1.25	4.32	84.68
15	1.26	4.10	88.50	1.24	4.16	85.86
10	1.25	3.97	89.21	1.24	4.08	85.98
5	1.24	3.84	89.76	1.23	3.94	86.86
0	1.23	3.74	89.88	1.22	3.80	87.61
-5	1.22	3.61	90.51	1.21	3.68	88.16
-10	1.21	3.54	90.03	1.21	3.61	88.28
-15	1.20	3.42	90.64	1.20	3.48	88.87
-20	1.20	3.33	91.12	1.19	3.37	89.45
-25	1.19	3.23	91.45	1.18	3.25	90.04

the sound velocity for binary mixtures. This constant was used to describe the properties of mixtures. The Rao constant<sup>226</sup> is defined by equation 7.1 which also equals:

$$R = Vc^{1/3} \quad 7.7$$

where V is the molar volume and for the mixture will have the form:

$$V = \left[ \frac{x_1 M_1 + x_2 M_2}{\rho} \right] \quad 7.8$$

where  $x_1$ ,  $x_2$ ,  $M_1$  and  $M_2$  are the mole fractions and molecular weights respectively of the pure components subscripted as 1 and 2 and  $\rho$  is the density of the binary mixture. Assuming the linearity of the molar sound velocity, the following relation for binary liquid mixtures can be established:

$$R_{\text{mix}} = x_1 R_1 + x_2 R_2 \quad 7.9$$

where  $x_1$ ,  $x_2$ ,  $R_1$  and  $R_2$  are the mole fractions and Rao constants of the pure components of the mixture respectively subscripted as 1 and 2. The  $R^E$  was calculated using the following equation:

$$R^E = R_{\text{calculated}} - R_{\text{experimental}} \quad 7.10$$

Values of the excess normalized by the values of R are presented in Table 7.16.

In all cases a deviation from ideal behaviour is observed. The basis of the Rao approach is that the sound velocity is directly related to the strength of the intramolecular potential which in turn reflects the

TABLE 7.16. Molar Sound Properties of  $[xC_7H_{16} + (1-x)$   
n-hexadecane] at 298.15K.

x	$R_{\text{mix}}(\text{exp}) /$ $(\text{cm}^3\text{mol}^{-1})$ $(\text{ms}^{-1})^{1/3}$	$R_{\text{mix}}(\text{theor}) /$ $(\text{cm}^3\text{mol}^{-1})$ $(\text{ms}^{-1})^{1/3}$	$R^E /$ $(\text{cm}^3\text{mol}^{-1})$ $(\text{ms}^{-1})^{1/3}$
x, 2, 2-dimethylpentane + (1-x) n-hexadecane			
0.130	3018.6	3019.4	0.8
0.237	2833.2	2835.6	2.4
0.521	2345.9	2348.8	2.9
0.744	1964.8	1966.9	2.1
0.901	1696.2	1697.6	1.4
x, 2, 3-dimethylpentane + (1-x) n-hexadecane			
0.083	3096.6	3098.2	1.6
0.241	2820.7	2824.2	3.5
0.411	2525.6	2529.9	4.3
0.638	2130.9	2136.9	6.0
0.835	1789.8	1795.8	6.0
0.942	1605.2	1610.0	4.8
x, 3, 3-dimethylpentane + (1-x) n-hexadecane			
0.102	3063.9	3065.2	1.3
0.243	2817.2	2820.0	2.8
0.512	2353.5	2353.9	0.4
0.727	1980.4	1980.6	0.2
0.890	1695.2	1698.3	3.1

TABLE 7.16 (cont.)

---

x	$R_{\text{Mix}}(\text{exp}) /$ $(\text{cm}^3\text{mol}^{-1})$ $(\text{ms}^{-1})^{1/3}$	$R_{\text{Mix}}(\text{theor}) /$ $(\text{cm}^3\text{mol}^{-1})$ $(\text{ms}^{-1})^{1/3}$	$R^{\text{E}} / (\text{cm}^3\text{mol}^{-1})$ $(\text{ms}^{-1})^{1/3}$
x, 2, 4-dimethylpentane + (1-x) n-hexadecane			
0.104	3062.6	3064.0	1.4
0.239	2830.0	2832.9	2.9
0.411	2536.7	2539.7	3.0
0.645	2134.8	2140.4	5.6
0.844	1794.0	1799.0	5.0
0.921	1662.1	1667.5	5.4
0.956	1602.4	1607.9	5.5

---

nature of the nonbonding interactions between molecules. If the molecule-molecule interactions were simply a consequence of additive non-bonding interactions, then the Rao constant should predict the observed behaviour. The fact that this is not the case implies that some additional interactions must be present in the mixtures compared with those which exist in the simple liquids.

Values of the excess thermodynamic quantities for the mixtures investigated here are presented in Table 7.17. The values<sup>148</sup> of the excess enthalpy and T-entropy product are strongly positive whilst those of the free energy are negative except in the case of 2,4-dimethylpentane which is positive. These data have been interpreted in terms of the Prigogine-Flory<sup>9,22</sup> theory in terms of two effects: first a decrease of order when correlations of orientation between n-C<sub>16</sub> molecules in the pure liquid are replaced in the solution by weaker correlations whose strengths depend on the shapes of the lower alkane isomers. Secondly, for lower alkane isomers of the same shape but highly sterically hindered, the enthalpy and T-entropy products are small manifesting a negative contribution, ascribed to a rotational ordering of the n-C<sub>16</sub> segments on the sterically hindered molecule. Enthalpy-entropy compensation is observed for these contributions from studies as a function of temperature. The compressibilities studied here exhibit a minimum in the region of 0.6-0.75 mole fraction, the region where the excess volume of mixing also exhibits

TABLE 7.17. Excess Thermodynamic Quantities for  
 $[xC_7H_{16} + (1-x)\text{n-hexadecane}]$  at 298.15K.

x	$\Delta V^E /$ $\text{cm}^3\text{mol}^{-1}$	$\Delta H^E /$ $\text{J mol}^{-1}$	$\Delta G^E /$ $\text{J mol}^{-1}$
x, 2,2-dimethylpentane + (1-x) n-hexadecane			
0.130	-0.25	107.7	-3.7
0.237	-0.47	172.0	-7.7
0.521	-0.68	237.1	-16.4
0.744	-0.70	189.6	-16.2
0.901	-0.52	92.5	-8.8
x, 2,3-dimethylpentane + (1-x) n-hexadecane			
0.083	-0.07	44.8	-8.6
0.241	-0.26	118.5	-29.3
0.411	-0.37	151.2	-50.2
0.638	-0.42	148.6	-62.3
0.835	-0.34	89.8	-43.7
0.942	-0.16	38.5	-19.9
x, 3,3-dimethylpentane + (1-x) n-hexadecane			
0.102	-0.14	47.9	-29.2
0.243	-0.32	98.0	-63.0
0.512	-0.46	138.1	-96.3
0.727	-0.46	112.5	-82.4
0.890	-0.32	57.5	-43.2

TABLE 7.17 (cont.)

---

x	$\Delta V^E /$ $\text{cm}^3 \text{mol}^{-1}$	$\Delta H^E /$ $\text{J mol}^{-1}$	$\Delta G^E /$ $\text{J mol}^{-1}$
x,2,4-dimethylpentane + (1-x) n-hexadecane			
0.104	-0.16	91.2	1.8
0.239	-0.35	167.5	4.6
0.411	-0.51	220.9	8.5
0.645	-0.61	213.7	11.0
0.844	-0.52	122.6	7.6
0.921	-0.40	71.9	4.7
0.956	-0.28	37.9	2.5

---

a minimum. The order of the magnitude of the deviation shows no apparent correlation with that presented for the free energy enthalpy terms. However, the order exhibited by the volume coincides with that observed with the compressibility.

An analysis of the acoustic absorption data at high frequency (section 6.4 ) indicated that the volume viscosity contribution changes with composition and structure and the magnitude varies approximately in the same order as that exhibited by the compressibility. The latter observations are subject to a significant uncertainty and therefore the absolute order of the deviation is difficult to quantify. The explanation advanced for this negative deviation involves a proposition that a fraction of the molecules can become organised into clustered regions. These regions would therefore also be less compressible and hence this would explain the deviation observed in the isoentropic compressibility. The fact that the deviation in the excess volume of mixing also coincides both in order and magnitude with that observed using the acoustic measurements provides further support for this hypothesis. The lack of correlation with the free energy, enthalpy and  $T$ -entropy product can be explained in the following manner. The formation of the ordered regions will occur as a consequence of a balance of entropy-enthalpy interactions. However, changes in the distribution of ordered-disordered molecules will also have an effect on the rotational isomeric contribution to the total energy. Thus increasing the

temperature will lead to the generation of a different distribution of isomeric structures and consequently a different number of structures available for cluster formation. Clearly, both effects are intimately connected and hence the overall average free energy, enthalpy and T-entropy product is a combination of clustering-ordering in the liquid and the change in the total energy distribution as a consequence of a change in the distribution of rotational isomeric structures.

### 7.5 Conclusions

(a) From the data presented it is clear that the propagation of a sound wave through the pure hydrocarbons is controlled not only by the nature of the molecular structure but also by the effects of the basic shape of the molecules on the intermolecular interactions. It is possible that clustering of the molecules may lead to ordered structures which in turn will influence the time volume average interactions.

(b) Analysis of the variation of the excess isoentropic compressibility with mole fraction and comparison with other excess thermodynamic properties indicates that the behaviour of mixtures of branched and linear hydrocarbons requires the proposition that ordering occurs in these mixtures. The apparent simple correlation of the free volume, acoustic attenuation and the isoentropic compressibility can be explained on the basis that these properties are more directly related to the extent of

ordering than to enthalpy, free energy and T-entropy product. The latter contain elements relating to the rotational isomeric state of these molecules and as such are not directly correlated with the ordering process in the mixtures.

CHAPTER 8  
ULTRASONIC INVESTIGATIONS OF MIXTURES  
OF ISOMERIC OCTANOLS WITH n-OCTANE

## CHAPTER 8

### ULTRASONIC INVESTIGATIONS OF MIXTURES OF ISOMERIC OCTANOLS WITH n-OCTANE

#### 8.1 Introduction

Thermodynamic studies of n-alkanols in various solvents have been extensively investigated<sup>247-249</sup>. Recent studies of the behaviour of binary mixtures of n-alkanols and n-alkanes have been undertaken in an attempt to interpret the way in which structure in the associated alkanols is modified by the addition of n-alkanes<sup>250-252,68</sup>. It has been suggested by Tresczanowicz and Benson<sup>254</sup> that the behaviour observed in the high alkanols dilution region for binary mixtures of n-alkanols and n-alkanes is the result of two opposing effects; self-association of alkanols and dipole-dipole interactions between alkanol monomers and multimers and change of 'free volume' in the real binary mixture.

Ultrasonic studies of aqueous solutions of n-alkanols<sup>60,59,253</sup> indicated that the large excess acoustic attenuation be attributed to the effect of the sound wave on the distribution of structural forms present at different concentrations.

Recently Dugue et al<sup>46</sup> studied the structural behaviour of the pure isomeric octanols using the ultrasonic and <sup>13</sup>C nmr techniques. They suggested that the relaxation observed in octan-1-ol and octan-2-ol be attributed to hydrogen bond exchange associated with structural relaxation of the pure liquids, an additional contribution associated with rotational relaxation. Later they

extended their work to the binary mixtures of these octanols with methanol<sup>45</sup>. The excess in acoustic attenuation was found to be similar to those observed for aqueous solutions of n-alkanols.

This study of binary mixtures of isomeric octanols with n-octane is an extension to the previous investigations of Dugue et al<sup>46,45</sup>. The main aim of this study is to clarify the role played by the environment of octanol's hydroxyl group in determining the extent and type of association and steric environments. This study will also provide an adequate basis for understanding the volumetric behaviour of these binary mixtures. Particular attention has been given to the dilute octanol region.

## 8.2 Materials

The isomeric octanols: octan-1-ol, octan-2-ol, 2-ethylhexan-1-ol, 2,3-dimethylhexan-3-ol, 2,4-dimethylhexan-3-ol and n-octane were all obtained from Aldrich Chemical Company Limited as better than 99% pure. The purity was confirmed using glc and the structural integrity using <sup>13</sup>C nmr spectroscopy. The liquids were all stored over molecular sieves, type 4A (BDH) and filtered before use. Densities, refractive indices and sound velocities of the pure components were measured, Table 8.1, and found in good agreement with those published in the literature<sup>46,60,155,255-258</sup>.

## 8.3 Results

### (i) Excess volumes' data

Values of the excess volumes,  $V^E$ , of the binary mixtures of isomeric octanols and n-octane were calculated

TABLE 8.1. Densities,  $\rho$ , Refractive Indices,  $n_D$ , Sound Velocity,  $c$ , of the Pure Components at 298.15K.

Molecule	$\rho/\text{g cm}^{-3}$		$n_D$		$c/\text{ms}^{-1}$	
	Obs.	Lit.	Obs.	Lit.	Obs.	Lit.
n-Octane	0.69876 -	0.69867 0.69861	1.39522 -	1.39518 1.39505	1177.8 -	1177.25 -
Octan-1-ol	0.82113 -	0.82139 0.82157	1.42724 -	1.42757 1.4275	1349.8 -	1348.83 -
Octan-2-ol	0.81627	0.81802	1.42434	1.424	1309.7	1307.75
2-ethylhexan-1-ol	0.82906	-	1.42920	-	1323.4	1321.8
2,4-dimethylhexan-3-ol	0.83205	0.83272	1.42921	-	1288.5	-
2,3-dimethylhexan-3-ol	0.83418	0.83481	1.43022	-	1286.5	-

using equation 2.33. The data were fitted to the empirical equation 6.5 and the fitting coefficients  $a_n$  of order  $n$  obtained from a least squares fit of the data presented in Table 8.2. The standard deviations associated with this analysis are also presented in Table 8.2 along with the coefficients for  $a_n$ . Comparison of the plots of actual data and the predictions of equation 6.5 indicate that the deviation is in all cases less than 0.1%. The excess volumes for the binary mixtures of branched-chain octanols and n-octane are all positive over the whole mole fraction range, figure 8.1. In the case of the straight chain octan-1-ol,  $V^E$  values are negative except at low mole fractions, where it is positive.

(ii) Acoustic velocity and isoentropic compressibility

The measured sound velocities at ca. 2 MHz for binary mixtures of isomeric octanols and n-octane at 298.15 are presented in Table 8.3 and illustrated in Figure 8.2. The isoentropic compressibilities,  $\kappa_s$ , and excess compressibilities,  $\kappa_s^E$ , were calculated using equations 2.35 and 2.34 respectively. Values of  $\kappa_s$  and  $\kappa_s^E$  so obtained are listed in Table 8.3 and  $\kappa_s^E$  is plotted as a function of mole fraction,  $x$ , of octanol at 298.15K, Figure 8.3.

(iii) Ultrasonic attenuation and viscosity measurements

Attenuation data ( $\alpha/f^2$ ) obtained over the frequency range 1.5 to 3 MHz presented in Figure 8.4 as a function of mole fraction of the mixture. The viscosities of the mixtures are presented in Figure 8.5. The

TABLE 8.2. Coefficients  $a_n$  and standard deviations  $\sigma V^E/\text{cm}^3 \text{ mol}^{-1}$  for least squares representations of excess volumes at 298.15K by equation 6.5.

$a_n$	Octan-1-ol	2-ethylhexan-1-ol	Octan-2-ol	2,4-dimethylhexan-3-ol	2,3-dimethylhexan-3-ol
$a_1$	0.2441	0.0040	0.0047	0.0958	0.0621
$a_2$	-0.9384	1.2413	2.5149	3.3962	3.9973
$a_3$	-5.9462	-7.0093	-12.9164	-13.7878	-23.5198
$a_4$	24.2826	18.7009	31.1446	33.6940	65.8922
$a_5$	-32.9092	-26.0802	-41.2848	-52.3344	-99.8554
$a_6$	21.1767	18.3939	28.4913	42.7372	76.3898
$a_7$	-5.6965	-5.1608	-7.9542	-13.8082	-23.0773
$\sigma V^E / \text{cm}^3 \text{ mol}^{-1}$	0.0004	0.0005	0.0009	0.0002	0.0007

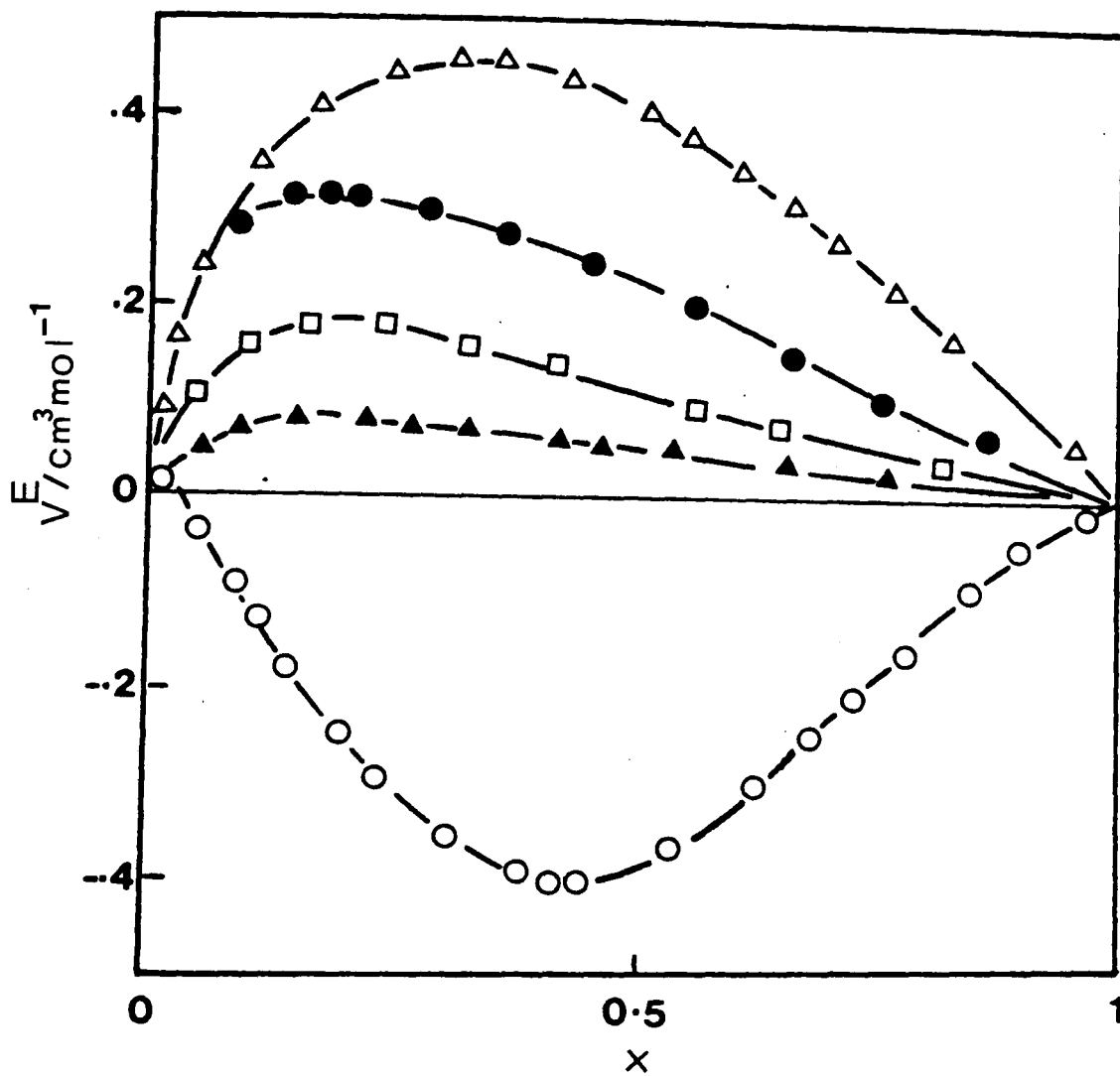


Figure 8.1. Excess volumes for  $[xC_8H_{17}OH + (1-x)$   
 n-octane] at 298.15K:  $\circ$ , octan-1-ol;  $\square$ , octan-2-ol;  
 $\blacktriangle$ , 2-ethylhexan-1-ol;  $\triangle$ , 2,3-dimethylhexan-3-ol;  
 $\bullet$ , 2,4-dimethylhexan-3-ol.

TABLE 8.3. Densities,  $\rho$ , sound velocities,  $c$ , isoentropic compressibilities,  $\kappa_S$ , and excess isoentropic compressibilities,  $\kappa_S^E$ , for  $[xC_8H_{17}OH+(1-x)$  n-octane] at 298.15K.

x	$\rho/\text{gcm}^{-3}$	$c/\text{ms}^{-1}$	$\kappa_S \times 10^{12}/\text{Pa}^{-1}$	$\kappa_S^E \times 10^{12}/\text{Pa}^{-1}$
x, octan-1-ol + (1-x) n-octane				
0.0000	0.6987	1177.8	1031.6	.....
0.0014	0.6989	1177.9	1031.2	0.05
0.0032	0.6991	1178.1	1030.7	0.10
0.0056	0.6994	1178.3	1029.7	0.13
0.0089	0.6999	1179.0	1027.8	0.14
0.0102	0.6999	1179.1	1027.6	0.18
0.0144	0.7008	1178.9	1026.7	0.29
0.0202	0.7010	1179.3	1025.7	0.51
0.0300	0.7029	1180.3	1021.1	0.91
0.0351	0.7035	1180.8	1019.6	1.05
0.0411	0.7042	1181.1	1017.9	1.20
0.0466	0.7044	1181.9	1016.3	1.35
0.0511	0.7049	1182.2	1015.0	1.49
0.0612	0.7062	1183.1	1011.5	1.71
0.0709	0.7075	1184.2	1007.9	1.75
0.0772	0.7077	1185.1	1005.9	1.78
0.0850	0.7080	1186.6	1003.1	1.74
0.0908	0.7094	1186.6	1001.0	1.72
0.1034	0.7107	1188.3	996.4	1.50
0.1428	0.7166	1192.3	981.5	0.63
0.2108	0.7236	1201.3	957.6	-0.88
0.3068	0.7355	1212.3	925.0	-3.01
0.3755	0.7456	1225.5	893.0	-4.63
0.4144	0.7494	1232.6	878.3	-5.25
0.4717	0.7574	1241.7	856.3	-6.52
0.5066	0.7602	1249.0	843.0	-7.13
0.5832	0.7708	1262.2	814.2	-8.01
0.6084	0.7728	1267.9	804.9	-8.25
0.6785	0.7821	1281.2	778.8	-8.50
0.7092	0.7851	1288.1	767.7	-8.38
0.7719	0.7933	1300.4	745.4	-7.55
0.8040	0.7967	1307.6	734.1	-6.99
0.9108	0.8096	1330.6	697.6	-3.77
0.9582	0.8160	1340.8	681.6	-1.88
0.9860	0.8193	1346.7	672.9	-0.38
1.0000	0.8211	1349.8	668.4	.....

TABLE 8.3 (cont.)

x	$\rho/\text{gcm}^{-3}$	$c/\text{ms}^{-1}$	$\kappa_S \times 10^{12}/\text{Pa}^{-1}$	$\kappa_S^E \times 10^{12}/\text{Pa}^{-1}$
x, octan-2-ol + (1-x) n-octane				
0.0045	0.6992	1178.0	1030.6	0.49
0.0074	0.6995	1178.1	1029.9	0.81
0.0102	0.6998	1178.2	1029.3	1.01
0.0223	0.7011	1178.9	1026.3	1.72
0.0298	0.7019	1179.2	1024.6	2.32
0.0420	0.7040	1179.2	1021.5	2.74
0.0535	0.7042	1180.9	1018.3	3.25
0.0594	0.7047	1181.2	1016.9	3.52
0.0722	0.7065	1182.0	1013.0	3.95
0.0811	0.7075	1182.6	1010.6	4.25
0.0900	0.7085	1183.3	1007.9	4.45
0.1006	0.7097	1184.1	1004.9	4.75
0.1586	0.7162	1188.5	988.4	6.25
0.2263	0.7240	1194.8	967.5	6.50
0.2534	0.7272	1197.5	958.9	6.38
0.3141	0.7344	1204.2	938.9	5.75
0.3470	0.7382	1207.9	928.5	5.38
0.4129	0.7459	1215.7	907.1	4.75
0.4538	0.7508	1220.7	893.8	4.38
0.5154	0.7581	1228.9	873.5	3.63
0.5624	0.7681	1235.4	853.1	3.13
0.6366	0.7725	1245.9	833.8	2.55
0.7047	0.7806	1256.5	811.3	1.82
0.7526	0.7863	1264.3	795.6	1.41
0.8054	0.7927	1273.2	778.2	1.03
0.8526	0.7924	1281.0	769.0	0.80
0.8973	0.8037	1289.7	748.0	0.51
0.9553	0.8107	1300.8	728.9	0.25
0.9834	0.8141	1306.3	719.7	0.13
1.0000	0.8162	1309.7	714.2	....

TABLE 8.3 (cont.)

x	$\rho/\text{gcm}^{-3}$	$c/\text{ms}^{-1}$	$\kappa_S \times 10^{12}/\text{Pa}^{-1}$	$\kappa_S^E \times 10^{12}/\text{Pa}^{-1}$
x, 2-ethylhexan-1-ol + (1-x) n-octane				
0.0051	0.6994	1178.2	1030.1	0.27
0.0112	0.7001	1178.5	1028.3	0.52
0.0154	0.7006	1178.8	1027.1	0.69
0.0262	0.7019	1179.6	1023.9	1.05
0.0316	0.7026	1180.0	1022.2	1.23
0.0424	0.7039	1180.7	1019.1	1.61
0.0510	0.7049	1181.3	1016.5	1.89
0.0660	0.7068	1182.4	1012.0	2.33
0.0710	0.7074	1182.7	1010.5	2.45
0.0845	0.7091	1183.8	1006.3	2.75
0.0912	0.7099	1184.3	1004.2	2.85
0.1156	0.7130	1186.3	996.5	3.28
0.1496	0.7173	1189.4	985.4	3.50
0.1836	0.7216	1192.8	974.1	3.49
0.2155	0.7256	1196.1	963.1	3.25
0.2623	0.7316	1201.4	946.9	2.75
0.3203	0.7391	1208.2	926.9	2.25
0.4123	0.7510	1219.8	894.9	1.50
0.4661	0.7580	1227.1	876.1	1.01
0.5206	0.7651	1234.6	857.4	0.98
0.5606	0.7706	1240.3	843.5	0.73
0.6218	0.7784	1249.9	822.2	0.68
0.6536	0.7826	1255.1	811.1	0.60
0.7009	0.7889	1262.9	794.6	0.51
0.7523	0.7958	1272.1	776.5	0.38
0.8070	0.8031	1282.3	757.3	0.31
0.8564	0.8097	1291.9	739.9	0.25
0.8863	0.8137	1298.1	729.3	0.21
0.9651	0.8244	1315.3	701.1	0.13
0.9824	0.8278	1319.2	694.1	0.01
1.0000	0.8290	1323.4	688.6	....

TABLE 8.3 (cont.)

x	$\rho/\text{gcm}^{-3}$	$c/\text{ms}^{-1}$	$\kappa_S \times 10^{12}/\text{Pa}^{-1}$	$\kappa_S^E \times 10^{12}/\text{Pa}^{-1}$
x, 2, 3-dimethylhexan-3-ol + (1-x) n-octane				
0.0114	0.7004	1177.7	1029.3	1.91
0.0200	0.7009	1177.9	1028.3	2.75
0.0313	0.7021	1178.2	1025.9	3.60
0.0360	0.7027	1178.3	1024.9	4.05
0.0406	0.7032	1178.5	1023.9	4.35
0.0514	0.7041	1179.0	1021.7	5.35
0.0568	0.7051	1179.1	1020.0	5.51
0.0636	0.7059	1179.1	1018.9	6.25
0.0712	0.7071	1179.4	1016.7	6.62
0.0767	0.7076	1179.6	1015.7	6.84
0.0807	0.7081	1179.7	1014.6	7.05
0.0904	0.7094	1179.9	1012.6	7.62
0.1124	0.7123	1180.7	1007.1	7.88
0.1397	0.7130	1181.5	1004.7	9.50
0.2180	0.7255	1186.9	978.5	11.74
0.2510	0.7298	1189.1	969.1	12.25
0.3348	0.7407	1195.7	944.2	12.63
0.4182	0.7521	1203.3	918.3	12.13
0.5079	0.7645	1212.7	889.3	10.70
0.5508	0.7704	1217.7	875.4	9.95
0.6096	0.7785	1224.9	855.9	8.80
0.6518	0.7846	1230.2	842.1	8.10
0.7098	0.7928	1238.3	822.6	6.75
0.7540	0.8011	1243.2	807.7	5.75
0.8029	0.8054	1252.8	791.0	4.55
0.8521	0.8133	1260.0	774.4	3.51
0.9058	0.8202	1270.0	755.8	2.13
0.9512	0.8279	1277.9	739.6	1.13
1.0000	0.8341	1286.5	724.3	....

TABLE 8.3 (cont.)

x	$\rho/\text{gcm}^{-3}$	$c/\text{ms}^{-1}$	$\kappa_S \times 10^{12}/\text{Pa}^{-1}$	$\kappa_S^E \times 10^{12}/\text{Pa}^{-1}$
x, 2, 4-dimethylhexan-3-ol + (1-x) n-octane				
0.0052	0.6994	1177.8	1030.7	0.75
0.0123	0.7001	1177.9	1029.5	1.65
0.0238	0.7013	1178.2	1027.2	2.38
0.0314	0.7020	1178.6	1025.4	3.21
0.0360	0.7026	1178.7	1024.4	3.51
0.0421	0.7033	1179.0	1022.8	3.75
0.0476	0.7039	1179.3	1021.6	4.15
0.0501	0.7042	1179.3	1021.0	4.35
0.0549	0.7052	1179.4	1019.4	4.61
0.0602	0.7055	1179.6	1018.6	4.95
0.0660	0.7061	1179.9	1017.3	5.35
0.0714	0.7067	1180.1	1016.0	5.68
0.0858	0.7083	1180.8	1012.6	6.49
0.0955	0.7095	1181.3	1010.1	6.87
0.1075	0.7111	1181.9	1006.8	7.13
0.2100	0.7239	1187.9	978.9	9.88
0.3204	0.7383	1196.7	945.8	10.11
0.3567	0.7470	1199.5	934.2	9.52
0.4247	0.7519	1207.1	912.6	8.75
0.5074	0.7650	1214.4	886.3	7.63
0.5512	0.7700	1220.4	871.9	6.91
0.5964	0.7750	1226.9	857.1	6.03
0.6544	0.7841	1233.6	838.1	5.08
0.7004	0.7904	1239.7	823.2	4.51
0.7504	0.7973	1246.9	806.6	3.63
0.8050	0.8032	1256.7	788.4	2.63
0.8521	0.8115	1262.7	772.8	1.98
0.8971	0.8156	1271.9	757.8	1.25
0.9512	0.8254	1279.6	739.9	0.63
0.9823	0.8298	1285.3	729.5	0.25
1.0000	0.8320	1288.5	723.9	....

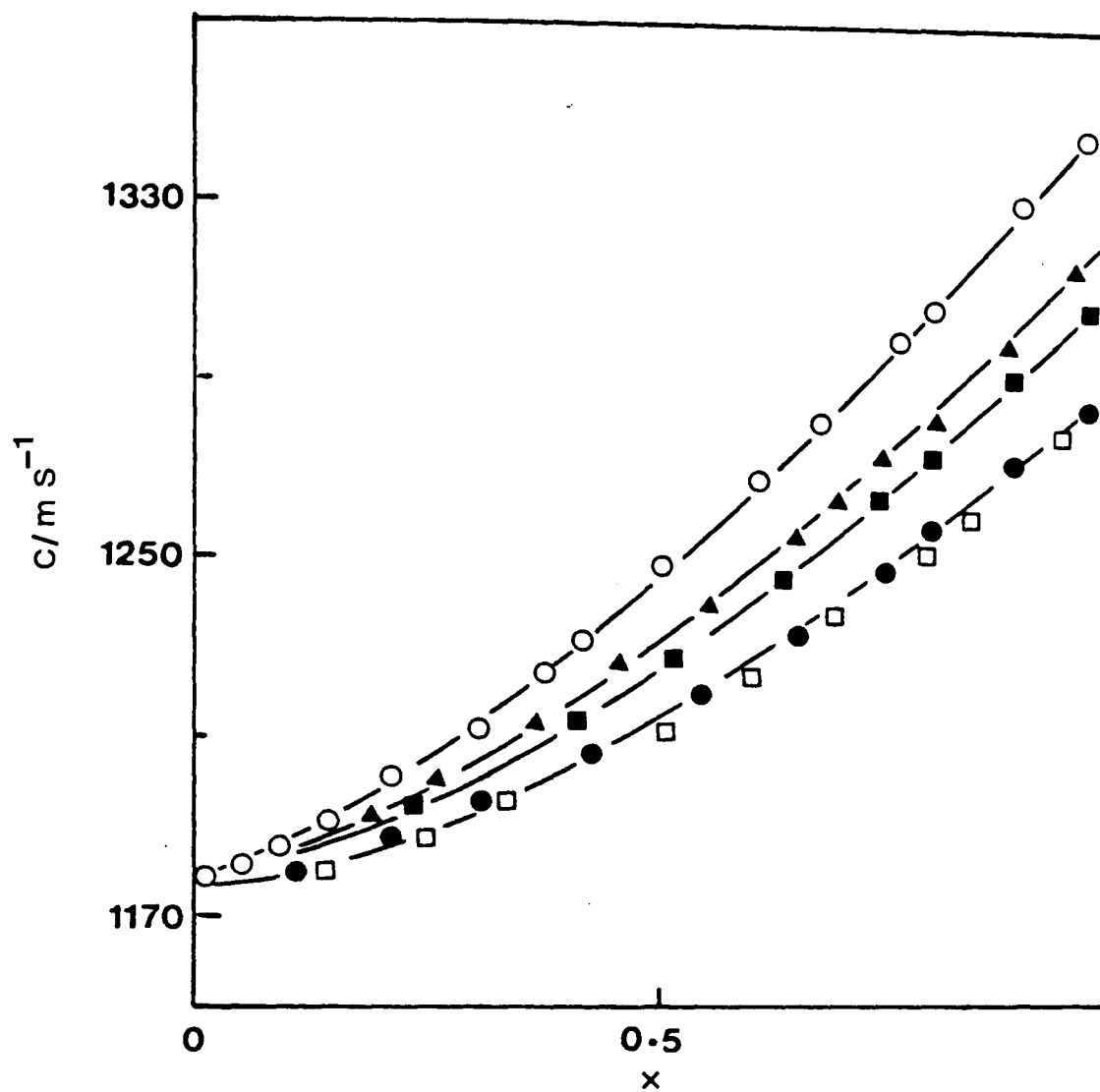


Figure 8.2. Sound velocity,  $c$ , for  $[xC_8H_{17}OH + (1-x)$  n-octane] at 298.15K: ○, octan-1-ol; ■, octan-2-ol; ▲, 2-ethylhexan-1-ol; □, 2,3-dimethylhexan-3-ol; ●, 2,4-dimethylhexan-3-ol.

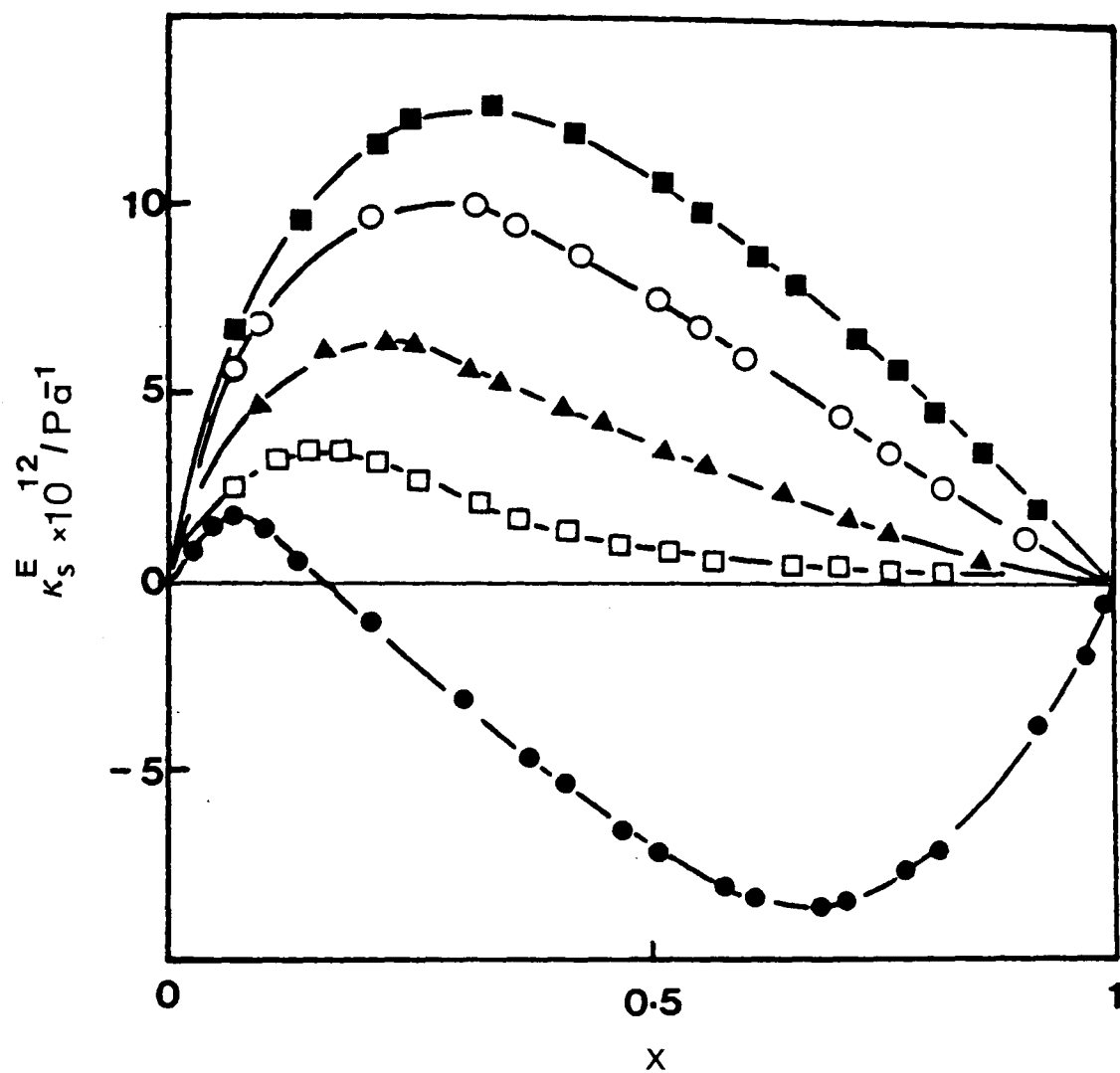


Figure 8.3. Excess isoentropic compressibility for  $[x\text{C}_8\text{H}_{17}\text{OH} + (1-x)\text{ n-octane}]$  at 298.15K: ●, octan-1-ol; ▲, octan-2-ol; □, 2-ethylhexan-1-ol; ■, 2,3-dimethylhexan-3-ol; ○, 2,4-dimethylhexan-3-ol.

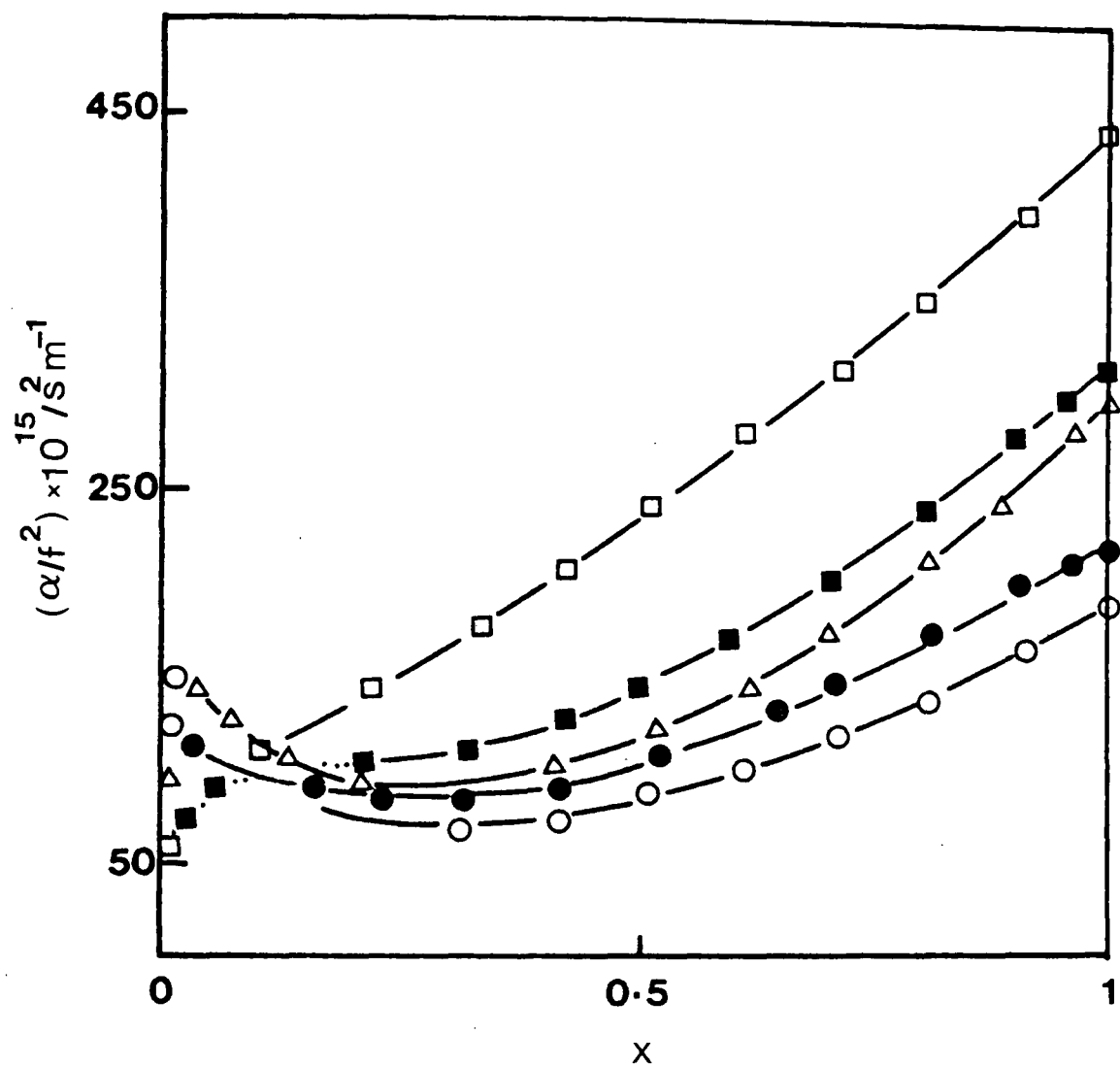


Figure 8.4. Ultrasonic absorption coefficient for  $[xC_8H_{17}OH + (1-x) \text{ n-octane}]$  at 298.15K and 2MHz.

○, octan-1-ol; ●, octan-2-ol; △, 2-ethylhexan-1-ol;  
 □, 2,3-dimethylhexan-3-ol; ■, 2,4-dimethylhexan-3-ol.

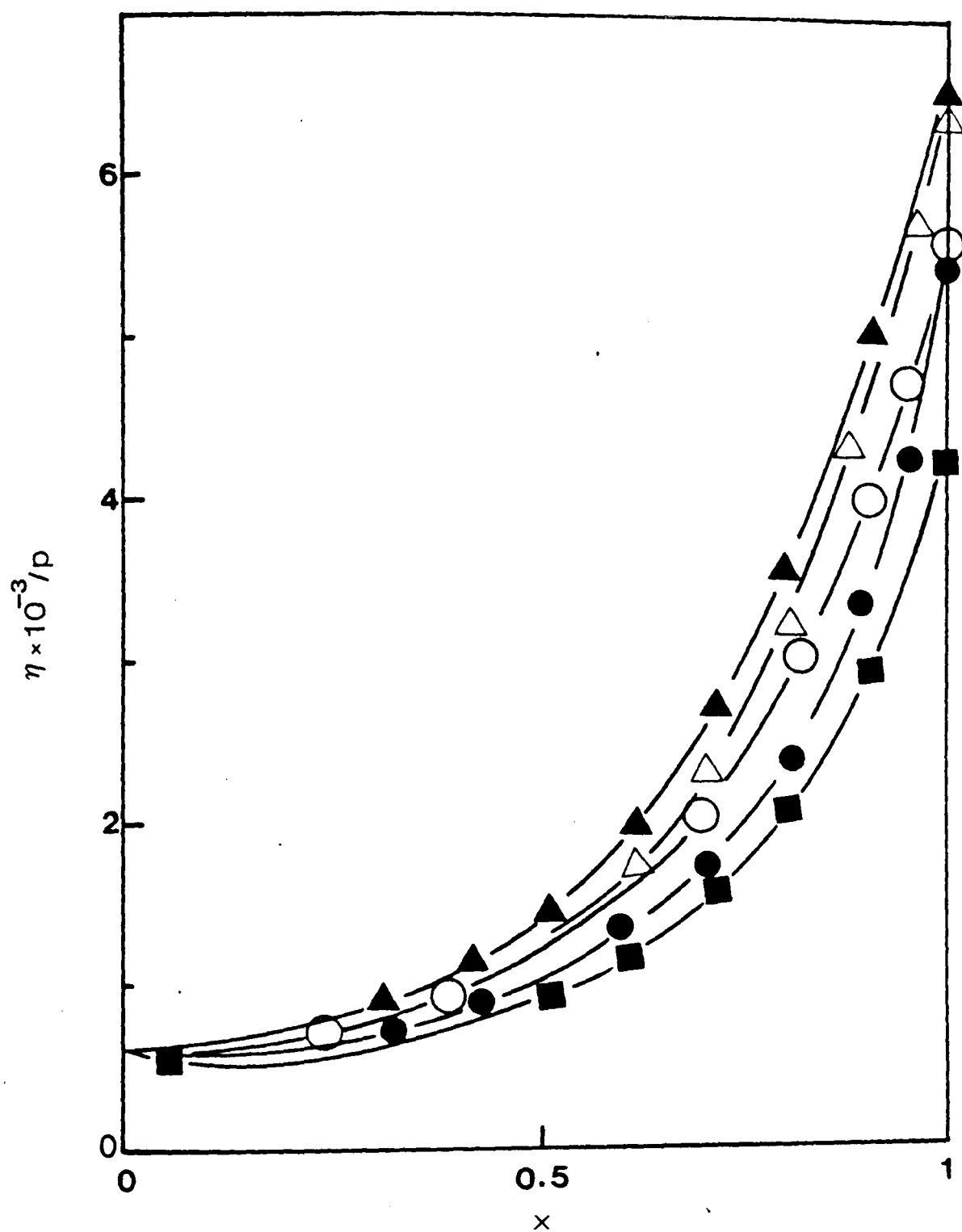


Figure 8.5. Variation of viscosity as a function of mole fraction,  $x$ , of octanols for  $[xC_8H_{17}OH + (1-x)$  n-octane] at 298.15K:  $\blacktriangle$ , octan-1-ol;  $\bigcirc$ , octan-2-ol;  $\triangle$ , 2-ethylhexan-1-ol;  $\blacksquare$ , 2,3-dimethylhexan-3-ol;  $\bullet$ , 2,4-dimethylhexan-3-ol.

attenuation of an organic liquid can be separated into two parts: a relaxational element associated with the disturbance of rotational isomeric equilibria or hydrogen bonded associated forms of the alcohol and a classical contribution associated with viscous and thermal contributions. The contribution from shear relaxation can be calculated from the viscosity using equation 2.3. The calculated shear contribution is presented in Figure 8.6. The viscous contribution contains a volume viscosity element and the total attenuation contains also a thermal conductivity loss. The latter for most organic liquids makes a contribution of much less than 1% to the observed attenuation. Estimates based on very imprecise literature data indicate that this is also true in the present case. In which case, the volume viscosity can be calculated from

$$(\alpha/f^2)_v = (2\pi^2\eta_v/\rho c^3)_v = (\alpha/f^2)_{obs} - (\alpha/f^2)_s \quad 8.1$$

where  $\eta_v$  is the volume viscosity of the mixture. Calculated values for  $(\alpha/f^2)_v$  are presented in Figure 8.7.

#### 8.4 Discussion

A survey of the literature indicates that few measurements have been performed in a systematic manner of the changes in the structure of alcohols with the addition of non polar molecules. This is in contrast to the considerable attention which has been given to alcohol with other hydrogen bonding molecules. In this present study the isomeric octanols allow the effects of chain isomerism, hydrogen bond accessibility and configurational mobility of the second molecule to be studied.

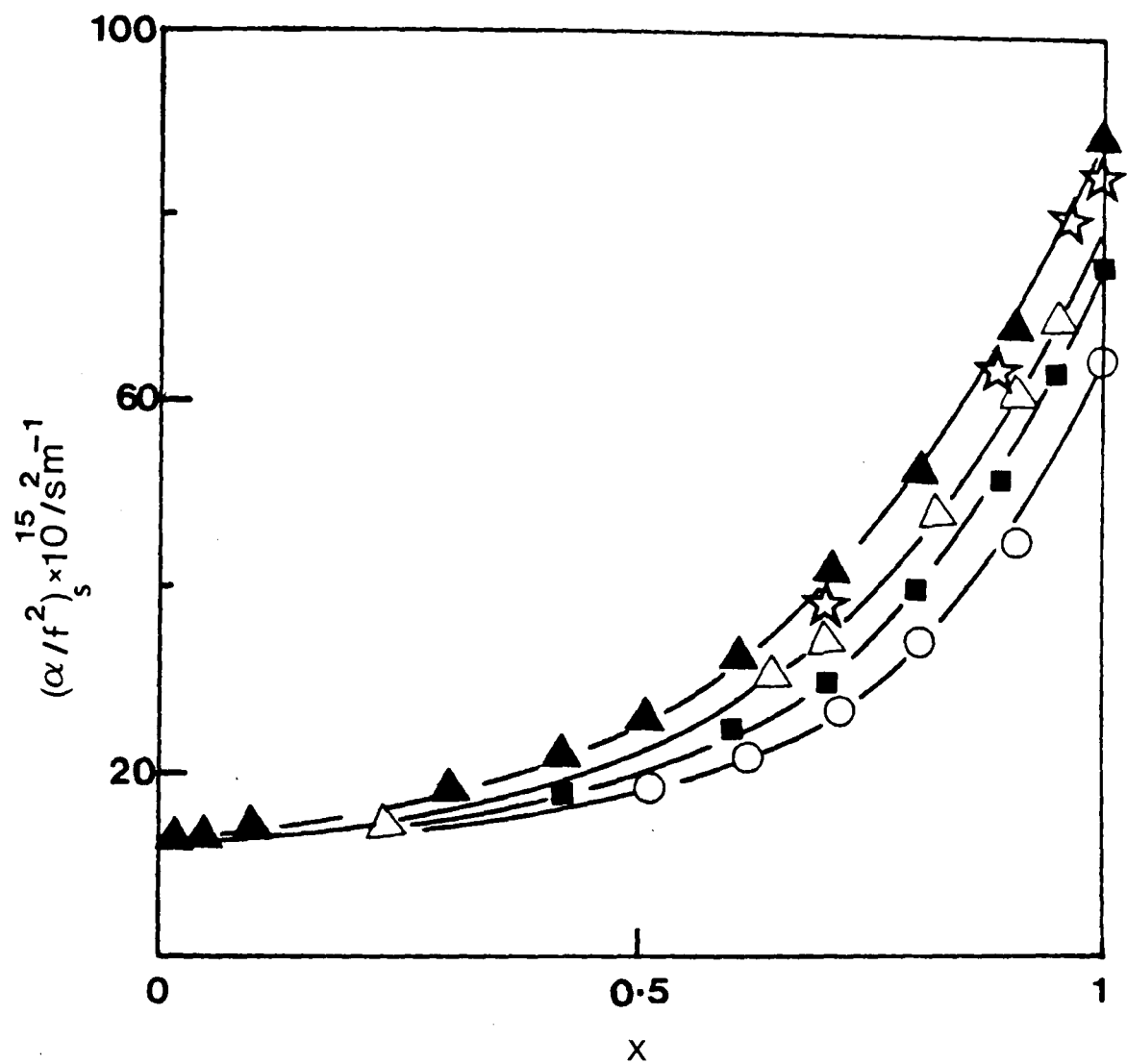


Figure 8.6. Ultrasonic absorption contribution from shear viscosity  $(\alpha/f^2)_s$  for  $[xC_8H_{17}OH + (1-x)$  n-octane] at 2MHz and 298.15K: ▲, octan-1-ol; △, octan-2-ol; ☆, 2-ethylhexan-1-ol; ○, 2,3-dimethylhexan-3-ol; ■, 2,4-dimethylhexan-3-ol.

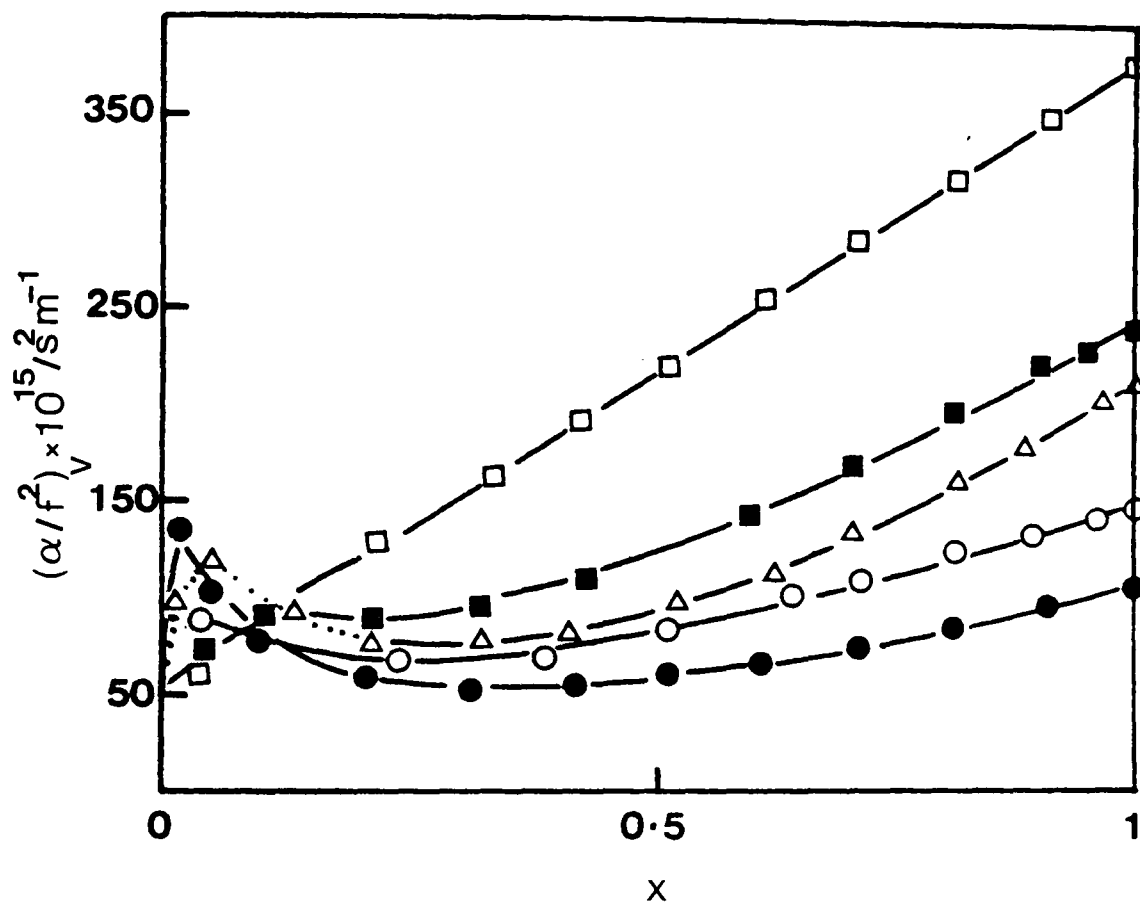


Figure 8.7. Ultrasonic absorption contribution from volume viscosity  $(\alpha/f^2)_V$  for  $[x\text{C}_8\text{H}_{17}\text{OH} + (1-x)\text{n-octane}]$  at 2MHz and 298.15K: ●, octan-1-ol; ○, octan-2-ol; △, 2-ethylhexan-1-ol; □, 2,3-dimethylhexan-3-ol; ■, 2,4-dimethylhexan-3-ol.

(i) Volume of mixing

The  $V^E$  values in the case of the straight chain octan-1-ol are negative except for mole fractions of less than 0.02 where they become positive, Figure 8.1. The maximum values of the excess volumes for branched octanols decrease in the order, 2,3-dimethylhexan-3-ol, 2,4-dimethylhexan-3-ol, octan-2-ol, 2-ethylhexan-1-ol. According to Tresczanowicz and Benson<sup>255</sup>, the  $V^E$  data for similar binary mixtures can be explained qualitatively by postulating that the excess is the result of two opposing effects; self association of the octanol and physical dipole-dipole interactions between octanol monomers and multimers, leading to increases in volume. Negative contributions arise from changes of 'free volume' in the real binary mixture. Additional contributions can be envisaged as arising from the restrictions in rotational motion<sup>46</sup> which arise when the octane molecule is accommodated interstitially within the branched octanol mixture.

The data presented in Figure 8.1 indicate that the negative contribution reaches a maximum at approximately 0.4 mole fraction of octan-1-ol, and at very low dilution octan-1-ol it becomes positive due to hydrogen bond breaking. The positive values of  $V^E$  for the branched chain octanols are a consequence of steric interactions associated with the branched alkyl chains reducing the extent of hydrogen bonding in the system. For instance, in the case of 2,3-dimethylhexan-3-ol, the hydroxyl group

is highly hindered by the alkyl group and gives the highest maximum excess volume values. As the steric effect of the alkyl group is increased, so the positive effect becomes more important than the negative. In octan-1-ol the octane molecules are accommodated in the octanol structure and a negative direction is observed. Similar effects have been reported by Benson for other alcohol/alkane systems<sup>254,255</sup>.

(ii) Acoustic velocity and isoentropic compressibilities

As indicated above the main effect of addition of octane is a change in the 'free' volume in the mixture compared with that in the pure components. Disruption of the alcohol structure and restriction of the rotational motion has been described as the condensation effect<sup>200,30</sup>. Interstitial accommodation and orientational order lead to a more compact structure and to an observed decrease in the excess compressibility, Figure 8.3. At low alkanol concentrations the negative deviations observed are attributed to the effects of break-up of the hydrogen bond structure and this tends to increase the compressibility and leads ultimately to the positive trend. The behaviour reported here is similar to that reported by Kiyohara and Benson<sup>248</sup> on various n-alkanol + n-octane systems.

The main conclusion with regard to the low mole fraction data is that breaking of multimer structure leads to a positive  $\kappa_S^E$  and a concomitant increase in the ability for interstitial accommodation of the alkane. This

behaviour is modulated by the steric interactions of the alkyl group both on the stability of the multimer structure but also on the ability of the liquid to accommodate the straight chain alkane. The infrared spectrum of these mixtures is very complex and does not allow either positive identification or estimation of the concentrations of the various multilinear structures present.

(iii) Viscothermal acoustic attenuation coefficient

The frequency dependence of the acoustic attenuation in the isomeric octanols has been reported previously<sup>46</sup>. In the following analysis, account has been taken of the contribution associated with rotational isomerism in octan-2-ol, 2,3-dimethylhexan-3-ol and 2,4-dimethylhexan-3-ol to the acoustic attenuation. In all cases the rotational isomeric contribution decreased linearly with the concentration of the octanol allowing the viscothermal acoustic attenuation to be defined as a frequency independent contribution.

The concentration variation of the viscosity reflects the complex manner in which the 'hydrogen bonded structure' with concentration and reflects the extent to which 'associated cyclic and linear hydrogen bonded structures are destabilized by the addition of non polar molecules. The observed deviations are negative, implying break up of associated structure in all cases. The ultrasonic attenuation is observed to increase rapidly on the addition of alcohol to the alkane and a maximum in the attenuation coefficient is observed in the dilute region for

octan-1-ol, octan-2-ol and 2-ethylhexan-1-ol and implies that as the alcohol concentration is increased so the probability of formation of cyclic forms increases. The maximum is probably of similar origin to that observed in water-alkanol systems where the excess is attributed to disturbance of the distribution between cyclic and linear structured pure forms and mixed associated forms<sup>60</sup>. The height of the absorption maximum decreases as the steric effects of the alkyl group increase. The height decreases in the order: octan-1-ol, 2-ethylhexan-1-ol, octan-2-ol, 2,4-dimethylhexan-3-ol and 2,3-dimethylhexan-3-ol. The steric effects in the 2,4- and 2,3-dimethylhexan-3-ol lead to less self association in these systems than in the corresponding linear systems. Introduction of n-octane to 2,3-dimethylhexan-3-ol leads to a slow increase in the attenuation and no maximum at low concentrations is observed, hydrogen bonding between these molecules being insufficiently strong to lead to association and hence the mechanism of relaxation observed in the other systems is excluded here. The excess absorption at low concentrations appears to be due to a structural relaxation contribution to the volume viscosity rather than to the classical shear viscosity absorption, Figures 8.6, 8.7 and 8.8.

As the concentration of the octanols increases, the disordering action of the n-octane molecules becomes less important in comparison with the effects of hydrogen bonding between neighbouring molecules. Studies of the

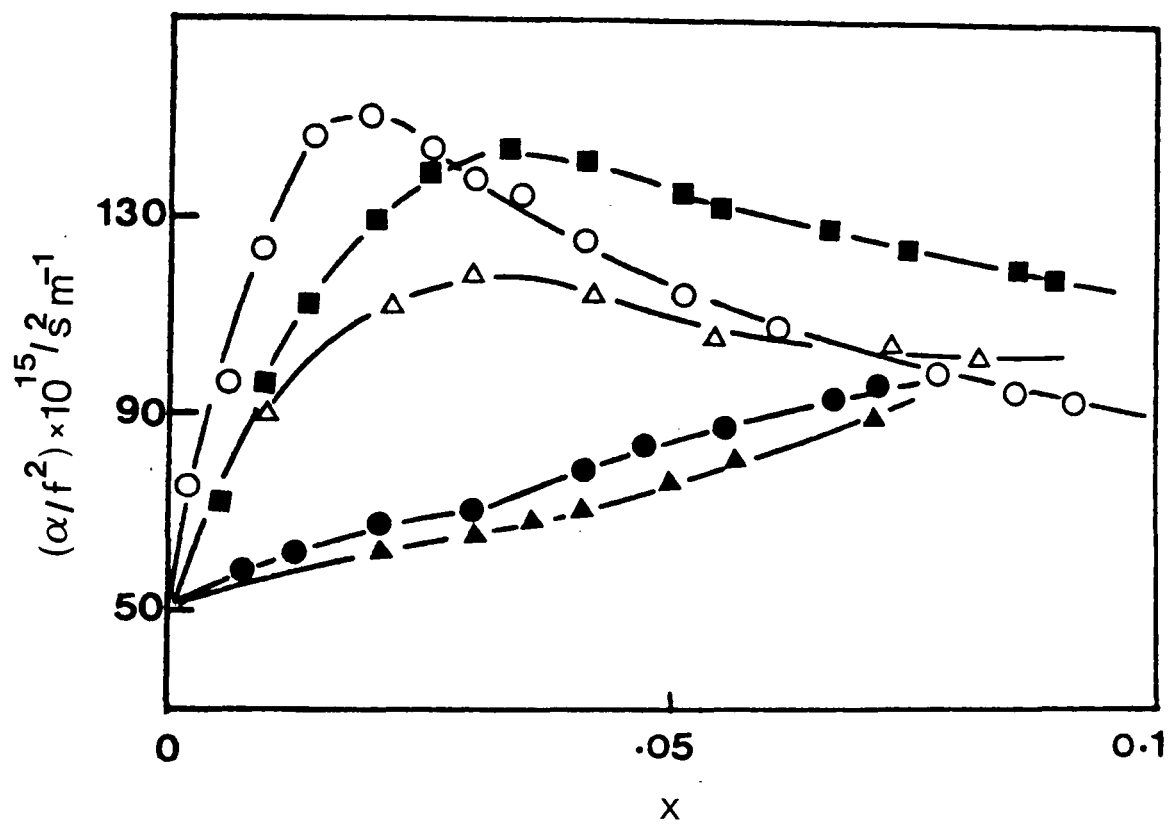


Figure 8.8. Ultrasonic absorption coefficient for  $[xC_8H_{17}OH + (1-x) \text{ n-octane}]$  at 298.15K, 2MHz and low mole fraction,  $x$ , of octanols  $< 0.1$ : ○, octan-1-ol; △, octan-2-ol; ■, 2-ethylhexan-1-ol; ▲, 2,3-dimethylhexan-3-ol; ●, 2,4-dimethylhexan-3-ol.

temperature frequency dependence of the attenuation in the pure alcohols have indicated that the total attenuation of the pure alcohol is a combination of contribution from rotation isomerism and processes associated with structural relaxation of hydrogen bonded clusters and dynamics of the structural association. This analysis is further supported by the trends observed at high mole fractions of alcohol, the rotational isomeric contribution being a linear function of the concentration of alcohol.

### 8.5 Conclusions

This study indicates that in mixtures of alcohol and alkane the observed excesses are a consequence of a number of competing effects. In the sterically unhindered alcohols, cyclic and linear associated forms can be formed. Addition of alkane allows the 'free' volume in the lattice to be filled and also will perturb the degree of clustering present. In the sterically hindered alcohols the cyclic associated forms cannot be formed and no excess features associated with critical association are observed. These latter effects are observed in the region of 0.1 mole fraction for the majority of systems studied. A lack of definitive spectroscopic data precludes a detailed analysis of these data at the present time in terms of linear and cyclic associated structures.

CHAPTER 9

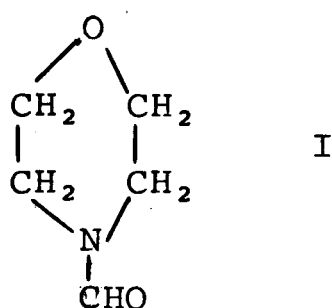
ULTRASONIC STUDIES OF N-FORMYLMORPHOLINE-  
WATER MIXTURES

## CHAPTER 9

### ULTRASONIC STUDIES OF N-FORMYLMORPHOLINE- WATER MIXTURES

#### 9.1 Introduction

Morpholine derivatives and their aqueous solutions are used for the extraction of monocyclic aromatic hydrocarbons from petroleum feedstocks<sup>70-74,259</sup>. N-formylmorpholine (NFM, I) is particularly useful because its high selectivity



and specific solvent power increase the activity coefficients of non-aromatics to a higher degree than aromatics in hydrocarbon-morpholine or hydrocarbon-morpholine-water systems, so permitting distillation or liquid-liquid separation. These solvation characteristics have their origin not only in the general pair interactions between polar and polarisable molecules, but also in the way the particular conformational geometry of N-formylmorpholine permits insertion into the bulk hydrocarbon or water structure. These specific aspects of the solvation interaction are not understood, and this work was undertaken so as to elucidate and evaluate their significance.

Since the economically attractive extraction processes use N-formylmorpholine-water mixtures, this study concentrates on the structural characteristics of aqueous solutions.

Water<sup>212,260,261</sup> has an ordered structure (at low temperatures) , mainly of ice I tetrahedral packing interspersed with numerous cavities containing more closely packed non-hydrogen-bonded molecules. Addition of an hydrogen bonding solute can both enhance the ordering of the non-bonded water and alter the structure of the ordered regions.

Ultrasonic studies of liquid systems can evaluate dynamic properties, such as conformational and structural changes (through relaxation observed in acoustic absorption) and 'static' thermodynamic properties, such as adiabatic compressibility (from sound velocity). Interpretation of ultrasonic measurements requires knowledge of both density and viscosity, and these properties too shed light on the structural characteristics of the liquid under investigation. Such methods have been used to investigate, in aqueous systems, the structural changes caused by non-electrolyte solutes<sup>60,61,262-268</sup>, and particularly the temperature dependence of the compressibility-composition relationship<sup>269-272</sup>. In this study, such observations have been extended to the N-formylmorpholine-water system.

## 9.2 Materials

N-formylmorpholine was obtained (glc grade) from Fluorochem (UK) Ltd. The liquid was refluxed over barium oxide for two hours, then degassed and stored over molecular sieves, type 4A (BDH). Its purity was found to be better than 99.9%. Solutions were prepared using deionized boiled water and filtered N-formylmorpholine. Densities

and sound velocities of pure N-formylmorpholine and deionized water were measured, Table 9.1, and found to be in good agreement with values published in the literature<sup>73,273-275</sup>

### 9.3 Results

#### (i) Volume of mixing data

The values of excess volumes,  $V^E$  for aqueous solutions of N-formylmorpholine were calculated using equation 2.33. The data were fitted to the empirical equation 6.5, where  $a_n$  is the fitting coefficient of order  $n$  obtained from a least squares fit of the data presented in Table 9.2. The standard deviations associated with this analysis are also presented in Table 9.2, along with the coefficients for  $a_n$ . Comparison of the plots of the actual data and the predictions of equation 6.5 indicates that the deviation is in all cases  $< 0.1\%$ . The excess volumes for the aqueous solutions of NFM are all negative over the whole mole fraction and temperature range studied, Figure 9.1.

#### (ii) Viscosity data

The measured viscosities of aqueous solutions of NFM at various temperatures are plotted as a function of mole fraction,  $x$  of NFM, Figure 9.2.

#### (iii) Sound velocity data

The measured sound velocities of aqueous solutions of NFM are presented in Table 9.3 and illustrated in Figure 9.3. The temperature dependence of the sound velocity for various mole fractions of NFM is presented in Figure 9.4. The sound velocity-mole fraction curves show maxima at low

TABLE 9.1. Densities,  $\rho$ , and sound velocities,  $c$ , for the component liquids.

	T/ $^{\circ}$ C	NFM		H <sub>2</sub> O	
		obs.	lit.	obs.	lit.
$\rho/\text{gcm}^{-3}$	20	1.1505	1.1528	-	0.998207
	25	1.1461	-	-	0.997048
	35	1.1374	-	-	0.994035
$c/\text{ms}^{-1}$	20	1639.0	-	1482.5	1482.383
	25	1623.6	-	1497.3	1496.739
	35	1588.1	-	1520.3	1519.81

TABLE 9.2. Coefficients  $a_n$  and standard deviations  $\sigma v^E/\text{cm}^3 \text{ mol}^{-1}$  for least squares representation of excess volume  $v^E/\text{cm}^3 \text{ mol}^{-1}$  for [x NFM + (1-x) water] by equation 6.5.

$a_n$	T/K			
	298.15	308.15	318.15	328.15
$a_1$	$-6.531 \times 10^{-4}$	$-3.005 \times 10^{-4}$	$6.63 \times 10^{-4}$	$-2.959 \times 10^{-3}$
$a_2$	-3.263	-3.051	-3.392	-2.442
$a_3$	-4.479	1.1019	22.237	-2.631
$a_4$	101.385	12.877	-274.222	49.592
$a_5$	-513.05	31.974	1953.424	-189.065
$a_6$	1464.171	-282.339	-7633.424	403.576
$a_7$	-2488.518	672.346	17700.84	-497.873
$a_8$	2465.539	-787.311	-25055.88	-325.822
$a_9$	-1308.987	466.361	-9917.329	-86.975
$a_{10}$	287.116	-111.877	1958.013	
$\sigma V_E/\text{cm}^3 \text{ mol}^{-1}$	$6.08 \times 10^{-3}$	$2.343 \times 10^{-3}$	$4.15 \times 10^{-3}$	$6.915 \times 10^{-3}$

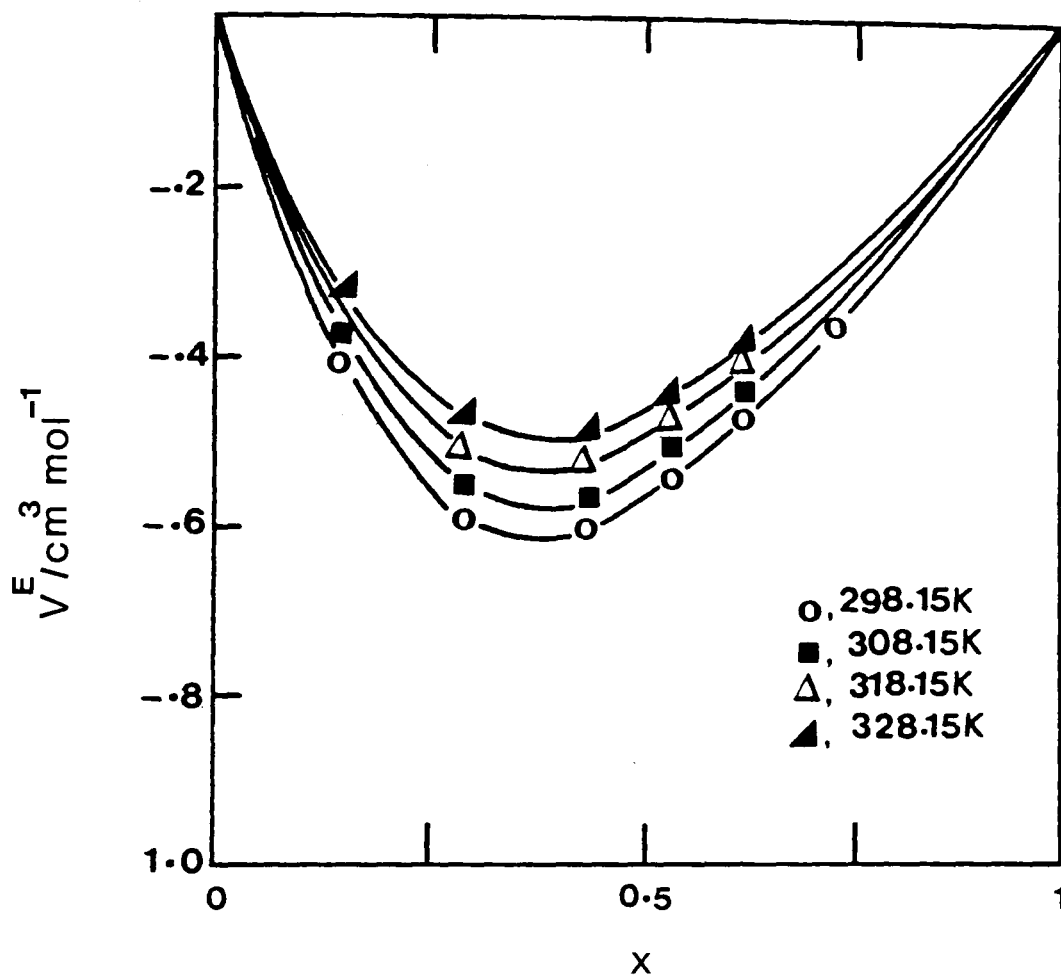


Figure 9.1. Excess volume of NFM-water mixtures as a function of mole fraction,  $x$ , of NFM at various temperatures.

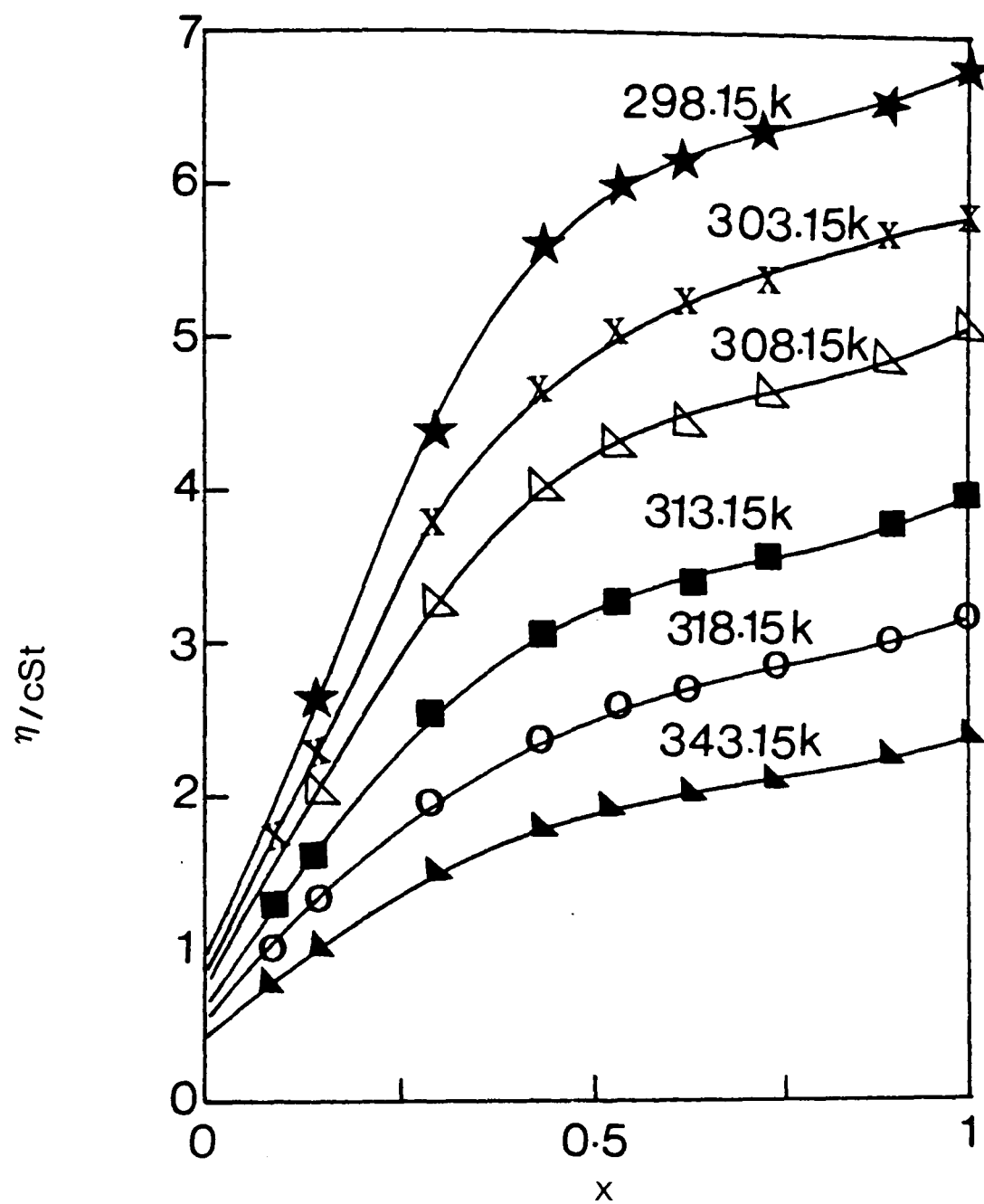


Figure 9.2. Viscosity of NFM-water mixtures as a function of mole fraction,  $x$ , of NFM at various temperatures.

TABLE 9.3. Density,  $\rho$ , sound velocity,  $c$ , isoentropic compressibility,  $\kappa_S$ , and excess isoentropic compressibility,  $\kappa_S^E$ , for [  $x$  NFM + (1- $x$ ) water]

$x$	$\rho/\text{gcm}^{-3}$	$c/\text{ms}^{-1}$	$\kappa_S \times 10^{12} / \text{Pa}^{-1}$	$\kappa_S^E \times 10^{12} / \text{Pa}^{-1}$
T = 298.15K				
0.0000	0.9970	1497.3	447.4	.....
0.0164	1.0126	1535.5	418.8	-18.65
0.0252	1.0201	1553.3	406.3	-26.43
0.0629	1.0467	1611.1	368.0	-47.73
0.0914	1.0624	1640.3	349.8	-55.70
0.1456	1.0845	1671.1	330.2	-60.59
0.2872	1.1159	1685.8	315.3	-51.62
0.4275	1.1299	1672.6	316.4	-37.24
0.5332	1.1341	1659.0	320.4	-26.50
0.6162	1.1389	1650.5	322.3	-20.42
0.7338	1.1412	1639.1	326.2	-11.95
0.8867	1.1448	1626.5	330.2	-3.42
0.9268	1.1451	1625.2	330.6	-2.00
0.9657	1.1457	1624.6	330.8	-1.03
1.0000	1.1461	1623.6	331.0	.....
T = 308.15K				
0.0000	0.9940	1520.3	435.3	.....
0.0164	1.0089	1547.1	414.1	-13.72
0.0252	1.0160	1559.8	404.5	-19.74
0.0629	1.0414	1603.0	372.7	-38.95
0.0914	1.0562	1625.6	358.3	-45.79
0.1456	1.0776	1651.8	340.1	-52.87
0.2872	1.1078	1659.3	327.8	-47.41
0.4275	1.1214	1641.7	330.9	-34.48
0.5332	1.1272	1628.4	334.6	-25.73
0.6162	1.1303	1616.4	338.6	-18.70
0.7338	1.1333	1604.7	342.6	-11.25
0.8867	1.1359	1591.1	347.7	-2.81
0.9268	1.1369	1590.0	347.9	-2.33
0.9657	1.1369	1589.3	348.2	-0.92

TABLE 9.3 (cont.)

x	$\rho/\text{gcm}^{-3}$	$c/\text{ms}^{-1}$	$\kappa_S \times 10^{12} / \text{Pa}^{-1}$	$\kappa_S^E \times 10^{12} / \text{Pa}^{-1}$
T = 318.15K				
0.0000	0.9902	1536.4	427.8	.....
0.0164	1.0045	1557.8	410.2	-12.40
0.0252	1.0115	1570.2	401.0	-19.11
0.0629	1.0355	1601.0	376.8	-34.46
0.0914	1.0498	1618.0	363.8	-42.12
0.1456	1.0702	1635.5	349.3	-48.92
0.2872	1.0993	1633.4	340.9	-44.91
0.4275	1.1126	1612.0	345.8	-33.12
0.5332	1.1183	1597.0	350.6	-24.88
0.6162	1.1212	1585.8	354.6	-17.71
0.7338	1.1244	1572.9	359.5	-11.50
0.8867	1.1272	1556.8	366.0	-2.64
0.9268	1.1275	1555.2	366.7	-1.48
0.9657	1.1281	1554.3	366.9	-0.80
1.0000	1.1286	1553.1	367.3	.....
T = 328.15K				
0.0000	0.9857	1547.7	423.5	.....
0.0164	0.9995	1563.6	409.2	-11.43
0.0252	1.0063	1573.3	401.4	-17.31
0.0629	1.0289	1595.5	381.8	-31.57
0.0914	1.0432	1607.8	370.8	-32.79
0.1456	1.0627	1618.1	359.4	-45.93
0.2872	1.0909	1608.9	354.1	-43.65
0.4275	1.1041	1584.4	360.8	-32.71
0.5332	1.1095	1567.3	366.9	-24.45
0.6162	1.1125	1555.0	371.2	-18.35
0.7338	1.1157	1540.5	377.7	-10.95
0.8867	1.1185	1524.0	384.9	-2.25
0.9268	1.1188	1522.8	385.4	-1.46
0.9657	1.1194	1521.5	385.9	-0.68
1.0000	1.1199	1520.3	386.3	.....
T = 343.15K				
0.0000	0.9777	1555.1	422.9	.....
0.0252	1.0042	1568.1	405.0	-17.43
0.0914	1.0329	1578.0	388.8	-32.68
0.1456	1.0524	1580.2	380.5	-45.24
0.2872	1.0799	1564.4	378.4	-41.79
0.4275	1.0911	1533.7	389.6	-30.11
0.5332	1.1008	1515.1	395.7	-23.73
0.6162	1.1018	1504.2	401.1	-18.27
0.7338	1.1035	1489.0	408.7	-10.45
0.8867	1.1056	1472.7	417.0	-2.02
1.0000	1.1067	1468.5	419.0	.....

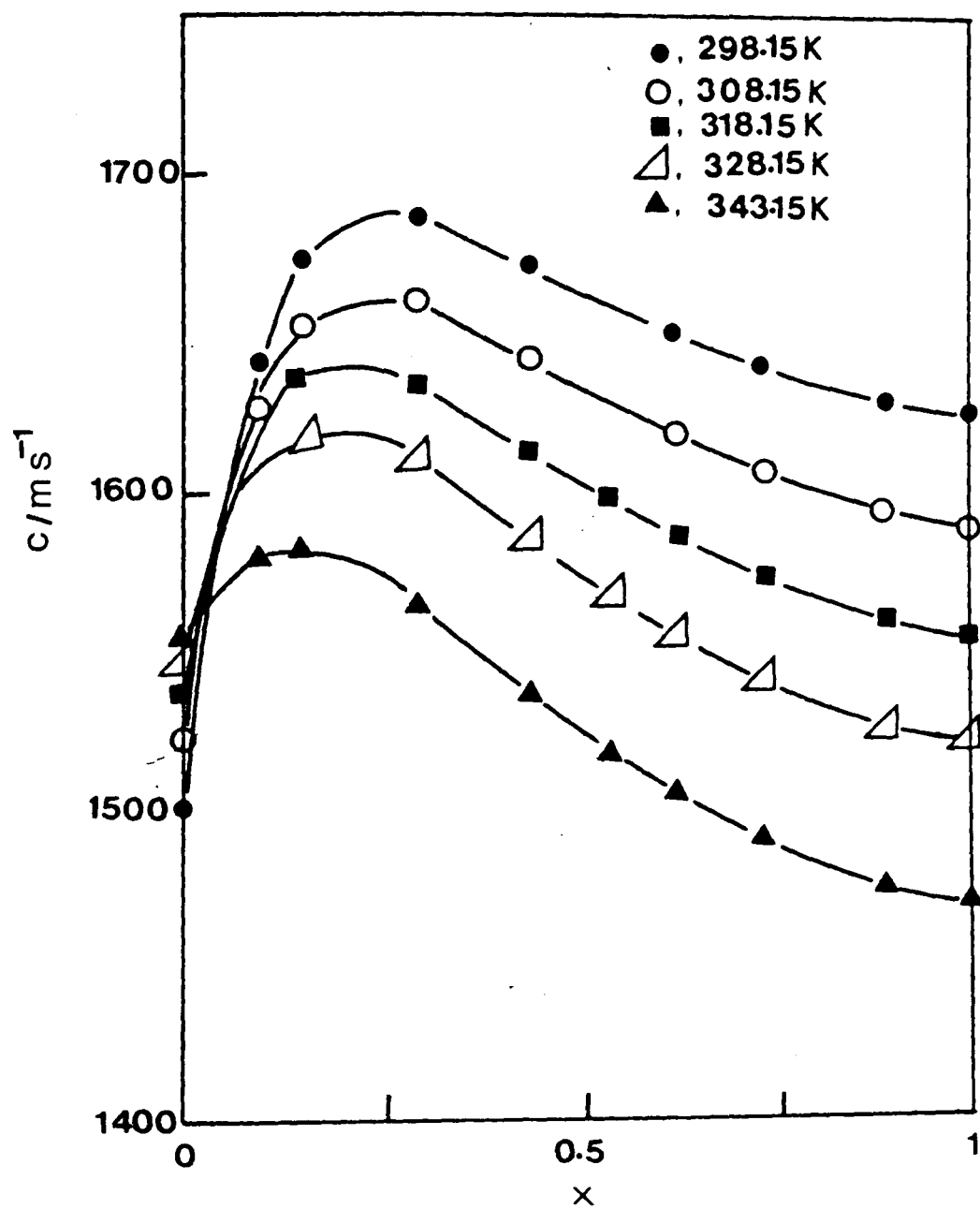


Figure 9.3. Ultrasonic velocity of NFM-water mixtures as a function of mole fraction,  $x$ , of NFM at various temperatures.

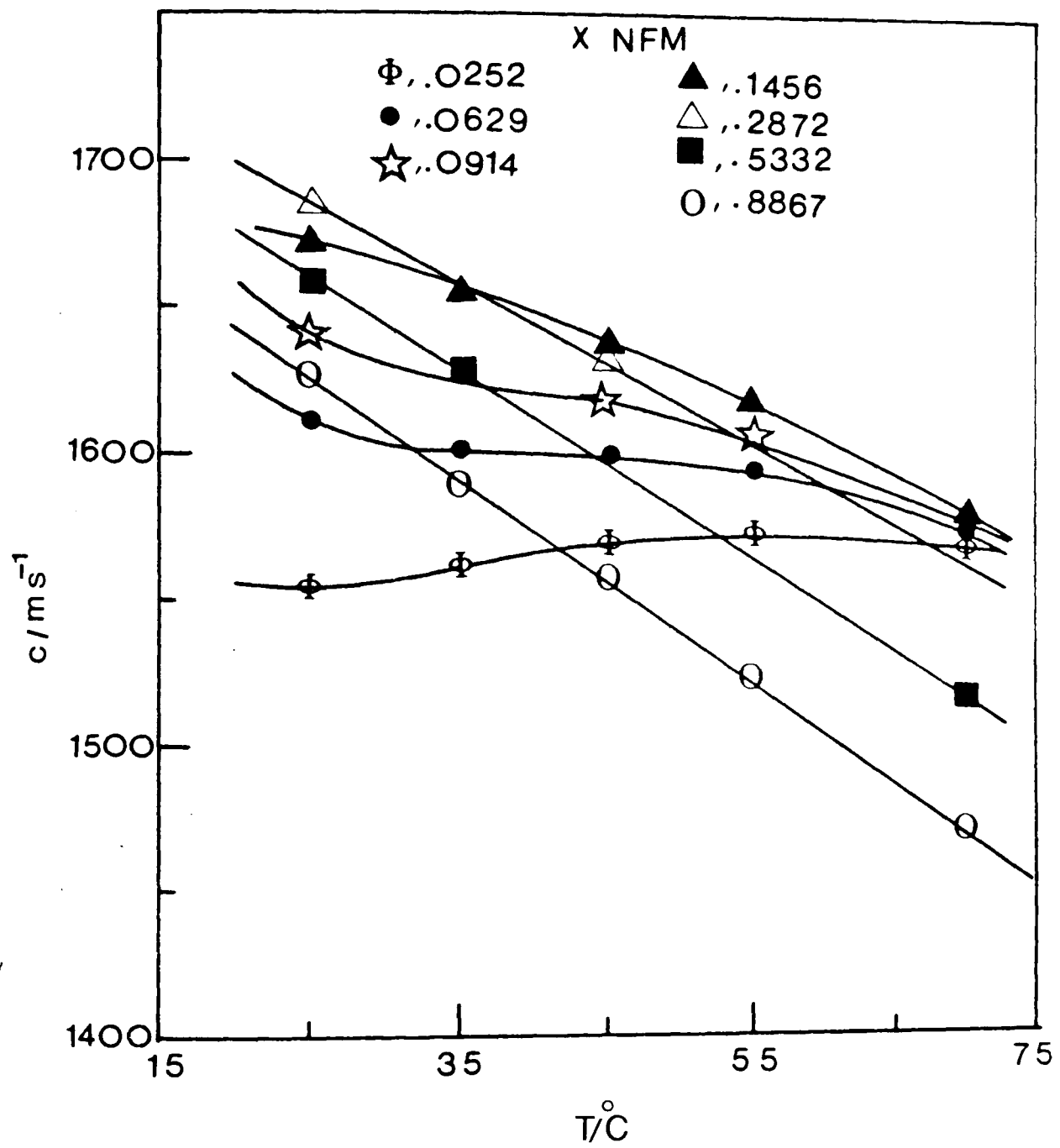


Figure 9.4. Temperature dependence on the sound velocity for NFM-water mixtures.

concentration and decreases as the temperature is increased.

(iv) Isoentropic compressibility and excess isoentropic compressibility data

Isoentropic compressibility,  $\kappa_S$ , of the pure components and aqueous solutions of NFM was calculated using equation 2.35. The data are presented in Table 9.3 and plotted as a function of mole fraction,  $x$ , of NFM at various temperatures, Figure 9.5.

The excess isoentropic compressibility  $\kappa_S^E$ , was calculated using equation 2.34 and the data so obtained are presented in Table 9.3. Figure 9.6 illustrates the variation of  $\kappa_S^E$  with mole fraction,  $x$ , of NFM at various temperatures. The excess isoentropic compressibilities for aqueous solutions of NFM are all negative over the whole mole fraction range and the various temperatures studied.

(v)  $^{13}\text{C}$  nmr spectra of N-formylmorpholine

The proton decoupled and non proton decoupled spectra of N-formylmorpholine are presented in Figures 9.7 and 9.8. The peak assignments and splitting constants are presented in Table 9.4. The  $^{13}\text{C}$  spectrum of this compound is analysed as follows. The highest field peak is associated with the formyl group and under conditions of non-proton decoupling is split into a doublet. The remaining carbons in the decoupled spectra are grouped into two separate regions, that at the higher field being associated with the carbon joined to the ring oxygen,

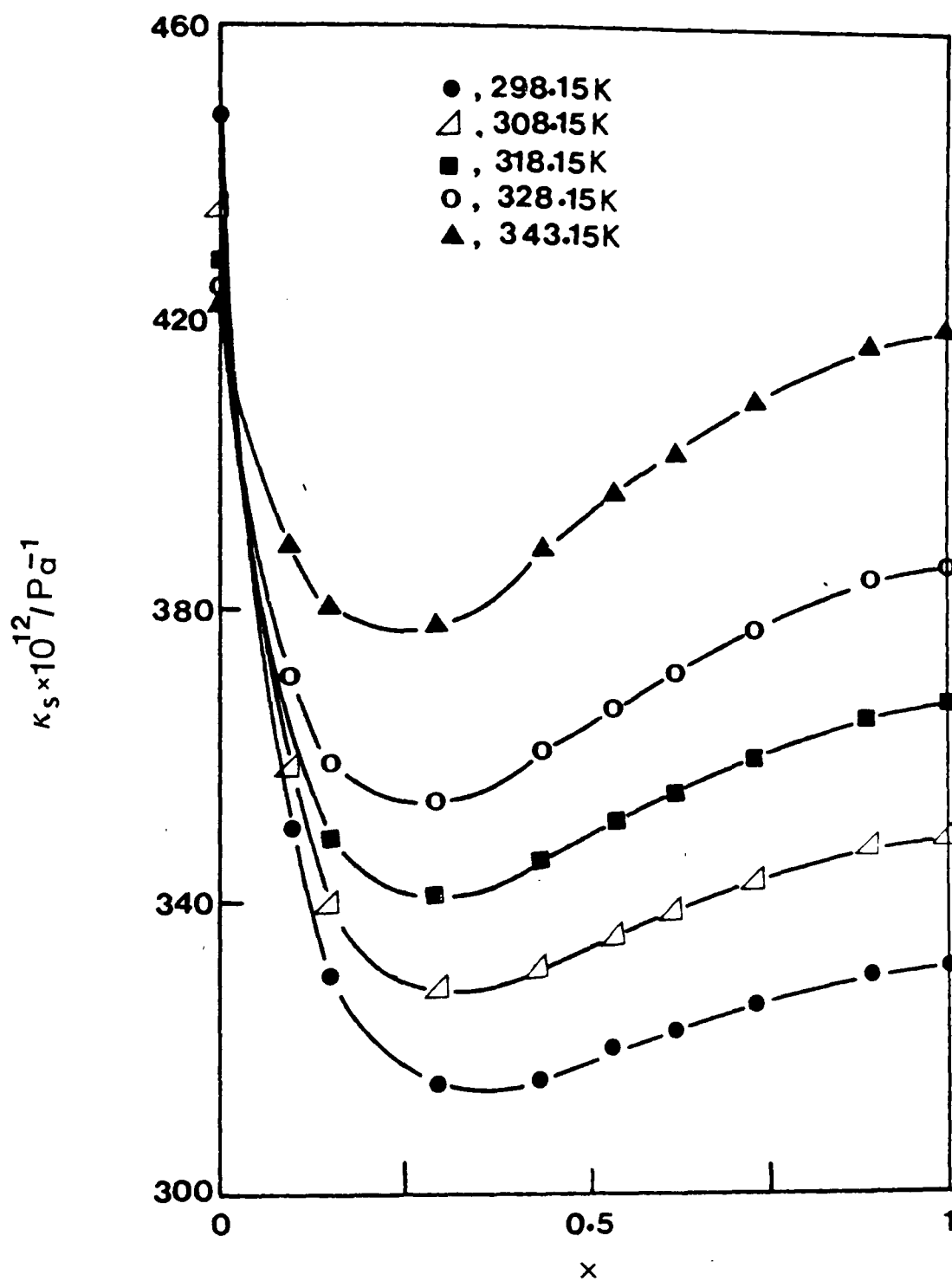


Figure 9.5. Isoentropic compressibility of NFM-water mixtures as a function of,  $x$ , of NFM at various temperatures.

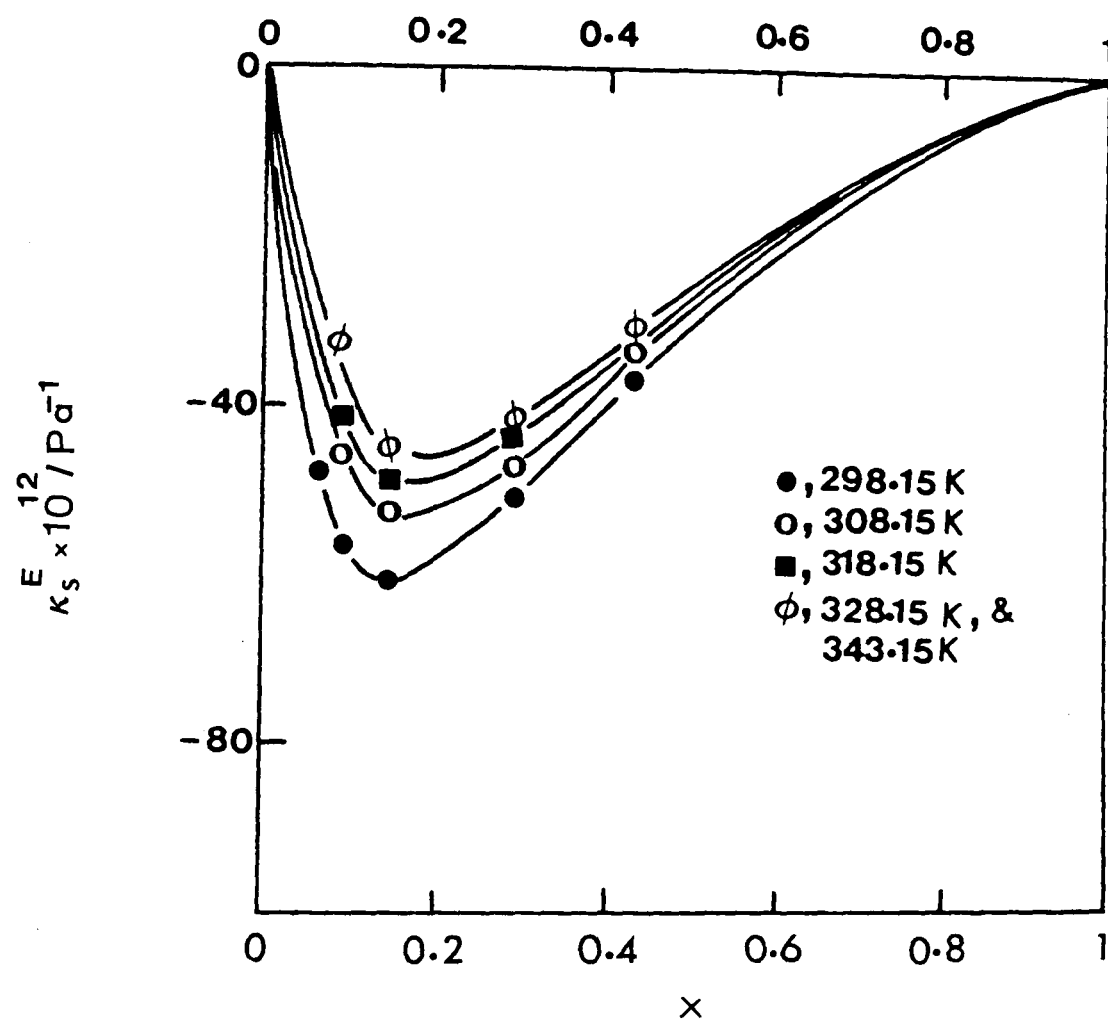


Figure 9.6. Excess isoentropic compressibility of NFM-water mixtures as a function of mole fraction,  $x$ , of NFM at various temperatures.

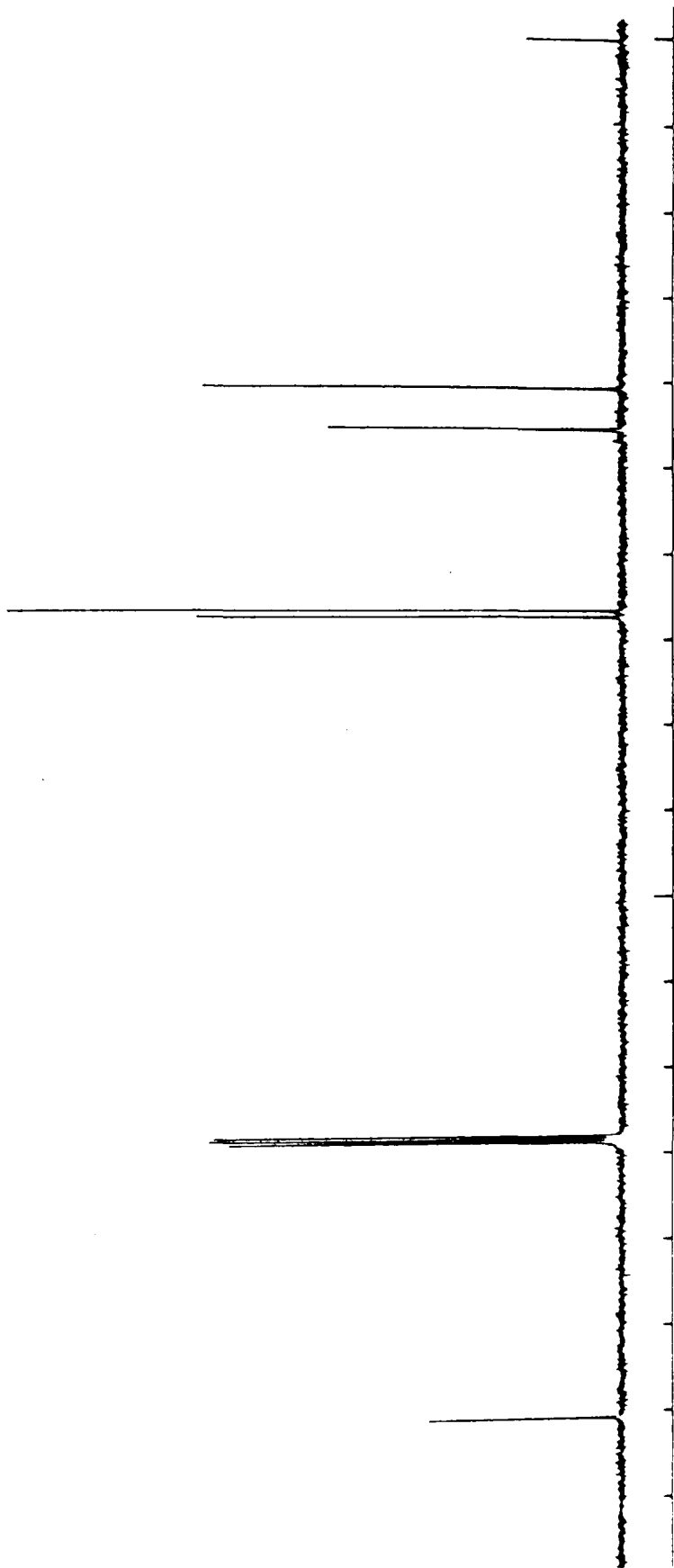


Figure 9.7.  $^{13}\text{C}$  nmr spectra of N-formylmorpholine-proton decoupled.

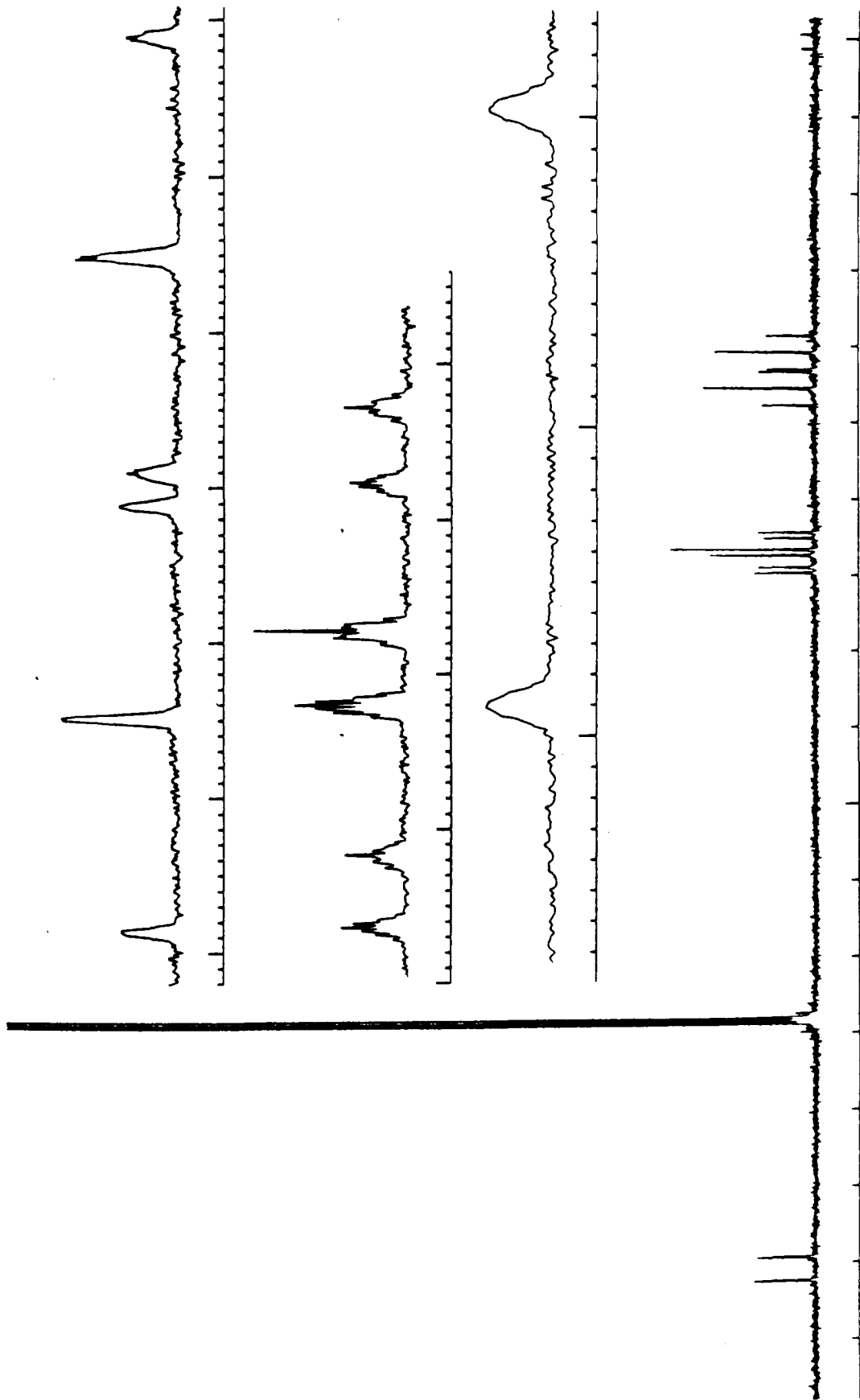


Figure 9.8.  $^{13}\text{C}$  nmr spectra of N-formylmorpholine-non-proton decoupled.

TABLE 9.4.  $^{13}\text{C}$  nmr spectrum of N-formylmorpholine.  
 C atoms labelled;  $\alpha$ ,  $\beta$  ring position from  
 N,  $\gamma$  formyl.

$\delta$ / ppm	C atom	Intensity	J/Hz
162.02	$\gamma$	1.61	192.35
158.96		1.54	
69.34	$\beta$	1.70	142.42
68.63		1.96	
67.03		1.61	
66.29	$\beta$	1.79	142.2
64.81		2.05	
63.48		1.10	
47.47	$\alpha$	1.81	139.64
45.28		3.77	
43.11		1.94	
42.77	$\alpha$	1.67	139.64
40.52		2.53	
38.32		1.70	

and that at the lower field to the carbon attached to the nitrogen atom. Each of these is split into a doublet under proton decoupled conditions, and further split into a doublet of triplets on non proton decoupling. The primary splitting is associated with different conformations of the ring. Examination of the beta carbon resonances indicates further splitting due to the quadruple of the nitrogen atom to which it is attached.

(vi) Ultrasonic attenuation data

The ultrasonic absorption coefficient as a function of frequency and mole fraction,  $x$ , of NFM at various temperatures is presented in Figures 9.9 – 9.11. The variation of absorption coefficient with frequency was fitted to the equation 2.8. Computer fits of the observed data for the aqueous solutions of NFM yielded the parameters summarized in Table 9.5.

Continuing the analysis as discussed in section 4.3(iv), the energy parameters associated with the rotational relaxation process could be derived. Plot of  $\log(T\mu_{\max}/c^2)$  against the reciprocal temperature is linear and has a slope  $\Delta H^\ominus/R$ . Arrhenius plots of the relaxation frequency, Figure 9.12, give the activation energy  $\Delta E^\ddagger$  for the overall relaxation processes. The values of  $\Delta H^\ominus$  and  $\Delta E^\ddagger$  are summarized in Table 9.6.

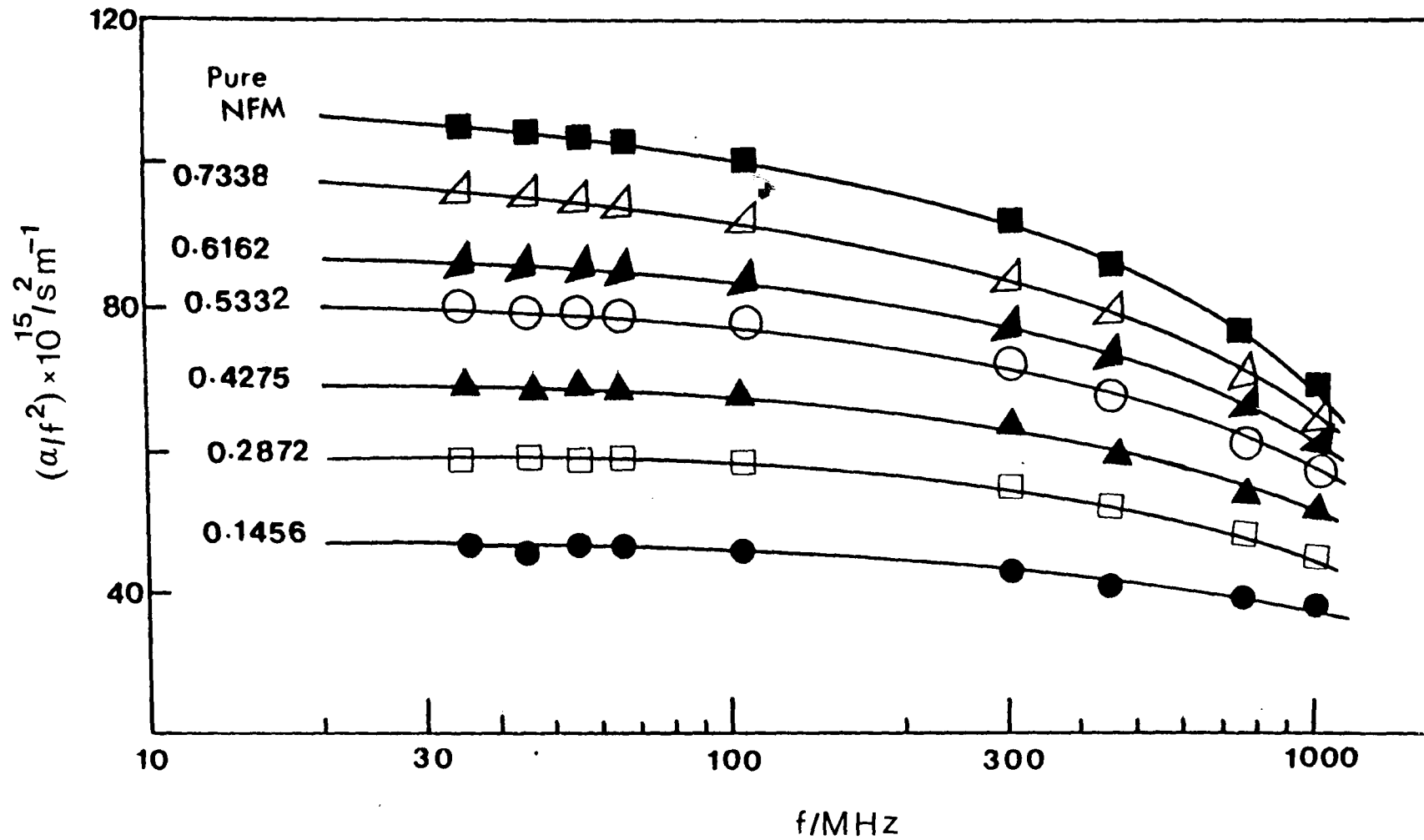


Figure 9.9. Variation of the ultrasonic absorption coefficient of NFM-water mixtures with frequency and mole fraction,  $x$ , of NFM at 292.15K.

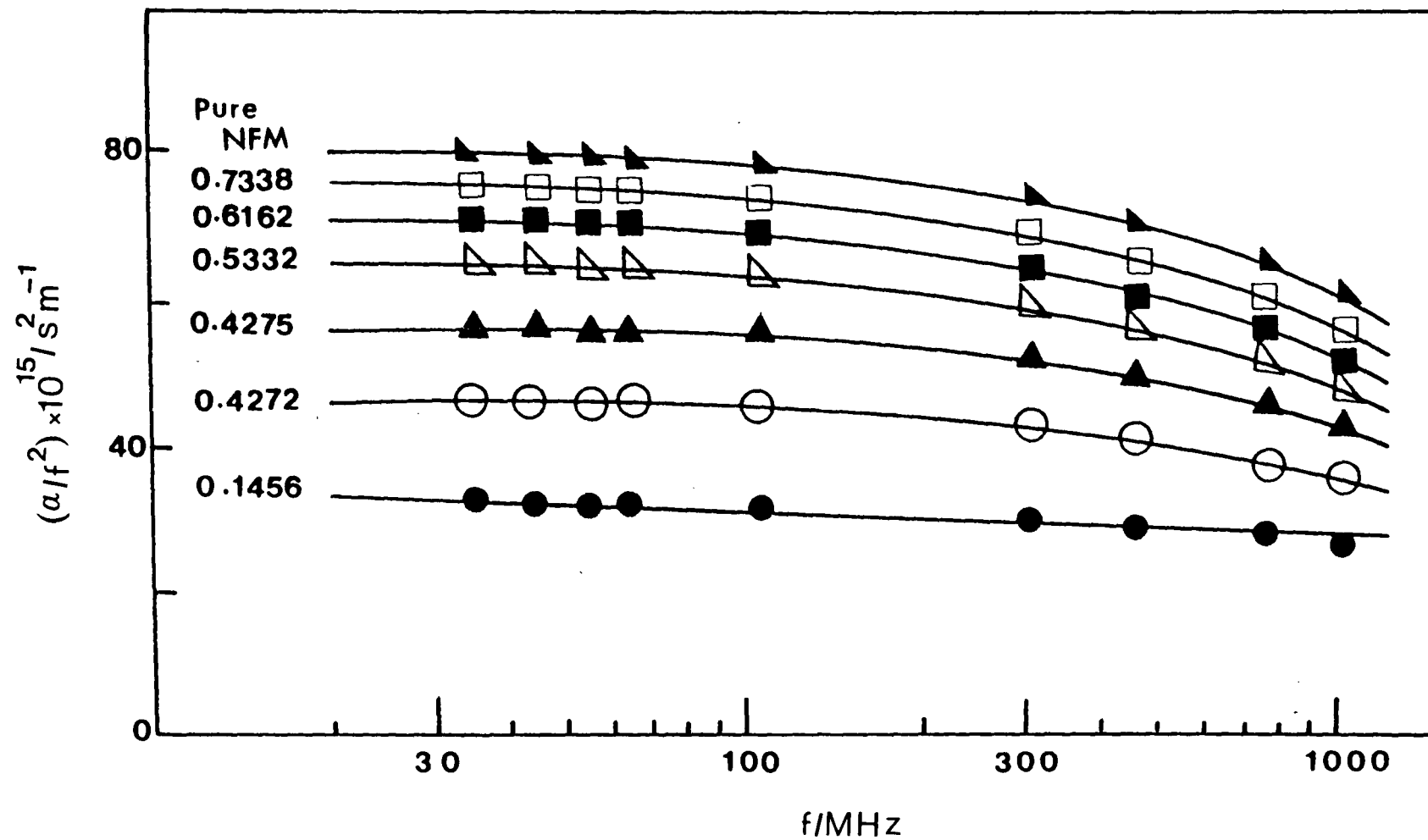


Figure 9.10. Variation of the ultrasonic absorption coefficient of NFM-water mixtures with frequency and mole fraction,  $x$ , of NFM at 298.15K.

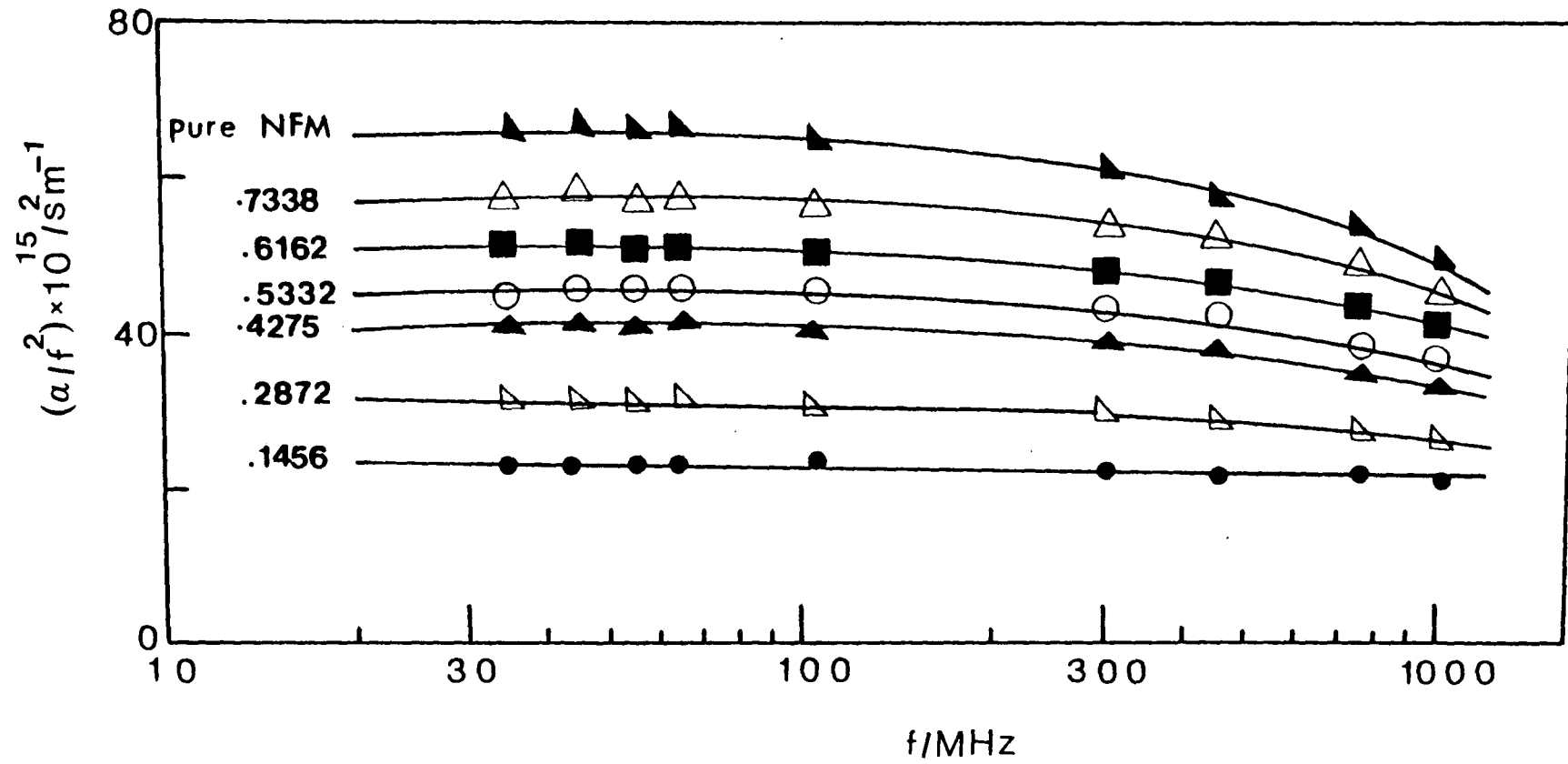


Figure 9.11. Variation of the ultrasonic absorption coefficient of NFM-water mixtures with frequency and mole fraction,  $x$ , of NFM at 318.15K.

TABLE 9.5. Ultrasonic relaxation parameters

Mole fraction of NFM	Temperature/K	A x 10 <sup>15</sup> /s <sup>2</sup> m <sup>-1</sup>	B x 10 <sup>15</sup> /s <sup>2</sup> m <sup>-1</sup>	f <sub>c</sub> /MHz
Pure NFM	292.95	34.5	67	500
	298.15	20.4	59.4	500
	318.15	12.5	52	552
0.7338	292.95	33	61.5	510
	298.15	19.7	55.6	516
	318.15	12.5	44.9	560
0.6162	292.95	28	57.5	520
	298.15	20	46.5	540
	318.15	11	35	575
0.5332	292.95	27	52.7	523
	298.15	20	46.5	540
	318.15	11	35	575
0.4275	292.95	21	48	540
	298.15	16	41	560
	318.15	9.5	32	575
0.2872	292.95	15	44	555
	298.15	14.5	33	570
	318.15	6	25.5	592
0.1456	292.95	11	36	568
	298.15	8.5	24.5	580
	318.15	4.5	19.5	600

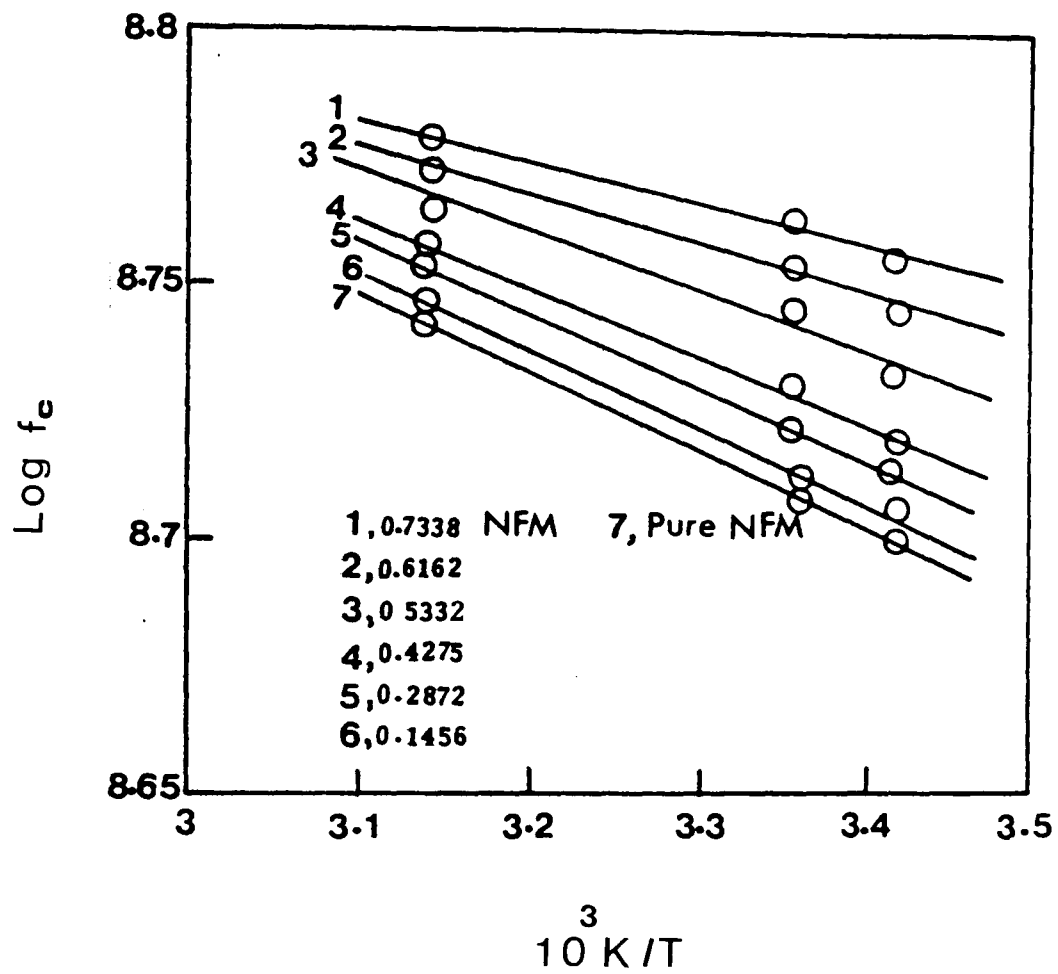


Figure 9.12. Arrhenius plot of relaxation frequencies of NFM and its aqueous solutions.

TABLE 9.6. Relaxation activation energies and enthalpy differences.

---

mole fraction of NFM	$\Delta E^\ddagger$ /kJ mol <sup>-1</sup>	$\Delta H^\ominus$ /kJ mol <sup>-1</sup>
1.0000	3.10	9.00
0.7338	2.97	8.52
0.6162	2.88	7.62
0.5332	2.80	7.10
0.4275	1.98	4.98
0.2872	1.71	
0.1456	1.59	

---

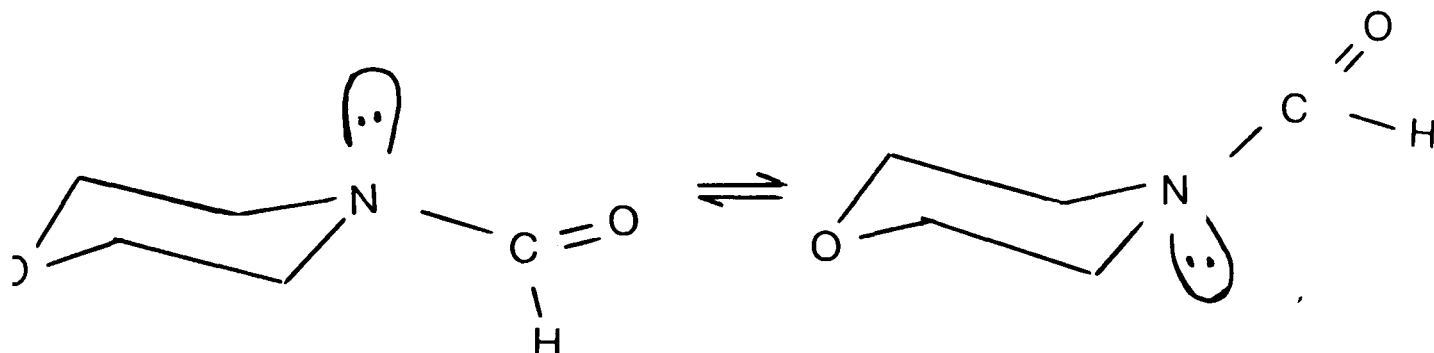
## 9.4 Discussion

### A. Conformational Dynamics of N-Formylmorpholine

There are two possible causes of the acoustic attenuation observed; rotational isomerism of the formyl group, and ring inversion. Rotational isomerism in formamide structures has been of interest for many years and in general the activation energies reported<sup>276</sup> lie in the range 60-120 kJ mol<sup>-1</sup>. In  $\alpha,\beta$  unsaturated aldehydes, however, values lie in the range 20-60 kJ mol<sup>-1</sup>. In such systems a correlation between the <sup>13</sup>C-<sup>1</sup>H coupling constant and the activation energy for aldehyde group rotation has been demonstrated, and this correlation would predict a value of 75 kJ mol<sup>-1</sup> for N-formylmorpholine. It is unlikely, therefore, that such a rotation is the cause of the ultrasonic relaxation observed in this study.

Turning now to ring inversion phenomena, an activation energy of 24.3 kJ mol<sup>-1</sup> has been found in N-methylmorpholine, and this has been ascribed<sup>277</sup> to inversion of the bonds to the nitrogen atom, which inversion occurs several times during the lifetime of any specific conformation of the remainder of the ring. Since the splitting of the <sup>13</sup>C nmr spectrum at 62 MHz indicates that in this case the ring geometry is effectively frozen at such frequencies, the acoustic process must be a localised change and is most likely again an inversion of the nitrogen atom. The very low activation energy indicates that electron delocalization of nitrogen to formyl creates a more planar structure at the N-atom. Thus the

conformational dynamics are seen as a rapid (low activation energy) inversion of an almost planar geometry at the N-atom superimposed on a much slower interchange between the normal six-membered ring conformations.



This suggests that the planarity is enhanced and diminished rate of more gross conformational change underlies the structural contribution to the greater specificity towards aromatics shown by N-formylmorpholine by comparison with other morpholine derivatives.

B. Conformational Dynamics of N-Formylmorpholine in the Presence of Water

In aqueous mixtures there is always the possibility of a proton transfer equilibrium (as observed in amine systems)<sup>276</sup> contributing to the observed acoustic relaxation. The fact that the acoustic relaxation amplitude changes almost linearly with the concentration of the N-formylmorpholine is consistent with the assumption that the relaxation is associated with a conformational change rather than with some form of proton transfer equilibrium<sup>278</sup>. Furthermore, the highly resolved nmr spectrum described earlier indicates that a proton exchange could not be taking place at the frequencies of the acoustic

relaxation.

The acoustic attenuation displayed in Figures 9.9 -9.11 and the energy parameters presented in Table 9.6 show that the presence of water modifies the conformational relaxation (lowering  $\Delta E^\ddagger$  and  $\Delta H^\ominus$ ) increasing the distinction between N-formyl and other derivatives of morpholine. This parallels an increased efficiency of aromatic extraction in the presence of small quantities of water<sup>71,73</sup>

### C. Structure of N-Formylmorpholine-Water Mixtures

#### (i) Excess volumes and compressibilities of mixing

An indication of packing changes in the structure of liquid mixtures can be obtained from excess functions of mixing, particularly the excess volume,  $V^E$ , and excess isoentropic compressibility,  $\kappa_s^E$ . The excess volumes are all negative over the whole composition and temperature range, Figure 9.1. This behaviour is similar to that familiar<sup>279-280</sup> in aqueous mixtures of liquids such as acetone, dimethylformamide and dimethylsulphoxide. The general explanation<sup>281</sup>, applicable in this case, is that hydrogen bonding to the carboxyl group is stronger than to water, so the solute enhances structure and close packing in the disordered regions.

Excess isoentropic compressibilities are illustrated in Figure 9.6. It is interesting that the largest negative excess compressibility occurs at a lower mole fraction of NFM (ca. 0.3) than does the largest negative excess volume (ca. 0.4). This must arise from the high volume but low compressibility of the ice I structure, and indicates that

larger amounts of NFM disrupt the structure so decreasing the volume without decreasing the compressibility.

It was also observed that on addition of NFM the sound velocity, Figure 9.3, and isoentropic compressibility, Figure 9.5, show that close packing is a maximum at low mole fraction of NFM and the temperature coefficient of sound velocity (at 310K) becomes positive at mole fraction of NFM  $\leq 0.06$ , as expected from thermal disruption of the water ice I structure. At given temperature, the sound velocity increases with increasing the mole fraction of NFM up to 0.29. Above this critical concentration the sound velocity profile is essentially dominated by NFM properties, Figure 9.4.

#### (ii) Viscosities

The viscosities of aqueous solutions of NFM are illustrated in Figure 9.2. Again an enhanced viscosity at intermediate mole fractions is indicative of intermolecular association. Viscosity measurements by themselves do not shed much light on the form of this interaction, but of course must be used in the calculation of the viscothermal contribution to ultrasonic absorption.

#### (iii) Ultrasonic absorption

The most interesting aspect of the attenuation measurements is found at low mole fractions NFM. The relaxation in water is ascribed to exchange of molecules between ordered and disordered regions. The amplitude of this must depend on the volume fractions of the ordered and disordered regions, and so like excess volume and

excess compressibility should show a correlation with break up of ice I structure or ordering of non hydrogen bonded molecules of NFM. The values of excess volume of Figure 9.1 and  $\kappa_s$ , Table 9.3, were used to calculate the structural volume contribution to the total relaxing amplitude

$$\mu_{vol} = \pi(\Delta V^\ominus)^2 / 2\kappa_s RT$$

A comparison of an excess absorption (calculated as usual from a Raoult's Law mole fraction of absorption coefficients of pure water and pure NFM) against the structural contribution calculated from excess volumes and compressibilities is shown in Figure 9.13. A good correlation is observed at low mole fractions NFM, lending strength to the general correctness of the hypotheses.

### 9.5 Conclusions

Ultrasonic attenuations and velocities,  $^{13}\text{C}$  nmr spectra densities and viscosities of NFM and its aqueous mixtures have been used in an interrelated way to investigate conformational and structural changes in the liquids. Conformational analysis (based mainly on nmr and ultrasonic relaxation) suggests that N-formylmorpholine is more planar than N-alkyl analogues, and that this planarity is increased by the presence of traces of water. This could explain the increased efficiency in extraction of aromatics from petroleum feedstocks. N-methylmorpholine < N-formylmorpholine < N-formylmorpholine/water. Structural analysis (based mainly on excess volumes and compressibilities of

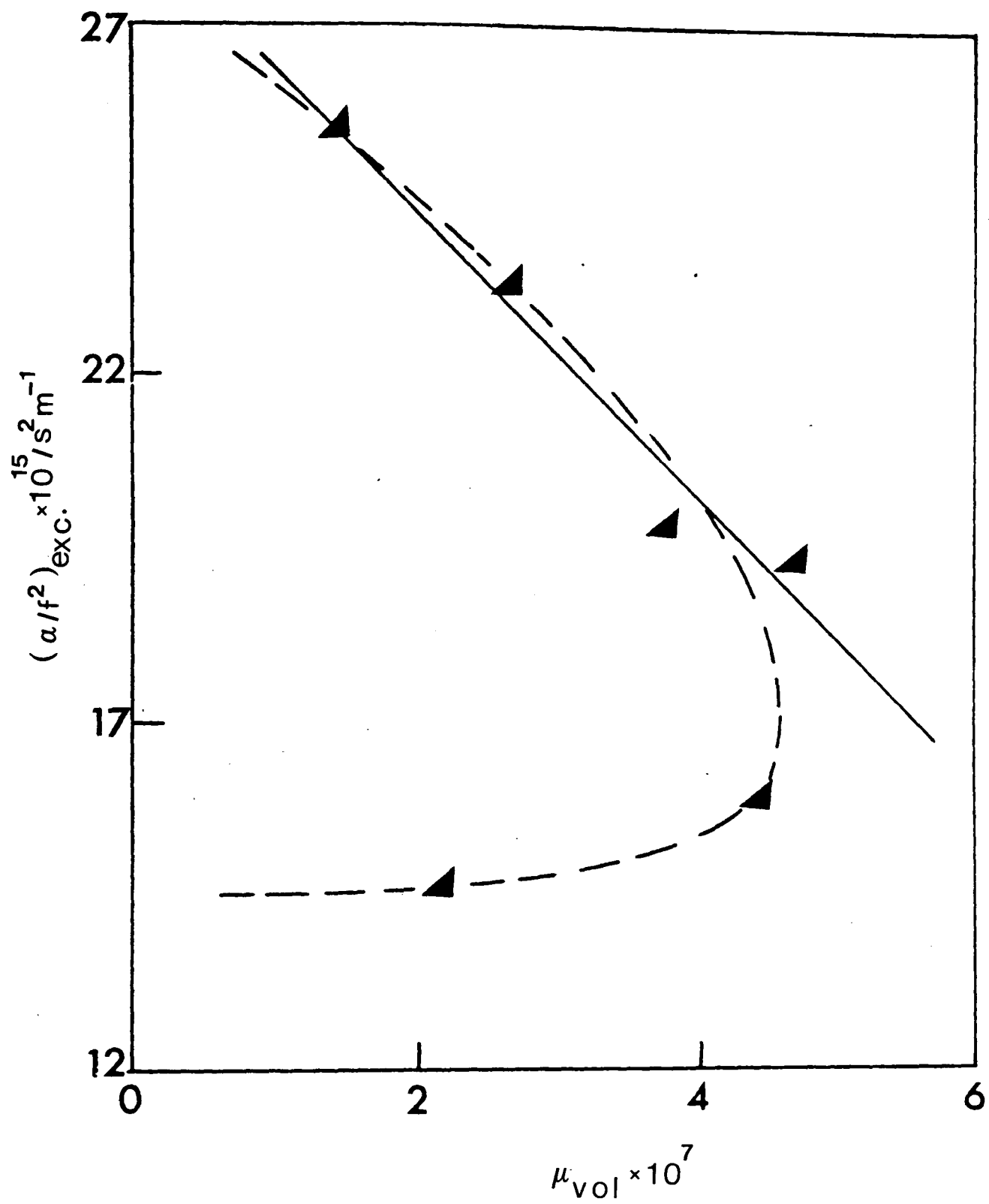


Figure 9.13. Excess attenuation compared with a calculated structural volume contribution to the total absorption at 298.15K.

mixing) suggests that as NFM is added to water, it first introduces hydrogen bonding and ordering to water molecules not bound into the ice I tetrahedral structure, then at higher concentrations it disrupts the ice I structure to a less open, but no less compressible, hydrogen bonded mixture. This array of solvated NFM is capable of absorbing the aromatic rings in the 'solvation' process.

## APPENDIX

## Publications

1. J. Chem. Soc. Faraday Trans. 2, 78, 1687 (1982),  
Ultrasonic Studies of Rotational Isomerism in Various  
Methylpentanes  
by A.M. Awwad, A.M. North and R.A. Pethrick.
2. J. Chem. Soc. Faraday Trans. 1, 78, 3203 (1982),  
Ultrasonic Investigations of Mixtures of n-octane  
with Isomeric Octanols  
by A.M. Awwad and R.A. Pethrick.
3. J. Chem. Soc. Faraday Trans. 2, 79, 449 (1983),  
Ultrasonic Studies of N-formylmorpholine-Water  
Mixtures  
by A.M. Awwad, A.M. North and R.A. Pethrick.
4. J. Chem. Soc. Faraday Trans. 2, 79, (1983),  
Ultrasonic Studies of Rotational Isomerism in Various  
Methylhexanes  
by A.M. Awwad, A.M. North and R.A. Pethrick.
5. J. Chem. Soc. Faraday Trans. 2, 79, (1983),  
Packing and Conformational Contributions in Binary  
Liquid Mixtures  
by A.M. Awwad, A.M. North and R.A. Pethrick.
6. J. Mol. Liquids, in press,  
Adiabatic Compressibility of Branched Chain Hydro-  
carbons - Pentanes and Hexanes  
by A.M. Awwad and R.A. Pethrick.

## REFERENCES

## REFERENCES

1. I.R. McDonald and K. Skinner, *Ann. Rep. Prog. Chem.*, 67A, 45 (1970).
2. P.A. Egelstaff, *Ann. Rev. Phys. Chem.*, 24, 159 (1973).
3. N.G. Parsonage, *Ann. Rep. Prog. Chem.*, 64A, 57 (1967).
4. J.A. Barker and D. Henderson, *Ann. Rev. Phys. Chem.*, 23, 439 (1972).
5. C. Schlier, *Ann. Rev. Phys. Chem.*, 20, 191 (1969).
6. J.S. Rowlinson, *Disc. Faraday Soc.*, 49, 30 (1970).
7. J.S. Rowlinson and I.D. Watson, *Chem. Eng. Sci.*, 24, 1565 (1969).
8. R.L. Scott and D.V. Fenby, *Ann. Rev. Phys. Chem.*, 20, 111 (1969).
9. P.J. Flory, *Disc. Faraday Soc.*, 49, 7 (1970).
10. D. Patterson and J.B. Bardin, *Trans. Faraday Soc.*, 66, 321 (1970).
11. D.E. Woessner, *J. Chem. Phys.*, 41, 84 (1964).
12. S. Chandra and J. Prakash, *J. Chem. Phys.*, 54, 5366 (1971).
13. D.C. Douglass and G.P. Jones, *J. Chem. Phys.*, 45, 956 (1966).
14. A.K.M. Masood, A.M. North, R.A. Pethrick, M. Towland and F.L. Swinton, *Adv. Mol. Relaxation Processes*, 9, 153 (1976).
15. M.A. Hamza, G. Serratrice, M.J. Stebe and J.J. Delpuech, *Adv. Mol. Relaxation Processes*, 20, 199 (1981).
16. M.L. Klein and I.R. McDonald, *J. Chem. Phys.*, 71, 298 3673 (1979).

17. S. Murad, D.J. Evans, K.E. Gubbins, W.B. Streett and D.J. Tidesley, *Mol. Phys.*, 37, 725 (1979).
18. K. Singer, J.V.L. Singer and A.J. Taylor, *Mol. Phys.*, 37, 1239 (1979).
19. M. Zeidler, *Angew. Chem. Int. Ed. Engl.*, 19, 697 (1980).
20. P. Clancy and K.E. Gubbins, *Disc. Faraday Soc.*, 66, 116 (1978).
21. F. Kohler, N. Quirke and J.W. Perram, *J. Chem. Phys.*, 71, 4128 (1979).
22. I. Prigogine, 'The Molecular Theory of Solutions', North Holland, Amsterdam, 1957.
23. P.J. Flory, *J. Am. Chem. Soc.*, 87, 1833 (1965).
24. B.E. Eichinger and P.J. Flory, *Trans. Faraday Soc.*, 64, 2035 (1968).
25. P.J. Flory, R.A. Orwoll and A. Vrij, *J. Am. Chem. Soc.*, 86, 3507 (1964).
26. D. Patterson and G. Delmas, *Disc. Faraday Soc.*, 49, 98 (1970).
27. P.J. Flory, *J. Chem. Phys.*, 10, 51 (1942).
28. M.L. Huggins, *J. Phys. Chem.*, 46, 151 (1942).
29. A.J.B. Cruickshank and C.P. Hicks, *Disc. Faraday Soc.*, 49, 106 (1970).
30. P. Tancrede, P. Bothorel, P. de St. Romain, D. Patterson, *J. Chem. Soc., Faraday Trans. 2*, 73, 15 (1977).
31. P. de St. Romain, H.T. Van and D. Patterson, *J. Chem. Soc., Faraday Trans. 1*, 75, 1700 (1979).
32. A. Desmyter and J.H. van der Waals, *Rec. Trav. Chim.*, 77, 53 (1958).

33. J.D. Gomez-Ibanez and C.T. Liu, *J. Phys. Chem.*, 67, 1388 (1968).
34. M.L. McGlashan and K.W. Morcum, *Trans. Faraday Soc.*, 57, 581 907 (1961).
35. J.H. van der Waals, *Trans. Faraday Soc.*, 52, 916 (1956).
36. M.L. McGlashan and A.G. Williamson, *Trans. Faraday Soc.* 57, 588 (1961).
37. A.J. Davenport and J.S. Rowlinson, *Trans. Faraday Soc.*, 59, 78 (1963).
38. V.F. Nozdrev, 'The Use of Ultrasonic in Molecular Physics', Pergamon, New York (1965).
39. J.E. Piercy and N.G.S. Rao, *J. Chem. Phys.*, 46, 3951 (1967).
40. J.H. Chen and A.A. Petrauskas, *J. Chem. Phys.*, 30, 304 (1959).
41. J.M. Young and A.A. Petrauskas, *J. Chem. Phys.*, 25, 943 (1956).
42. M.A. Cochran, P.B. Jones, A.M. North and R.A. Pethrick, *J. Chem. Soc., Faraday Trans. 2*, 68, 1719 (1972).
43. F. Franks and D.S. Reid, 'Water - A Comprehensive Treatise', Vol. 2, Ed. F. Frank, Plenum Press, New York (1973).
44. J. Emery, S. Gasse, R.A. Pethrick and D.W. Phillips, *Adv. Mol. Relaxation Processes*, 12, 47 (1978).
45. C. Dugue, J. Emery and R.A. Pethrick, *Mol. Phys.*, 42, 1453 (1981).
46. C. Dugue, J. Emery and R.A. Pethrick, *Mol. Phys.*, 41, 703 (1980).

47. G. Rao, B.K. Singh, O.N. Awashi and U.S. Tandor, *Phys. Letters*, A36, 319 (1971).
48. S.K. Kor, B.K. Singh and R. Pasad, *Phys. Letters*, A35, 100 (1971).
49. S.K. Garg and C.P. Smyth, *J. Phys. Chem.*, 69, 1294 (1965).
50. C. Campbell, J. Crossley and L. Glasser, *Adv. Mol. Relaxation Processes*, 8, 63 (1976).
51. J. Crossley, *Adv. Mol. Relaxation Processes*, 2, 69 (1970).
52. V.A. Dorgan, *Dokl. Akad. Nauk., SSSR*, 232, 114 (1977).
53. R. Zana and J. Lang, *Adv. Mol. Relaxation Processes*, 7, 21 (1975).
54. W.G. Rothschild, *J. Chem. Phys.*, 53, 3265 (1970).
55. E.D. Becker, E.E. Tucker and C.N.R. Rao, *J. Chem. Soc., Faraday Trans. 2*, 73, 438 (1977).
56. F. Franks and D.J.G. Ives, *Quart. Rev.*, 20, 1 (1966).
57. R.A. Pethrick, 'Molecular Interactions', Vol. 3, Ed. H. Ratajczak and W.J. Orville-Thomas, John Wiley and Sons Ltd., London (1982).
58. C.J. Burton, *J. Acoust. Soc. Am.*, 20, 186 (1948).
59. M.J. Blandamer and D. Waddington, *Adv. Mol. Relaxation Processes*, 2, 1 (1970).
60. J. Emery and S. Gasse, *Acustica*, 43, 205 (1979).
61. S. Gasse and J. Emery, *J. de Chim. Phys.*, 77, 262 (1980).
62. J.H. Andreae, P.D. Edmonds and J.K. McKeller, *Acustica*, 15, 74 (1965).

63. G.C. Benson and H.D. Pflug, *J. Chem. Eng. Data*, 15, 382 (1970).
64. J. Singh and G.C. Benson, *Can. J. Chem.*, 46, 1249, 2065 (1968).
65. M.P. Diaz and C.P. Sotomayor, *An. Quim.*, 67, 461, 467 (1971).
66. R.H. Stokes, K.N. Marsh, *Ann. Rev. Phys. Chem.*, 23, 65 (1972).
67. R.S. Ramalho and M. Ruel, *Can. J. Chem. Eng.*, 46, 456 (1968).
68. M.P. Diaz and C.D. Rodriguez, *An. Quim.*, 66, 637 (1970).
69. H. Wolff and H.E. Hoepfel, *Ber. Bunsenges, Phys. Chem.*, 72, 710, 722 (1968).
70. P. Gerhard, S. Martin and R. Klaus, *German Patent*, 1, 916, 255 (1970).
71. M. Stein, *Hydrocarbon Process.*, 52, 139 (1973).
72. G. Preusser, M. Stein and F. Franzen, *The Oil and Gas J.*, 71, 114 (1973).
73. E. Cinelli, S. Noe and G. Paret, *Hydrocarbon Process.*, 51, 141 (1972).
74. V.F. Trefny, *Erdol und Khole-Edrgas - Petrochem.*, 23, 337 (1970).
75. J.F. Hueter and R.H. Bolt, *'Sonics'*, Wiley, Interscience, New York (1960).
76. K.F. Herzfeld and T.A. Litovitz, *'Absorption and Dispersion of Ultrasonic Waves'*, Academic Press, New York (1959).

77. J. Lamb, 'Physical Acoustics', Vol. 2A, Ed. W.P. Mason, Academic Press, London (1971).
78. A.J. Matheson, 'Molecular Acoustics', Wiley-Interscience, London (1971).
79. C. Truesdell, J. Rational Mech. Anal., 2, 643 (1955).
80. C. Kirchoff, Poggendorf's Ann. Phys., 134, 177 (1868).
81. T.A. Litovitz, J. Acoust. Soc. Am., 31, 681 (1959).
82. E. Wyn-Jones and R.A. Pethrick, 'Topics in Stereochemistry', Vol. 5, Ed., E.L. Eliel and N.L. Allinger, Wiley-Interscience, London (1970).
83. R.A. Pethrick, Sci. Progr., 58, 563 (1970).
84. S. Glasstone, K.J. Laidler and H. Eyring, 'The Theory of Rate Processes', McGraw-Hill, New York (1941).
85. E.L. Heasell and J. Lamb, Proc. Roy. Soc., A237, 233 (1956).
86. R.O. Davies and J. Lamb, Quart. Rev. Chem. Soc., 11, 134 (1957).
87. R.A. Padmanaban, 'Ultrasonic Relaxation due to Rotational Isomerism in Organic Liquids', M.Sc. Thesis, London University (1959).
88. J.S. Rowlinson and F.L. Swinton, 'Liquids and Liquid Mixtures', Butterworths, London (1982).
89. M.L. McGlashan, 'Chemical Thermodynamics', Academic Press, London (1979).
90. I. Brown and A.H. Ewald, Aust. J. Sci. Res., A3, 306 (1950).
91. J. A. Larkin and M.L. McGlashan, J. Chem. Soc., 3425 (1961).

92. P. Picker, J. Jolicourr and J.E. Desnoyers, J. Chem. Thermodyn., 1, 469 (1969).
93. J.L. Fortier and G.C. Benson, J. Chem. Thermodyn., 8, 411 (1976).
94. W.A. Duncan, J.P. Sheridan and F.L. Swinton, Trans. Faraday Soc., 62, 1090 (1966).
95. L.A. Beath, S.P. O'Neill and A.G. Williamson, J. Chem. Thermodyn., 1, 293 (1969).
96. W.G. Cady, 'Piezoelectricity', McGraw-Hill, New York (1946).
97. W.P. Mason, 'Piezoelectric Crystals and their Application to Ultrasonics', Van Nostrand, New York (1950).
98. P. Vigoureux and C.F. Booth, 'Quartz Vibrators and their Applications', H.M.S.O., London (1950).
99. P. Curie and J. Curie, Compt. Rend., 91, 294(1881).
100. K.N. Baranskii, Sov. Phys. Doklady, 2, 237 (1957).
101. J. Lamb and J. Richter, J. Acoust. Soc. Am., 41, 1043 (1969).
102. R.B. Hemphill, Appl. Phys. Lett., 9, 35 (1966).
103. M.T. Wauk and D.K. Winslow, Appl. Phys. Lett., 13, 286 (1968).
104. B.T. Curtis, J. Chem. Phys., 40, 433 (1964).
105. J. de Klerk and E.F. Kelly, Rev. Sci. Inst., 36, 506 (1965).
106. K.R. Keller and B. Abeles, J. Appl. Phys., 37, 1937 (1966).

107. T.B. Bateman and J.H. McFee, *J. Appl. Phys.*, 39, 4471 (1968).
108. N.F. Foster, *J. Acoust. Soc. Am.*, 70, 1609 (1981).
109. B.A. Auld, *J. Acoust. Soc. Am.*, 70, 1577 (1981).
110. J. Blitz, 'Fundamentals of Ultrasonics', Butterworths, London (1963).
111. E.G. Spender and P.V. Lenzo, *J. Appl. Phys.*, 38, 423 (1967).
112. C.P. Wen and R.F. Mayo, *Appl. Phys. Lett.*, 9, 135 (1966).
113. A.B. Smith, *J. Appl. Phys.*, 40, 2687 (1969).
114. H. Sussner, D. Michas, A.A. Assflag, S. Hunklinger and K. Dransfied, *Phys. Lett.*, A45, 475 (1973).
115. L. Bui, H.J. Shaw and L.T. Zitell, *Electronics Lett.*, 12, 393 (1976).
116. W.H. Chen, H.J. Shaw, D.C. Weinstein and L.T. Zitelli, *Proc. IEEE*, 75, 780 (1978).
117. H. Kawai, *Japan J. Appl. Phys.*, 8, 975 (1969).
118. J. Stuehr, E. Yeager, J. Sachs and F. Hoverka, *J. Chem. Phys.*, 38, 587 (1963).
119. L.E. Lawley and R.D.C. Reed, *Acustica*, 5, 316 (1954).
120. J. Karpovich, *J. Acoust. Soc. Am.*, 26, 819 (1954).
121. F. Eggers, *Acustica*, 19, 232 (1967/68).
122. R.A. Pethrick, *J. Phys. E.*, 5, 57 (1972).
123. J.R. Pellam and J.K. Galt, *J. Acoust. Soc. Am.*, 18, 251 (1946).
124. J.M.M. Pinkerton, *Proc. Phys. Soc.*, B 62, 286 (1949).
125. E.L. Heasell and J. Lamb, *Proc. Phys. Soc.*, B 69, 869 (1956).

126. K.G. Plass, *Acustica*, 19, 236 (1967).
127. T. Wright and D.D. Campbell, *J. Phys. E.*, 10, 1241 (1977).
128. P. Debye and F.W. Sears, *Proc. Nat. Acad. Sci.*, 18, 409 (1932).
129. M.M. Farrow, S. Oslen, N. Purdie and E.M. Eyring, *Rev. Sci. Instrum.*, 47, 657 (1976).
130. G. Benedek, and T. Graytak, *Proc. IEEE*, 53, 1623 (1965).
131. J.H. Andreae, R. Bass, E.L. Heasell and J. Lamb, *Acustica*, 8, 131 (1958).
132. M.A. Cochran, Ph.D. Thesis, University of Strathclyde. (1974).
133. K.G. Plass, *Ber. Bunsenges. Phys. Chem.*, 74, 343 (1970).
134. P.K. Khabibullaev, M.G. Khaliuin and K. Pariev, *Sov. Phys. Acoust.*, 15, 406 (1970).
135. E.G. Spencer, P.V. Lenzo and K. Nassau, *Appl. Phys. Lett.*, 7, 67 (1965).
136. R.S. Musa, *J. Acoust. Soc. Am.*, 30, 215 (1958).
137. P.J. Flory, 'Statistics of Chain Molecules', Wiley-Interscience, London (1970).
138. D.C. Douglass and D.W. McCall, *J. Phys. Chem.*, 62, 1102 (1958).
139. P.A. Egelstaff and D.H.C. Harries, *Disc. Faraday Soc.*, 49, 193 (1970).
140. G.J. Szasz, N. Sheppard and D.H. Rank, *J. Chem. Phys.*, 16, 704 (1948).
141. N. Sheppard and G.J. Szasz, *J. Chem. Phys.*, 17, 86 (1949).

142. L.S. Bartell and D.A. Kohl, J. Chem. Phys., 39, 3097 (1963).
143. R.A. Boham and L.S. Bartell, J. Am. Chem. Soc., 81, 3491 (1959).
144. M.S. De Groot and J. Lamb, Proc. Roy. Soc., A 242, 36 (1957).
145. T.H. Thomas, E. Wyn-Jones and W.J. Orville-Thomas, Trans. Faraday Society, 65, 974 (1969).
146. R.A. Pethrick and E. Wyn-Jones, J. Chem. Phys., 49, 5349 (1968).
147. K. Krebs and J. Lamb, Proc. Roy. Soc., A 244, 558 (1958).
148. M. Barbe and D. Patterson, J. Solution Chem., 9, 753 (1980).
149. M. Barbe and D. Patterson, J. Phys. Chem., 82, 40 (1978).
150. V.T. Lam, P. Picker, D. Patterson and P. Tancrede, J. Chem. Soc., Faraday Trans. 2, 70, 1465 (1974).
151. A. Heintz and R.N. Lichtenthaler, Angew. Chem., Int. Ed., Engl., 21, 184 (1982).
152. J. Timmermans, 'Physico-Chemical Constants of Pure Organic Compounds', Elsevier, Vol. 2 (1965).
153. W. Schaaffs, in Molecular Acoustics, Vol. 5 of Landolt-Bornstein New Series Group II; K-H Hellwege and A.M. Hellwege, Editors Springer-Verlag, Berlin-Heidelberg, New York (1967).
154. G. Allen, G. Gee and G.J. Wilson, Polymer, 1, 456 (1960).
155. Selected Values of Properties of Hydrocarbons and Related Compounds, API Project 44, Thermodynamics Research Center, Texas A and M University, College

- Station, Texas, April 30, 1956, June 30, 1945, Dec. 31, 1948, Oct. 31, 1952.
156. H. Geelen, H.I. Waterman, J.B. Westerdijk and R.F. Klaver, *Riv. Combust.*, 9, 355 (1955).
  157. A.J. Barlow, J. Lamb and A.J. Matheson, *Proc. Roy. Soc.*, A 292, 322 (1969).
  158. E.N. Lassetre and L.B. Dean, *J. Chem. Phys.*, 16, 151 (1948).
  159. E.N. Lassetre and L.B. Dean, *J. Chem. Phys.*, 17, 317 (1949).
  160. W.V. Smith and R.R. Howard, *Phys. Rev.*, 79, 132 (1950).
  161. J.G. Aston, S. Isserow, G.J. Szasz and R.M. Kennedy, *J. Chem. Phys.*, 12, 336 (1944).
  162. F.A. French and R.S. Rasmussen, *J. Chem. Phys.*, 14, 389 (1946).
  163. E.M. Mason and M.M. Kreevoy, *J. Am. Chem. Soc.*, 77, 5808 (1955).
  164. M.M. Kreevoy and E.M. Mason, *J. Am. Chem. Soc.*, 79, 485 (1957).
  165. J.E. Lennard-Jones, *Proc. Roy. Soc.*, A 106, 463 (1924).
  166. B.E.F. Fender and G.D. Halsey, *J. Chem. Phys.*, 36, 1881 (1962).
  167. R.A. Buckingham, *Proc. Roy. Soc.*, A 168, 264 (1938).
  168. R.A. Scott and H.A. Scheraga, *J. Chem. Phys.*, 42, 2209 (1965).
  169. L. Pauling, *Proc. Nat. Acad. Sci.*, 44, 211 (1958).
  170. L. Pauling, 'The Nature of the Chemical Bond', Cornell University Press, New York (1960).

171. J.C. Slater and J.G. Kirkwood, *Phys. Rev.*, 37, 682 (1931).
172. K.S. Pitzer, *J. Chem. Phys.*, 7, 583 (1939).
173. J. Overend and J.R. Scherer, *J. Opt. Am. Soc.*, 50, 1203 (1960).
174. E.B. Smith, *Ann. Rep. Prog. Chem.*, 63, 13 (1966).
175. J.T. Edwards, *Can. J. Chem.*, 59, 3192 (1981).
176. S.W. Benson, 'Thermodynamical Kinetics', John Wiley and Sons, New York (1976).
177. E.B. Freyer, J.C. Hubbard and D.H. Andrews, *J. Am. Chem. Soc.*, 51, 759 (1929).
178. W. Schaaffs, *Z. Phys. Chem.*, A 196, 413 (1950/51).
179. J.H. Hildebrand, J.S. Sweny, *J. Phys. Chem.*, 43, 109, 297 (1939).
180. H. Tompa, *Trans. Faraday Soc.*, 45, 101 (1949).
181. K.N. March, J.B. Ott and A.E. Richards, *J. Chem. Thermodyn.*, 12, 897 (1980).
182. J.R. Goates, J.B. Ott and R.B. Grigg, *J. Chem. Thermodyn.*, 13, 907 (1981).
183. J.G. Fernández-García, M. Guillemin and Ch. G. Boissonnes, *Helv. Chim. Acta.*, 51, 1451 (1968).
184. H.B. Evans and H.L. Clever, *J. Phys. Chem.*, 68, 3433 (1964).
185. F. Danusso, *Rend. Reale Accad. Naz. Lincei.*, 17, 109 (1954).
186. K. Ridgway and P.A. Butler, *J. Chem. Eng. Data*, 12, 509 (1967).

187. A.R. Mathieson and J.C.J. Thynne, *J. Chem. Soc.*, 3708 (1956).
188. T.E. Mairs and F.L. Swinton, *J. Chem. Thermodyn.*, 12, 575 (1980).
189. R.J. Hill, T.E. Mairs and F.L. Swinton, *J. Chem. Thermodyn.*, 12, 581 (1980).
190. S.S. Chen and B.J. Zwolinski, *J. Chem. Soc., Faraday Trans. 2*, 70, 1133 (1974).
191. J. Reeder, C.M. Knobler and R.L. Scott, *J. Chem. Thermodyn.*, 7, 345 (1975).
192. M. Steiger, Ch. G. Boissonass, J.G. Fernandez and H.F. Stoickli, *Helv. Chim. Acta.*, 55, 1329 (1972).
193. M. Steiger and H.F. Stoeckli, *Helv. Chim. Acta.*, 57, 521 (1974).
194. G. Delmas, P. de St. Romain and P. Purves, *J. Chem. Soc., Faraday Trans. 1*, 71, 1181 (1975).
195. J.A. Larkin, D.V. Fenby, T.S. Gilman and R.L. Scott, *J. Phys. Chem.*, 70, 1959 (1966).
196. D.V. Fenby, J.R. Khurma, Z.S. Kooner, T.E. Block, C.M. Knobler, J. Reeder and R.L. Scott, *Aust. J. Chem.*, 33, 1927 (1980).
197. J.B. Ott, R.B. Grigg and J.R. Goates, *Aust. J. Chem.*, 33, 1921 (1980).
198. B. Kronberg and D. Patterson, *J. Chem. Soc., Faraday Trans. 2*, 77, 1223 (1981).
199. S.N. Bhattacharyya and D. Patterson, *J. Soln. Chem.*, 9, 247 (1980).
200. D. Patterson, *Pure and Appl. Chem.*, 47, 305 (1976).

201. R.A. Orwoll and P.J. Flory, *J. Am. Chem. Soc.*, 89, 6814, 6822 (1967).
202. H. Klunder, W.E. Hammers and C.L. de Ligny, *J. Soln. Chem.*, 7, 485 (1978).
203. A.J. Treszczanowicz, O. Kiyohara and G.C. Benson, *J. Chem. Thermodyn.*, 13, 253 (1981).
204. M. Diaz Pena and G. Tardajus, *J. Chem. Thermodyn.*, 10, 19 (1978).
205. G.C. Benson and H.P. Hanoda, *J. Chem. Thermodyn.*, 13, 887 (1981).
206. J.P. Wiabaut and H. Brand, *Rec. Trav. Chim.*, 80, 97 (1961).
207. J.E. Piercy, *J. Chem. Phys.*, 43, 4066 (1966).
208. J.E. Piercy and J. Lamb, *Trans. Faraday Soc.*, 52, 930 (1956).
209. V.P. Romanov and V.A. Solouyev, *Sov. Phys. Acoust.*, 11, 68, 219 (1965).
210. O. Nomoto, *J. Phys. Soc. Jap.*, 11, 827, 818 (1956).
211. L. Hall, *Phys. Rev.*, 73, 775 (1948).
212. C.M. Davis, J.R. and T.A. Litovitz, *J. Chem. Phys.*, 42, 2563 (1965).
213. H.S. Frank and W.Y. Wen, *Discuss. Faraday Soc.*, 24, 133 (1957).
214. G. Nemethy and H.A. Scheraga, *J. Chem. Phys.*, 36, 3382 (1962).
215. T.A. Litovitz and C.M. Davis, 'Physical Acoustics', Vol. 2 A, Ed. W.P. Mason, Academic Press (1965).

216. J.R. Pellam and J.K. Galt, *J. Chem. Phys.*, 14, 608 (1946).
217. G.W. Willard, *J. Acoust. Soc. Am.*, 19, 235 (1947).
218. R.T. Lagemann, D.R. McMillan, Jr. and M. Woolsey, *J. Chem. Phys.*, 16, 247 (1948).
219. V. Suryaprakasam, *Proc. Ind. Acad. Sci.*, A 12, 341 (1940).
220. C.V.J. Rao, *Proc. Ind. Acad. Sci.*, A 9, 312 (1939).
221. J.C. Hubbard and A.L. Loomis, *Nature*, 120, 189 (1927).
222. R. Bar, *Helv. Phys. Acta*, 8, 500 (1935).
223. M.R. Rao, *Ind. J. Phys.*, 14, 109 (1940).
224. R.T. Lagemann and W.S. Dunbar, *J. Phys. Chem.*, 49, 428 (1945).
225. R.T. Lagemann, D.R. McMillan, Jr. and W.E. Woolf, *J. Chem. Phys.*, 17, 369 (1949).
226. M.R. Rao, *J. Chem. Phys.*, 9, 682 (1941).
227. G. Weissler, *J. Am. Chem. Soc.*, 70, 1634 (1948).
228. I.G. Mikhailov and D.M. Nizhin, *Dokl. Akad. Nauk. S.S.S.R.*, 58, 1689 (1947).
229. H.I. Leon, *J. Chem. Phys.*, 28, 748 (1958).
230. D.V.S. Jain, A.M. North and R.A. Pethrick, *Trans. Faraday Soc.*, 70, 1292 (1974).
231. K. Seshadri and K.C. Reddy, *Acustica*, 29, 59 (1973).
232. V. Tiwari and J.D. Pandey, *Acoust. Lett.*, 2, 116 (1980).
233. J.D. Pandey, R.L. Mishra and T. Bhatt, *Acustica*, 38, 83 (1977).
234. N. Prasad and S. Prakash, *J. Chem. Eng. Data*, 22, 49 (1977).

235. W. Schaaffs, *Acustica*, 33, 272 (1975).
236. W. Schaaffs, *Acustica*, 30, 275 (1974).
237. W. Schaaffs, *Z. Phys. Chem.*, 114, 110 (1939).
238. D. Chandler, *Ann. Rev. Phys. Chem.*, 29, 441 (1978).
239. D. Chandler, *J. Chem. Phys.*, 67, 1113 (1977).
240. B.M. Ladanyi, and D. Chandler, *J. Chem. Phys.*, 62, 4308 (1975).
241. B. Jacobsen, *Acta Chem. Scand.*, 5, 1214 (1951).
242. B. Jacobsen, *Acta Chem. Scand.*, 6, 1485 (1952).
243. H. Eyring, *J. Chem. Phys.*, 4, 283 (1936).
244. H. Eyring and J. Hirschfelder, *J. Phys. Chem.*, 41, 249 (1937).
245. H.M. Huffman, M.E. Grass, D.W. Scott and J.P. McCullough, *J. Phys. Chem.*, 65, 495 (1961).
246. R. Shaw, *J. Chem. Eng. Data*, 14, 461 (1961).
247. K.N. Marsh and C. Burfitt, *J. Chem. Thermodyn.*, 7, 955 (1975).
248. O. Kiyohara and G.C. Benson, *J. Chem. Thermodyn.*, 11, 861 (1979).
249. L.A.K. Staveley and B. Spice, *J. Chem. Soc.*, 406 (1952).
250. G. Dharmaraju, G. Nayayanaswamy and G.K. Raman, *J. Chem. Thermodyn.*, 12, 563 (1980).
251. H.C. Van Ness, C.A. Soczek and N.K. Kochar, *J. Chem. Eng. Data*, 12, 346 (1967).
252. G.N. Swamy, G. Dharmaraju and G.K. Raman, *Can. J. Chem.*, 58, 229 (1980).
253. S. Nishikawa, M. Mashima and T. Yasunaga, *Bull. Chem. Soc. Japan*, 49, 1413 (1976).

254. A.J. Tresczanowicz and G.C. Benson, *J. Chem. Thermodyn.*, 10, 967 (1978).
255. A.J. Tresczanowicz and G.C. Benson, *J. Chem. Thermodyn.*, 12, 173 (1980).
256. J.L. Hales and J.H. Ellender, *J. Chem. Thermodyn.*, 8, 1177 (1976).
257. E. Alcart, G. Tardajou and M. Diaz Pena, *J. Chem. Eng. Data*, 25, 140 (1980).
258. G.W. Marks, *J. Acoust. Soc. Am.*, 41, 103 (1967).
259. W.E. Kuhn, United States Patent, 2.357.6667, 9 (1944).
260. J. Morgan and B.E. Warren, *J. Chem. Phys.*, 6, 666 (1938).
261. H. Narten, M. Danford and H. Levy, *Disc. Faraday Soc.*, 43, 97 (1967).
262. K.M. Swamy and P. Sitaramaswaamy, *J. Phys. Soc. Japan*, 28, 535 (1970).
263. N.I. Larionov, *Z. Fiz. Khim.*, 27, 1002 (1953).
264. H. Endo, *Bull. Chem. Soc. Japan*, 46, 1586 (1973).
265. E.K. Baumgartner and G.J. Atkinson, *J. Phys. Chem.*, 75, 2336 (1971).
266. H. Endo, *Bull. Chem. Soc. Japan*, 46, 1106 (1973).
267. A. Giacomini, *J. Acoust. Soc. Am.*, 19, 702 (1947).
268. N.V. Chekalin and M.I. Schakhparonov, *Sov. Phys. Acoust.*, 17, 147 (1971).
269. R. Kuhnkies and W. Schaaffs, *Acustica*, 12, 254 (1962).
270. A. Al-Kassim and S.B. Palmer, *Acoust. Lett.*, 3, 192 (1980).

271. P.N. Girija and K.C. Reddy, *Acoust. Lett.*, 3, 184 (1980).
272. E. Baumgartner and G. Atkinson, *Z. Phys. Chem., Leipzig*, 252, 392 (1973).
273. W. Kroebel and K.H. Mahrt, *Acustica*, 35, 154 (1976).
274. G.S. Kell, *J. Phys. Chem. Ref. Data*, 6, 1109 (1977).
275. H.J. McSkimin, *J. Acoust. Soc. Am.*, 37, 325 (1965).
276. R.A. Pethrick and E. Wyn-Jones, *J. Chem. Soc., A*, 713 (1969).
277. V.M. Gittins, P.J. Heywood and E. Wyn-Jones, *J. Chem. Soc. Perkin 2*, 14, 1642 (1975).
278. D. Grimshaw and E. Wyn-Jones, *J. Chem. Soc., Faraday Trans. 2*, 69, 168 (1973).
279. C. de Visser, G. Perron, J.E. Desnoyers, W.J. Heuvelsland and G. Somsen, *J. Chem. Eng. Data*, 22, 74 (1977).
280. O. Kiyohara, G. Perron and J.E. Desnoyers, *Can. J. Chem.*, 53, 3263 (1975).
281. R.C. Petersen, *J. Phys. Chem.*, 64, 184 (1960).